Universidade do Minho
Escola de Engenharia

Paula Matilde López Pérez

Some hints on using surface phenomena for the design and performance optimization of distinct biomedical devices

Janeiro de 2010

Some hints on using surface phenomena for the design and performance optimization of distinct biomedical devices
Paula Matilde López Pérez
UMinho | 2010

Universidade do Minho
Escola de Engenharia

Paula Matilde López Pérez

Some hints on using surface phenomena for the design and performance optimization of distinct biomedical devices

Tese de Doutoramento em
Engenharia Biomédica

Trabalho efectuado sob a orientação de
Professor Doutor Rui Luís Gonçalves dos Reis
Doutora Iva Pashkuleva

Janeiro de 2010

To my family (a mi familia)

“Scientific work must not be considered from the point of view of the direct usefulness of it. It must be done for itself, for the beauty of science”

Marie Curie (1867-1934)

Acknowledgments

After writing more than 150 pages, when you start to think that the writing process is finished you realize that you have still to write the easiest and at the same time hardest page. The presentation of this thesis would be not possible at all without the presence and assistance of several people. It is with pleasure that I express my gratitude to them in here.

First and foremost, I am greatly thankful to my thesis supervisor Prof. Rui Reis who offered me a chance being a PhD candidate in his group. He gave me all the support and freedom to choose my research topics (even when they were “fundamentalist”) and provided me all the necessary conditions to perform my work. I am completely grateful to my cosupervisor, Dr. Iva Pashkuleva. Thank you very much for the day to day support, friendship and encouragement in my more pessimistic days. Thank you also for being not only a supervisor in the lab but to be also present in the important moments of my personal live.

If this thesis is going to “see the light” is without any doubts because of the personal and scientific support of Prof. Julio San Roman gave me from the very beginning of this journey. Julio, ni siquiera se me ocurre una forma con la que se pueda expresar el agradecimiento por todo el apoyo y amistad durante estos últimos años; ¡MUCHÍSIMAS GRACIAS!.

The personal and scientific issues are very important for a thesis development but it is true that without a material part, i.e., the money, it would be not possible even to start the work. For that reason, I can not forget to thank the financial support that I receive from the Marie Curie European program, that provide me the PhD scholarship by the Alea Jacta Est project (MEST-CT-2004-008104), and the European network of excellence EXPERTISSUES (NMP3-CT-2004-500283), that partially support the described research work.

I would like to acknowledge to all people that somehow was involved in my scientific work. Thank to Prof. Paula Margarida Ferreira from the Chemistry department for introducing me in the peptide synthesis and to Elisa Pinto from the NMR service for her availability. Thank also to Carmen Serra from the University of Vigo for the help and guidance on the surface characterization issues. Thanks to Gema, Eva and Carolina at CSIC in Madrid for helping with the GPC. Finally my colleges from·3B´s: Vitor Correlo, Paula Sol and Rui Amandi for the SPCL scaffolds issues; Xana that introduce me in the biology lab; Liliana always available in the reagents matter; Rogério that kindly help me with the fluorescence microscopy, Johan observing the surfaces “smooth like crazy” by AFM and Marina that invest her last day of holidays before leaving to Sevilla on helping me with the confocal microscopy (Marinocas eres un sol).

In my journey in the 3B´s I had the opportunity to interact with a great number of people and I want to take this opportunity to acknowledge to all of them for the goods and bad moments we lived together. However it would be not fair if I do not thank specifically those who really did the difference in my personal live. I would like to thank to Tommaso (and Elena) that share with me the hard beginning and end of the thesis but also very good moments in the middle; to Ricardo Pires, that was always next to me hearing with patience my problems, complaints and stupid theories.

Thanks to Cassilda my personal “Tinkerbell”. Thanks also to Helena Lima, Silvia and Vitor for all the conversations without any sense that were always making me smile, and to Vitor ES, Daniela Ferreira, Catarina Custodio and a tola da Mendes for the support words you gave me in the last year. Finally, thank to Helena Azevedo, Ana Leite, Sofia, Belinha, Bruno, Sandra Luna, Ricardo Pichioqui, Ana Martins, Joao Oliveira, Kadrus, Marco Antonio, Ivo, Daniela Coutinho, Adriano, Rui Pereira, Ana Rita, Tó, Erkan and Wojtek, because they were there always that I needed.

A toda la gente del laboratorio en Madrid que hizo mi adaptación al país extranjero durante mi estancia mucho más fácil. A Blanca por su comprensión y cariño. A todos los “Manolistas” por ayudarme a entender la gastronomía local y sin los cuales aquellas animadas comidas no habrían sido lo mismo. Un gracias muy especial a Luilli el Rojo por las profundas discusiones lingüísticas (y no sólo lingüísticas) y porque aunque cueste creerlo nuestro momento de Manolo y Benito fue un punto de inflexión en mi tesis. A mis dos mejicanos favoritos Rodri y Raúl (más conocidos por Machupichu y Guachipango) por aguantar estoicamente todas mis bromas (como está última). Al Paco Paquillo y su estilo puramente chulapo que me ayudó a recordar la importancia de un buen químico orgánico. Como no agradecer a mis cuatro fantásticas: a Sandra (la hierbas) por haberme sacao la pulga que me traje de Marruecos; a “esa Feli y olé” y su quarto y mitad de chope con su alegría andalusa; a mi Patri (jiji) por su dulzura desmedida y a mi pequeña Lorenilla (la mayor Friki niña de los Flanders que jamás he conocido), que aguantó todos mis quejas, lloros y lamentos al igual que compartió mis alegrías; por nuestros paseos de camino a casa. Gracias por tantos momentos dentro y fuera del laboratorio: por el drenaje que me salvó la vida, por el café de las 11, por las toneladas de risquetos, por los viajes hechos y por los que nos quedan por hacer… A Marita y Cristina porque la vida en Pradillo sin vosotras no habría tenido comparación; por todas las series no vistas y las cenas compartidas.

A todos los amigos que he ido haciendo por allí por donde he pasado. Por haber mostrado siempre su apoyo en los momentos bajos y haber sabido entender y respetar mi ausencia en sus vidas por mi mala gerencia del tiempo. A las niñas un gracias especial porque aunque ahora nos veamos muy poco siempre seréis “mis niñas”.

Por último tengo que decir que la realización de esta tesis tampoco habría sido posible sin el cariño de mi familia. A ellos les debo no sólo el haber llegado hasta aquí sino haber llegado a donde quiera que sea. A mis padres, a los que con mis inseguridades he hecho sufrir a lo largo de los años y aun así nunca se han rendido y han continuado animándome a acabar todo aquello que había empezado. A mis hermanos (Joaquín, Elvi, Mario, Marta y Andrés), cuñados y a la reciente prole por su apoyo incondicional a lo largo de los años y por los buenos momentos brindados cuando estamos todos juntos. A mi abuelo Joaquín y como no a mi tercera abuela Maruja porque durante años siempre me ha dado su hombro para llorar mis penas. À minha familia por afinidade pelo seu apoio e carinho.

Oh! Ricardo a minha “preguiza”. Esto habría sido como un cubo de Rubik en mis manos, dando vueltas y más vueltas sin encontrar solución, si tú no hubieses hecho parte de mi vida. Gracias por ayudarme a colocar todas las piezas en su lugar. Gracias por tu cariño y paciencia que han sido, sin duda, vitales para ir viendo poco a poco la luz sin que los rayos me cegasen.

Some hints on using surface phenomena for the design and performance optimization of distinct biomedical devices

Abstract

The surface properties of materials in contact with biological systems play a key role in determining the outcome of biological-material interactions. Most of the conventional materials do not meet simultaneously the demands required for biomaterials surface and bulk properties. An effective approach for optimizing biomaterials performance is to modify the surface of a specific material which already has excellent functionality and bulk properties. Anionic scaffolds have been investigated in order to create tissue engineering substitutes mainly because of their capability to facilitate morphogenetic processes. For example, the negative charge of glucosaminoglycans (GAGs) is associated with their bioactivity via interaction with the positively charged amino groups of extracellular proteins. On the other hand, it is also reported that many bone promoting proteins naturally interact with acidic polymers. This thesis addresses the influence of such anionic, acidic groups on the surface of biomedical devices. In a first approach, plasma induced polymerization of vinyl monomers with pendent acidic moieties on chitosan membranes (2D) is described (Chapter 3). Acrylic acid and vinyl sulfonic acid was used to introduce respectively, carboxylic or sulfonic groups on the surface. A plasma activation method was chosen because it does not influence the bulk attributes of the material. On the other hand, carboxylic and sulfonic groups were studied because they are present as the major anionic functional groups on natural GAGs structures. In Chapter 4, the same strategy was followed to introduce phosphonic groups on chitosan membranes surface. The importance of the phosphonic groups, mimicking bone promoting proteins and mineral bone matrix, has been recognized before by the biomaterials scientific community. We have demonstrated herein that plasma induced polymerization is an effective methodology for grafting vinyl polymers on 2D chitosan membranes, without modifying the bulk properties of the material. Moreover, we found that the presence of sulfonic and phosphonic groups induced remarkably different osteoblast-like cells (SaOs-2) response in terms of attachment, spreading, viability and proliferation. In Chapter 5, the effectiveness of this surface modification method was tested on 3D structures with complex shapes. For that, the same modification process was used to introduce sulfonic and phosphonic groups on the surface of fiber mesh scaffolds made of a blend of starch and ε-polycaprolactone. We found that grafting of negatively charged units such as

sulfonic and phosphonic groups induced rather different response in both protein adsorption from serum and osteoblast-like cells adhesion and proliferation.

In the second part of the thesis, ionic thermo-responsive vinyl polymers were synthesized by conventional free radical polymerization. Random terpolymers composed of *N*-isopropylacrylamide (NIPAAm), 2-Acrylamido-2-methyl-1-propanesulphonic acid (AMPS) and *N-tert*-butylacrylamide (NTBAAm) were obtained. The technological relevance of this type of polymer relies on their ability to form surfactant-free nanoparticles stabilized by surface charge above the low critical solution temperature (LCST) or to interact with oppositely charged macromolecules, allowing for instance surface modification using techniques of polyelectrolyte layer-by-layer construction. In Chapter 6 the effect of polymer composition, salt and polymer concentration in the aggregation-redissolution behavior in solution was evaluated. Turbidity was used to assess the macroscopic phase separation and dynamic light scattering (DLS) was employed to elucidate some aspects regarding the molecular scale mechanism of the temperature-induced phase separation. The cloud point temperature (CPT) determined by turbidimetry was found to be systematically much higher than the LCST determined by DLS; nanosized aggregates were observed at temperatures between the LCST and the CPT. Both CPT and LCST decreased when increasing the polymer hydrophobicity (molar ratio of NTBAAm). It was found that polymers with higher NTBAAm contents present a slow macroscopic phase separation and the large aggregates formed only redissolve when LCST is reached. This behavior was explained on the basis of a delicate balance between the electrostatic repulsion and the hydrophobic attractive forces, which contribute cooperatively to the formation of metastable nanosized aggregates. In addition, the behavior observed for more hydrophobic polymers was further explored in Chapter 7 as a way to develop a method for the synthesis of thermoresponsive nanoparticles providing a tight control over particle size (between 35 - 200 nm) and that can also be reversibly disentangled at a temperature below the LCST, with recovery of soluble terpolymer chains. The nanoassemblies are formed in aqueous and surfactants free medium. For that, the polymer solution is just maintaining at high temperature for some time and the temperature is decreasing to 21ºC when particles achieve the desired size. This thermoresponsive system may be potentially useful for a range of applications, including drug and gene delivery, biosensing, or separation and purification of biological molecules and cells.

Algumas considerações sobre o uso de fenómenos superficiais na concepção e na optimização do desempenho de diversos dispositivos biomédicos

Resumo

As propriedades superficiais de materiais em contacto com sistemas biológicos têm um papel determinante no resultado das interacções entre os dois meios. A maior parte dos materiais convencionais não obedece simultaneamente aos requisitos exigidos para as propriedades totais e superficiais dos biomateriais. Uma abordagem para a optimização do desempenho de biomateriais consiste na modificação da superfície dum material que já tenha demonstrado possuir propriedades totais e funcionalidade adequadas.

Têm havido vários estudos sobre suportes poliméricos aniónicos para a formação de tecidos biológicos de substituição, advogando a sua capacidade de facilitar o processo de morfogénese. No caso dos glicosaminoglicanos (GAGs), carregados negativamente, a bioactividade foi associada a interacções com os grupos amina positivamente carregados das proteínas extracelulares. Por outro lado, também têm sido referido na literatura que muitas das proteínas que promovem a morfogénese óssea interagem naturalmente com polímeros acídicos.

Esta tese debruça-se sobre a influência de grupos aniónicos (acídicos) na superfície de dispositivos biomédicos. Numa primeira abordagem, é descrita a polimerização de monómeros vinílicos com grupos funcionais laterais acídicos induzida em membranas de quitosano pré-tratadas por plasma (capítulo 3). Os ácidos acrílico e vinil sulfónico foram usados para introduzir na superfície grupos carboxílicos e sulfónicos, respectivamente. O método de activação por plasma foi escolhido, por não influenciar as propriedades totais dos materiais. Os grupos carboxílicos e sulfónicos foram escolhidos para estudo por serem os grupos funcionais aniónicos mais abundantes nas estruturas naturais dos GAGs. No capítulo 4, foi seguida a mesma estratégia para introduzir grupos fosfónicos na superfície de membranas de quitosano. A importância dos grupos fosfónicos, que mimetizam as proteínas que promovem a morfogénese e a própria matriz mineral do osso, foi anteriormente reconhecida pela comunidade científica dos biomateriais. Nesta tese demonstra-se que a polimerização induzida por plasma é uma metodologia adequada para o enxerto de vários polímeros vinílicos em membranas de quitosano (2D), sem modificar as propriedades totais do material. Também se observou que a presença de grupos sulfónicos e fosfónicos se traduz em diferenças notáveis na resposta celular de células do tipo osteoblasto (SaOs-2) em termos de adesão, morfologia, viabilidade e proliferação. No capítulo 5, a eficácia deste método de modificação superficial foi testada

em estruturas 3D com formas mais complexas. O mesmo método de modificação foi usado para introduzir grupos sulfónicos e fosfónicos na superfície de suportes para engenharia de tecidos à base de fibras de uma mistura polimérica de amido e ε-policaprolactona. Concluiu-se que o enxerto de cadeias poliméricas com grupos sulfónicos e fosfónicos induzem um resposta diferente tanto em termos de adsorção de proteínas do soro, como, de adesão e proliferação de células do tipo osteoblasto.

Na segunda parte da tese foram sintetizados polímeros iónicos com resposta à temperatura por métodos convencionais de polimerização radical, obtendo-se terpolímeros aleatórios compostos por *N*-isopropilacrilamida (NIPAAm), ácido 2-acrilamida-2-metil-1-propanosulfónico (AMPS) e *N-tert*-butilacrilamida (NTBAAm). A relevância tecnológica deste tipo de polímeros está relacionada com a sua capacidade para formar nanopartículas, sem recurso a surfactantes, estabilizadas pela carga superficial quando acima da temperatura crítica de solubilidade inferior (LCST); ou pela sua capacidade de interagir com macromoleculas com carga oposta, permitindo, por exemplo, a modificação de superfícies por deposição electrostática alternando camadas de carga oposta. No capítulo 6, foi avaliado o efeito da composição do polímero e das concentrações de sal e polímero na agregação e redissolução. A separação de fases foi avaliada macroscopicamente pelo aparecimento de turbidez. Alguns dos aspectos dos mecanismos moleculares inerentes à separação de fases induzida pelo aumento da temperatura foram revelados por difusão dinâmica de luz (DLS). A temperatura de turvação (CPT), determinada por turbidimetria, foi sistematicamente superior à LCST determinada por DLS; agregados à escala nanométrica foram observados entre a LCST e a CPT. Tanto a CPT como a LCST diminuíram com o aumento da hidrofobicidade (fracção molar de NTBAAm). Polímeros com maior conteúdo em NTBAAm apresentaram uma separação de fases lenta a nível macroscópico, e os agregados de “grandes” dimensões entretanto formados apenas redissolveram quando arrefecidos abaixo da LCST. Este comportamento, observado para os polímeros mais hidrófobos, foi usado no capítulo 7 para desenvolver um método de síntese de nanopartículas com resposta à temperatura, permitindo um alto controlo sobre o tamanho de partícula (entre 35 - 200 nm). Para isso, a solução de polímero foi mantida a temperatura elevada durante algum tempo e, quando as partículas atingiram o tamanho especificado, arrefecida a 21 ºC. Estas construções nanométricas são formadas em meio aquoso, sem recurso a surfactantes, e podem ser desagregadas reversivelmente a temperatura inferior à LCST, levando à redissolução das cadeias poliméricas. Este sistema com resposta à temperatura tem alto potencial para um conjunto de aplicações tão diversas como a administração localizada de fármacos e genes, o desenvolvimento de biosensores, ou a separação e a purificação de macromoléculas biológicas ou de células.

Table of Contents

	Page
Acknowledgements	v
Abstract	vii
Resumo	ix
List of Figures	xv
List of Tables	xix
List of Abbreviations and nomenclature	xxi
1 Introduction. Surface modification of natural-based biomedical polymers.	**1**
1.1 Introduction	2
1.2 Some terms and classifications	2
1.3 Wet chemistry in surface modification	4
1.3.1 Wet chemical etching	5
1.3.2 Oxidation by wet surface modification methods	6
1.3.3 Hydrolysis	7
1.4 Physical methods for surface alternations	9
1.4.1 Plasma activation and modification	9
1.4.2 UV-irradiation	13
1.4.3 β- and γ-irradiation	14
1.5 Grafting	14
1.6 Bio-approaches: Mimicking the cell-cell interactions	16
1.6.1 Protein immobilization	16
1.6.2 Lipid coatings	20
1.7 Future directions	21
1.8 References	22
2 Materials and Methods	**33**
2.1 Part I: Surface functionalization by plasma induced polymerization	33
2.1.1 Materials	33
2.1.2 Membranes/scaffolds production and modification	40
2.1.3 Surface characterization	41
2.1.4 *In vitro* biological evaluation	46
2.2 Part II: Thermoresponsive alkylacrylamide based ionic terpolymers.	49
2.2.1 Terpolymers synthesis	49

2.2.2 Copolymers compositions 50
2.2.3 Molecular weight distribution 50
2.2.4 Turbidity measurements 51
2.2.5 Dynamic light scattering measurements 51
2.2.6 Nanoparticles Electrophoretic Mobility determination 53
2.3 References. 53
3 Effect of chitosan membranes' surface modification via plasma induced polymerization on the adhesion of Osteoblast-like cells 59
3.1 Abstract 59
3.2 Introduction 61
3.3 Materials and Methods 62
3.3.1 Membranes preparation 62
3.3.2 Surface modification 63
3.3.3 X-ray Photoelectron spectroscopy (XPS) 63
3.3.4 Fourier-transform infrared spectroscopy (FTIR) 63
3.3.5 Scanning electron microscopy (SEM) 64
3.3.6 Contact angle measurements 64
3.3.7 Cell culture 64
3.3.8 Cell morphology 65
3.3.9 MTS assay 65
3.4 Results and discussion 66
3.4.1 XPS analysis 66
3.4.2 SEM analysis 68
3.4.3 FTIR analysis 68
3.4.4 Contact angle measurements 69
3.4.5 Cell morphology 72
3.4.6 MTS assay 74
3.5 Conclusions 75
3.6 Acknowledgments 75
3.7 References 76
4 Surface phosphorylation of chitosan significantly improves Osteoblast cells viability, attachment and proliferation **79**
4.1 Abstract 79
4.2 Introduction 80
4.3 Materials and methods 81
4.3.1 Materials 81

4.3.2 Preparation and modification of chitosan membranes 82
4.3.3 Surface characterization 82
4.3.4 Cell culture 84
4.4 Results and discussion 86
4.4.1 Surface Chemistry 86
4.4.2 Surface Topography 90
4.4.3 Surface energy and water wettability 91
4.4.4 Cell behavior 94
4.5 Conclusions 97
4.6 Acknowledgements 98
4.7 References 98
4.8. Support information 63
5 Plasma-induced polymerization as a tool for surface functionalization of polymer scaffolds for bone tissue engineering: an *in vitro* study **105**
5.1 Abstract 105
5.2 Introduction 106
5.3 Materials and Methods 107
5.3.1 Materials 107
5.3.2 SPCL meshes production and modification 107
5.3.3. Surface chemical composition 108
5.3.4. Surface topography 109
5.3.5. Protein adsorption 109
5.3.6 Cell culture conditions and seeding 110
5.4 Results and discussion 110
5.4.1 Surface chemistry 111
5.4.2 Surface topography 114
5.4.3 *In vitro* biological evaluation 114
5.5. Conclusions 118
5.6 Acknowledgements 118
5.7 References 119
6 Hydrophobic-electrostatic balance driving the LCST offset aggregation-redissolution behavior of N-alkylacrylamide based ionic terpolymers **123**
6.1 Abstract 123
6.2 Introduction 125
6.3 Materials and Methods 127

6.3.1 Copolymers synthesis and characterization 127
6.3.2 Turbidity measurements 128
6.3.3 Dynamic Light Scattering (DLS) 128
6.4. Results and Discussion 129
6.5. Conclusions 140
6.6 Acknowledgements 141
6.7 References 141
7 Temperature as a single on-off parameter controlling nanoparticles growing, stabilization and fast disentanglement **145**
7.1 Abstract 145
7.2 Introduction 146
7.3 Results and discussion 147
7.4 Conclusions 152
7.5 Experimental 152
7.6 Acknowledgements 153
7.7 References 154
8 General conclusions and final remarks 157

List of Figures

1.1 SaOs-2, cultured for 7 days on SPCL (A and B) and SEVA-C (C and D) before (A and C) and after (B and D) surface oxidation by potassium permanganate. 7

1.2 Enzymatic (α-amylase) hydrolysis of starch 8

1.3 Hydrolysis of esters catalyzed by acid (up) or base (down) 8

1.4 Hydrolytic process involved in the conversation of chitin into chitosan 9

1.5 Transitional states of the matter 10

1.6 Effect of plasma working conditions on the surface morphology of starch/cellulose acetate (SCA) blend (50/50 wt): SEM micrographs of untreated SCA (A); and Ar plasma modified SCA at 80W, 15 min (B); at 30W,15 min (C) and at 80W for 5 min (D) 11

1.7 SEM micrographs showing the effect of oxygen plasma modification (30W, 15 min) on SaOs-2 adhesion (3 days of culture): untreated chitosan membrane (A and B) and modified one (C and D) 12

1.8 Immunostaining (PECAM, Phaloiedin and nuclei) of HUVEC cultured for 7 days on SPCL untreated (left) fibers mesh and SPCL fibers mesh modified by oxygen plasma (right) 12

1.9 Optical micrographs of osteoblast-like cells stained with methylene blue and cultured on untreated (A, C) and UV-irradiated (B, D) SCA (up) and SPCL (down) for 7 days 13

1.10 SPCL untreated (left) and surface modified by acrylic acid grafting (Ar plasma activation, right): effect of the treatment on cell (SaOs-2) adhesion after 7 days of culture – methylene blue staining 15

1.11 SEM micrographs of SaOs-2 cultured for 7 days on untreated chitosan membranes (up) and membranes grafted with vinyl sulfonic acid after oxygen plasma activation (down) 15

1.12 Two examples of natural polyions: chitosan (left) which is polycation at low pH and the polyanion hyaluronan (right). 17

1.13 Schematic representation of layer by layer (LbL) deposition technique depicting film deposition starting with a positively charged substrate 17

1.14 Illustration of the Langmuir-Blodgett technique 21

2.1 Chemical structures of the compounds used in the part I of the thesis. (For starch are only showed the α-(1→4) linkages but α-(1→6) bonds are also possible) 34
2.2 Example of linear regressions obtained by plotting η_{sp}/C (Huggins) or $\ln(\eta_{rel}/C)$ (Kraemer) against C (M_v = 790 kDa, K_H = 0.31;K_K = 0.17) 36
2.3 Chemical structure of monomers used in ionic terpolymer synthesis 49

3.1 C_{1s} core level spectra of non treated chitosan (a), plasma treated (b), AA grafted (c) and VSA grafted (d) materials 67
3.2 FTIR-ATR spectra of: untreated chitosan (a) and modified by O_2 plasma (b); AA grafted (c) and VSA grafted (d) materials 69
3.3 Optical micrographs of osteoblast-like cells stained with methylene blue cultured for 3 and 7 days 73
3.4 SEM micrographs showing SaOs-2 cultured for 3 days on the surface of plasma treated (a) and VSA grafted (b) membranes 74
3.5 Viability of SaOs-2 adhered to untreated and modified surfaces after 1, 3 and 7days of culture at 5% CO_2 at 37ºC 74

4.1 C1s, O1s, P2p core level spectra of native and PVPA grafted chitosan membranes 87
4.2 Positive (up) and negative (down) ToF-SIMS spectra of chitosan before and after (displayed in reverse) modification with poly (vinyl phosphonic acid) 88
4.3 High resolution ToF-SIMS, showing both higher concentration of NH (left) and presence of P(right) as a result of the applied treatment (the spectra displayed in the reverse) 89
4.4 Images of a 500 μm^2 area of VPA-grafted chitosan surface as reconstructed from the negative ion mass spectrum measured by static ToF-SIMS. From left to right: all ions; M59 (C2H3O2); M63 (PO2); M79 (PO3) 90
4.5 90x120μm^2 Optical Profiler images of chitosan (left) and PVPA grafted (right) membranes. Both images were taken in the membranes face dried in contact with the air 90
4.6 SEM micrographs of SaOs-2 cultured on chitosan (left) and PVPA (right) membranes during 1, 7 and 14 days (from up to down) 94
4.7 Calcein AM staining of SaOs-2 cultured for 7 days on chitosan (up) and PVPA (down) substrates 95
4.8 Cell viability (by MTS assay) of SaOs-2 cultured on unmodified and PVPA 96

grafted membranes
4.9 DNA concentration corresponding to SaOs-2 cultures in direct contact with CTS and PVPA substrates 96
4.SI1 XPS Survey spectra of non-treated and PVPA grafted materials 103
4.SI2 AFM images of chitosan (left) and PVPA grafted (right) membranes 103

5.1 Micro computed tomography image from SPCL fiber mesh scaffold 108
5.2 XPS core level spectra of untreated and grafted samples in the regions of C1s (left) and O1s (right) 112
5.3 Chemical structures of the components of the blend 113
5.4 Optical profile images: From left to right untreated SPCL, VSA grafted and VPA grafted scaffolds 114
5.5 Confocal Laser Scanning Microscopy photographs of non-modified and grafted scaffolds stained for Fn and Vn 115
5.6 SEM microphotographs of SaOs-2 cultures on SPCL, VSA grafted and VPA grafted scaffolds (from left to right) after 3, 7 and 14 days of culture (from up to down) 116
5.7 Viability of SaOs-2, evaluated by MTS assay, cultured on untreated and grafted SPCL fiber meshes 117
5.8 DNA concentration corresponding to SaOs-2 cultured on non-modified and functionalized scaffolds 117

6.1 poly(NIPAAm-co-NTBAAm-co-AMPS) chemical structure 127
6.2 Turbidity curves showing the effect of copolymer composition on the macroscopic phase separation for heating (a) and cooling (b) scans (1 g/L, 0.154M NaCl, 1 ºC/min). 131
6.3 Cloud point temperature (CPT) (filled squares) and macroscopic phase separation sharpness (ΔCPT) (filled triangles) in function of NTBAAm molar fraction (x_{NTBAAm}) (a). Comparision between CPT (filled squares) and redissolution temperature (empty squares) as a function of NTBAAm molar ratio (b). 131
6.4 Isothermal aggregation kinetics of 60/35/5 (1g/L) dissolved in 0.154M NaCl aqueous solution at temperatures above the cloud point temperature. 133
6.5 Effect of the NaCl concentration on the turbidity *vs* temperature curves on heating and cooling scans for 60/35/5 (a) and 80/15/5 (b). In both curves the polymers concentrations and scan rates were 1g/L and 1 ºC/min respectively. 135

6.6 Effect of the polymer concentration on the transmittance *vs* temperature curves on heating and cooling scans for 60/35/5 (a) and 80/15/5 (b). In both curves the salt concentrations and scan rates were 0.154M and 1 ºC/min respectively 135

6.7 Temperature dependence of the apparent hydrodynamic diameter (D_h) at several NaCl concentrations for 60/35/5 (polymer concentration 1g/L). The inset figure shows the hydrodynamic diameter distribution at temperatures before and after the aggregation (0.120M NaCl) 136

6.8 Isothermal aggregation kinetics of 60/35/5 determined by DLS (1g/L polymer concentration and 0.120M NaCl) at 19 ºC (triangles) and 25 ºC (square). Filled symbols represent the hydrodynamic diameter and empty symbols represent scattered light intensity (173º) 138

6.9 Temperature dependence of the apparent hydrodynamic diameter (D_h) at several NaCl concentrations for 80/15/5 (polymer concentration 1g/L). Inset shows the temperature dependence of D_h in water 138

7.1 Hydrodynamic diameter (D_h) and solution turbidity (*Transmittance*) changes observed as a function of temperature for (a) 80/15/5 and (b) 60/35/5. (c) Aggregation isotherms for 60/35/5 above the LCST. (d) Nanoparticles size control using a temperature programme. All measurements were done at polymer concentration of 1 g/l in NaCl aqueous solution (0.120M) 149

7.2 Nanoparticles z-average hydrodynamic diameter ($<D_h>_z$) observed as a function of temperature for 60/35/5. Aggregation is triggered at (a) 30 ºC or at (b) 40 ºC for well defined time periods and subsequently inhibited at 21 ºC. All measurements were done at polymer concentration of 1 g/l in NaCl aqueous solution (0.120M). (c) Schematic representation of the nanoparticles size manipulation using the thermoresponsive aggregation behaviour 150

7.3 (a) Electrophoretic mobility (μ_e) observed as a function of temperature for 60/35/5. Linear regression trendlines are shown independently for the datasets above and below 21 ºC. (b) μ_e measured isothermally for the studied aggregation kinetic states, followed by isothermal determination at 21 ºC. All measurements were done at polymer concentration of 1 g/l in NaCl aqueous solution (0.120M) 151

List of Tables

1.1 Material approach: Some of the used methods and related references 3

1. 2 Some bio-approaches: methods and applications 4

1.3 Some of the identified active sequences from different proteins and the receptors, which recognized them 19

2.1 Chitosan degree of deacetylation (DD) determined by different methods. (Average and standard deviation of *N* data points) 37

2.2 Calibration curves to determine the degree of deacetylation (DD) using the FTIR spectrum of chitosan. The absorbance (*A*) is the height at the band maximum corrected by the intercept with the respective baseline 37

2.3 Comparison of the resolution and sample/environment requirements for VSI optical profiler, AFM and SEM 46

2.4 Chemical Shifts (δ) and assignments for p(NIPAAm-*co*-NTBAAm-*co*-AMPS 50

3.1 Chemical composition of untreated and modified materials determined by XPS 66

3.2 C1s core level spectra of untreated and modified samples; composition (%) and Binding Energy (eV, in parenthesis) 68

3.3 Equilibrium contact angle values for untreated and modified samples (air, room temperature) 70

3.4 Surface Energy (± standard deviation) and its components calculated by OWRK (glycerol and diiodomethane) and AB (glycerol, formamide and diiodomethane) methods 71

4.1 Relative peaks composition (%) of C1s, O1s high resolution spectra 86

4.2 Equilibrium water contact angle and adhesion tension for PVPA grafted and non-treated chitosan membranes 92

4.3 Surface Energy and its components calculated by OWRK and AB methods 93

4.SI1 Chemical composition in atomic percentage of native and PVPA grafted chitosan membranes determined by XPS 103

5.1 Elemental composition of untreated and modified SPCL fiber meshes determined by XPS 111

5.2 Values for the roughness, calculated from the optical profiler images (107X magnification) 114

6.1 Copolymers composition and molecular weight 129

List of abbreviations and nomenclature

AA	Acrylic Acid
AcOH	Acetic acid
AcONa	Sodium acetate
AFM	Atomic Force Microscopy
AIBN	2,2'-azobis-isobutyronitrile
AMPS	2-Acrylamido-2-methyl-1-propanesulphonic acid
ATR	Attenuated total reflection
C	Concentration
CAE	Constant Analyser Energy mode
Calcein AM	Calcein-acetoxymethylester staining
CLSM	Confocal Laser Scanning Microscope
CPT	Cloud point temperature
CTS	Chitosan
CW	Continuous wave
D	Diffusion coefficient
DA	Degree of *N*-acetylation
DD	Degree of deacetylation
D_h	Hydrodynamic diameter
DLS	Dynamic light scattering
DMEM	Dulbecoo's modified Eagle's medium
DMF	Dimethylformamide
DVB	Scale proposed by Della Volpe and Sibone for surface energy of solvents
ECACC	European Collection of Cell Cultures
ECM	Extracellular matrix
EtO	Ethylene oxide
FBS	Fetal bovine serum
Fn	Fibronectin
FTIR-ATR	Fourier transform infrared spectroscopy

GAGs	Glucosaminoglycans
GlcN / GluN	D-glucosamine
GlcNAc /GluNAc	N-acetyl-D-glucosamine
GPC	Gel permeation chromatography
HMDS	Hexamethyldisilazane
HUVEC	Human umbilical vein cells
K_a	Acid ionization constant
K_B	Boltzmann constant
K_H	Huggins coefficient
K_K	Kraemer coefficient
LB	Langmuir-Blodgett technique
LbL	Layer by Layer
LCST	Low critical solution temperature
LDV	Laser Doppler Velocimetry
M_n	Number average molecular weight
MTS	((3-(4,5-dimethylthiazol-2-yl)-5-(3-carboxymethoxyphenyl)-2-(4-sulfophenyl)-2H tetrazolium
M_v	Viscosity molecular weight
M_w	Weight average molecular weight
M_w/M_n	Polydispersity
NIBS	Non-invasive backscattering
NIPAAm	*N*-isopropylacrylamide
NMR	Nuclear Magnetic Resonance spectroscopy
NTBAAm	*N-tert*-butylacrylamide
OD	Optical Density
OEG	Oligo(ethylene glycol)
OWRK	Owens, Wendt, Rabel and Kaelble method for surface energy calculation

PBS	Phosphate buffer solution
PCL	Polycaprolactone
PCS	Photon Correlation Spectroscopy
PEG	Poly(ethylene glycol)
PES	Polyethersulfone
PNIPAAm	Poly(*N*-isopropylacrylamide)
PVPA	Poly(vinylphosphonic acid)
Ra	Average absolute distance from average flat surface
RES	Reticuloendothelial system
R_h	Hydrodynamic radius
Rq	Root mean square from average flat surface
SAMs	Self-assembling monolayers,
SCA	Blend of starch andcellulose acetate
SEC	Size exclusion chromatography
SEM	Scanning electron microscopy
SEVA-C	Blend of starch and poly(ethylenevinyl alcohol
SMBV™	Supra molecular Biovector™
SPCL	Blend of starch and polycaprolactone
T	Temperature
TE	Tissue engineering
TGA	Thermo-gravimetric analysis
THF	Tetrahydrofuran
ToF-SIMS	Time-of-Flight Secondary Ion Mass Spectrometry
UV	Ultraviolet
Vn	Vitronectin
vOCG	Van Oss-Chaudury-Good theory
VPA	Vinyl phosphonic acid
VSA	Vinyl sulfonic acid
VSI	Vertical Scanning Interferometry mode
x_{NTBAAm}	Molar fraction of *N-tert*-butylacrylamide

XPS	X-ray photoelectron spectroscopy
ΔCPT	Phase separation sharpness
η_r	Relative viscosity
η_{sp}	Specific viscosity
θ	Contact angle
μCT	Micro computed tomography
μ_e	Electrophoretic mobility
τ	Water adhesion tension
γ_s^p	Polar components of the surface energy
γ_s^d	Dispersive component of the surface energy
γ_s	Surface tension
γ_S^{LW}	Surface energy corresponding to Lifshitz-Van der Waals forces
γ_S^{AB}	Contribution of the acid-base interaction to the surface tension:
γ_S^-	Lewis base contribution to the surface energy
γ_S^+	Lewis acid contribution to the surface energy
γ_w	Water surface tension
ϕ	Diameter
[η]	Intrinsic viscosity
$<D_h>_z$	z-average Hydrodynamic diameter

Chapter 1

Introduction

Surface modification of natural-based biomedical polymers

This chapter is based on the following publication:
Iva Pashkuleva; Paula M. López Pérez; Rui L. Reis. In **Natural-based polymers for biomedical applications**, eds. Reis RL, Neves NM, Mano JF, Gomes ME, Marques AP, Azevedo HS, Woodhead Publishing Limited, Cambridge, 163-192.

1.1 Introduction

Surface is defined as the outside or top layer of the material. If the analogy with a human is used, one can say that the bulk properties of a material determine its "character", while the surface is its "face". Similar to the human society, the initial acceptance or rejection of a biomaterial in the cell society is very dependent on its face whereas material character determines its long performance and proper function. Unfortunately, it is very difficult to find a biomaterial which simultaneously possesses both suitable mechanical properties in order to function properly in a certain bioenvironment and to not be harmful for the host tissue [1]. Therefore, a common approach is to fabricate biomaterials with adequate bulk properties and then to make-up those by a specific treatment resulting in enhanced surface properties.

The materials' surfaces (as people faces) are very different and it is not possible to have a universal modification for all of them [2]. Moreover, the environment and the role, which certain biomaterial is expected to play, call for a specific, unique and enough resistant modification which to ensure its good performance. To make this task even more complex, the requirements in the biomedical material research and development field are growing very fast. While few years ago, bioinert surfaces, protecting biomaterials from bacterial invasion, were sufficient for a material to be successful [3], over the past decade the requirements shift [4] to surfaces that interact and functionally integrate with their biological environment in a predictable and controllable way. Nowadays, design of surfaces helping the body to heal itself [5] by stimulating specific cellular responses at the molecular level is in the target of the research.

1.2 Some terms and classifications

A crucial concept to understand about the tissue-biomaterial interface is that many things happen there! The environment inside the body is dynamic and active, and the interface between an implanted biomaterial and the body is the location of a variety of dynamic biochemical processes and reactions [6]. During contact of non-bio surfaces with biological fluids, protein adsorption occurs almost instantaneously. This proteins layer will further mediate the key bio/material interactions. Therefore, protein adsorption plays a fundamental role in dictating the cellular response elicited by biomedical systems implanted in the human body. Thus, the ability to control these phenomena at the biomaterial surface largely determines the biological performance of biomedical systems.

Prevention of non-specific adhesion of proteins and polymer functionalization with cell-type specific molecules can propel to direct control of cell adhesion on biomaterials [7].
In the field of biomaterials, two historical approaches have been utilized [8] to understand and tailor cell adhesion to the materials' surfaces. The elder one, so-called **material approach,** correlates cell response (morphology, adhesion, retention or higher cellular function) to the character of the material surface. Different chemistry and physics based methodologies have been developed (Table 1.1) in order to tailor material surface in terms of composition, surface energy, morphology, and chemistry.

Table 1.1 Material approach: Some of the used methods and related references

Process	Methods	References
Etching	Chemical	[9, 15, 16, 86, 87]
	Physical	[30-32, 36, 88, 89]
Functionalization	Chemical	[9-12]
Oxidation	Physical:	
	• Plasma	[1, 21, 27-30, 32, 34-38, 40, 41, 65, 88, 90]
	• UV irradiation	[40-42, 56]
Hydrolysis	Chemical	[23-26]
	Enzymatic	[91]
Coatings	Layer by Layer (LbL)	[92, 93]
Grafting[47, 48]	Chemical	[49-53, 64, 94-104]
	Enzymatic	[105-107]
	Physical activation:	
	• Plasma	[31, 33, 34, 51, 64, 72, 108-110]
	• Irradiation (gamma, UV, laser)	[54-56, 86, 111-114]

According to the second, **biology-driven approach,** cell/biomaterial surface interactions are governed by the same biologically specific chemistry as cell/cell surface interactions. Following this approach, the material surface must be designed in a way to mimic the cell surface as close as possible (Table 1.2). Intensive exploration/exploitation of cell surface and its different components (e.g. proteins, phospholipids, enzymes, etc.) was the outcome from the development of this approach.

Nowadays, these two approaches have merged and combined methodologies using the best achievements from biology and material sciences are used for directing the interaction between tissue cells and biomaterials.

1.3 Wet chemistry in surface modification

Chronologically, this is the first surface modification approach used in order to improve surface properties of polymers. The wet chemical methods in the surface modification field can be compared with a cosmetic surgery (but not with a simple make up!!!) if the analogy material surface/human face is used. The ultimate goal of this approach is to create **stable, well-defined** functional substrates characterized by **controlled surface properties,** which are available for further chemistry.

Table 1.2 Some bio-approaches: methods and applications

Targeted Application	**Methods**	**References**
Cell adhesion	Protein immobilization	[53, 64, 115-117]
	Active peptide sequences conjugation	[69, 96, 98, 118-121]
Drug delivery	Self assembled structures (e.g. phospholipid cell membranes)	[83, 84, 122-125]
	Other chemical approaches	[126, 127]

The wet chemistry surface modification methods are based on the knowledge from general solution chemistry. Thus, for example starch-based blends have been surface oxidized by the well known oxidizing system acid-permanganate [9] or surface crosslinked using tri-sodium tri-meta phosphate solution [10]; chitosan can be surface sulfonated by SO_3 [11] or surface phosphonated by P_2O_5 [12] in different solvents. Although, the experience from the solution chemistry is indispensable, several specific “surface issues” must be considered:

Which are the functional groups available on the surface? Are they the same as the ones in the bulk?

Surface chemistry depends on the processing of the material. Therefore, prior any further modification, full surface characterization and knowledge of the processing “history” of the

material are required. When a solvent is involved in the preparation of the sample (e.g. solvent casting technique), the ability of the used solvent to form hydrogen bonds with the functional groups of the material, can show up or hide these functional groups. Usually polar, protic solvents result in more hydrophilic surfaces compared to aprotic ones. On the other hand, the mould's surface, which is in contact with the sample, has similar effect via hydrophobic/hydrophilic forces. A simple example is the contact angle of PCL membranes prepared by solvent casting using different solvents: $CHCl_3$ 85.08 (Petri dish contact surface)/93.3 (air contact surface); THF 105.8 (Petri dish contact surface)/101.7 (air contact surface) [13].

Where the reaction actually occurs? Are the wet chemistry methods surface modification methods?

The dynamics of the surface chemical composition in the wet surface chemistry methods complicates additionally the process. In this case, a solvent is also involved in the modification step. Once again, its interactions with the material to be modified can alter the surface chemistry. Moreover, if these interactions result in swelling, the modification will not confined to the surface and will go deeply into the bulk of the material.
All these issues must be considered in the choice of a system/method for surface modification of a certain material. The most common wet modification methods and some general trends in their application are described below. It must be noted that these methods are widely used in industry to treat large objects that would be difficult to treat by other commonly used techniques.

1.3.1 Wet chemical etching

Etching is a process of removal surface material, similar to the face lifting. It has a long history, starting in the beginning of the Middle Ages. The old masters such as Rembrandt and Goya used it as one of the main techniques to create their art works. However, the "art application" of this method is constricted only to metals as materials. The widely used nowadays micro- and nano-fabrication techniques [14] are based on the same principles. Natural-based polymers are much more sensitive and the strong acids, usually used for etching of metals or glasses, cannot be applied for them. Generally, weaker chemical etchants (e.g. diluted bases and acids [15], oxidizing agents [9, 16]) are used to convert smooth hydrophobic surfaces to rough hydrophilic surfaces usually by dissolution of amorphous

regions and surface oxidation and hydrolysis. The alternative plasma etching or so-called dry etching is preferable for surface modification and surface cleaning of biopolymers.

1.3.2 Oxidation by wet surface modification methods

Which is the role of the oxygen in the surface chemistry of the applied biomaterials? Do we want it there, on the surface, or not? Which is its optimal surface content?
Usually the surface oxidation alternates the proteins' adsorption and therefore cell behavior via:

(a) Modulation of the surface hydrophilicity; i.e. the physical bonds surface/proteins. Generally, the introduction of oxygen containing groups, such as hydroxyl (-OH), carbonyl (=C=O) or carboxyl (-COOH) groups, is related to an increase of the surface's hydrophilicity.
(b) Alternation of the surface charge. Negatively charged groups have shown [17-20] positive effect on cell adhesion and growth and this is attributed to the favourable protein conformation on these surfaces. The polarity of these groups allows formation of additional hydrogen bonds with the proteins, which will keep them fixed onto the surface.
(c) Creating active places, where a chemical bond between the proteins and surface functional groups can occur. However, this process is not always advantageous since denaturation of the proteins could also occur.

As mentioned before, the general knowledge from organic solution chemistry can be used and solutions with known oxidative properties can be adjusted (concentration) and applied. An example is the oxidation of starch-based biomaterials by the system nitric acid-potassium permanganate [9]. The functionalization of the surface resulted (Figure 1.1) in both higher number of cells attached to the surface and changes in their morphology. Integrins, through which the cells communicate with the surrounding environment, recognize the introduced changes and prove them by binding to the surface. As a result, it was possible to observe cells spreading and extending their filopodia in an oriented way after the oxidation.

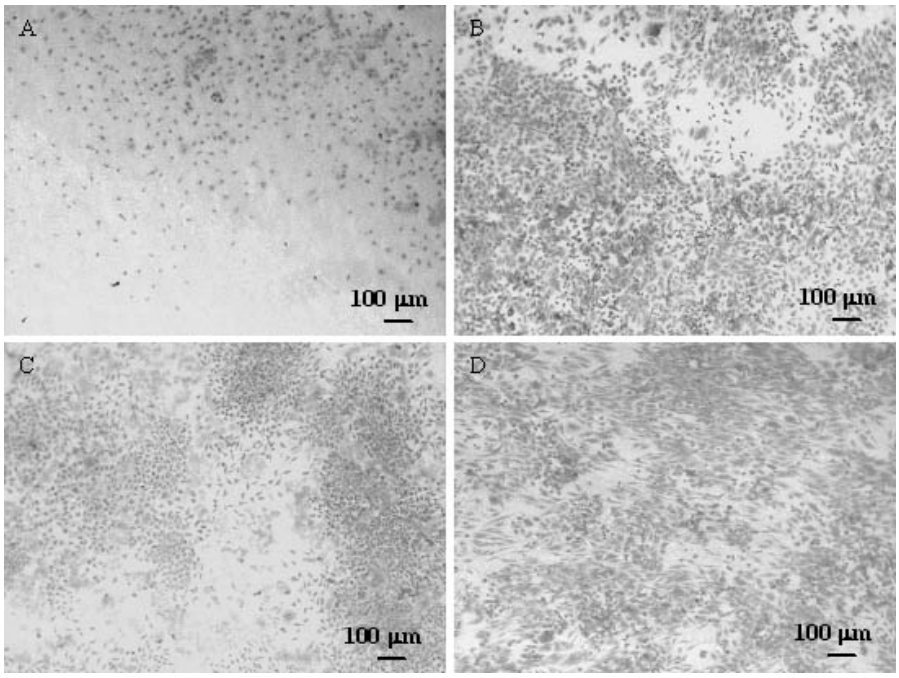

Figure 1.1 SaOs-2, cultured for 7 days on SPCL (A and B) and SEVA-C (C and D) before (A and C) and after (B and D) surface oxidation by potassium permanganate.

It should be noticed that there must be a compromise between functionalization and hydrophilicity. Proteins need some active places (in terms of charge and functionality) on the surface, where they can bind. On the other hand, the introduction of these active places is related with an increase of the hydrophilicity. Generally, proteins have hydrophobic nature and therefore repulsion but not adhesion can be observed when surface with very high hydrophilicity is produced. Actually, surface passivation with hydrophilic molecules is used for modification of devices in contact with blood. The passivated surface reduces or prevents the adhesion of thrombogenic cells and proteins onto the underlying substrate or material, thereby preventing surface-induced blood clotting. After studying a wide variety of substrate polymers, Tamada and Ikada found [21] that there is an optimal wettability for cell adhesion and that is approximately 70° water contact angle.

1.3.3 Hydrolysis

The ability of a material to be resorbed over time is an important property in many biomedical applications. Hydrolysis is the most common way through which the natural polymers degrade in the organism to normal metabolic compounds. All biomaterial surfaces are potentially susceptible to hydrolysis, simply due to the fact that they are

surrounded of warm aqueous environment (the body fluids), containing hydrolyzing agents (e.g. enzymes). Catabolism of starch by α-amylase (Figure 1.2.), which is available in the human blood and in the saliva [22], is one example for those processes.

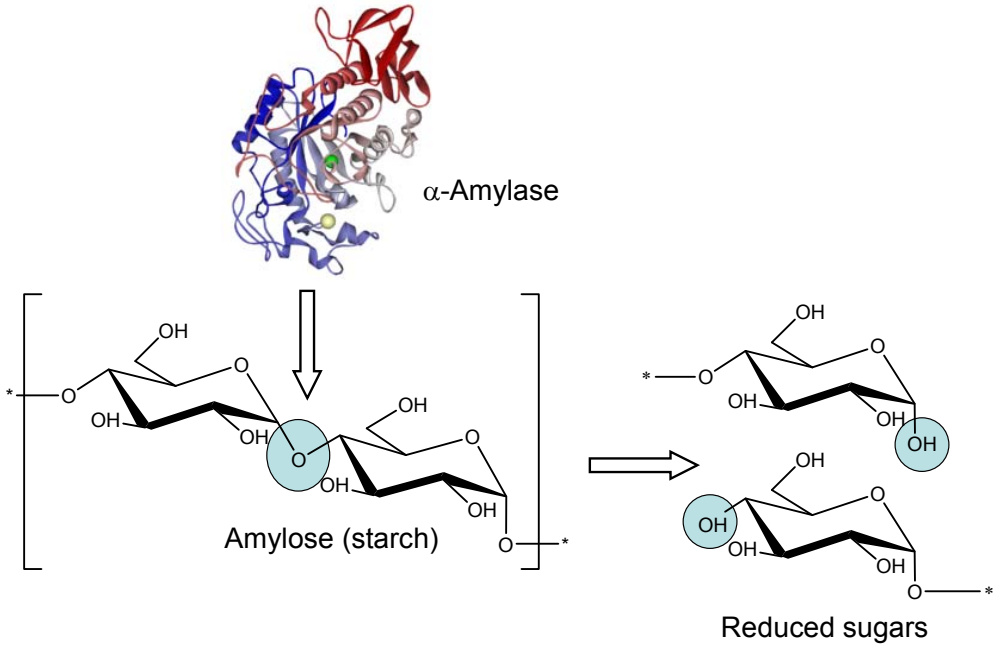

Figure 1.2 Enzymatic (α-amylase) hydrolysis of starch.

Natural polymers containing ester, amid or other carboxylic derivative groups undergo degradation by a simple hydrolytic mechanism (Figure 1.3). The reaction is base- or acid catalyzed and sensitive to temperature above 37°C. Chitosan, well known biomaterial for different applications, is produced from chitin (Figure 1.4) using this process.

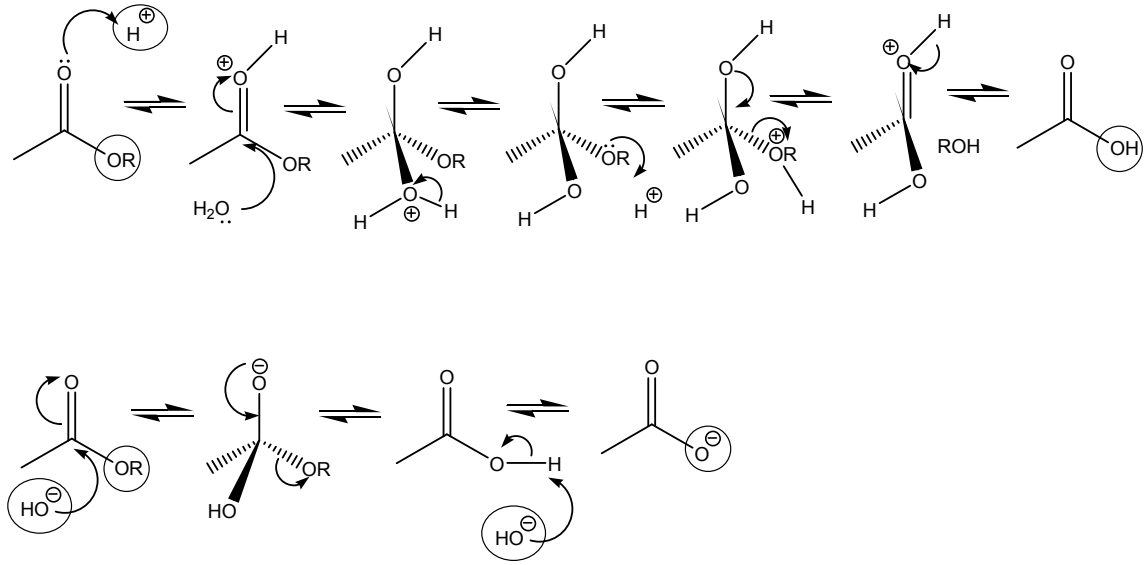

Figure 1.3 Hydrolysis of esters catalyzed by acid (up) or base (down)

On the other hand, the hydrolysis is a powerful surface modification method. More hydrophilic surfaces can be produced via the attack of a nucleophile agent [23-26]. Sodium and potassium hydroxides are the most used nucleophiles. The alternated surface functionality can be used in the further chemistry [24-26] including immobilization of biomolecules.

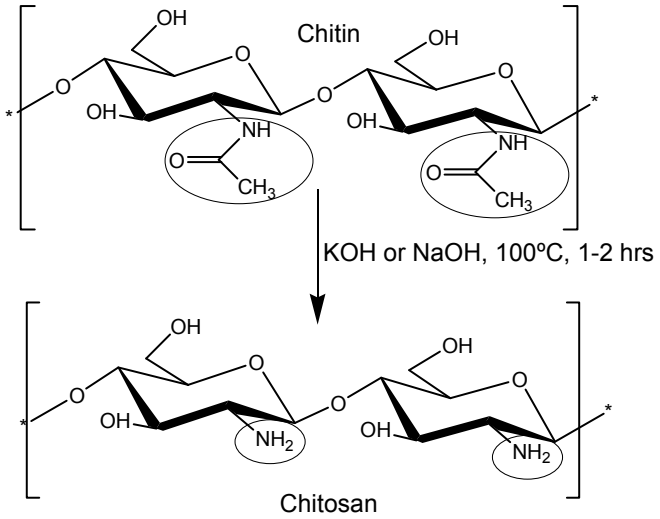

Figure 1.4 Hydrolytic process involved in the conversation of chitin into chitosan.

1.4 Physical methods for surface alternations

1.4.1 Plasma activation and modification

The plasma is considered as the forth state of the matter (Figure 1.5) [27]. It contains various (atomic, molecular, ionic and radical) energetic, reactive, positively and negatively charged species but as a whole, the plasma is neutral. The energy required to create and sustain plasma is supplied by an external electrical field. Different plasma sources can be used: gaseous (radio frequency glow discharge and corona discharge), metallic, and laser based. The plasma state exists only at a low pressure (less than $1\text{-}10^{-2}$ torr).
Several plasma techniques are widely used for surface modification of natural based polymers:

- Plasma sputtering and etching;
- Plasma functionalization;
- Plasma polymerization.

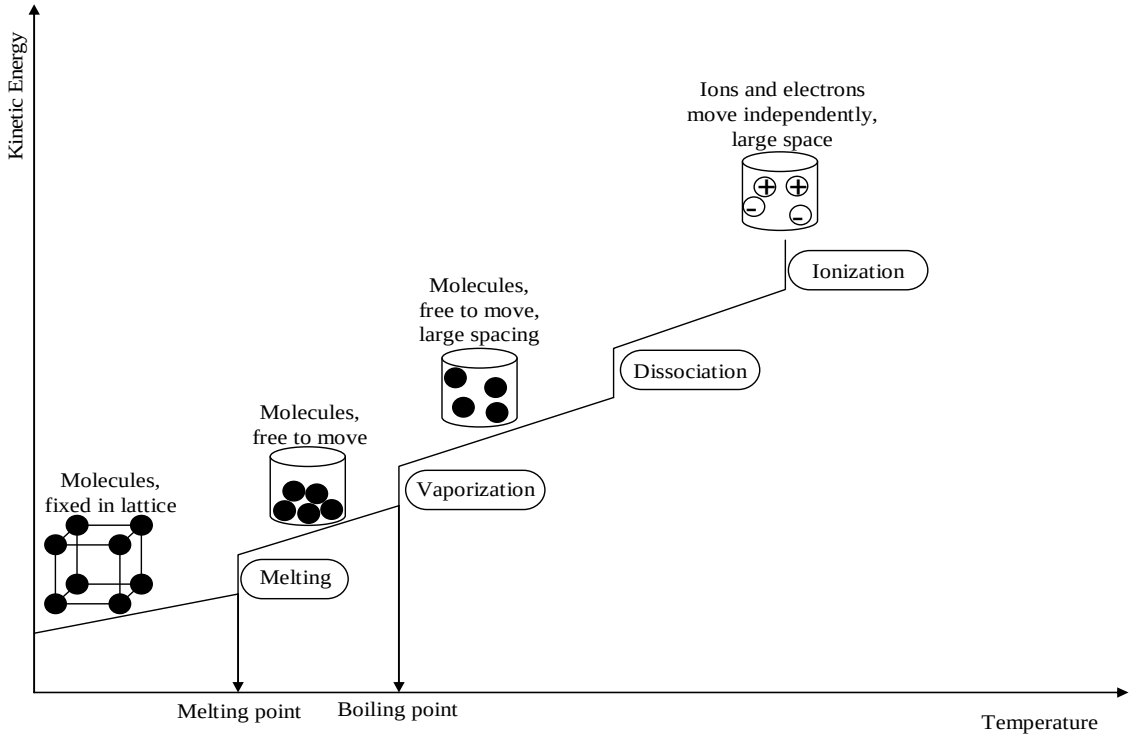

Figure 1.5 Transitional states of the matter.

All these plasma techniques have several advantages:

(a) All processes are restricted to the topmost (angstroms) layer and therefore the modified material has similar chemical and physical properties to the original one;

(b) Modification is fairly uniform over the whole surface even for samples with complex shapes;

(c) Surfaces of all kind of materials can be modified, regardless of their structures and chemical reactivity.

How does it work? When the plasma becomes in a contact with the biomaterial surface, the activated species are accelerated towards the substrate by the applied electric field. Since some parts of the surfaces are exposed to energies higher than the bonding energy of polymers, these parts undergo chain scission. Chain scission process will initiate different chemical and physical events [2, 28, 29]. Surface degradation can be observed with sufficient sputtering time and enough (different for different materials) high power applied. Figure 1.6 shows an example of how the conditions, used for the plasma treatment, can alternate the surface morphology of a material. A blend of starch and cellulose acetate (50/50 %wt) was treated at different powers and for different time. As can be seen from the scanning electron microscopy (SEM) micrographs, all modified samples presented much rougher surface compared to the original one.

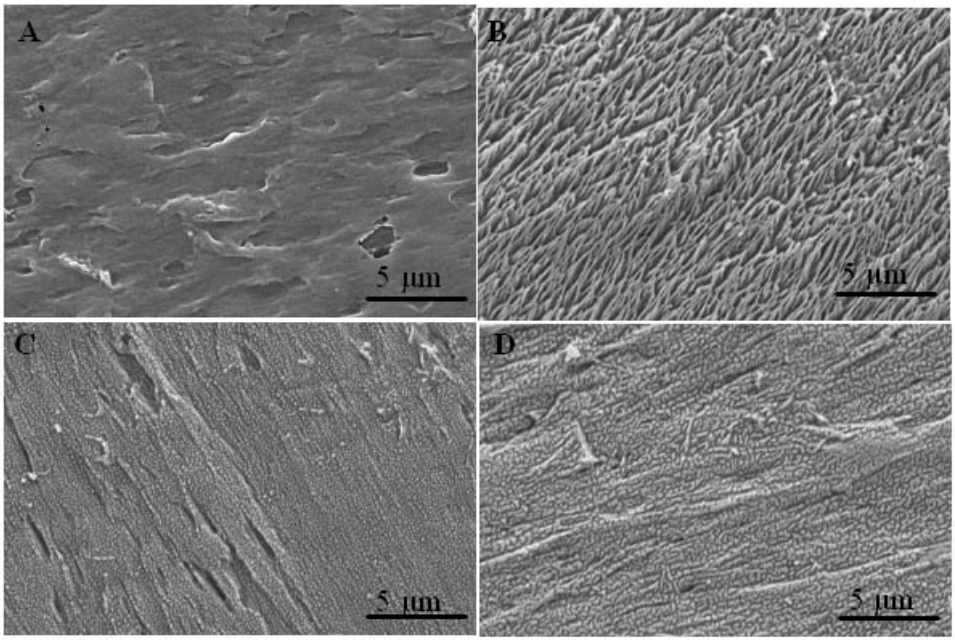

Figure 1.6 Effect of plasma working conditions on the surface morphology of starch/cellulose acetate (SCA) blend (50/50 wt): SEM micrographs of untreated SCA (A); and Ar plasma modified SCA at 80W, 15 min (B); at 30W,15 min (C) and at 80W for 5 min (D).

This effect depends on the used power, which determines the acceleration of the active species toward the material surface, as well as on the time during which the material is exposed to this bombarding with active species [30]. Plasma etching can be used either for cleaning off the surface of the material or as a surface morphology modification technique. Engineering of new composites with improved adhesion between the components [31] and surfaces with better biocompatibility [30, 32] are only two examples of the enormous benefits, which surfaces with tailored roughness/surface area, can bring to the material sciences arena.

On the other hand, the chain scission results in the formation of highly reactive radicals on the surface. Those radicals can be used either in a subsequent plasma depositions/polymerization processes [33, 34] or they can recombine (e.g. crosslinking reactions) with the other active species available in the reactor. Additionally to the power and the expose time, the working atmosphere is of main importance for these processes. Gases as CH_4 [35] or CF_4 [30, 36, 37] are usually used to decrease the wettability of the surface. Contrary, the use of oxygen (–OH, –C=O, –COOH groups introducing) or nitrogen (–NO_2, –NH_2, –$CONH_2$ groups) plasma is one of the most powerful methods for increasing of material hydrophilicity which usually results in improved adhesion strength, biocompatibility, and other pertinent properties [29, 38]. Chitosan, modified by oxygen [34] or nitrogen [32] plasma displayed higher number of cells attached on the surface (Figure 1.7)

and higher proliferation rate compared to the untreated chitosan membranes, for which next to no cell adhesion was observed.

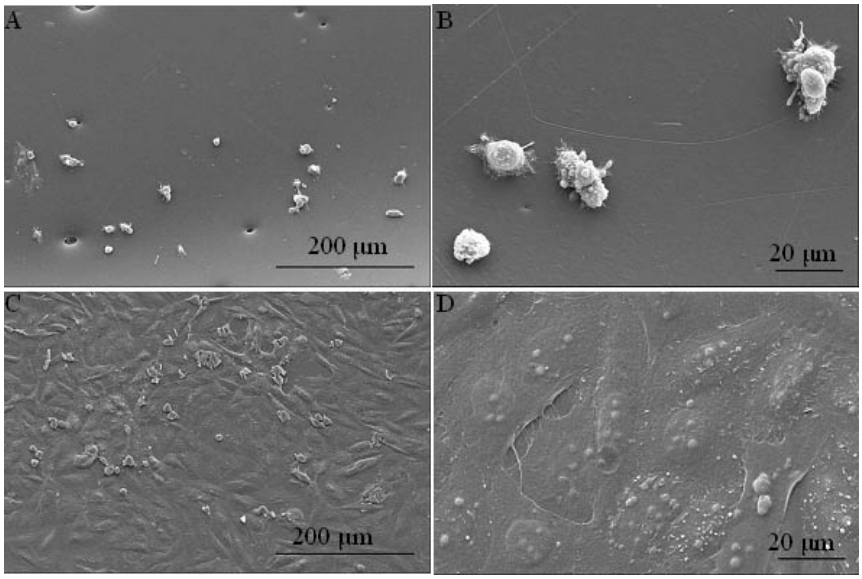

Figure 1.7 SEM micrographs showing the effect of oxygen plasma modification (30W, 15 min) on SaOs-2 adhesion (3 days of culture): untreated chitosan membrane (A and B) and modified one (C and D).

All these processes can be applied for three dimensional (3D) samples only if the holes/trenches are wider than the mean free path of the electrons and the Debye length [39]. Only in this case the discharge, which generates the active species, will be sustained. Highly porous and interconnected starch based (starch/polycaprolactone 30/70 wt%) scaffolds were modified by oxygen plasma. Dramatic improvement of human umbilical vein cells (HUVEC) adhesion on the modified samples can be seen on Figure 1.8.

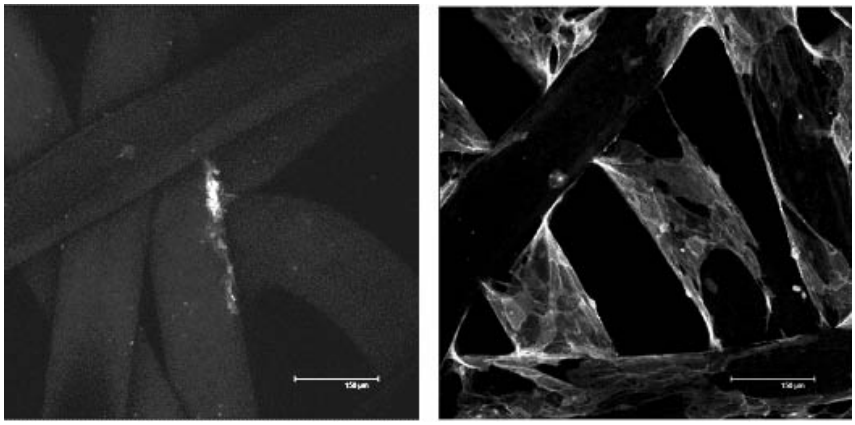

Figure 1.8 Immunostaining (PECAM, Phaloiedin and nuclei) of HUVEC cultured for 7 days on SPCL untreated (left) fibers mesh and SPCL fibers mesh modified by oxygen plasma (right).

1.4.2 UV-irradiation

The UV irradiation resembles getting the tan under the sun and the same rules are followed: time and intensity of the irradiation are important factors and "sunburn" could be caused if they are not in the limits. Similarly to the plasma treatment, the UV irradiation can result in chemical (photo-crosslinking, photo-oxidation in air, or photochemical reactions in reactive atmosphere) or physical (surface morphology, etc.) changes [38, 40-42]. These photochemical reactions can be surface-limited or can take place deep inside the bulk (different from plasma!) depending on the UV absorption coefficient at the specific UV-wavelength (Lambert-Beer's law). There are two groups of sources: continuous wave (CW) UV-lamps with a moderate light or pulsed laser. The laser sources cause mainly surface etching. They can be used to modify very small surface area and this is the reason for their wide application in micro- and nano-fabrication technologies. The CW UV-lamps are used for surface oxidation [41, 42]. Starch-based biomaterials have been modified by CW UV-lamp. As it was expected, no significant effect on surface morphology was observed. The irradiation resulted in surface oxidation and higher number of cells adhered to the surface (Figure 1.9).

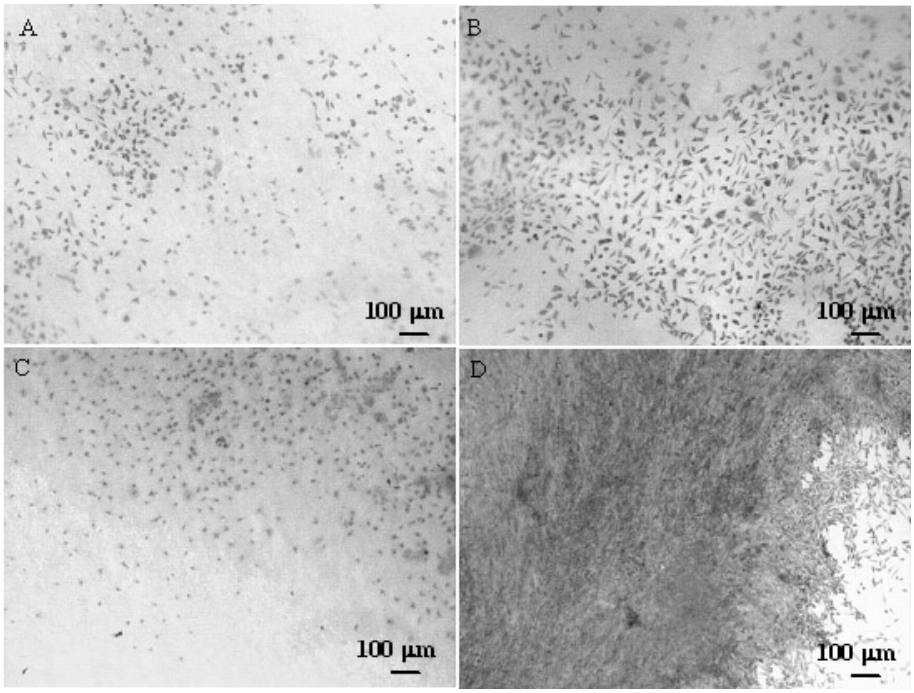

Figure 1.9 Optical micrographs of osteoblast-like cells stained with methylene blue and cultured on untreated (A, C) and UV-irradiated (B, D) SCA (up) and SPCL (down) for 7 days.

1.4.3 β- and γ-irradiation

The perfect sterilization procedure for natural based biomaterials is the one, which does not include any changes in the chemistry, the mechanical properties and the degradation behavior. In other words, the final make-up of a biomaterial should not destroy all the work done before. Radiation with γ- or β-rays is often used to sterilize extracorporeal and intracorporeal medical devices made from polymers. High-energy radiation in addition to killing bacterial life, may also affect material properties. The surface is not an exception - surface chemistry and surface energy could be inadvertently altered by cleaning and sterilization procedures [43]. Sometimes, the sterilization process can be used as a surface modification technique. For example, it was found [44] that sterilization of membranes from chitosan-soybean protein isolate by β-irradiation increases the surface energy but does not affect the bulk properties of the material. Unfortunately, not always the synergy modification/sterilization works out. Studies [45, 46] on the effect of gamma irradiation on collagen structure clearly indicate chain scission resulting in a fraction of lower molecular weight material. Material degradation leads to a loss of mechanical properties as well as to change in the surface roughness. Additionally, crosslinking could occur. Crosslinking reactions affect initial tensile strength (increase), surface hydrophilicity (decrease) and the properties related to these. In general, aromatic polymers are more resistant to high-energy radiation than aliphatic ones, while the presence of impurities and additives may enhance degradation and/or crosslinking.

1.5 Grafting

The main advantage of surface grafting is the long-term stability of the introduced chains onto the material surface. In contrast to physically coated polymer chains, in this method the chains are attached to the surface by covalent bonding which avoids their delamination [2, 47]. Many different synthetic routes can be employed to introduce graft chains onto the surface of polymeric substrates but generally, the grafting methods can be divided into two groups [48]. **Grafting-from** methods utilize active species created on the polymer surfaces to initiate the polymerization of monomers (usually acrylic or vinyl) from the surface toward the bulk phase. In the case of **grafting-to** methods, the reactive species are carried by the preformed polymer chains, which are going to be covalently coupled to the surface. The fundamental step in grafting is the creation of reactive groups on the substrate surface. This could be done either chemically [49-53] or more often by

irradiation [54-56]. Great majority of grafting processes involves a radical mechanism of polymerization of vinyl monomers.

Plasma processes can be also used [31, 33-35, 37, 51] for surface functionalization via grafting. In this process, created on the surface radicals interact with monomers which can be introduced in the plasma reactor either as vapor or by pre-adsorption [33] of the material surface. Alternatively, the surface can be pre-activated by plasma with subsequent immersing in the monomer solution. Some examples of the use of plasma treatment as a pre-activation technique are shown on Figures 1.10 and 1.11. Higher number of osteoblasts like cells, adhered to the surface of SPCL (starch/poly (ε-caprolactone 30/70) after acrylic acid grafting, was observed. However, the cell did not show (Figure 1.10) the typical osteoblasts morphology. When chitosan was modified in a similar fashion, cells were much more spread, with extended filopodias (Figure 1.11).

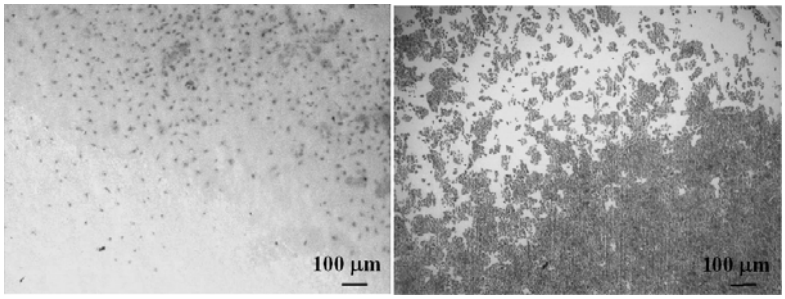

Figure 1.10 SPCL untreated (left) and surface modified by acrylic acid grafting (Ar plasma activation, right): effect of the treatment on cell (SaOs-2) adhesion after 7 days of culture – methylene blue staining.

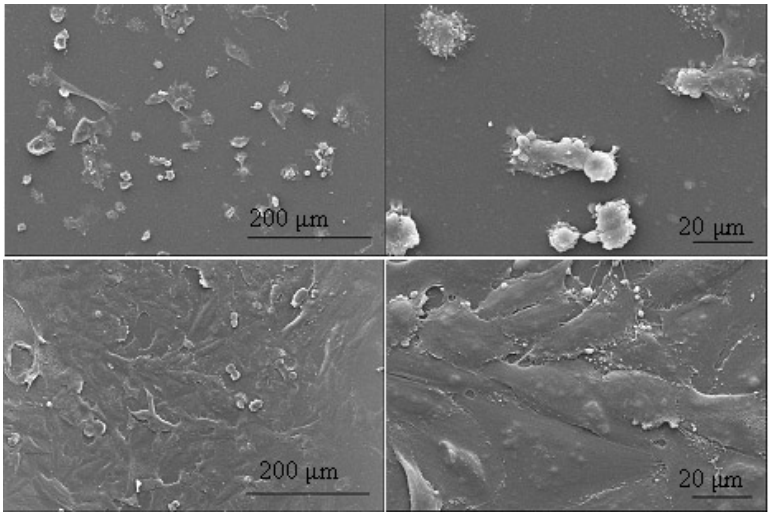

Figure 1.11 SEM micrographs of SaOs-2 cultured for 7 days on untreated chitosan membranes (up) and membranes grafted with vinyl sulfonic acid after oxygen plasma activation (down).

1.6 Bio-approaches: Mimicking the cell-cell interactions

As mentioned before, cells interact with a foreign device primary trough proteins adsorbed onto the surface. Parts 3 to 5 of this chapter described some methods for tailoring the protein adsorption and consequently the cell behaviour trough modification/functionalization of the material surface. However, the described methods are quite general, i.e. they are not selective for a certain protein or cell type. On the other hand, the body fluids are rich in highly competitive protein molecules and very often, the ones, which are not desired, are "faster" and cover the available space onto the surface. How to overcome this problem and to engineer a selective surface? One of the approaches is to pre-immobilize an instructive component on the surface, which will further direct the cell behavior. Carefully selected proteins, as a part of the communication system of the cell, can be used as an interpreter, which to translate the desired information surface-cell. On the other hand, phospholipids are the main building part of different bio-membranes. Therefore, they can be useful in a strategy, aiming to dupe the cell. Several methodologies for mimicking these two cell's components are described bellow.

1.6.1 Protein immobilization

Several different methodologies have been used in order to immobilize different proteins on the material surface. Coating with proteins can be achieved by a simple **physical adsorption**. Protein physical adsorption will occur when the change in Gibbs free energy of the system decreases during the adsorption process. Generally, proteins adhere to hydrophobic surfaces [57], because of their hydrophobic nature, and are repelled by hydrophilic surfaces. A comparative study between starch-based materials showed [58] that the most hydrophilic blend (starch/cellulose acetate, 50/50 wt%, SCA) adsorbs less protein than the blend with the biggest water contact angle (starch-poly(ethylenevinyl alcohol, 50/50%, SEVA-C) in unitary (fibronectin or vitronectin) or complex proteins solution system. However, most of the natural available materials are reach in polar groups (-OH, $-NH_2$, -COOH, $-SO_3H$, etc.) and therefore relatively hydrophilic. How then proteins can be irreversible deposited on the natural materials' surface? Fortunately, more of the natural polymers bear charges, which can be used in physical protein adsorption. Chitosan is an example for polycation and hyaluronic acid can illustrate what is the polyanion (Figure 1.12).

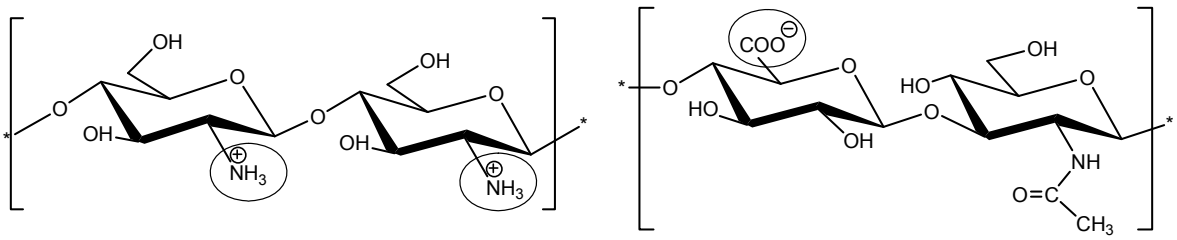

Figure 1.12 Two examples of natural polyions: chitosan (left) which is polycation at low pH and the polyanion hyaluronan (right).

Electrostatic interactions between charged peptide residues presented by a protein's surface and surface functional groups greatly contribute to the Gibbs free energy of protein adsorption [59]. The **layer-by-layer technique** (LbL) [60-62] is based on these interactions and follows quite simple procedure (Figure 1.13). Recently, it was reported[63] that both number of the deposited layers and the charge of the last layer influence the adsorption of fibronectin. Furthermore, modulation of HUVEC attachment on the natural polymers, modified by fibronectin adsorption by meaning of LbL technique, was achieved. When the surface does not bear a charge, pre-activation or pre-modification, using one of the described already techniques, and subsequent protein immobilization can be a solution. There are several examples when this step-treatment was very successful. Laminin was incorporated [64] onto chitosan, pre-activated by plasma or wet chemistry methods. Although significant increase of cell attachment was observed for both cases, plasma treatment was indicated as a better methodology for the protein grafting on chitosan membranes. Similar effect was reported [65] for starch-based biomaterials, pre-activated by plasma and subsequently immersed in different protein solution.

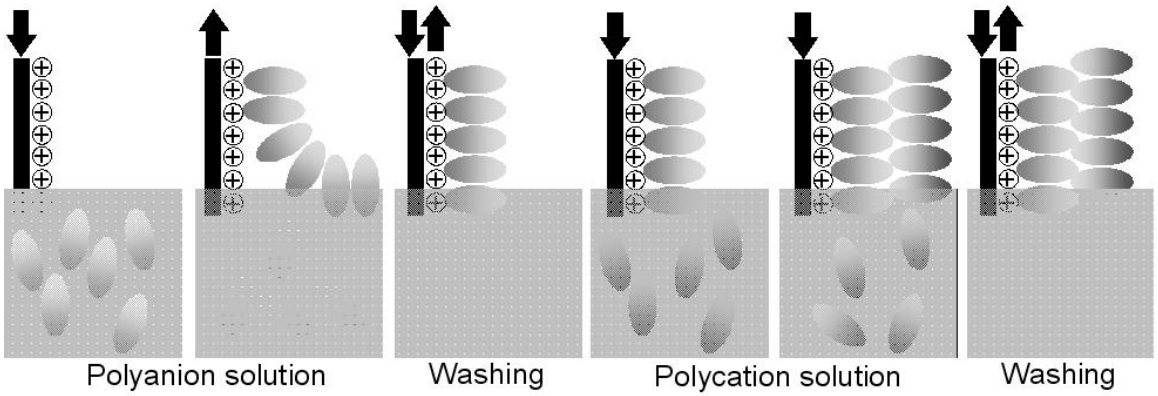

Figure 1.13 Schematic representation of layer by layer (LbL) deposition technique depicting film deposition starting with a positively charged substrate.

The use of whole proteins carries some disadvantages for the application in the medical field. Proteins must be isolated from other organism and purified. Consequently, they may elicit undesirable immune responses and increase infection risks. Normally they are expensive and often no available in a clinically acceptable form. Due their stochastic orientation on the surface, not all the proteins have the appropriate orientation for cell adhesion [66]. The incorporation of short oligopeptides having specific binding domains can overcome most of the indicated problems. The advantages of using small peptides rather than whole proteins are that they are relatively inexpensive to synthesize and easy to purify. Additionally, they exhibit higher stability to sterilization processes, heat treatment and pH variation, storage and conformation shifting and they can be characterized easily [67]. Furthermore, when they are covalently bonded to the surface, they are more stable to cellular proteolysis than adsorbed cell adhesion proteins, since protein desorption is eliminated and the active groups are not exposed to soluble proteases.

In 1984, Pierschbacher and Ruoslahti published a pioneer work [68], in which Arg-Gly-Asp (RGD) was identified as the first adhesive recognition sequence in fibronectin. Subsequently, the same motif was identified in other cell-adhesion proteins such as vitronectin, collagen or laminin [69]. Nowadays, there are several short oligopeptides' sequences used [69-71] to mediate cell-specific adhesion and function (Table 1.3).

As in the grafting process several different methodologies can be used in order to create a chemical bond between the oligopeptides and the surface of the material. Photografting of GRGD onto chitosan was reported [72] to improve the adhesion and proliferation of endothelial cells on the modified surfaces. On the other hand, chemical methods can be also used.also used. Carbodiimide chemistry is very often used [73, 74] strategy for protein conjugation.This strategy has several advantages. Either membranes or samples with complex geometry can be coated. Moreover, the reaction can be performed in aqueous or organic media by using different carbodiimides. Therefore, the solubility should not be an obstacle for the process. Taking the advantage of the highly reactive chitosan amine group, GRGD was grafted[74] on 3D chitosan structures. The peptide density on the surface was measured to be around 10^{-12} mol/cm^2, promoting cell adhesion and proliferation as well as enhancing the formation of mineralized foci. Nevertheless, this reaction has a disadvantage. Two different acid moieties (end group on Ser and the carboxyl acid of Asp) in the RGD are present. This presence imposes additional step - protection of the acid group on Asp, without which the control of the reaction is difficult. There is an alternative strategy, which uses succinic anhydride [73] to generate carboxyl groups (but not amine) on the chitosan surface. The created carboxyl groups can further react with the free amine group of the peptide forming the necessary spacing between the surface and the peptide [67]. The same strategy was applied [75] for alginate hydrogels, which bring the carboxyl

groups in their native structure and no additional transformation before the conjugation is needed.

Table 1.3 Some of the identified active sequences from different proteins and the receptors, which recognized them

Protein	Recognition sequence	Receptor
Fibronectin	Gly-Arg-Gly-Asp-Se (RGD)	$\alpha_5\beta_1$, $\alpha_{IIb}\beta_3$, $\alpha_v\beta_3$, $\alpha_3\beta_1$, $\alpha_v\beta_1$
	Leu-Asp-Val	$\alpha_4\beta_1$
	Arg-Glu-Asp-Va (REDV)	$\alpha_4\beta_1$
Laminin	Tyr-Ile-Gly-Ser-Arg (YIGSR)	67-kDa binding protein
	Pro-Asp-Ser-Gly-Arg (PDSGR)	?
	Arg-Tyr-Val-Val-Leu-Pro (RYVVLPR)	?
	Leu-Gly-Thr-Ile-Pro-Gly (LGTIPG)	67-kDa binding protein
	Arg-Gly-Asp (RGD)	?
	Ile-Lys-Val-Ala-Val (IKVAV)	110- kDa
Vitronectin	Arg-Gly-Asp (RGD)	$\alpha_v\beta_3$, $\alpha_v\beta_5$, $\alpha_{IIb}\beta_3$
Fibrinogen	Arg-Gly-Asp (RGD)	$\alpha_v\beta_3$, $\alpha_{IIb}\beta_3$
von Willebrand factor	Arg-Gly-Asp (RGD)	$\alpha_{IIb}\beta$
Entactin	Arg-Gly-Asp (RGD)	?
Collagen type I	Arg-Gly-Asp (RGD)	30, 70, and 250 kDa
	Asp-Gly-Glu-Ala (DGEA)	$\alpha_2\beta_1$

Besides the surface functionality, which determines the binding oligopeptide-surface, the surface concentration and distribution of the immobilized active sequence are other issues, which need attention. The minimal RGD surface concentration necessary for maximal cell spreading is 1fmol/cm [276]. The formation of focal contacts and stress fiber was observed at 10fmol/cm^2. These values were calculated for RGD peptide immobilized on a poorly adhesive glass substrate. On the other hand, Jin Li, *et al* confirmed [73] the dependency on the concentration of the peptide, immobilized on chitosan membranes surfaces. Higher peptide concentration enhances process as cell attachment, proliferation, migration and mineralization.

Finally, there are also some disadvantages of using short protein sequences. Lost of both affinity and specificity of the sequence, when taken out of the context of the protein, are some of them. For example, the hexapeptide Gly-Arg-Gly-Asp-Ser-Pro (GRGDSP), which is the active sequence from fibronectin, is 1000 times less effective.

1.6.2 Lipid coatings

Lipids are not always useless burden! Contrary, in the biomedical field they are even covetable. There are several reasons for this:

(a) Fact that the lipid bilayers are the major building blocks of biological membranes;
(b) Their hemo-compatible and non-thrombogenetic properties;
(c) The ability of phospholipids to self-organize into specific supramolecular aggregates.

A simple approach for generating membrane-mimetic surfaces is to create supported lipid mono- or bilayers at the surface of bulk materials [77]. Different methodologies (Table 1.2) as self-assembling monolayers (SAMs), Langmuir-Blodgett technique or covalent binding can be applied. Similarly to the proteins, SAMs are used [57, 59, 77, 78] as models since they are well defined and organized structures. Langmuir-Blodgett technique (LB) is the main technique, used for the formation of lipids mono- or multilayers on natural-based polymers [79-82]. The principle of the LB is illustrated on Figure 1.14 Phospholipid bilayer formation on chitosan and agarose has been performed [79] using LB. It was found that the bilayer lipid membranes, cushioned by thin chitosan films, are more stable than the agarose-cushioned membranes. Charge, which the chitosan poses, is most probably the reason for this stabilization. Molecular weight of the used polymer is another factor to be considered [83].

Lipid coated vesicles but not membranes are also object of great scientific interest [77, 84] because of their application as release systems. The cell membrane, which is built by phospholipids among other bioactive components, can not “recognize” the lipid vesicles and allow them to penetrate inside the cell and to deliver the target component which is previously loaded in the core of the vesicle. Phospholipid coating on plasmid DNA adsorbed starch-chitosan nanoparticles has been investigated [84] in order to create a barrier between DNAse sensitive genetic material and body fluids. Such a system posses both surface properties of a liposome and drug loading effectiveness of polymeric nanoparticles. Another example is so-called synthetic biomimetic supra molecular Biovector^{TM} (SMBV^{TM}) [85], which has been proven in preclinical and clinical evaluation to be a suitable candidates for the delivery of nasal vaccines. In general, the SMBV^{TM} is a

virus like particle made of an inner core of polysaccharide hydrogel. It can be further surrounded by a lipid bilayer formed by ionic/hydrophobic interactions. Due to their bi-compartmental structure SMBV^{TM} can be loaded with various active substances. All these studies show that fundamental biological processes can be successfully mimicked with the help of the lipid coated natural materials.

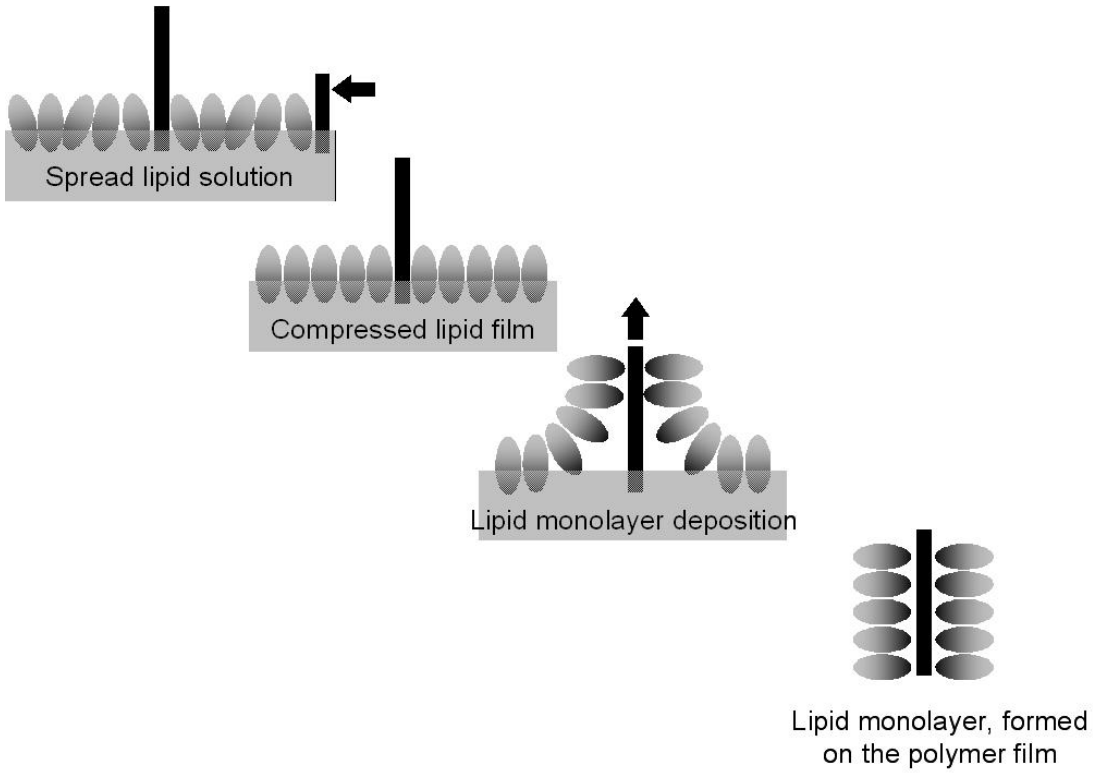

Figure 1.14 Illustration of the Langmuir-Blodgett technique.

1.7 Future directions

Using the advances in the material sciences, biology and nanotechnology, we have learnt much from the Nature. These lessons imposed a shift toward third generation [5], resorbable nanostructured surfaces, enriched with specific biosignals, that once implanted will help the body healing itself. Nevertheless, we are still a long way from recreating the complexity and dynamics of the natural three-dimensional environment of cells, their ECM. It is likely that cells require the full context of this 3D nano-fibrous matrix to maintain their phenotypic shape and establish natural behaviour patterns. Achieving effective temporal control over the signals that are presented to cell in 3D artificial matrices is still a key challenge in optimization the outside-in signaling.

1.8 References

1. Chu, P.K.; Chen, J.Y.; Wang, L.P.; Huang, N. Plasma surface modification of biomaterials*. Material science and engeenering*, 2002, **R36**, 143-206.

2. Pashkuleva, I.; Reis, R., *Surface activation and modification - a way for improveing the biocompatibility of degradable biomaterials*, in *Biodegradable Systems in Medical Functions: Design, Processing, Testing and Application*, R. Reis and J.S. Roman, Editors. 2004, CRC press: Boca Ranton, USA. 429-454.

3. Hench, L.L. Biomaterials*. Science*, 1980, **208**, 826-831.

4. Hench, L.L.; Wilson, J. Surface active biomaterials*. Science*, 1984, **226**, 630-636.

5. Hench, L.L.; Polak, J.M. Third-Generation Biomedical Materials*. Science*, 2002, **295**, 1016-1017.

6. Dee, K.C.; Puleo, D.A.; Bizios, R. *An introduction to tissue-biomaterial interactions*. 2002, Hoboken, New Jersey: John Wiley & Sons, Inc.

7. Bearinger, J.P.; Castner, D.G.; Healy, K.E. Biomolecular modification of p(AAm-co-EG/AA) IPNs supports osteoblast adhesion and phenotypic expression*. J Biomat Sci - Polymer edition*, 1998, **9,** (7), 629-652.

8. Schamberger, P.C.; Gardella, J.A., Jr. Surface chemical modification of materials which influence animal cell adhesion*. Colloids and surfaces B: Biointerfaces*, 1994, **2**, 209-223.

9. Pashkuleva, I.; Marques, A.P.; Vaz, F.; Reis, R.L. Surface modification of starch based blends using potassium permanganate-nitric acid system and its effect on the adhesion and proliferation of osteoblast-like cells*. Journal of Materials Science-Materials In Medicine*, 2005, **16**, 81-92.

10. Demirgoz, D.; Elvira, C.; Mano, J.; Cunha, A.; Piskin, E.; Reis, R. Chemical modification of starch based biodegradable polymeric blends: effects on water uptake, degradation behavior and mechanical properties*. Polymer degradation and stability*, 2000, **70**, 161-170.

11. Lin, C.-W.; Lin, J.-C. Surface characterization and platelet compatibility evaluation of surface-sulfonated chitosan membrane*. Journal of Biomaterials Science, Polymer Edition*, 2001, **12,** (5), 543-557.

12. Amaral, I.F.; Granja, P.L.; Melo, L.V.; Saramago, B.; Barbosa, M.A. Functionalization of chitosan membranes through phosphorylation: Atomic force microscopy, wettability, and cytotoxicity studies*. Journal of Applied Polymer Science*, 2006, **102,** (1), 276-284.

13. Tang, Z.G.; Black, R.A.; Curran, J.M.; Hunt, J.A.; Rhodes, N.P.; Williams, D.F. Surface properties and biocompatibility of solvent-cast poly[epsilon-caprolactone] films*. Biomaterials*, 2004, **25,** (19), 4741–4748.

14. Folch, A.; Toner, M. Microengineering of cellular interactions. *Annual Review of Biomedical Engineering*, 2000, **2**, 227-256.

15. Leonor, I.B.; Reis, R. An innovative auto-catalytic deposition route to produce calcium-phosphate coatings on polymeric biomaterials. *Journal of Materials Science-Materials In Medicine*, 2003, **14**, 435-441.

16. Dong, Y.; Yuan, Q.; Wu, Y.; Wang, M. Fine structure in cholesteric fingerprint texture observed by scanning electron microscopy. *Polymer Bulletin*, 2000, **44**, 85-91.

17. Lee, M.H.; Ducheyne, P.; Lynch, L.; Boettiger, D.; Composto, R.J. Effect of biomaterial surface properties on fibronectin–a5b1 integrin interaction and cellular attachment. *Biomaterials*, 2006, **27**, 1907-1916.

18. Keselowsky, B.G.; Collard, D.M.; Garcia, A.J. Surface chemistry modulates fibronectin conformation and directs integrin binding and specificity to control cell adhesion. *Journal of Biomedical Materials Research Part A*, 2003, **66,** (2), 247-259.

19. Keselowsky, B.G.; Collard, D.M.; Garcia, A.J. Surface chemistry modulates focal adhesion composition and signaling through changes in integrin binding. *Biomaterials*, 2004, **25,** (28), 25 (28): 5947-5954.

20. Faucheux, N.; Tzoneva, R.; Nagel, M.-D.; Groth, T. The dependence of fibrillar adhesions in human fibroblasts on substratum chemistry. *Biomaterials*, 2006, **27**, 234-245.

21. Tamada, Y.; Ikada, Y. Cell adhesion on plasma treated polymer surfaces. *Polymer*, 1993, **34**, 2208-2212.

22. Lorentz, K. Properties of human alpha-amylases from urine, pancreas, and saliva. *Enzyme*, 1982, **28**, 233-241.

23. Lim, D., *Treatment of cellulose acetate butyrate contact lenses* U. Patents, Editor. 1984, Barnes-Hind/Hydrocurve, Inc.: US, California.

24. Lim, D.; Morris, P.C., *Surface modification of hydrophilic contact lenses*, U. Patent, Editor. 1986, Barnes-Hind, Inc.: US, California.

25. Bledzki, A.K.; Reihmane, S.; J. Gassan, J. Properties and modification methods for vegetable fibers for natural fiber composites. *Journal of Applied Polymer Science*, **59,** (8), 1329-1336.

26. Rahman, M.M.; Mallik, A.K.; Khan, M.A. Influences of various surface pretreatments on the mechanical and degradable properties of photografted oil palm fibers. *Journal of Applied Polymer Science*, 2007, **105**, 3077–3086.

27. Poncin-Epaillard, F.; Legeay, G. Surface engineering of biomaterials with plasma techniques. *Journal of Biomaterials Science, Polymer Edition*, 2003, **14,** (10), 1005.

28. Inagaki, N. *Plasma surface modification and plasma polymerization*. 1996, Basel, Switzerland: Technomic Publishing AG.

29. Oehr, C. Plasma surface modification of polymers for biomedical use*. NIM B*, 2003, **208**, 40-47.

30. Riekerink, M.B.; Engbers, G.H.; Wessling, M.; Feijen, J. Tailoring the properties of asymmetric cellulose acetate membranes by gas plasma etching*. Journal of Colloid and Interface Science*, 2002, **245**, 338-348.

31. Morales, J.; Olayo, M.G.; Cruz, G.J.; Herrera-Franco, P.; Olayo, R. Plasma modification of cellulose fibers for composite materials*. Journal of Applied Polymer Science*, 2006, **101,** (6), 3821-3828.

32. Silva, S.; Luna, S.; Gomes, M.; Benesh, J.; Pashkuleva, I.; Mano, J.; Reis, R. Plasma surface modification of chitosan membranes and its effect on cell adhesion and proliferation*. Macromolecular Bioscience*, 2008, .**8,** (6), 568-576.

33. Li, Y.; Liu, L.; Fang, Y. Plasma-induced grafting of hydroxyethyl methacrylate (HEMA) onto chitosan membranes by a swelling method*. Polymer International*, 2003, **52,** (2), 285-290.

34. López, P.M.; Marques, A.P.; Pashkuleva, I.; Reis, R. Plasma surface modification of chitosan membranes using different monomers aiming to improve the adhesion of Osteoblast-like cells*. On-line Journal of E-MRS Fall Meeting*, 2006, **Symposium J**.

35. Wang, H.; Fang, Y.-E.; Yan, Y. Surface modification of chitosan membranes by alkane vapor plasma*. Journal of Materials Chemistry*, 2001, **11**, 1374-1377.

36. Sahin, H.T. RF-CF4 plasma surface modification of paper: Chemical evaluation of two sidedness with XPS/ATR-FTIR*. Applied Surface Science*, 2007, **253,** (9), 4367-4373.

37. Poncin-Epaillard, F.; Legeay, G.; Brosse, J.-C. Plasma modification of cellulose derivatives as biomaterials*. Journal of Applied Polymer Science*, 2003, **44,** (9), 1513-1522.

38. Chan, C.M. *Polymer Surface modification and characterization*. 1994, Cincinnati: Hanser.

39. Hollander, A. Surface oxidation inside of macroscopic porous polymeric materials*. Surface & Coatings Technology*, 2005, **200**, 561-564.

40. Kaczmarek, H.; Kowalonek, J.; Szalla, A.; Sionkowska, A. Surface modification of thin polymeric films by air plasma or UV irradiation*. Surface Science*, 2002, **507-510**, 883-888.

41. Chan, C.M.; Ko, T.-M. Polymer surface modification by plasmas and photons*. Surface Science Reports*, 1996, **24**, 1-54.

42. Sionkowska, A.; Kaczmarek, H.; Wisniewski, M.; Skopinska, J.; Lazare, S.; Tokarev, V. The influence of UV irradiation on the surface of chitosan films*. Surface Science*, 2006, **600**, 3775–3779.

43. Ratner, B.D.; Hoffman, A.S.; Schoen, F.J.; Lemons, J.E. *Biomaterials science: An introduction to materials in medicine*. 1996, San Diego, California, USA: Academic press.

44. Silva, R.M.; Elvira, C.; Mano, J.; San Roman, J.; Reis, R. Influnce of beta-radiation sterilization in properties of new chitosan/soybean protein isolate membranes for guided bone regeneration. *Journal of Materials Science-Materials In Medicine*, 2004, **15**, 523-528.

45. Friess, W. Collagen - biomaterial for drug delivery. *European Journal of Pharmaceutics and Biopharmaceutics*, 1998, **45**, 113-136.

46. Noah, E.M.; Chen, J.; Jiao, X.; Heschel, I.; Pallua, N. Impact of sterilization on the porous design and cell behavior in collagen sponges prepared for tissue engineering. *Biomaterials*, 2003, **23**, 2855-2861.

47. Kato, K.; Uchida, E.; Kang, E.-T.; Uyama, Y.; Ikada, Y. Polymer surface with graft chains. *Progress in Polymer Science*, 2003, **28**, 209-259.

48. Bhattacharya, A.; Misra, B.N. Grafting: a versatile means to modify polymers - Techniques, factors and applications. *Progress in Polymer Science*, 2004, **29,** (8), 767-814.

49. Amornchai, W.; Hoven, V.P.; Tangpasuthadol, V. Surface modification of chitosan films-grafting ethylene glycol oligomer and its effect on protein adsorption. *Macromolecular Symposia*, 2004, **216**, 99-107.

50. Shantha, K.L.; Harding, D.R.K. Synthesis and characterization of chemically modified chitosan microspheres. *Carbohydrate Polymers*, 2002, **48**, 247-253.

51. Elvira, C.; Yi, F.; Azevedo, M.C.; Rebouta, L.; Cunha, A.; Roman, J.S.; Reis, R.L. Plasma and chemical indused graft polymerization on the surface of starch based biomaterials aimed at improving cell adhesion and proliferation. *Journal Of Materials Science-Materials In Medicine*, 2003, **14**, 187-194.

52. Sashiwa, H.; Aiba, S.-i. Chemically modified chitin and chitosan as biomaterials. *Progress in Polymer Science*, 2004, **29**, 887-908.

53. Subramanian, A.; Rau, A.V.; Kaligotla, H. Surface modification of chitosan for selective surface–protein interaction. *Carbohydrate Polymers*, 2006, **66**, 321-332.

54. Sawpan, M.A.; Khan, M.A.; Abedin, M.Z. Surface modification of jute yarn by photografting of low-glass transition temperature monomers. *Journal of Applied Polymer Science*, 2003, **87**, 993-1000.

55. Rajam, S.; Ho, C.C. Graft coupling of PEO to mixed cellulose esters microfiltration membranes by UV irradiation. *Journal of Membrane Science*, 2006, **281,** (1-2), 211-218.

56. Mao, C.; Qiu, Y.Z.; Sang, H.B.; Mei, H.; Zhu, A.P.; Shen, J.; Lin, S.C. Various approaches to modify biomaterial surfaces for improving hemocompatibility. *Advances in Colloid and Interface Science*, 2004, **110,** (1-2), 5-17.

57. Prime, K.L.; Whitesides, G.M. Self-Assembled Organic Monolayers: Model Systems for Studying Adsorption of Proteins at Surfaces. *Science*, 1991, **252**, 1164-1167.

58. Alves, C.M.; Reis, R.L.; Hunt, J.A. Preliminary study on human protein adsorption and leucocyte adhesion to starch-based biomaterials. *Journal of Material Science: Materials in Meicine.*, 2003, **14**, 157-165.

59. Basalyga, D.M.; Latour, R.A. Theoretical analysis of adsorption thermodynamics for charged peptide residues on SAM surfaces of varying functionality. *Journal of Biomedical Materials Research Part A*, 2003, **64,** (1), 120-130.

60. Decher, G. Fuzzy Nanoassemblies: Toward Layered Polymeric Multicomposites. *Science*, 1997, **277**, 1232-1237.

61. Tang, Z.; Wang, Y.; Podsiadlo, P.; Kotov, N.A. Biomedical Applications of Layer-by-Layer Assembly: From Biomimetics to Tissue Engineering. *Advanced Materials*, 2006, **18**, 3203-3224.

62. Groth, T.; Lendlein, A. Layer-by-Layer Deposition of Polyelectrolytes—A Versatile Tool for the In Vivo Repair of Blood Vessels. *Angewandte Chemie International Edition*, 2004, **43,** (8), 926-928.

63. Wittmer, C.R.; Phelps, J.A.; Saltzman, W.M.; Van Tassel, P.R. Fibronectin terminated multilayer films: Protein adsorption and cell attachment studies. *Biomaterials*, 2007, **28**, 851-860.

64. Huang, Y.-C.; Huang, C.-C.; Huang, Y.-Y.; Chen, K.-S. Surface modification and characterization of chitosan or PLGA membrane with laminin by chemical and oxygen plasma treatment for neural regeneration. *Journal of Biomedical Materials Research Part A*, 2007, **82**, 842-851.

65. Alves, C.M.; Yang, Y.; Carnes, D.L.; Ong, J.L.; Sylvia, V.L.; Dean, D.D.; Agrawal, C.M.; Reis, R.L. Modulating bone cells response onto starch-based biomaterials by surface plasma treatment and protein adsorption. *Biomaterials*, 2007, **28,** (2), 307-315.

66. Elbert, D.L.; Hubbell, J.A. Surface treatments of polymers for biocompatibility. *Annual Review of Materials Science*, 1996, **26**, 365-394.

67. Hersel, U.; Dahmen, C.; Kessler, H. RGD modified polymers: biomaterials for stimulated cell adhesion and beyond. *Biomaterials*, 2003, **24,** (24), 4385-4415.

68. Pierschbacher, M.D.; Ruoslahti, E. Cell Attachment Activity Of Fibronectin Can Be Duplicated By Small Synthetic Fragments Of The Molecule. *Nature*, 1984, **309,** (5963), 30-33.

69. Yamada, K.M. Adhesive Recognition Sequences. *Journal Of Biological Chemistry*, 1991, **266,** (20), 12809-12812.

70. Shin, H.; Jo, S.; Mikos, A.G. Biomimetic materials for tissue engineering. *Biomaterials*, 2003, **24,** (24), 4353-4364.

71. Hubbell, J.A. Biomaterials In Tissue Engineering. *Bio-Technology*, 1995, **13,** (6), 565-576.

72. Chung, T.W.; Lu, Y.F.; Wang, S.S.; Lin, Y.S.; Chu, S.H. Growth of human endothelial cells on photochemically grafted Gly-Arg-Gly-Asp (GRGD) chitosans. *Biomaterials*, 2002, **23,** (24), 4803-4809.

73. Li, J.; Yun, H.; Gong, Y.D.; Zhao, N.M.; Zhang, X.F. Investigation of MC3T3-E1 cell behavior on the surface of GRGDS-coupled chitosan. *Biomacromolecules*, 2006, **7,** (4), 1112-1123.

74. Ho, M.H.; Wang, D.M.; Hsieh, H.J.; Liu, H.C.; Hsien, T.Y.; Lai, J.Y.; Hou, L.T. Preparation and characterization of RGD-immobilized chitosan scaffolds. *Biomaterials*, 2005, **26,** (16), 3197-3206.

75. Rowley, J.A.; Madlambayan, G.; Mooney, D.J. Alginate hydrogels as synthetic extracellular matrix materials. *Biomaterials*, 1999, **20,** (1), 45-53.

76. Massia, S.P.; Hubbell, J.A. An Rgd Spacing Of 440nm Is Sufficient For Integrin Alpha-V-Beta-3-Mediated Fibroblast Spreading And 140nm For Focal Contact And Stress Fiber Formation. *Journal Of Cell Biology*, 1991, **114,** (5), 1089-1100.

77. Collier, J.H.; Messersmith, P.B. Phospholipid strategies in biomineralization and biomaterials research. *Annual Review of Materials Research*, 2001, **31**, 237-63.

78. Scotchford, C.A.; Gilmore, C.P.; Cooper, E.; Leggett, G.J.; Downes, S. Protein adsorption and human osteoblast-like cell attachment and growth on alkylthiol on gold self-assembled monolayers. *Journal of Biomedical Materials Research*, 2002, **59**, 84-99.

79. Baumgart, T.; Offenhausser, A. Polysaccharide-supported planar bilayer lipid model membranes. *Langmuir*, 2003, **19**, 1730-1737.

80. Thompson, M.; Krull, U.J.; Kallury, K.M., *Lipid membrane-based device*, U. Patent, Editor. 1989, Allied-Signal Inc.: USA.

81. Baumgart, T.; Offenhausser, A. Lateral Diffusion in Substrate-Supported Lipid Monolayers as a Function of Ambient Relative Humidity. *Biophysical Journal*, 2002, **83**, 1489–1500.

82. Ionov, R.; El-Abed, A.; Goldmann, M.; Perettia, P. Interactions of lipid monolayers with the natural biopolymer hyaluronic acid. *Biochimica et Biophysica Acta*, 2004, **1667**, 200-207.

83. Fang, N.; Chan, V.; Mao, H.-Q.; Leong, K.W. Interactions of phospholipid bilayer with chitosan: effect of molecular weight and pH. *Biomacromolecules*, 2001, **2**, 1161-1168.

84. Baran, E.T.; Reis, R., *Biomimetic approach to drug delivery and optimization of nanocarrier systems*, in *Nanocarrier technologies: Frontiers of nanotherapy*, M.R. Mozafari, Editor. 2006, Springer: Dordrecht. 75-86.

85. von Hoegen, P. Synthetic biomimetic supra molecular Biovector™ (SMBV™) particles for nasal vaccine delivery. *Advanced Drug Delivery Reviews*, 2001, **51**, 113-125.

86. Khan, M.A.; Bhattacharia, S.K.; Kabir, M.H.; Chowdhury, A.M.S.A.; Rahman, M.M. Effect of mercerization on surface modification of Henequen (Agave fourcroydes) fiber by photo-curing with 2-hydroxyethyl methacrylate (HEMA). *Polymer-Plastics Technology and Engineering*, 2005, **44,** (6), 1079-1093.

87. Pashkuleva, I.; Azevedo, H.S.; Reis, R. Surface structural investigation into starch-based biomaterials. *Macromolecular Bioscience*, 2007, **8,** (2), 210-219.

88. Vander Wielen, L.C.; Ostenson, M.; Gatenholm, P.; Ragauskas, A.J. Surface modification of cellulosic fibers using dielectric-barrier discharge. *Cabohydrate Polymers*, 2006, **65,** (2), 179-184.

89. Zanini, S.; Riccardi, T.C.; Canevali, C.; Orlandi, M.; Zoia, L.; Tolppa, E.-L. Modifications of lignocellulosic fibers by Ar plasma treatments in comparison with biological treatments. *Surface & Coatings Technology*, 2005, **200**, 556-560.

90. Szymanowski, H.; Kaczmarek, M.; Gazicki-Lipman, M.; Klimek, L.; Wozniak, B. New biodegradable material based on RF plasma modified starch. *Surface & Coatings Technology*, 2005, **200**, 539-543.

91. Gubitz, G.; Cavaco-Paulo, A. New substrates for reliable enzymes: enzymatic modification. *Current Opinion in Biotechnology*, 2003, **14**, 577-582.

92. Ogawa, T.; Ding, B.; Sone, Y.; Shiratori, S. Super-hydrophobic surfaces of layer-by-layer structured film-coated electrospun nanofibrous membranes. *Nanotechnology*, 2007, **18**, 165607.

93. Renneckar, S.; Zink-Sharp, A.; Esker, A.R.; Johnson, R.K.; Glasser, W.G. *Novel methods for interfacial modification of cellulose-reinforced composites*. in *A.C.S. symposium series* 2006.

94. Pasquini, D.; Belgacem, M.N.; Gandini, A.; Aprigio, A.; Curvelo, S. Surface esterification of cellulose fibers: Characterization by DRIFT and contact angle measurements. *Journal of Colloid and Interface Science*, 2006, **295,** (1), 79-83.

95. Lindqvist, J.; Malmström, E. Surface modification of natural substrates by atom transfer radical polymerization. *Journal of Applied Polymer Science*, 2006, **100,** (5), 4155-4162.

96. Li, J.; Yun, H.; Gong, Y.; Zhao, N.; Zhang, X. Investigation of MC3T3-E1 cell behaviour on the surface of GRGDS-coupled chitosan. *Biomacromolecules*, 2006, **7**, 1112-1123.

97. Tsubokawa, N.; Takayama, T. Surface modification of chitosan powder by grafting of 'dendrimer-like' hyperbranched polymer onto the surface. *Reactive and Functional Polymers*, 2000, **43,** (3), 341-350.

98. Nurdin, N.; François, N.; Descouts, P., *GRGDS-grafted chitosan for biomimetic coating*, in *Advances in Chitin Science*, A. Domard, G.A.F. Roberts, and K.M. Varum, Editors. 1998, J. André Publishers: Lyon. 378-383.

99. Roy, D. Controlled modification of cellulosic surfaces via the reversible addition - Fragmentation chain transfer (RAFT) graft polymerization process*. Australian Journal of Chemistry*, 2006, **59,** (3), 229.

100. Morao, A.; Escobar, I.C.; de Amorim, M.T.P.; Lopes, A.; Goncalves, I.C. Postsynthesis modification of a cellulose acetate ultrafiltration membrane for applications in water and wastewater treatment*. Environmental progress*, 2005, **24,** (4), 367-382.

101. Vilaseca, F.; Corrales, F.; Llop, M.E.; Pelach, M.A.; Mutije, E. Chemical treatment for improving wettability of biofibres into thermoplastic matrices*. Composite Interfaces*, 2005, **12,** (8-9), 725-738.

102. Zhang, J.; Yuan, J.; Yuan, Y.; Shen, J.; Lin, S. Chemical modification of cellulose membranes with sulfo ammonium zwitterionic vinyl monomer to improve hemocompatibility*. Colloids and Surfaces B: Biointerfaces*, 2003, **30**, 249-257.

103. Yuan, J.; Zhang, J.; Zang, X.P.; Shen, J.; Lin, S. Improvement of blood compatibility on cellulose membrane surface by grafting betaines*. Colloids and Surfaces B: Biointerfaces*, 2003, **30,** (1-2), 147-155.

104. Thielemans, W.; Belgacem, M.N.; Dufresne, A. Starch nanocrystals with large chain surface modifications*. Langmuir*, 2006, **22,** (10), 4804-4810.

105. Zhou, Q.; Baumann, M.J.; Piispanen, P.S.; Teeri, T.T.; Brumer, H. Xyloglucan and xyloglucan endo-transglycosylases (XET): Tools for ex vivo cellulose surface modification*. Biocatalysis and Biotransformation*, 2006, **24,** (1-2), 107-120.

106. Kumar, G.; Smith, P.J.; Payne, G.F. Enzymatic grafting of a natural product onto chitosan to confer water solubility under basic conditions*. Biotechnology and Bioengineering*, 1999, **63**, 154-165.

107. Chao, A.; Shyu, S.; Lin, Y.; Mi, F. Enzymatic grafting of carboxyl groups onto chitosan - to confer on chitosan the property of a cationic dye adsorbent*. Bioresource technology*, 2004, **91**, 157-162.

108. Ogino, A.; Kral, M.; Narushima, K.; Yamashita, M.; Nagatsu, M. Surface amination of biopolymer using surface-wave excited ammonia plasma*. Japanese Journal of Applied Physics*, 2006, **45** (10B), 8494-8497.

109. Abidi, N.; Hequet, E. Cotton Fabric Graft Copolymerization Using Microwave Plasma. II. Physical Properties*. Journal of Applied Polymer Science*, 2005, **98**, 896-902.

110. Mukherjeea, P.; Jonesb, K.L.; Abitoyec, J.O. Surface modification of nanofiltration membranes by ion implantation*. Journal of Membrane Science*, 2005, **254**, 303-310.

111. Kiatkamjornwong, S.; Mongkolsawat, K.; Sonsuk, M. Synthesis and property characterization of cassava starch grafted poly(acrylamide-co-(maleic acid)) superabsorbent via g-irradiation. 2002, **43**, 3915-3924.

112. Woo, C.K.; Schiewe, B.; Wegner, G. Multilayered assembly of cellulose derivatives as primer for surface modification by polymerization. *Macromolecular Chemistry and Physics*, 2006, **207,** (2), 148-159.

113. Khan, F.; Ahmad, S.R. Graft Copolymerization and Characterization of 2-Hydroxyethyl Methacrylate onto Jute Fiber by Photoirradiation. *Journal of Applied Polymer Science*, 2006, **101**, 2898–2910.

114. Hassan, M.M.; Islam, M.R.; Khan, M.A. Surface modification of cellulose by radiation pretreatments with organo-silicone monomer. *Polymer-Plastics Technology and Engineering*, 2005, **44,** (5), 833-846.

115. Yi, H.; Wu, L.-Q.; Bentley, W.E.; Ghodssi, R.; Rubloff, G.W.; Culver, J.N.; Payne, G.F. Biofabrication with Chitosan. *Biomacromolecules*, 2005, **6,** (6), 2881-2894.

116. Kongdee, A.; Bechtold, T.; Teufel, L. Modification of cellulose fiber with silk sericin. *Journal of Applied Polymer Science*, 2005, **96,** (4), 1421-1428.

117. Alves, C.M.; Reis, R.L.; Hunt, J.A. Preliminary study on human protein adsorption and leukocyte adhesion to starch-based biomaterials. *Journal of Materials Science-Materials In Medicine*, 2003, **14,** (2), 157-165.

118. Hersel, U.; Dahmen, C.; Kessler, H. RGD modified polymers: biomaterials for stimulated cell adhesion and beyond. *Biomaterials*, 2003, **24**, 4385–4415.

119. Chung, T.-W.; Lu, Y.-F.; Wang, H.-Y.; Chen, W.-P.; Wang, S.-S.; Lin, Y.-S.; Chu, S.-H. Growth of human endothelial cells on different concentrations of Gly-Arg-Gly-Asp grafted chitosan surface. *Artificial Organs*, 2003, **27,** (2), 155–161.

120. Itoh, S.; Matsuda, A.; Kobayashi, H.; Ichinose, S.; Shinomiya, K.; Tanaka, J. Effects of a laminin peptide (YIGSR) immobilized on crab-tendon chitosan tubes on nerve regeneration. *Journal of Biomedical Materials Research Part B*, 2005, **73,** (2), 375-382.

121. Taillac, L.; Porte-Durrieu, M.C.; Labrugere, C.; Bareille, R.; Amedee, J.; Baquey, C. Grafting of RGD peptides to cellulose to enhance human osteoprogenitor cells adhesion and proliferation. *Composites Science and Technology*, 2004, **64,** (6), 827-837

122. Morigaki, K.; Tobias Baumgart, T.; Jonas, U.; Offenhausser, A.; Knoll, W. Photopolymerization of diacetylene lipid bilayers and its application to the construction of micropatterned biomimetic membranes. *Langmuir*, 2002, **18**, 4082-4089.

123. Fang, N.; Chan, V. Interaction of liposome with immobilized chitosan during main phase transition. *Biomacromolecules*, 2003, **4**, 581-588.

124. Yang, F.; Cui, X.; Yang, X. Interaction of low-molecular-weight chitosan with mimic membrane studied by electrochemical methods and surface plasmon resonance. *Biophysical Chemistry*, 2002, **99**, 99-106.

125. Girod, S.; Cara, L.; Maillols, H.; Salles, J.P.; Devoisselle, J.M. Relationship between conformation of polysaccharides in the dilute regime and their interaction with a phospholipid bilayer. *Luminiscence*, 2001, **16**, 109-116.

126. Ye, S.H.; Watanabe, J.; Takai, M.; Iwasaki, Y.; Ishihara, K. Design of functional hollow fiber membranes modified with phospholipid polymers for application in total hemopurification system. *Biomaterials* 2005, **26**, 5032-5041.

127. Ye, S.H.; Watanabe, J.; Takai, M.; Iwasaki, Y.; Ishihara, K. High functional hollow fiber membrane modified with phospholipid polymers for a liver assist bioreactor. *Biomaterials*, 2006, **27,** (9), 1955-1962.

Chapter 2

Materials and Methods

The aim of this chapter is to describe and contextualized the experimental methods used throughout the thesis. Chapters 3 to 7 are based on submitted or published studies and have an own materials and methods section. However, this chapter includes additional experimental details helping for better understanding of the performed studies and permitting their faster replication. Furthermore, this chapter will explain the evolution process and the reason behind some decisions on the experimental design.

The research performed in this thesis and described in the following 5 chapters can be divided in two parts. The first one (Chapters 3, 4 and 5) is focused on the surface functionalization of 2D and 3D biomaterial structures by plasma induced polymerization and the influence of the modification process on the surface properties and the material *in vitro* performance. The second part (chapters 6 and 7) describes the synthesis and characterization of thermoresponsive ionic polymers and their use for the production of nanoparticles with controlled size. The materials, procedures and characterization techniques used for each of this research lines are not related and hence, this chapter will be divided in two parts.

2.1 Part I: Surface functionalization by plasma induced polymerization

2.1.1 Materials

Plasma induced polymerization was used for grafting of negatively charged functional groups on the surface of biomaterials devices previously proposed by 3B's Research Group for different biomedical applications [1-4]. Surface modification of chitosan membranes, described in chapters 3 and 4, is an example of strategies and characterization techniques which can be applied to 2D devices. Scaffolds made of a blend of starch with ε-polycaprolactone were modified and characterized in Chapter 5. The reported methodologies are examples for approaches useful in surface analysis and treatment of 3D scaffolds.

Chitosan (CTS) is a biopolysaccharide obtained by an alkaline N-deacetylation of chitin which is the primary structural polymer in arthropod exoskeletons [5]. It is composed of *N*-

acetyl-D-glucosamine (GlcNAc) and D-glucosamine (GlcN) units linked by β-D (1→4) glycosidic bonds (Figure 2.1). In fact, the term chitosan refers to a series of deacetylated chitins with different molecular weight (50 kD to 2000 kD), viscosity, and degree of *N*-deacetylation (40 to 98%) [6]. CTS from crab shells was purchased from Sigma-Aldrich. A purification procedure was set up and the products obtained from independent purifications were mixed to obtain a final homogeneous batch of purified chitosan. This batch was used along the entire experimental work reported in this thesis to prevent concerns about the influence of the degree of *N*-deacetylation (DD)/ *N*-acetylation (DA) or molecular weight (M_w) on the material modification and *in vitro* behaviour. The purification process and the characterization of the purified chitosan are described below since the details of these processes are not presented in chapters 3 and 4.

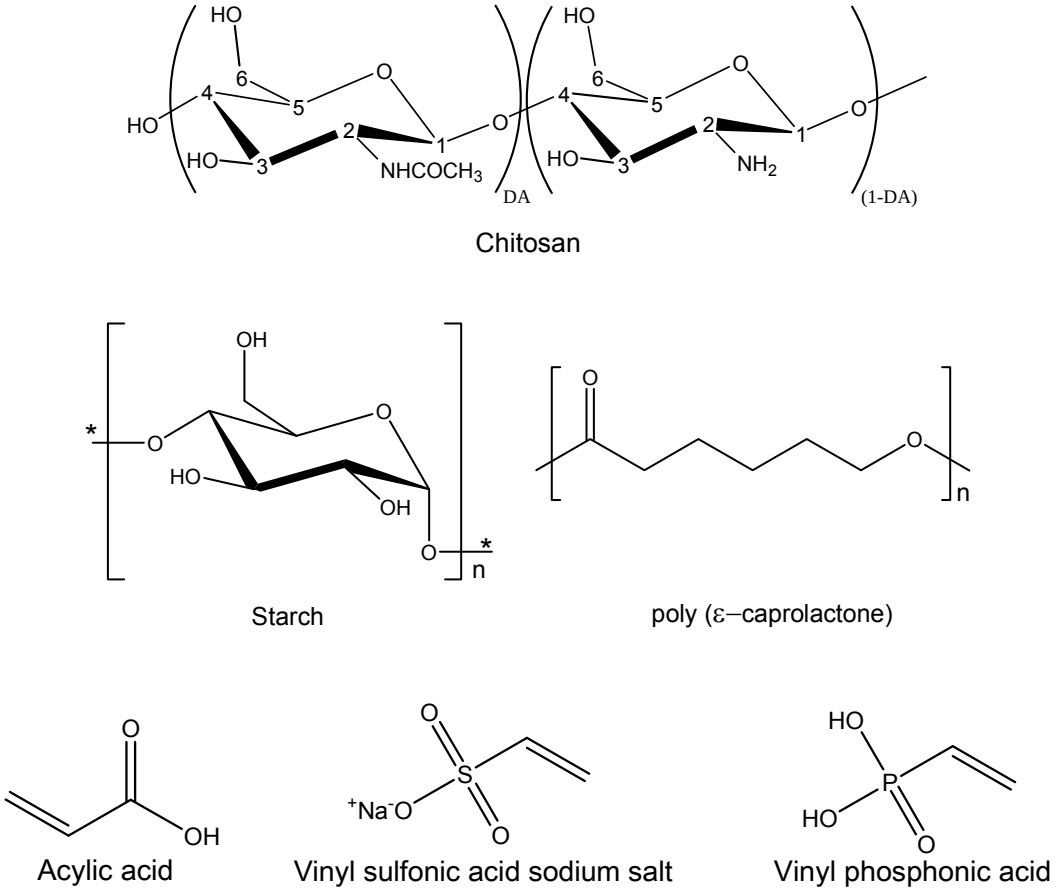

Figure 2.1 Chemical structures of the compounds used in the part I of the thesis. (For starch are only showed the α-(1→4) linkages but α-(1→6) bonds are also possible).

For the purification process, CTS was dissolved in an aqueous acetic acid solution (1%) at ~1% (w/v). The obtained solution was filtrated (Whatman® ashless filter paper, 20-25 μm) and then precipitated by adding a NaOH solution (final pH ~ 8). The formed white gel was

sieved to remove the exuded liquid and thoroughly rinsed with distilled water until stable pH. The chitosan gel was further washed with ethanol, freeze-dried, ground to powder and dried at 60ºC overnight. Viscosity molecular weight (M_v) and degree of *N*-deacetylation (DD) of the purified CTS were determined as follow.

The molecular weight was determined by viscosity. Viscosity depends on the hydrodynamic volume of the macromolecule, which is a function of the molecular weight, conformational properties and polymer-solvent interactions [7-9]. Measurements of solution viscosity are made by comparing the flow time *t* required for a specific volume of polymer solution to flow through a capillary tube with the correspondent flow time t_0 for the solvent. Relative viscosity (η_r) and specific viscosity (η_{sp}) are calculated from *t and* t_0, according to the following equations:

$$\eta_r = \eta/\eta_0 \cong t/t_0 \tag{2.1}$$

$$\eta_{sp} = \frac{\eta - \eta_0}{\eta_0} = \eta_r - 1 \tag{2.2}$$

Several mathematical equations are available for determining the intrinsic viscosity [η] of a polymer. These equations are found to be valid at sufficiently low concentrations, assuring that the polymer chains are free to move individually in the solvent, i.e., the kinetic units are not aggregates but single polymer molecules. The equations derived by Huggins[8] (equation 2.3) and Kraemer[9] (equation 2.4) relate η_r and η_{sp}, respectively, with the polymer concentration in the solvent (*C in* g/dL or any other units proportional to this), according to the following expressions:

$$\frac{\eta_{sp}}{C} = [\eta] + K_H[\eta]^2 C \tag{2.3}$$

$$\frac{\ln \eta_r}{C} = [\eta] - K_K[\eta]^2 C \tag{2.4}$$

The Huggins (K_H) and the Kraemer (K_K) coefficients give information on the polymer-solvent interactions, being the K_H lower values (ranging from 0.25 to 0.5) and the K_K negative values related to a better solvation of the polymer chains[10]. Theoretically, $K_H + K_K$ should be equal to 0.5. The intrinsic viscosity [η] is a theoretical value calculated at the limit of infinite dilution using those equations:

$$[\eta] = (\eta_{sp}/C)_{c=0} \quad \text{(Huggins)} \tag{2.5}$$

$$[\eta] = (\ln \eta_r/C)_{c=0} \quad \text{(Kraemer)} \tag{2.6}$$

The graphical extrapolation (*C*=0) using both equations is expected to produce more or less the same values of [η] for a particular polymer-solvent system. The quality of the results was assessed by comparing the values of [η] and evaluating K_H and K_K. Fresh solutions of CTS were prepared with five different concentrations in the range that gives η_r

between 1.1 and 1.9. The flow time was obtained from five reproducible measurements for each solution, using an Ubbelohde viscometer (T = 25.0 ± 0.1ºC). The intrinsic viscosity [η] was calculated by linear regression plotting η_{sp}/C and $\ln(\eta_r)/C$ against C(g/dL) (Figure 2.1). The solutions were carefully prepared since the method is very sensitive to small errors in the concentration, solutions ageing and the presence of dust particles, which due to the small diameter of the capillary can decrease significantly the flow section area. The purified CTS powder was dried overnight and accurately weighted. In any case the amount of weighted chitosan was inferior to 20.0 mg in order to minimise weighting errors. The residual water was determined thermo-gravimetrically (TGA) and the weight was corrected accordingly. CTS was completely dissolved in 0.5 M acetic acid (AcOH). Then, sodium acetate (AcONa) was added to a final concentration of 0.2 M. The obtained solution was filtered and transferred to a volumetric flask. The volumetric flask was filled up to the mark with the same 0.5 M AcOH solution. The blank solution was prepared in the same way, but without adding chitosan. Finally, the pH was checked (it should be around 4.3-4.4) and the flow time was analysed immediately to avoid chitosan hydrolysis.

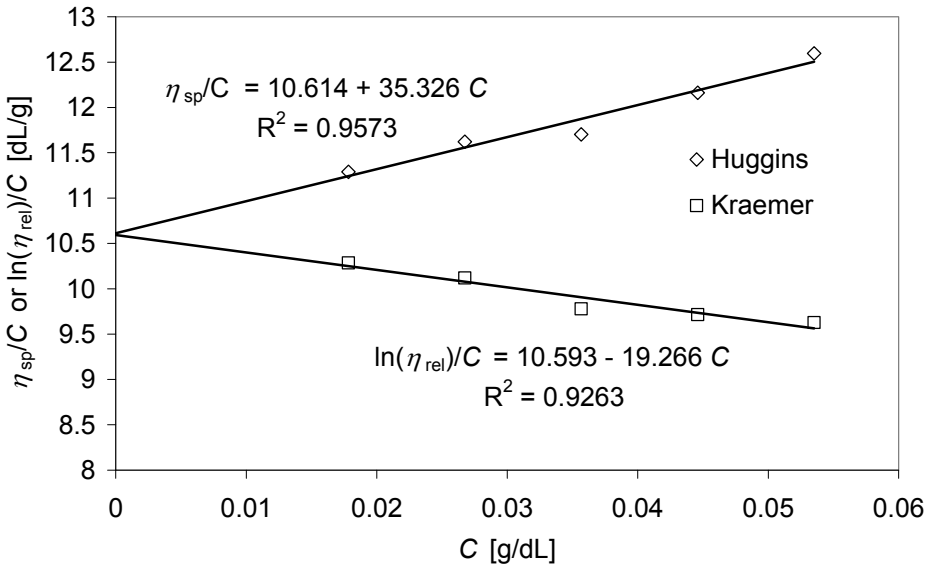

Figure 2.2 Example of linear regressions obtained by plotting η_{sp}/C (Huggins) or $\ln(\eta_{rel}/C)$ (Kraemer) against C (M_v = 790 kDa, K_H = 0.31;K_K = 0.17).

The viscosity average molecular weight (M_v) was calculated based on the Mark-Houwink equation:

$$[\eta] = k(M_v)^a \qquad (2.7)$$

with, [η] in dL/g, M_v in Da, k = 3.5 x 10^{-4} and a = 0.76 for 0.5 M AcOH/0.2 M NaOAc aqueous solution as solvent at 25ºC (independent of the DD at these conditions)[7, 11]. For the purified CTS used in the thesis a M_v of 790 kDa was obtained.

The properties of chitosan vary considerably with the DD. Although the determination of DD appears to be a simple analytical problem, a huge number of methods have been proposed in the literature to obtain this value [12-28]. In fact, these methods differ in reliability, robustness, precision and accuracy over the entire DD range. We have used several methods [12, 14, 24, 29] and compared them in terms of precision and accuracy of the obtained values, but we have also evaluated practical issues such as the amount and harmfulness of the produced residues or if the methods encompass time-spending and laborious procedures. The obtained *DD* values are shown in table 2.1.

Table 2.1 Chitosan degree of deacetylation (DD) determined by different methods. (Average and standard deviation of *N* data points)

Method	DD (%)	N
FTIR – method I (A1655/A3450) [12]	82.0 ± 2.2	5
FTIR – method II (A1320/A1420) [14]	93.6 ± 1.8	5
FTIR – method III (A1320/A3450) [14]	82.0 ± 4.4	5
^{1}H-NMR [24]	92.9 ± 0.9	3
1st derivative UV spectrophotometry [29]	93.3 ± 0.1	3

Fourier transformed infrared spectroscopy (FTIR) methods are widely used to determine CTS DD [12-15] In our first attempt to determine the DD by FTIR (Table 2.2.), we have used three different base line methods, previously optimized by several authors. The FTIR spectra were recorded in an IRPrestige 21 FTIR spectrophotometer with a resolution of 4 cm^{-1} and averaged over 36 scans.

Table 2.2 Calibration curves to determine the degree of deacetylation (DD) using the FTIR spectrum of chitosan. The absorbance (*A*) is the height at the band maximum corrected by the intercept with the respective baseline

Method	Band (cm^{-1})	Baseline (cm^{-1})	Calibration curve *DD* (%)
I [12]	*A1655*	1800 - 1600	$DD = 100 - (A_{1655}/A_{3450}) \times 115$
	A3450	4000 - 2500	
II [14]	*A1320*	1355 - 1270	$A_{1320}/A_{1420} = 0.3822 + 0.03133\ (100 - DD)$
	A1420	1495 - 1405	
III [14]	*A1320*	1355 - 1270	$A_{1320}/A_{3450} = 0.03146 + 0.00226\ (100 - DD)$
	A3450	4000 - 2500	

Generally, the methods that use the –OH stretching band at 3450 cm^{-1} gave lower values than the ones obtained by using the band at 1420 cm^{-1}. This is likely due to the fast uptake of moisture from the atmosphere that oven-dried chitosan materials present [29].

Moreover, we found that the values obtained using as a reference the band at 1420 cm^{-1} did not consistently match the DA obtained by ^{1}H-NMR (Nuclear Magnetic Resonance spectroscopy). This discrepancy between the results obtained using different calibration curves or different reference methods has been described in the literature [13]. The use of FTIR for quantification purposes have some drawbacks associated with the hydrogen-bonding networks different for each chitin polymorphic form [13]. Hence, the selection of suitable bands and baselines is quite problematic. Recently, statistical studies comparing the vast number of proposed bands and baselines combinations have been employed to optimize that selection based on robust criteria [15]. Despite its drawbacks, FTIR has been often preferred because it is a quick, user-friendly and low-cost method, but mostly because it can also be applied to the insoluble chitin. Nevertheless, the construction of a specific calibration line for each particular isolation and deacetylation procedure may be necessary to obtain reliable values of DD [15]. The calibration requires the use of standards previously assessed for the DD, which, in the case of insoluble samples, is normally done using solid state ^{13}C-NMR as a reference method [13-15]. Taking into consideration all those issues, we did not consider the FTIR technique as the most appropriate method to assess the DD of CTS raw-materials used in this thesis and focused on two other methods, namely ^{1}H-NMR (Chapter 3) and 1st derivative UV spectrophotometry (Chapter 4).

The NMR methods are often referred as the gold standard techniques, being employed to calibrate or to assess the accuracy of other methods. The experimental parameters should be carefully adjusted in order that the signal is proportional to the nuclei concentration. Unfortunately, the costs and complicate technical considerations hinder its widespread as routine technique at the industrial scale and in non-specialized laboratories. In our studies, we have dissolved 10 mg CTS in 1 ml of 0.4% (w/v) DCl in D_2O solution at room temperature. In order to minimise the deacetylation catalysed by the presence of deuterium chloride, only freshly prepared solutions were used. The ^{1}H-NMR spectra were acquired in a Varian Unity Plus (300 MHz) spectrometer at 70ºC, temperature at which the solvent signal (HOD) does not interfere with the chitosan peaks. The acquisition (64 transients) started after 10 min, considered to be enough to reach the thermal equilibrium. The pulse repetition delay, 6 s, and the acquisition time, 2 s, were set to assure complete relaxation of the nuclei before each pulse application. This procedure (repetition time of 8 s) guarantees that the relative intensities of the resonances correlate with the exact number of nuclei originating that signal. We have used several methods to calculate the DA, namely the method proposed by Hirai *et al* [24], which makes use of the

peak areas from the protons H2, H3, H4, H5, H6, H6' (Figure 2.1) to estimate the sum of both monomers and the signal arising from the acetyl group protons (HAc) to the amount of GluNAc:

$$\mathrm{DD}(\%) = 1 - \left(\frac{\mathrm{HAc}/3}{(\mathrm{H2} + \mathrm{H3} + \mathrm{H4} + \mathrm{H5} + \mathrm{H6} + \mathrm{H6}')/6} \right) \times 100 \qquad (2.8)$$

Recently, it was reported [24] that despite the good internal consistency, the determination of DA by ^{1}H-NMR may be systematically affected by the choice of the peaks to be used in that calculation and in the way those peaks are combined to estimate the GluN and GluNAc quantities. Therefore, in chapter 4 the DD determination was performed using a methodology proposed by our group [29]. which involves the 1st derivative ultraviolet (UV) spectrophotometry firstly proposed by Muzzarelli and Rocchetti [19]. The proposed method allows DD determination directly from the mass concentration of chitosan solutions and the first derivative value of its UV spectra at 202 nm (the acetic acid solutions zero crossing point), over the entire range of the DD of chitosan using a mathematical model. This approach avoids the use of empiric corrections for highly deacetylated samples.

Blend of starch with ε-polycaprolactone (30/70 wt%). Starch (Figure 2.1) is a natural polymer present in plants as corn, rice and potato. It is composed by two isomers, amylase and amylopectine being the relative amount of both components dependent on the source of starch [30]. Amylase is a linear molecule of (1→4) bonded α-D-glucopiranosyl units, slightly branched by α-(1→6) linkages, while amylopectine is a highly branched molecule containing both α-(1→4) and α-(1→6) bonds at 25-30 glucose units distance. We have used corn starch which contains approximately 30 % amylase and 70 % amylopectine. Because starch has poor mechanical properties and it is difficult to process, blends of starch with other polymers have been developed in order to join the low cost and widely availability of starch with the good mechanical properties and processing easiness of synthetic polymers[31, 32]. In this thesis, a commercial available blend of corn starch (30 %wt) with ε-polycaprolactone (70 %wt), previously used in many studies by our groups [1, 2, 33, 34], was employed.

Monomers. Scaffolds, containing anionic units have been investigated because of their capability to facilitate morphogenetic processes for tissue engineering substitutes [35, 36]. For example, the negative charge of glucosaminoglycans (GAGs) is associated with their bioactivity. GAGs interact with the positively charged amino groups of extracellular proteins and these interactions determine cell-matrix adhesion. Therefore, our aim was to study the effect of different negatively charged functional groups on biomaterials in vitro

behaviour. In chapter 3 we have investigated carboxylic (-COOH) and sulfonic groups (-SO_3) grafting on 2D chitosan membranes. Following the results and conclusions obtained from this first study, we have added to this set of anionic units the phosphonic groups (-PO_3) which was focussed in Chapter 4. Taking in consideration the outcomes obtained for 2D structures, sulfonic and phosphonic groups were grafted on 3D scaffolds. Acrylic acid (AA, Merck), vinyl sulfonic acid sodium salt (VSA) and vinyl phosphonic acid (VPA) both from Sigma-Aldrich (Figure 2.1) were kept at room temperature and used without further purification

2.1.2 Membranes/scaffolds production and modification

Chitosan membranes with smooth surface used in chapters 3 and 4 were prepared by solvent casting method. Chitosan (1% wt.) was dissolved in acetic acid solution (1% v/v). The solution was carefully stirred in order to avoid the formation of any air bubble, poured on Petri Dishes (5 mg of chitosan/cm^2) and dried at room temperature in a dust free environment. The obtained membranes (thickness approx. 50μm) were neutralized in 0.1M NaOH solution for 10 min, washed thoroughly with distilled water and dried fixed in a frame.

SPLC scaffolds. Fibers of SPCL were produced by melt spinning using a modular co-rotating twin screw extruder (Leistritz AG-LSM 36/25D, Germany), a screw speed of 3 rpm and a temperature profile in the barrel (from feed to die zones) between 60 and 130 °C. The average output rate was 0.3 kg/h. Upon extrusion through the die, the filament was spun in two consecutive steps to a final draw ratio of approximately 1:100. The cooling of the filament was performed in air (average temperature of 17 ºC). Melt spun fibers presented a diameter in the 105-345 μm range and a mean fiber diameter of 213 ± 50 μm. The fibers were cut into 0.5 mm length segments and used in the production of fiber mesh scaffolds by a custom-designed mould. Fiber bundles were randomly displaced into the mould cavities and subjected to thermal treatment at 60°C for 30 minutes before predefined compression levels along the z-axis were applied for assuring the bonding between neighboring fibers using a final compression ratio of 22%.

Surface modification of chitosan membranes and SPCL scaffolds. The modification of both 2D and 3D structures was performed by O_2 plasma induced polymerization. A plasma could be considered as the forth state of matter and can be broadly defined as a gas containing charged and neutral species including some or all the following: electrons,

positive and negative ions, radicals, atoms and molecules [37]. A glow discharge plasma is a low-temperature, relatively low-pressure gas in which a degree of ionization is sustained by energetic electrons. A glow discharge can be generated and sustained by applying an electric field to a gas under low pressure between two electrodes. Work with alternating electric field in the megahertz region (RF) provides a higher plasma density and better stability of RF plasma [37, 38]. In this thesis, we have performed the surface activation in radio frequency (13.56 MHz) plasma reactor (Plasma Prep5, Gala Instrument, Germany) using oxygen as a working atmosphere. Oxygen and oxygen containing plasmas are commonly employed to modify polymer surfaces. In oxygen plasma two processes occur simultaneously: etching of the polymer surface and the formation of oxygen functional groups at the polymer surface. The balance of these two process depends on the operation parameters [37]. In our studies, the samples were exposed to O_2 plasma at 30W of power for 15 minutes. During the treatment the pressure inside the reactor was maintained below 20 Pa by adjusting the gas flow. Before the experiments, the plasma chamber was purged with a continuous flow of O_2 to reduce the trace amounts of air. The activated samples with free radicals formed on the surface were subsequently immersed in a degassed monomer solution, where the present radicals act as initiator for the polymerization of the vinyl monomers. The specific conditions (temperatures, times and concentrations) are given in each chapter. At the final step, the membranes were thoroughly washed with the same solvent used in the polymerization to remove the unreacted monomer and dried at room temperature.

2.1.3 Surface characterization

Characterization methods are fundamental for checking the status of polymer surfaces, and even more importantly, for understanding the effectiveness of a modification technique. Since the objective of surface modification is just to change the composition and structure of the outer few atomic layers of materials, characterization techniques that detect changes in this small amount of the material are required.

Fourier-transform infrared spectroscopy (FTIR)

Fourier transform infrared spectroscopy (FTIR) is a standard analytical method that can reveal information about the sample chemical structure, since the absorption of infrared (IR) light is related to discrete energy transitions of the vibrational states of atomic and molecular units within a molecule. In transmission mode, the FTIR spectra give

information related to the bulk material. The attenuated total reflection (ATR) sampling mode can be used to increase the intensity of the surface signal, because it observes the region near the surface. However, FTIR-ATR is not truly surface sensitive due to the high penetration depth of the IR beam (1 – 5 μm) [39]. Nevertheless, the rich structural information that the IR spectra provide makes the FITR-ATR an interesting technique to evaluate greater chemical changes, such as the grafting of polymers both at the surface and also at a broader region nearby the surface. Hence, in Chapter 3 we have used the FTIR to prove the success of the modification process on the chitosan membranes surfaces. Spectra were recorder on FTIR spectrophotometer (IRPrestige, 21 Shimadzu) with an attenuated total reflectance (ATR) with a resolution of 4 cm^{-1} and averaged over 36 scans.

X-ray photoelectron spectroscopy (XPS)

The X-ray photoelectron spectroscopy (XPS) method (also called Electron Spectroscopy for Chemical Analysis, ESCA) is based on the photoelectric effect. The interaction of the X-rays focused on the sample with its atoms causes the emission of a core level (inner shell) electrons (photoelectrons). The energy of these photoelectrons is measured and its value provides information about the nature (survey spectrum) and environment (high resolution spectrum) of the atoms from which they came [37, 40]. Being so, information about the elemental composition and chemistry can be obtained at the surface level of the sample within a depth of 10-250 Å [39].

Chemical changes occurring on the surfaces as a result of the modifications performed in Chapters 3, 4 and 5 were evaluated by XPS. The spectra were obtained using an ESCALAB 200A instrument from VG Scientific (East Grinstead, UK) with PISCES software for data acquisition and analysis. A monochromatic Al-Kα radiation (hv = 1486.60 eV) operating at 15 kV (300 W) was used. The measurements were performed in a constant Analyser Energy mode (CAE) and take off angle of 90º relative to the sample surfaces. Survey spectra were acquire using a pass energy of 50 eV, over a binding energy range of 0 to 1100 eV, and were used to calculate the elemental composition of the surfaces. Element atomic percentages were calculated from the integrated intensities of the survey spectra using the sensitivity factor of the instrument data system. High resolution spectra for different regions were obtained using a pass energy of 20 eV and were peak-fitted using a least-squares peak analysis software, XPSPEAK version 4.1, using the Gaussian/Lorenzian sum function. Background counts were subtracted using a linear baseline and the sample charging was corrected assigning a binding energy of 285.0 eV to the saturated hydrocarbons C1s peak.

Time-of-Flight Secondary Ion Mass Spectrometry (ToF-SIMS)

Secondary Ion Mass Spectrometry (SIMS) is a very useful technique for high sensitivity elemental analysis. The use of SIMS in analyzing polymers has attracted a great deal of interest because is a good complement to XPS. It is a more surface-sensitive technique, with a typical sampling depth of approximately 1 nm [37]. In a SIMS experiment, the surface is bombarded by energetic primary particles of low current density. The emitted or sputter particles consists largely of secondary neutral species with a small fraction of secondary positive and negative ions. The secondary ions are detected and analysed in a mass spectrometer. A detailed analysis of the positive and negative ion spectra can provide structural and chemical information about the polymer. Studies in Chapter 4 were performed using a ToF-SIMS IV instrument (ION-TOF GmbH, Germany). The samples were bombarded with a pulsed bismuth ion beam (25 keV) at 45º incidence over an area with size 500 μm^2. The generated secondary ions were extracted with a voltage of 10 kV and their mass was determined by measuring their time of flight from the sample to the detector. Electron flood gun for charge compensation was necessary during the measurements. The experimental conditions (ion type, beam voltage and primary ion dose) were maintained constant for comparative studies. Additionally, high mass resolution spectra were obtained by bunching the raw pulse. These spectra can be attained without concurrent loss of counts, however, this is at cost of spatial resolution (in this mode no better than 2-5 μm).

Contact angle measurements

The energy of the surface, which is directly related to its wettability, is a useful parameter that has often been strongly correlated with the cell-biomaterial interfacial interactions. Unfortunately, there are not direct methods to measure surface energy or surface tension of solids. However, a number of indirect empirical and semi-empirical methods have been developed based on contact angle measurements. The contact angle of a liquid drop with a solid surface is a consequence of the force balance between the liquid-vapour surface tension of the drop and the interfacial tension between the solid and the drop. The surface energy can be calculated with data from liquids of different surface tensions. The contact angle methods are very surface-sensitive, being the analysed depth of around 3-20 Å [39]. The equilibrium water contact angle (measured under static conditions) of some polymer substrates has been shown to correlate with the cell adhesion and proliferation, which are both optimal at around 70º [41].

In Chapter 3 and 4, contact angle (θ) measurements were undertaken at room temperature (c.a. 20ºC) using (contact angle meter OCA 15+ with high-performance image processing system from DataPhysics Instruments , Germany and sessile drop method At least six measurements were performed for each solvent. A 1 µl drop of the tested liquid was added at room temperature on the sample surface by a motor driving syringe. The surface tension (γ_s) was calculated from the contact angle data by two different methods: the Owens, Wendt, Rabel and Kaelble (OWRK) method [42], that discerns polar (γ_s^p) and dispersive (γ_s^d) components of the surface energy; and the acid-base method (AB method), which allows calculation of the Lewis acid (γ_S^+) and basic (γ_S^-) contributions using the van Oss-Chaudury-Good theory (vOCG) [43]. Moreover, in chapter 4 values of water adhesion tension (τ) are also given. The water adhesion tension is often used to predict or explain biomaterial-cell interactions as an alternative to surface energy and it is defined as:

$$\tau = \gamma_w \cdot \cos\theta \qquad (2.9)$$

where γ_w is the water surface tension.

Scanning Electron Microscopy (SEM)

Etching processes are unavoidable when polymers are exposed to plasma. Usually, these processes are very dependent on the used time and power and they are limited to the topmost material surface layer. Scanning electron microscopy (SEM) can be used to evaluate morphological changes. SEM images are obtained from the low-energy secondary electrons emitted from each spot of the sample where the focused electron beam impacts. It possess a penetration depth of 5 Å [39]. The samples should be previously dehydrated. Non-conductive samples are typically coated with a thin, electrically deposited metal layer, to minimise charge accumulation. For our studies, we have used an SEM, (S360, Leica Cambridge, UK)). Micrographs at different magnification were taken in order to observe eventual morphological changes in details.

Interferometric Optical Microscopy (Optical profiler)

The surface profilometer is suitable for measuring surface macrostructures. Optical interferometers are specialized interference microscopes where nanometer level characteristics of a sample surface may be obtained through the interpretation of light reflected from a surface. The interference of two beams of light is used for characterizing

surface topographies. With optical interferometry is possible to scan-samples with sizes up to a square millimetre with a vertical resolution of approximately 2 nm [44]. This large scanned area (in comparison with the area scanned by atomic force microscopy, AFM) allows for a more comprehensive analysis of surface roughness and is very useful complement to the small scan-sizes (typically 100 μm^2) that are possible with an AFM. Optical profiler analysis were performed in Chapters 4 and 5 by an Interferometric profiler Wyko-NT 1100 (Veeco) using Vertical Scanning Interferometry (VSI) mode. The images were processed and analyzed with the analytical software package WycoVision®32.

Atomic Force Microscopy (AFM)

Atomic Force Microscopy (AFM) set up consists of a sharp tip fixed at the end of a flexible cantilever which moves across a sample surface. When the tip approaches the surface a deflection of the cantilever is registered. This deflection depends on the interaction between the tip and the sample surface and involves mechanical contact forces, van der Waals forces, capillary forces, chemical bonding, electrostatic forces, magnetic forces etc. The deflection of a cantilever is usually measured by reflecting a laser beam on the back of the cantilever into a split photodiode detector. The two commonly used modes of operation are contact mode AFM and tapping mode AFM, which are conducted in air or liquid environments [37, 45]. AFM has a very high spatial resolution and is more suitable than optical profiler for microstructures determination. AFM measurements were carried out in Chapter 4 in air atmosphere using a Multimode Nanoscope V (Veeco). Tapping mode was employed with non coated Phosphorous (n) dopped Silicon probe with cantilever length of 115 to 135 μm and resonant frequency from 257 to 342 kHz. Images were processed and analyzed by multimode software version V7.20 and analytical software package WycoVision®32.

The last three techniques described above are widely used in studying the surface nano- and micromorphology. Each method has its own limitations and the proper choice of analytical technique depends on features of analyzed surface and primary goals of research. Table 2.3 summarizes the resolution and sample/environment requirements for VSI optical profiler, AFM and SEM.

Table 2.3 Comparison of the resolution and sample/environment requirements for VSI optical profiler, AFM and SEM[39, 40, 44]

	Optical Profile (VSI)	**AFM**	**SEM**
Lateral resolution	0.5-1.2 μm	0.5 nm	0.5-1 nm
Vertical resolution	2 nm	0.5 Å	Only 2D images
Field of view	845 x 630 μm (10x)	100 x100 μm	1-2 mm
Vertical range of scan	1 mm	10 μm	-
Preparation of a sample	-	-	Required coating of conducted material
Required environment	Air	Air, liquid	Vacuum

2.1.4 *In vitro* biological evaluation

The effect of the surface modification on cell morphology, viability and proliferation was evaluated in chapters 3, 4 and 5. To complement these studies, protein adsorption experiments were performed in chapter 5.

Cell culture and seeding

The materials studied in this thesis are to be used for mineralised tissue regeneration; therefore the effect of the surface modifications was assessed by cells with the osteoblastic phenotype, the principal cell type facing these devices *in vivo*. A human osteosarcoma cell line (SaOs-2), was obtained from European Collection of Cell Cultures (ECACC, UK) and was used in cell culture studies reported in this thesis (Chapters 3-5). The cells were cultured at 37 ºC and 5% CO_2 in Dulbecoo's modified Eagle's medium (DMEM; Sigma-Aldrich, Inc, USA) supplemented with 10000 U/ml penicillin-G sodium, 10000 μg/ml streptomycin sulfate and 25 μg/ml amphotericin B in a 0.85% saline (Gibco, Invitrogen Corporation, UK) and 10% of heat-inactivated foetal bovine serum (FBS; Biochrom AG, Germany).

After sterilization with ethylene oxide under standard consitions, the samples were placed into well culture plates, seeded with a cell suspension for different time periods at 37 ºC, 5% CO_2 in a humidified atmosphere in order to follow their behaviour in contact with the studied surfaces. In Chapters 3 and 4 chitosan membranes with a circular shape and 14 mm diameter were used.

Cell morphology

Cell morphology represents the global manifestation of the cell's structural organization of the cytoskeleton and thus reflects the migratory behavior of different cell types. Therefore, the morphology of cells cultured on materials can be a sign of the cell response.
The morphology of SaOs-2 cells growing on untreated and modified materials was observed by Scanning Electron Microscopy (S360, Leica Cambridge, UK). After each predetermined incubation time cells were fixed using a 2.5% glutaraldehyde (Sigma, USA) solution in Phosphate Buffered Saline (PBS; Sigma-Aldrich, Inc, USA). Prior the analysis, the samples were dehydrated, dried at air, mounted onto brass stubs and sputtered coated with gold.

Cell viability

The **MTS** ((3-(4,5-dimethylthiazol-2-yl)-5-(3-carboxymethoxyphenyl)-2-(4-sulfophenyl)-2H tetrazolium)) is a biochemical test based in the reduction of a tetrazolium product into a aqueous soluble formazan product by the cell mitochondrial enzyme succinate dehydrogenase. At death, cells rapidly lose the ability to reduce tetrazolium products and, therefore, the production of colored formazan is proportional to the number of viable cells in the culture. Cell viability on the materials at different time points was determined in chapters 3, 4 and 5 by using Cell Titer 96® Aqueous One Solution Cell Proliferation Assay kit (Promega, USA) and following manufactures' instructions. Samples were washed with sterile PBS. Fresh medium without phenol red and MTS reagent were added to each well in 5/1 proportion. The materials were incubated for 3 h at 37 ºC in a humidified atmosphere containing 5% CO_2. After reaction, 100 µl of incubated medium was transferred to 96-well plate and Optical Density (OD) was read in a microplate reader (Bio-Tek, USA) at 490 nm.

Additionally to SEM and MTS assay in chapter 4 the cell morphology and viability were evaluated by **Calcein-acetoxymethylester staining (Calcein AM)**. Calcein-AM is a non-fluorescent, cell permeant compound, which is converted by intracellular esterases into calcein, an anionic fluorescent form. It is used in microscopy and fluorometry and provides both morphological and functional information of viable cells. For Calcein AM staining, the samples were treated with 0.002% Calcein-AM (MolecularProbes) solution in DMEM culture medium and incubated in dark for 15 min at 37 ºC in a humidified atmosphere of 5% CO_2. Cells fluorescence was examined by an Axioplan Imager Z1 from Zeiss, Germany.

Cell proliferation

Cell proliferation was evaluated in Chapters 4 and 5 by double-stranded DNA (dsDNA) quantification using the PicoGreen dsDNA kit (MolecularProbes). This reagent is an ultra-sensitive fluorescent nucleic acid stain for quantifying dsDNA in molecular biology procedures. Traditionally DNA concentration has been determined by measuring absorbance of the sample at 260 nm. Disadvantages of this method include its poor sensitivity and the impossibility to distinguish between single-stranded and double-stranded DNA. PicoGreen undergoes a dramatic fluorescence enhancement upon binding to dsDNA that can be measured using a microplate fluorometer. For the assay cells cultured on the materials were washed with sterile PBS and lysed by osmotic and thermal shock (-80 ºC). The obtained supernatant was used for DNA analyse according the manufacture instructions. The fluorescence was read (485 nm/528 nm of excitation/emission) in a microplate reader (Bio-Tek, USA) and the DNA amounts calculated from a standard curve.

Protein adsorption

In Chapter 5 the effect of the surface treatments on protein adsorption was analyzed by fluorescent immunolabelling. Two adhesion proteins were studied: fibronectin (Fn) because it is commonly used in a standard procedure applied to improve adhesion of cells [46-48] and Vitronectin (Vn) because of its influence on cell spreading and migration [47, 49, 50]. Samples were incubated for 1 hour at 37 ºC with a complex protein solution composed of 10 v/v% heat-inactivated fetal bovine serum (FBS; Biochrom AG, Germany) in Dulbecoo's modified Eagle's medium (DMEM; Sigma-Aldrich, Inc, USA). Samples immersed in PBS were used as blanks. After the incubation time was over, the samples were washed with PBS and incubated at room temperature for 1 hour with primary antibody mouse anti-cow Vn (Santa Cruz, USA) or mouse anti-cow Fn (Santa Cruz, USA). Both primary antibodies were diluted at ratio 1:50 (v/v) in 1% (w/v) Bovine Serum Albumin (BSA, Sigma-Aldich, USA) solution in PBS. All samples were again washed and incubated for 1 hour at room temperature with goat anti-mouse Alexa Fluor 488 IgG (H+L) secondary antibody (Invitrogen, USA). Labelled samples were analyzed by an Olimpus IX81 Confocal Laser Scanning Microscope (CLSM)

2.2 Part II: Thermoresponsive alkylacrylamide based ionic terpolymers

In this part series of random terpolymers composed of *N*-isopropylacrylamide (NIPAAm), 2-Acrylamido-2-methyl-1-propanesulphonic acid (AMPS) and *N-tert*-butylacrylamide (NTBAAm) monomers (Figure 2.3) were synthesized by free radical polymerization. In Chapter 6 turbidity measurements were used to evaluate the influence of the relative amount of NIPAAm and NTBAAm, polymer concentration, as well as solution ionic strength on the cloud point and redissolution temperatures (macroscopic phase separation). Dynamic light scattering (DLS) was employed to elucidate some aspects regarding the molecular scale mechanism of the temperature-induced phase separation and to determine the low critical solution temperature (LCST). The interesting aggregation/redissolution profile observed for more hydrophobic polymers was used in Chapter 7 to produce thermoresponsive nanoparticles with a tight control over particle size (between 20- 200 nm).

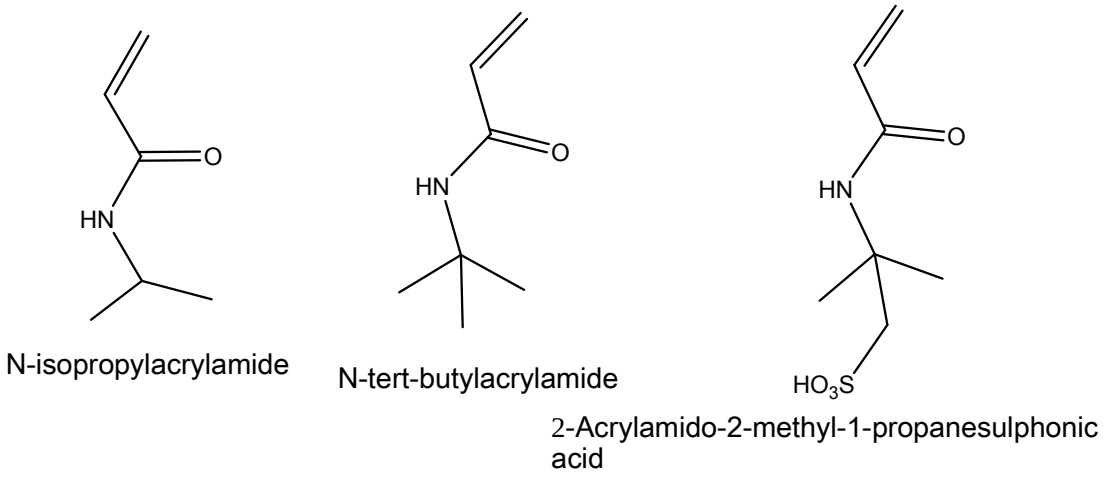

Figure 2.3 Chemical structure of monomers used in ionic terpolymer synthesis.

2.2.1 Terpolymers synthesis

Random linear terpolymers p(NIPAAm-*co*-NTBAAm-*co*-AMPS) were synthesized by free-radical copolymerization using AIBN as initiator (see chart 6.1). In both Chapters (6 and 7) the copolymers are designed as XX/YY/ZZ being XX, YY and ZZ the molar percentages of NIPAAm, NTBAAm, and AMPS in the reaction mixture, respectively. Monomers with a total concentration of 0.5 M were dissolved in an 50:50 isopropanol:water mixture and AIBN (1 mol% with respect to the total monomer) was added to the solution. After degasification of the reactants solution with nitrogen for about 15 min, the reaction vessel was sealed and placed in an oven at 60 ºC for 16 h. The solution containing the obtained

polymers was neutralized with NaOH, dialyzed against distilled water using dialysis tubes with a cut-off molecular weight of 3500 Da and freeze-dried.

2.2.2 Copolymers compositions

Terpolymers composition was analyzed by combining Elemental analyses and ^{1}H-NMR. The chemical structure of all monomers is quite similar and it was not possible to determine the ratio of each monomer in the polymer using one technique alone. The AMPS content was determined using the sulfur content on the sample (%S) determined by Elemental analysis (Leco CHNS-932). The ^{1}H-NMR was performed in a *Varian* Inova 300 using $CDCl_3$ as solvent. After peak assignation (Table 2.4) the NIPAAm/NTBAAm ratio on the copolymer was calculated by the integrated areas of methyl groups from NIPAAm δ(1.142) and NTBAAm δ(1.314) and considering that the AMP in the copolymer content in the copolymer is 5%.

Table 2.4 Chemical Shifts (δ) and assignments for p(NIPAAm-*co*-NTBAAm-*co*-AMPS)

δ/ppm	**Assignment**
1.142	-CH_3 (NIPAAm)
1.314	-CH_3 (NTBAAm)
1.578	-CH_3 (AMPS)
1.802	-CH_2 (NIPAAm, AMPS; NTBAAm -$\underline{C}H_2$-CH) overlapping
2.015	-CH (NIPAAm, AMPS; NTBAAm CH_2-$\underline{C}$H) overlapping
3.311—3.365 *	-CH_2 (AMPS; -$\underline{C}H_2$-SO_3H)
4.001	-CH (NIPAAm, $\underline{C}$H-$(CH_3)_2$)

*Observed for NIPAAm/AMPS copolymers[51]; not detected for the studied terpolymers due to the low AMPS content

2.2.3 Molecular weight distribution

Gel permeation chromatography (GPC) (also called size exclusion chromatography SEC) is a separation method based on the size or hydrodynamic volume of the analytes. GPC is a powerful technique to determine the relative molecular weight and the molecular weights distribution of polymer samples. In GPC a dilute polymer solution is injected in a solvent

stream which flows through a column packed with beads of a porous gel. The smaller polymer molecules can penetrate the pores and therefore retained in a greater extent than larger molecules, increasing their retention time into the column [52].

Molecular weight and polydispersity of the synthesized polymers were determined by GPC using 0.1% (w/v) LiBr solution in DMF as an eluent at a flow rate of 0.3 mL min^{-1} at 70 ºC and narrow disperse poly (ethylene glycol) (PEG) as a calibration standards.

2.2.4 Turbidity measurements

Turbidimetry is a common technique used to estimate the cloud point temperature (CPT) of thermoresponsive polymers in aqueous solutions, motivated by the tendency of polymer molecules to aggregate at the poor solvent region above the Θ-temperature, which causes a marked change in the solution optical properties. CPT of the polymer solutions was measured in a Varian-Cary 3 UV/Visible spectrophotometer, equipped with a Peltier cell holder for temperature control. The turbidity of the solutions was monitored as a function of temperature at 400 nm and under magnetic stirring. The solutions were prepared using distilled water with varying NaCl concentrations. They were frozen at -20 ºC to ensure complete dissolution. Immediately after melting, the solutions were placed in a cuvette and heating scans were performed between 15-80 ºC at a scanning rate of 1 ºC/min. The first measured point at 15 ºC was used as blank (it corresponds to the clear polymer solution). The transmittance of the polymer solution at different concentration and ionic strength (adjusted with NaCl) was monitored as a function of temperature. The redissolution temperature of the formed aggregates was evaluated by cooling scans in the range 80-5ºC immediately after heating at the same rate.

In Chapter 6 the aggregation kinetic isotherms were also evaluated by turbidity. Solutions were frozen before each temperature measurement and blank was record at 15 ºC, as for the temperature scanning experiments. Afterwards, the solutions were rapidly heated to set of temperature values near and above the CPT and transmittance was recorded as a function of time.

2.2.5 Dynamic light scattering measurements

Dynamic Light Scattering (DLS), also known as Photon Correlation Spectroscopy, (PCS) measures Brownian motion and relates this to the size of the particles. Particles, emulsions and molecules in suspension undergo Brownian motion. This is the motion

induced by the collision with the solvent molecules that are moving due to their thermal energy. An important feature of Brownian motion for DLS is that small particles move quickly and large particles move slowly and therefore a correlation function can be defined and related to the diffusion coefficient (D). The relationship between the size of a particle, this is hydrodynamic radius (R_h), and its speed due to Brownian motion is defined in the Stokes-Einstein equation [53]:

$$R_h = \frac{K_B T}{(6\Pi \eta D)} \qquad (2.10)$$

with K_B, T and η being the Boltzman constant, the absolute temperature and the solvent viscosity and respectively

DLS measurements were performed using a Zetasizer NanoZS Instrument (ZEN3600, Malvern Instruments, Worcestershire, UK) equipped with a 4 mW He-Ne laser (λ_0=633 nm) and with non-invasive backscattering (NIBS) detection at a scattering angle of 173º. Owing to this configuration, the equipment can decrease the scattered light path length through the sample by adjusting automatically the measuring position, hence reducing multiple scattering for larger particle size, i.e. opaque samples. This is especially useful in colloidal aggregation experiments, where scattered light intensity can rapidly increase several orders of magnitude, because it reduces the need of sample dilution. Both measuring position and attenuator were adjusted automatically before each measurement. The autocorrelation function was converted in a volume weighted particle size distribution with Dispersion Technology Software 5.06 from Malvern Instruments. Terpolymer solutions with varying salt concentration were prepared in ultrapure water and filtered using a 0.20 µm disposable PES membrane filter (TPP, Trasadingen, Switzerland).The apparent hydrodynamic diameters with the temperature (D_h) were taken in Chapters 6 and 7 as the mean position of the peak in volume-D_h distributions. The measurements were performed in the temperature range 5-85 ºC with a temperature interval of 2 ºC and an equilibration time of 2 min. Regarding the stability measurements reported in chapter 6, samples were initially frozen, melted and equilibrated at 5 ºC inside the measurement cell to assure complete dissolution. Thereafter, samples were submitted to a temperature jump and measured at constant temperature for 12 h.

In Chapter 7 nanoparticles were preparing by submitting the copolymer solution to a temperature jump to a certain temperature at which the growing of aggregates occurs (30 ºC and 40 ºC) and z-average D_h ($\langle D_h \rangle_z$) was recorded for some time. When the particles achieve the desire size, the temperature was drop down at 21 ºC; where the particles size remained constant.

2.2.6 Nanoparticles Electrophoretic Mobility determination

When an electric field is applied across an electrolyte, charged particles dispersed in the electrolyte are attracted towards the electrode of opposite charge. Viscous forces acting on the particles tend to oppose this movement. When equilibrium is reached between these two opposing forces, the particles move with constant velocity. The velocity of a particle in an electric field is commonly referred to as its electrophoretic mobility (μ_e) [54]. In Chapter 7 the nanoparticles' electrophoretic mobility (μ_e) was obtained by Laser Doppler Velocimetry (LDV) using a Zetasizer NanoZS Instrument (ZEN3600, Malvern Instruments, Worcestershire, UK) at a scattering angle of 17º and a Folded Capillary cell (DTS1060, Malvern) electrophoretic cell. The measurements were performed with an applied voltage of ± 20 V in the temperature range 8-64 ºC after an equilibration time of 4 min. For both DLS and electrophoretic mobility measurements, the terpolymer solutions were prepared in ultrapure water and filtered using a 0.20 µm disposable polyethersulfone (PES) membrane filter (TPP, Trasadingen, Switzerland).

2.3 References

1. Gomes, M.E.; Holtorf, H.L.; Reis, R.L.; Mikos, A.G. Influence of the porosity of starch-based fiber mesh scaffolds on the proliferation and osteogenic differentiation of bone marrow stromal cells cultured in a flow perfusion bioreactor. *Tissue Engineering*, 2006, **12,** (4), 801-809.

2. Gomes, M.E.; Sikavitsas, V.I.; Behravesh, E.; Reis, R.L.; Mikos, A.G. Effect of flow perfusion on the osteogenic differentiation of bone marrow stromal cells cultured on starch-based three-dimensional scaffolds. *Journal of Biomedical Materials Research Part A*, 2003, **67,** (1), 87-95.

3. Silva, R.M.; Silva, G.A.; Coutinho, O.P.; Mano, J.F.; Reis, R.L. Preparation and characterisation in simulated body conditions of glutaraldehyde crosslinked chitosan membranes. *Journal of Materials Science-Materials In Medicine*, 2004, **15,** (10), 1105-1112.

4. Silva, S.S.; Luna, S.M.; Gomes, M.E.; Benesch, J.; Pashkuleva, I.; Mano, J.F.; Reis, R.L. Plasma surface modification of chitosan membranes: Characterization and preliminary cell response studies. *Macromolecular Bioscience*, 2008, **8,** (6), 568-576.

5. Li, Q.; Grandmaison, E.W.; Goosen, M.F.A.; Dunn, E.T. Applications and Properties of Chitosan. *Journal of Bioactive and Compatible Polymers*, 1992, **7,** (4), 370-397.

6. Gallardo, A.; Aguilar, M.R.; Elvira, C.; Peniche, C.; San Roman, J. *Chitosan-Based Microcomposites- From Biodegradable Microparticles to Self-Curing Hydrogels*. Biodegradables Systems in Tissue Engieering and Regenerative Medicine, ed. R.L. Reis and J. San Roman. 2005, Boca Raton, U.S.A.: CRC Press. 145-161.

7. Terbojevich, M.; Cosani, A., *Molecular weight determination of chitin and chitosan*, in *Chitin handbook*, R. Muzzarelli and M. Peter, Editors. 1997, European chitin society. 87-101.

8. Huggins, M.L. The Viscosity of Dilute Solutions of Long-Chain Molecules. IV. Dependence on Concentration. *Journal of the American Chemical Society*, 1942, **64,** (11), 2716-2718.

9. Kraemer, E.O. Molecular Weights of Celluloses and Cellulose Derivates. *Industrial and Engineering Chemistry*, 1938, **30,** (10), 1200-1203.

10. Delpech, M.C.; Oliveira, C.M.F. Viscometric study of poly(methyl methacrylate-g-propylene oxide) and respective homopolymers. *Polymer Testing*, 2005, **24,** (3), 381-386.

11. Terbojevich, M.; Cosani, A.; Muzzarelli, R.A.A. Molecular parameters of chitosans depolymerized with the aid of papain. *Carbohydrate Polymers*, 1996, **29,** (1), 63-68.

12. Baxter, A.; Dillon, M.; Taylor, K.D.A.; Roberts, G.A.F. Improved Method for IR Determination of the Degree of *N*-Acetylation of Chitosan. *International Journal of Biological Macromolecules*, 1992, **14,** (3), 166-169.

13. Van de Velde, K.; Kiekens, P. Structure analysis and degree of substitution of chitin, chitosan and dibutyrylchitin by FTIR spectroscopy and solid state C-13 NMR. *Carbohydrate Polymers*, 2004, **58,** (4), 409-416.

14. Brugnerotto, J.; Lizardi, J.; Goycoolea, F.M.; Arguelles-Monal, W.; Desbrieres, J.; Rinaudo, M. An infrared investigation in relation with chitin and chitosan characterization. *Polymer*, 2001, **42,** (8), 3569-3580.

15. Duarte, M.L.; Ferreira, M.C.; Marvao, M.R.; Rocha, J. An optimised method to determine the degree of acetylation of chitin and chitosan by FTIR spectroscopy. *International Journal of Biological Macromolecules*, 2002, **31,** (1-3), 1-8.

16. Jiang, X.A.; Chen, L.R.; Zhong, W. A new linear potentiometric titration method for the determination of deacetylation degree of chitosan. *Carbohydrate Polymers*, 2003, **54,** (4), 457-463.

17. Roberts, G.A.F., *Determination of the degree of N-acetylation of chitin and chitosan*, in *Chitin handbook*, R. Muzzarelli and M. Peter, Editors. 1997, European chitin society. 127-132.

18. Liu, D.S.; Wei, Y.N.; Yao, P.J.; Jiang, L.B. Determination of the degree of acetylation of chitosan by UV spectrophotometry using dual standards. *Carbohydrate Research*, 2006, **341,** (6), 782-785.

19. Muzzarelli, R.A.A.; Rocchetti, R. Determination of the Degree of Acetylation of Chitosans by 1st Derivative Ultraviolet Spectrophotometry. *Carbohydrate Polymers*, 1985, **5,** (6), 461-472.

20. Tan, S.C.; Khor, E.; Tan, T.K.; Wong, S.M. The degree of deacetylation of chitosan: advocating the first derivative UV-spectrophotometry method of determination. *Talanta*, 1998, **45,** (4), 713-719.

21. Prochazkova, S.; Varum, K.M.; Ostgaard, K. Quantitative determination of chitosans by ninhydrin. *Carbohydrate Polymers*, 1999, **38,** (2), 115-122.

22. Raymond, L.; Morin, F.G.; Marchessault, R.H. Degree of Deacetylation of Chitosan Using Conductometric Titration and Solid-State NMR. *Carbohydrate Research*, 1993, **246**, 331-336.

23. Varum, K.M.; Anthonsen, M.W.; Grasdalen, H.; Smidsrod, O. High-Field NMR-Spectroscopy of Partially N-Deacetylated Chitins (Chitosans) .1. Determination of the Degree of N-Acetylation and the Distribution of N-Acetyl Groups in Partially N-Deacetylated Chitins (Chitosans) by High-Field NMR-Spectroscopy. *Carbohydrate Research*, 1991, **211,** (1), 17-23.

24. Hirai, A.; Odani, H.; Nakajima, A. Determination of Degree of Deacetylation of Chitosan by 1H-NMR Spectroscopy. *Polymer Bulletin*, 1991, **26,** (1), 87-94.

25. Lavertu, M.; Xia, Z.; Serreqi, A.N.; Berrada, M.; Rodrigues, A.; Wang, D.; Buschmann, M.D.; Gupta, A. A validated 1H-NMR method for the determination of the degree of deacetylation of chitosan. *Journal of Pharmaceutical and Biomedical Analysis*, 2003, **32,** (6), 1149-1158.

26. Ottoy, M.H.; Varum, K.M.; Smidsrod, O. Compositional heterogeneity of heterogeneously deacetylated chitosans. *Carbohydrate Polymers*, 1996, **29,** (1), 17-24.

27. Duarte, M.L.; Ferreira, M.C.; Marvao, M.R.; Rocha, J. Determination of the degree of acetylation of chitin materials by C-13 CP/MAS NMR spectroscopy. *International Journal of Biological Macromolecules*, 2001, **28,** (5), 359-363.

28. Heux, L.; Brugnerotto, J.; Desbrieres, J.; Versali, M.F.; Rinaudo, M. Solid state NMR for determination of degree of acetylation of chitin and chitosan. *Biomacromolecules*, 2000, **1,** (4), 746-751.

29. da Silva, R.M.P.; Mano, J.F.; Reis, R.L. Straightforward determination of the degree of N-acetylation of chitosan by means of first-derivative UV spectrophotometry. *Macromolecular Chemistry and Physics*, 2008, **209,** (14), 1463-1472.

30. Singh, N.; Singh, J.; Kaur, L.; Sodhi, N.S.; Gill, B.S. Morphological, thermal and rheological properties of starches from different botanical sources. *Food Chemistry*, 2003, **81,** (2), 219-231.

31. Gomes, M.E.; Reis, R.L. Biodegradable polymers and composites in biomedical applications: from catgut to tissue engineering - Part 1 - Available systems and their properties. *International Materials Reviews*, 2004, **49,** (5), 261-273.

32. Sousa, R.A.; Correlo, V.M.; Chung, S.; Neves, N.M.; Mano, J.F.; Reis, R.L., *Processing of starch-based blends for biomedical applications*, in *Natural-based polymers for biomedical applications*, R.L. Reis, Editor. 2008, CRC Press LLC: Boca Raton, FL, U.S.A. 85-105.

33. Bastioli, C.; Belliotti, V.; Cella, G.; Del Guidice, L.; Montino, S.; Perego, G., *Bodegradable polymeric compositions comprising starch and a thermoplastic polymer*, PCT, Editor. 1998, Novamont S. p. A., Novara, italy.

34. Bastioli, C.; Bellotti, V.; Del Tredici, G.; Lombi, R., *Biodegradable polymeric compositions based on starch and thermoplastic polymers*, E.P. Office, Editor. 1997, Novamont S.p.A.: Italy.

35. Chen, Y.M.; Shiraishi, N.; Satokawa, H.; Kakugo, A.; Narita, T.; Gong, J.P.; Osada, Y.; Yamamoto, K.; Ando, J. Cultivation of endothelial cells on adhesive protein-free synthetic polymer gels. *Biomaterials*, 2005, **26,** (22), 4588-4596.

36. Moreira, P.L.; An, Y.H.; Santos, A.R.; Genari, S.C. In vitro analysis of anionic collagen scaffolds for bone repair. *Journal of Biomedical Materials Research Part B-Applied Biomaterials*, 2004, **71,** (2), 229-237.

37. Chan, C.M. *Polymer Surface Modification and Characterization*, ed. C.M. Chan. 1993, Munich: Hanser Publishers. 226-263.

38. Fracassi, F., *Architecture of RF plasma reactors*, in *Plasma Processing of Polymers*, R. d`Agostino, P. Favia, and F. Fracassi, Editors. 1997, Kluwer Academic Publishers: Dordrecht/Boston/London.

39. Ratner, B.D., *Surface properties of materials*, in *Biomaterials Science*, B.D. Ratner, et al., Editors. 1996, Academic Press. 21-35.

40. Ratner, B.D.; Castner, D.G., *Electron Spectroscopy for Chemical Analysis*, in *Surface Analysis. The Principal Techniques*, J.C. Vickerman and L.S. Gilmore, Editors. 2009, Jonh Wiley &Sons Ltd: Chichester, West Sussex, UK. 47-112.

41. Tamada, Y.; Ikada, Y. Fibroblast growth on polymer surfaces and biosynthesis of collagen. *Journal of Biomedical Materials Research*, 1994, **28,** (7), 783-789.

42. Owens, D.K.; Wendt, R.C. Estimation Of Surface Free Energy Of Polymers. *Journal Of Applied Polymer Science*, 1969, **13,** (8), 1741-1747.

43. van Oss, C.J.; Chaudhury, M.K.; Good, R.J. Interfacial Lifshitz-Vanderwaals and Polar Interactions in Macroscopic Systems. *Chemical Reviews*, 1988, **88,** (6), 927-941.

44. Koyuncu, I.; Brant, J.; Luttge, A.; Wiesner, M.R. A comparison of vertical scanning interferometry (VSI) and atomic force microscopy (AFM) for characterizing membrane surface topography. *Journal of Membrane Science*, 2006, **278,** (1-2), 410-417.

45. Leggett, G.J., *Scaning Probe Microscopy*, in *Surface Analysis. The Principal Techniques*, J.C. Vickerman and L.S. Gilmore, Editors. 2009, John Wiley &Sons Ltd: Chichester, West Sussex, UK. 479-562.

46. Knox, P. Kinetics of Cell Spreading in the Presence of Different Concentrations of Serum or Fibronectin-Depleted Serum. *Journal of Cell Science*, 1984, **71**, 51-59.

47. Underwood, P.A.; Bennett, F.A. A Comparison of the Biological-Activities of the Cell-Adhesive Proteins Vitronectin and Fibronectin. *Journal of Cell Science*, 1989, **93**, 641-649.

48. Santos, M.I.; Pashkuleva, I.; Alves, C.M.; Gomes, M.E.; Fuchs, S.; Unger, R.E.; Reis, R.L.; Kirkpatrick, C.J. Surface-modified 3D starch-based scaffold for improved endothelialization for bone tissue engineering. *Journal of Materials Chemistry*, 2009, **19,** (24), 4091–4101.

49. Hayman, E.G.; Pierschbacher, M.D.; Suzuki, S.; Ruoslahti, E. Vitronectin - a Major Cell Attachment-Promoting Protein in Fetal Bovine Serum. *Experimental Cell Research*, 1985, **160,** (2), 245-258.

50. Thomas, C.H.; McFarland, C.D.; Jenkins, M.L.; Rezania, A.; Steele, J.G.; Healy, K.E. The role of vitronectin in the attachment and spatial distribution of bone-derived cells on materials with patterned surface chemistry. *Journal of Biomedical Materials Research*, 1997, **37,** (1), 81-93.

51. Zhang, C.; Easteal, A.J. Study of free-radical copolymerization, of N-isopropylac lamide with 2-acrylamido-2-methyl-1-propanesulphonic acid. *Journal of Applied Polymer Science*, 2003, **88,** (11), 2563-2569.

52. Cloizeaux, J.D.; Jannink, G. *Polymers in Solution. Their Modelling and Structure*. 1987, New York, US: Oxford University Press. 32-41.

53. Berry, G.C.; Cotts, P.M., *Static and Dynamic Light Scattering*, in *Modern Techniques in Polymer Characterisation*, R.A. Pethrick and J.V. Dawking, Editors. 1999, John Wiley & Sons: Chichester, West Sussex, England. 81-95.

54. Hunter, R.J. *Zeta Potential in Colloid Science. Principles and Applications*. 1988, London, UK: Academic Press

Chapter 3

Effect of chitosan membranes' surface modification via plasma induced polymerization on the adhesion of Osteoblast-like cells

3.1 Abstract

The surface of solvent cast chitosan membranes was modified using a two-step procedure. Oxygen plasma treatment was used at the first, activation step, followed by vinyl monomers graft polymerization. Two monomers were used in order to compare the influence of different functional groups on cell adhesion and proliferation; acrylic acid (AA) was used to introduce carboxyl groups and vinyl sulfonic acid (VSA) was used as a source of sulfonic groups.

The surface chemistry/energy changes were characterized by means of X-Ray photoelectron spectroscopy (XPS), Fourier transform infrared spectroscopy (FTIR-ATR), and contact angle measurements. Additionally, alterations in the surface morphology were investigated by scanning electron microscopy (SEM).

XPS analyses confirmed the polymer grafting on the surface; S_{2s} peak appears in the VSA survey spectrum and O–C=O peak emerge in C_{1s} high resolution spectrum after AA grafting. Moreover, contact angle measurements showed an increment in the values of the surface energy polar and Lewis base components for all treated samples, confirming the introduction of additional polar groups by the modification processes. FTIR-ATR spectra showed no significant difference between treated and original materials. These results confirmed that only very top (few angstroms) surface layer, but not the bulk of the material was modified.

The effect of the modification on the adhesion and proliferation of osteoblast-like cells was studied in a preliminary basis. Direct contact tests were performed using a human osteosarcoma cell line (SaOs-2). Cell morphology (optical microscopy and SEM) and cell viability (MTS test) were evaluated for untreated and surface modified membranes.

The results revealed that both, plasma treatment and the presence of sulfonic groups on the surface of chitosan membranes, improve SaOs-2 adhesion and proliferation when compared to untreated or AA-grafted membranes. This effect was strongly related with the polar and Lewis basic components of the total surface energy.

This chapter is based on the following publication:

Paula M. López-Pérez; Alexandra P. Marques; Ricardo M.P. da Silva; Iva Pashkuleva; Rui L. Reis. **Journal of Materials Chemistry**, 2007, 17 (38): 4064-4071.

3.2 Introduction

Chitin, derived from exoskeleton of crustaceans and insects, is the second most abundant polysaccharide in nature next to cellulose. Chitosan is a copolymer composed of *N*-acetyl-D-glucosamine (GlcNAc) and D-glucosamine (GlcN) units linked by β-D (1→4) bonds, and it is obtained by partial *N*-deacetylation of chitin. In fact, the term chitosan refers to a series of deacetylated chitins with different molecular weigh (50 kD to 2000 kD), viscosity, and degree of *N*-deacetylation (40 to 98%) [1].

Due to its special properties, namely biocompatibility, biodegradability and non-toxicity [2], this natural polymer has been proposed for a number of applications in the biomedical field such as wound dressings, drug delivery or skin regeneration [2, 3].

The pH-dependent solubility of chitosan offers a suitable membrane-processing route under mild conditions [4]. However, it was found that native chitosan membranes do not support cell adhesion and proliferation [5, 6].

The surface is the first contact between the living body and the biomaterial when a certain device is implanted into the body. It is well known [7] that the surface properties of biomaterials, namely chemistry, topography and/or surface energy, are essential factors for cell adhesion and proliferation and consequently for the performance (rejection or acceptance) of a potential device. Therefore, adequate surface modifications of chitosan membranes can improve its biocompatibility in terms of better cell adhesion and proliferation without changing the key physical properties of chitosan itself. The alternation of presence and density of polar groups on the material's surface can be used to tailor its wettability and surface free energy [8-10] and hence to adjust surface biocompatibility in accordance with the application. Furthermore, the introduced polar groups can be used for the immobilization of bioactive molecules or to control protein adsorption on the surface [11].

In the medical field, surface modifications resulting in very thin layers with a thickness of some ten to hundred nanometres are considered to be suitable [12]. Several methods have been used to render biomaterials with appropriate surface properties. Among them, plasma-surface modification is an effective and economical technique, applicable for many materials and of growing interest in the biomaterials field. The main advantage of plasma modification techniques is that the surface properties can be enhanced selectively, while the bulk attributes of the materials remain unchanged. Plasma based treatments have been largely used for medical applications with different aims, such as introduction of new functionalities, enhancement of surface wettability, increase of the surface oxygen concentration and improvement on the interfacial adhesion [13].

This work reports a graft polymerization of acrylic and vinylsulfonic polar monomers on the surface of chitosan membranes preactivated by oxygen plasma treatment. The effects of the plasma treatment itself, as well as of the different functional groups introduced by the subsequent surface grafting polymerization, on the osteoblast like cell behavior (adhesion and proliferation) are also reported.

3.3 Materials and methods

Chitosan (CHT), purchased from Sigma-Aldrich, was purified as follow. Chitosan was dissolved at a concentration of 1% (w/v) in 1% acetic acid (AcOH) aqueous solution. The solution was filtrated and re-precipitated with a slight excess of a sodium hydroxide (NaOH) solution, until a sudden decrease in the viscosity of the solution was observed, corresponding to the equivalent point. The product was thoroughly washed with water until a stable pH. The obtained precipitate was washed with ethanol and freeze-dried. Acrylic acid (AA, Merck) and Vinyl sulfonic acid, sodium salt (VSA, Aldrich) were used without further purification.

The chitosan degree of deacetylation (DD) was determined by ^{1}H-NMR using the method proposed by Hirai A, *et al*. [14]. The molecular weight (Mv) was determined by viscometry using a 0.5M AcOH/0.2M NaOAc aqueous solution as a solvent. The measurements were performed at 25 ºC. The Mark-Houwink parameters determined by Terbojevich M, *et al*.[15] were used for the calculations. The obtained values for the DD and Mv were 93% and 790 kDa, respectively.

3.3.1 Membranes preparation

Chitosan films (thickness approx. 50 μm) were prepared by solvent casting. Purified chitosan powder was dissolved in aqueous AcOH 1% (v/v) solution at a concentration of 1% wt. The solution was carefully stirred to avoid air bubbles formation, cast into Petri dishes (0.5g/cm^2) and dried at room temperature. The obtained membranes were neutralized by immersion in a 0.1 M NaOH solution, washed with water and dried at room temperature.

3.3.2 Surface modification

Plasma treatment was applied to activate the surface of the chitosan films by free radicals formation. These radicals were expected to initiate further graft copolymerization of vinyl monomers. The plasma treatment was performed using radio frequency (13.56 MHz) Plasma Prep5 equipment from Gala Instrument. Samples were exposed to O_2 plasma at 30 W of power during 15 minutes. The pressure in the reactor was maintained around 20 Pa by regulating the gas flow. Subsequently, the activated samples were immersed in a degassed 10%wt monomer solution (solvents: 2-propanol for AA and acetone for VSA grafting) and kept at room temperature during 2h. The pH of the AA solution was adjusted (pH=5) by triethylamine. In order to remove the nongrafted monomer, samples were washed thoroughly with a suitable solvent (2-propanol for AA and water for VSA grafted membranes).

3.3.3 X-ray Photoelectron spectroscopy (XPS)

XPS was used to characterise the surface chemistry of treated and untreated samples. The XPS analyses were performed using a VG Escalab 250 iXL ESCA instrument form VG Scientific. A monochromatic Al-Kα radiation (hv=1486.92 eV) and take off angle of 90º relative to the sample surface were used. The measurements were carried out in a Constant Analyzer Energy mode (CAE) with 100 eV pass energy for survey spectra and 20 eV pass energy for high resolution spectra. Charge referencing was adjusted by setting the lower binding energy hydrocarbon C_{1s} peak at 285.0 eV. Overlapping peaks were resolved into their individual components by XPSPEAK 4.1 software.

3.3.4 Fourier-transform infrared spectroscopy (FTIR)

The surface chemical analysis was also performed by FTIR spectroscopy using an IRPrestige 21 FTIR spectrophotometer with an attenuated total reflectance (ATR) device from Shimadzu. Spectra were taken with a resolution of 4 cm^{-1} and averaged over 36 scans.

3.3.5 Scanning electron microscopy (SEM)

The surface morphology changes were observed by S360 SEM Equipment from Leica Cambridge, UK. Prior to SEM examination, a conductive thin gold film was deposited on the samples surface by a Sputter Jeol JFC 1000.

3.3.6 Contact angle measurements

Changes of the surface wettability and the surface free energy for the modified surfaces were evaluated by contact angle measurements. Static contact angle measurements were carried out by the sessile drop method using a contact angle meter OCA 15+ with high-performance image processing system from DataPhysics Instruments. A drop (1μL) of the used liquids (methylene iodide, glycerol or formamide) was added by a motor driving syringe at room temperature. Two different samples of each material were used and at least three measurements were carried out for each sample. The presented data correspond to the final average value. The surface energy and its components (polar and dispersive) were calculated by means of the Owens, Wendt, Rabel and Kaelble (OWRK) method [16], using the contact angle values obtained both for glycerol and methylene iodide. Additionally, the Lewis acid and basic contributions to the surface energy were calculated using the acid-base method (AB method). This method based on the Van Oss-Chaudury-Good theory allowed determining the ion pair acceptor and ion pair donor behavior of the studied surfaces. The AB method requires at least a three liquids system from which two should be polar and one non-polar. Glycerol and formamide were used as polar liquids and methylene iodide was employed as the non-polar one. Contact angle measurements were also performed using water, but the values were not included in the calculations of the surface free energy, because such values lack of physical meaning, as discussed below.

3.3.7 Cell culture

Direct contact assays were performed in order to evaluate the effect of the applied surfaces treatments on cell adhesion and proliferation. A human osteosarcoma cell line (SaOs-2), an immortalized cell line with an osteoblastic phenotype, was obtained from European Collection of Cell Cultures (ECACC, UK) and was used in the cell culture studies. The cells were cultured in Dulbecoo's modified Eagle's medium (DMEM; Sigma-

Aldrich, Inc, USA) supplemented with 10000U/ml penicillin-G sodium, 10000 µg/ml streptomycin sulfate and 25 µg/ml amphotericin B in a 0.85 % saline (Gibco, Invitrogen Corporation, UK) and 10% of heat-inactivated fetal bovine serum (FBS; Biochrom AG, Germany) in a humidified atmosphere with 5 % of CO_2. Cells were seeded onto the materials at a concentration of $3x10^4$ cells/ml, 1ml per well and incubated for 1, 3 and 7 days.

Prior culturing, all samples were sterilized with ethylene oxide (EtO) under the conditions previously described [17].

3.3.8 Cell morphology

Cell morphology was observed by SEM and optical microscopy at each time point. The cultured materials were washed with 0.1 M phosphate buffered saline solution (PBS, Sigma Chemical Co., USA) and then fixed with 2.5 % glutaraldehyde (BDH, UK) solution in PBS for 30 min at room temperature. Once again, the membranes were washed and kept in PBS at 4 ºC until being stained or prepared for SEM observation. When optical microscopy was used for observation, the surface of the materials was stained with 0.4% methylene blue solution in water and examined in an Axioplan Imager Z1 from Zeiss, Germany. The samples, subjected to SEM observation, were first dehydrated by gradient ethanol concentrations. Complete drying was achieved by using Hexamethyldisilazane (HMDS; Electron Microscopy Sciences, USA) to substitute critical point drying equipment. After overnight drying, samples were coated by sputtering of gold and observed by SEM.

3.3.9 MTS assay

Cell viability was quantified by MTS assays. The assays were performed after 1, 3 and 7 days. The cultured materials were washed with 0.1M phosphate buffered saline solution (PBS, Sigma Chemical Co., USA) and then treated with 500 µl of MTS solution in DMEM culture medium without phenol red (Sigma-Aldrich, Inc, USA). The cell culture plates were incubated during 3 hours at 37 ºC in a humidified atmosphere of 5% CO_2. Optical Density (OD) was read in a microplate reader (Bio-Tek, USA) at 490 nm. The reported data are averaged over two sets of assays. Four replicates of each material per set were used.

3.4 Results and discussion

Tailoring material surface properties is of great importance especially for biomedical materials in direct contact with the body environment. Changes in surface chemistry/topography may enhance the cell adhesion and proliferation leading to an improvement of the material biocompatibility. The hypothesis, checked out in this study, is that alterations in surface polarity of chitosan membranes by simple O_2 plasma treatment or by plasma activation and subsequent grafting of monomers with ionisable, hydrophilic groups will lead to significant changes in cell behavior. The ultimate aim of this study is to get some insights of general trends leading to better materials biocompatibility in what concerns their interactions with biological systems (proteins, cells, etc).

3.4.1 XPS analysis

The XPS analysis was carried out to determine the surface chemical composition of modified and non-modified materials. As it was expected, three main elements: carbon, oxygen and nitrogen were present in the survey spectrum of chitosan membranes. Silicon was also detected for all samples at a concentration around 3 at%. The chitosan used in this study is produced from crab shells and it seems that the manufacturing and purification methods can not remove the entire silicon. Other elements (Cl, Ca, Al, Mo and Sn) appear in the composition of some samples, normally in very small concentration (less than 0.5 at%), and were excluded for the element analysis (at%) showed in Table 3.1.

Table 3.1 Chemical composition of untreated and modified materials determined by XPS

Material	C_{1s} (%)	O_{1s} (%)	N_{1s} (%)	S_{2s} (%)	Si_{1s} (%)	O:C ratio
Chitosan	71.5	21.8	3.4	-	3.4	0.30:1
Plasma O_2	65.0	24.4	8.2	-	2.3	0.38:1
AA grafting	74.1	19.6	2.9	-	3.3	0.26:1
VSA grafting	70.2	22.6	3.5	0.3	3.3	0.32:1

The modification only by oxygen plasma resulted in higher oxygen content for the treated samples compared to the untreated ones. When vinyl sulfonic acid was grafted onto the activated surfaces, a characteristic signal corresponding to Sulfur (S_{2s}) was present in the

survey spectrum of the modified samples. The S_{2s} transition was used to quantify this element, because the most intense and quantitative signal for Sulfur (S_{2p}) was overlapped with the Si_{2s} (loss) peak.

Figure 3.1 shows the C_{1s} high-resolution spectra of the studied materials. The respective data are summarized in Table 3.2. The C_{1s} core level spectrum of chitosan membranes reveals four peaks. The 285.0 eV peak was assigned to C-H and C-C bonds in chitosan backbone. The peak at 285.57 eV corresponds to C-NH_2 from glucosamine rings. The peak present at 286.7 1eV was assigned to C-O, C-OH and C-N-C=O and the peak at 288.18 eV to O-C-O and N-C=O chemical bindings. A lost in the relative intensity of the hydrocarbon peak was measured after plasma treatment. This is accompanied by an increase on the intensity of oxygen containing bands. After AA grafting a new band appeared in the C_{1s} high resolution spectra (289.2 eV). This band was assigned to the O=C-O lateral group in the grafted polymer. The absence of the C-SO_3 band from the spectra of VSA modified membranes was somewhat unexpected, since the presence of the S_{2s} peak in the survey spectrum confirmed that VSA was successfully grafted. The difficulty to resolve the C-SO_3 band arises from the small chemical shift [18] of the C-S band, which is superimposed on the band of the hydrocarbons chemical bonds in chitosan observed at 285eV. Additionally, the relatively small amount of Sulfur (see Table 3.1) and the high intensity of the hydrocarbons band is hindering the correct resolution of the bands.

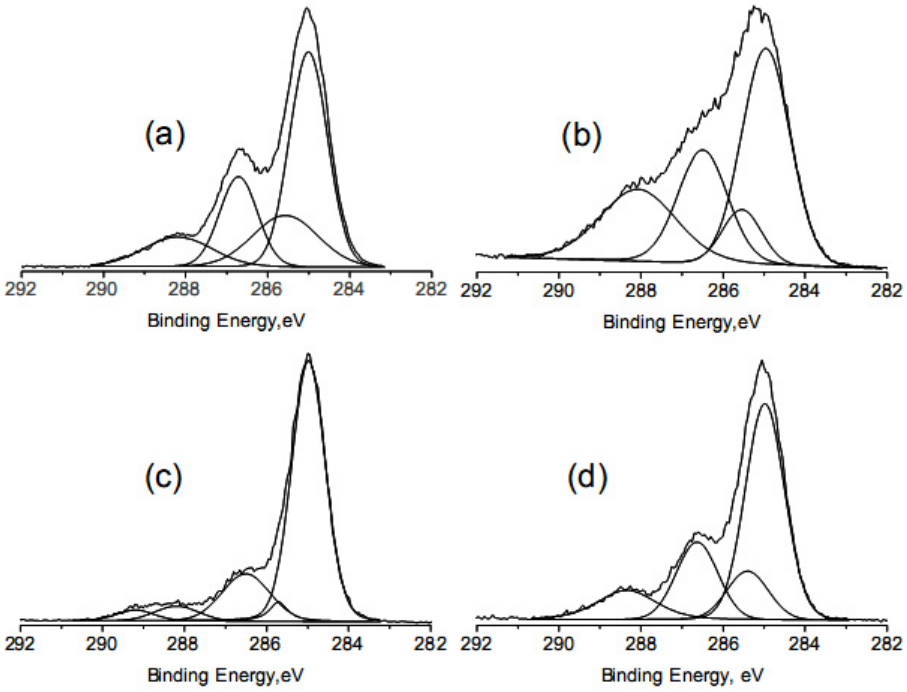

Figure 3.1 C_{1s} core level spectra of non treated chitosan (a), plasma treated (b), AA grafted (c) and VSA grafted (d) materials.

Table 3.2 C1s core level spectra of untreated and modified samples; composition (%) and Binding Energy (eV, in parenthesis)

Sample	C-H	C-NH_2	C-O	C=O	O=C-O
Chitosan	48.7 (285.00)	19.8 (285.57)	20.1 (286.71)	11.9 (288.18)	-
Plasma O_2	43.4 (284.96)	8.8 (285.54)	23.9 (286.49)	23.9 (288.07)	-
Grafted AA	70.4 (284.97)	3.9 (285..71)	17.7 (286.50)	4.9 (288.19)	3.1 (289.20)
Grafted VSA	54.69 (284.94)	12.65 (285.41)	20.32 (286.63)	12.348 (288.34)	-

3.4.2 SEM analysis

Etching processes are unavoidable when polymers are exposed to plasma. Usually, these processes are very dependent on the used time and power and they are limited to the topmost material surface layer. SEM was used to observe eventual morphology changes of the materials surface. SEM micrographs of the untreated chitosan film revealed a smooth surface without pores, nodes or defects (data not showed). The analysis of the treated materials indicated that none of the modification process, either oxygen plasma treatment or grafting polymerization, affected the surface morphology of the modified membranes.

3.4.3 FTIR analysis

Figure 3.2 shows the FTIR spectra of untreated and modified membranes. In the chitosan spectrum (Figure 3.2(a)), the NH_2 characteristic absorption band is observed at 1600cm^{-1}. The bands assigned to the stretching vibration of C-O-C linkages in the saccharide structure (glucosamine rings) appear at 1155, 1067, 1030 and 894 cm^{-1}. The absorptions at 1324 and 1380 cm^{-1} reflect the stretching vibration of C-N bond (amide III) and the C-H binding modes of the methylene, respectively. Very weak bands at 1420 and 1645 cm^{-1} corresponding to the C-H bond in the methyl and stretching vibration. of carbonyl group (amide I) reveal the high deacetylation degree of the used chitosan [19].

FTIR spectra of the treated materials (Figures 3.2(b), (c), and (d)) show no significant difference compared with the untreated material. This is not surprising since it is well

known that at each internal reflection, the penetration depth of the IR radiation beam is around 1-5 μm into the polymer membrane [20]. Moreover, the thickness of the modified layer by plasma treatments is usually confined to few nanometres of the top surface layer and has no effect on the bulk of treated polymers [13]. On the other hand, the changes indicated by the XPS analysis (more sensitive) reveals that the performed surface modifications have no effect on the bulk properties of the material but only on the very top surface layer.

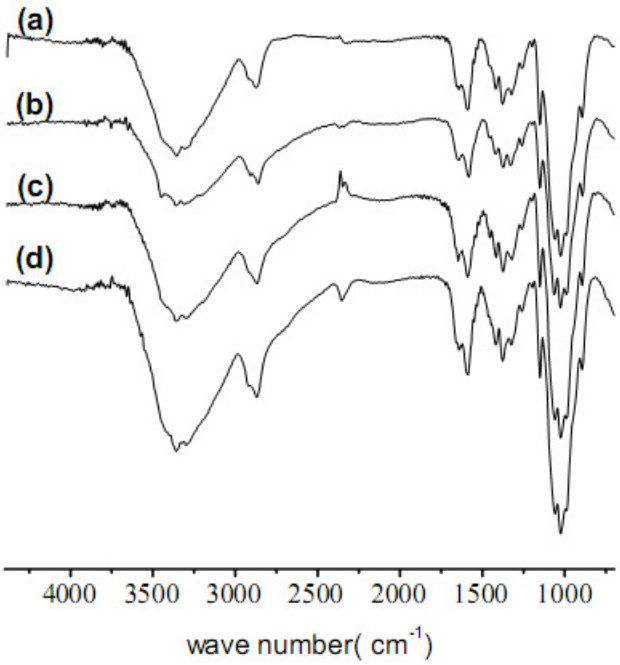

Figure 3.2 FTIR-ATR spectra of: untreated chitosan (a) and modified by O_2 plasma (b); AA grafted (c) and VSA grafted (d) materials.

3.4.4 Contact angle measurements

The energy of the surface, which is directly related to its wettability, is a useful parameter that has often been strongly correlated with the cell-biomaterial interfacial interactions. Unfortunately, there are not direct methods to measure surface energy or surface tension of solids. However, a number of indirect empirical and semiempirical methods have been developed based on contact angle measurements. Table 3.3 shows the equilibrium contact angle values of the used solvents for both untreated and modified materials.

Table 3.3 Equilibrium contact angle values for untreated and modified samples (air, room temperature)

Material	Glycerol C. Angle(º)	Diiodomethane C. Angle(º)	Formamide C. Angle(º)
Chitosan	83.0 ± 2.0	52.35 ± 2.3	68.4 ± 1.3
Plasma treated	73.0 ± 3.7	48.95 ± 4.0	50.8 ± 5.7
VSA grafted	78.1 ± 1.1	55.4 ± 0.7	51.8 ± 4.6
AA grafted	70.6 ± 2.7	52.0 ± 3.2	34.6 ± 4.7

Owens, Wendt, Rabel and Kaelble method has been widely used for the calculation of the total surface energy and its corresponding polar and dispersive components. Generally, the polar component value is used as an estimation of the concentration of the polar groups on the polymer surface. The surface energy values obtained for untreated, plasma treated and grafted samples are shown in Table 3.4. No apparent significant changes in the total surface energy were observed for any of the studied samples. However, the introduction of additional polar groups by the modification processes was confirmed by an increase in the values of the polar components for all treated samples. Plasma activation itself resulted in a higher value of the polar component (3.5mN/m) compared to the one calculated for untreated chitosan (1.1mN/m). The same effect was observed after VSA grafting (3.0mN/m). The most noteworthy difference was observed for AA grafted samples for which a value of 5.9mN/m was calculated.

Usually, the term “polar” is used to designate three classes of compounds [21], namely: *i*) dipolar compounds; *ii*) hydrogen bonding compounds and *iii*) compounds that interact as Lewis acids and bases. The Van Oss-Chaudhury-Good theory distinguishes the acid-base (AB) interactions as a component of the surface free energy:

$$\gamma_S = \gamma_S^{LW} + \gamma_S^{AB} \tag{3.1}$$

where γ_S^{LW} is the surface energy corresponding to Lifshitz-Van der Waals forces and γ_S^{AB} describes the contribution of the AB interaction to the surface tension:

$$\gamma_S^{AB} = 2 \cdot \left(\gamma_S^- \cdot \gamma_S^+\right)^{1/2} \tag{3.2}$$

where γ_S^- and γ_S^+ represent the ion pair donor (Lewis base) and the ion pair acceptor (Lewis acid) contributions, respectively.

Table 3.4 Surface Energy (± standard deviation) and its components calculated by OWRK (glycerol and diiodomethane) and AB (glycerol, formamide and diiodomethane) methods

Material	OWRK method			AB method			
	γ_s (mN/m)	γ_s^d (mN/m)	γ_s^p (mN/m)	γ_s (mN/m)	γ_s^{LW} (mN/m)	γ_s^+ (mN/m)	γ_s^- (mN/m)
Chitosan	32.9±0.3	31.8±0.3	1.1±0.2	32.7±0.3	32.7±0.0	0.0±0.0	3.0±0.3
Plasma treated	35.8±0.6	32.2±0.3	3.5±0.5	35.4±0.9	35.0±0.0	0.0±0.0	9.1±1.0
AA grafted	35.4±1.0	29.5±0.4	5.9±0.9	34.6±1.5	32.6±0.0	0.1±0.1	14.6±1.6
VSA grafted	31.9±0.5	28.9±0.3	3.03±0.5	31.0±0.1	31.0±0.1	0.0±0.0	12.1±1.0

γ_s =surface energy; γ_s^d and γ_s^p = dispersive and polar components of surface energy calculated by OWRK method; Lifshitz-Van der Walls (γ_s^{LW}), acid (γ_s^+) and basic (γ_s^-) components of the surface energy calculated by AB method

The total surface energy (γ_S) values obtained by the AB method correlate very well with the values achieved using the OWRK method (see Table 3.4). Over again, little differences were found between the total surface energy values throughout the several studied surfaces. Moreover, the acid component was found to be zero or negligible if compared with the basic component. This means that the modified surfaces present a monopolar character. It is interesting to notice that the tendency observed for the polar component of the surface energy calculated according to the theory of OWRK is similar to that observed for the basic component calculated using the acid-base theory. The non-modified chitosan membranes present the lower values (3.0mN/m), followed by the O_2 plasma modified and the VSA grafted films (9.1 and 12.1mN/m respectively). Samples grafted with AA present the highest value of the basic component (14.6mN/m). We found that this tendency is strongly correlated with the cell behavior, as detailed in the following section.

The water contact angle values were not used in the computation of surface energy, because these values lack of physical meaning. If fact, the chitosan membranes uptake water up to 130% of its own weight [4]. In this way, the measured contact angle is associated with non-equilibrium events resulting from the swelling of the membranes. This swelling also creates a surface deformation in the samples beneath the liquid water drop. This effect is more pronounced in the modified surfaces in which the sorption events were

notably faster, likely due to its increased hydrophilicity. Moreover, when the water contact angle values were tentatively included in the computation of the surface energy using both methods, the resultant correlation coefficients were found to be close to zero (good correlation should give a correlation coefficient close to 1). These initial calculations also presented high chi-square values, revealing that the theories would not describe such a set of experimental data. In this sense, the water contact angle was skipped from the calculations.

3.4.5 Cell morphology

Anchorage-dependent cells (fibroblast, osteoblast or endothelial cells) need to adhere in order to proliferate. Since the materials studied in this work are to be used for bone-guided regeneration, the effect of the surface modifications was assessed by cells with the osteoblastic phenotype, the principal cell type facing these devices *in vivo*.

Figure 3.3 shows the optical photographs of cells adhered to untreated and modified materials after 3 and 7 days of culture. It can be observed that cells adherent to chitosan surfaces did not show the characteristic morphology of osteoblast-like cell at any of the tested times of culture, which may indicate a deficient long-tem cell response. Poor cell attachment on chitosan has been reported [5] before. The AA surface grafting did not induce any improvement in the cell behavior; cells presented a round shape and the surface showed reduced cell adhesion. On the other hand, SaOs-2 in contact with plasma treated and VSA grafted materials demonstrate very good adherence to these surfaces. These treatments appear to render chitosan membranes with appropriate physico-chemical properties for adherence and proliferation of SaOs-2. This hypothesis was confirmed by the observation after 7 day of culture when a significant surface area was covered by a monolayer of cells (Figure 3.3). Moreover, cell morphology was positively affected by both treatments. SEM micrographs for 3 days of culture (Figure 3.4) showed that cells present the typical morphology for osteoblastic cells with cytoplasm extensions.

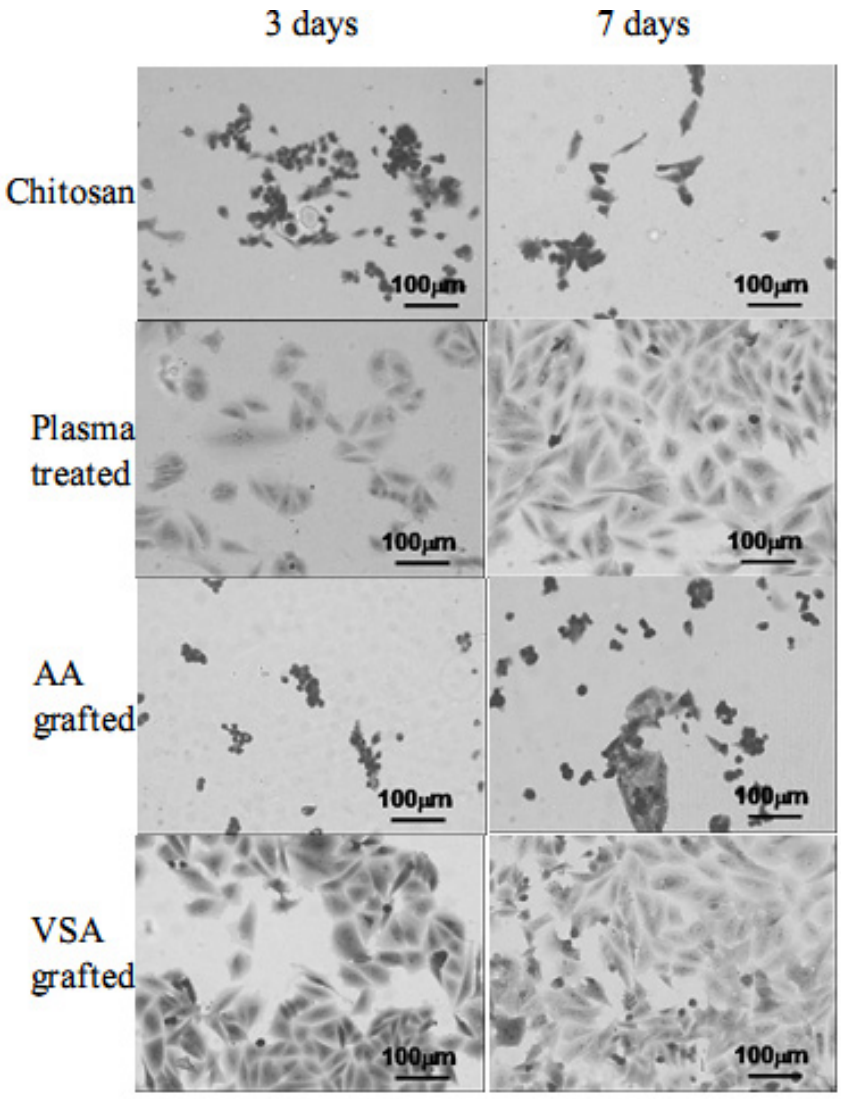

Figure 3.3 Optical micrographs of osteoblast-like cells stained with methylene blue cultured for 3 and 7 days.

In their normal mechanism, cells in contact with the surface will initially attach, adhere and spread. Protein adsorption is a determining step for this first phase and will further control cell morphology, as well as their proliferation capacity. It is proved [22] that the type of adsorbed proteins and their orientation are related to the surface properties, especially to the surface energy. Moreover, it has been reported [23] that the dispersive and polar components of the surface energy are of key importance for the interfacial interactions. Therefore, an optimal distribution of the two components is required. As can be seen from the contact angle results (Table 3.4), neither very low polar component (untreated chitosan) nor very high (AA grafted material) were favorable for the correct cell attachment/morphology. On the contrary, intermediate polar components achieved for

plasma treated and VSA grafted samples, influenced positively the cell behavior on these surfaces.

It has been also reported that Lewis basicity is a key factor in surface biocompatibility[24]. In the herein studied systems, the surfaces holding moderate basic component values (Table 3.4) presented improved SaOs-2 behavior, if compared to the samples showing both lower and higher values for the Lewis basicity. The similarity between this result and the one already described for the correlation between the surface energy polar component and the cell behavior is noteworthy.

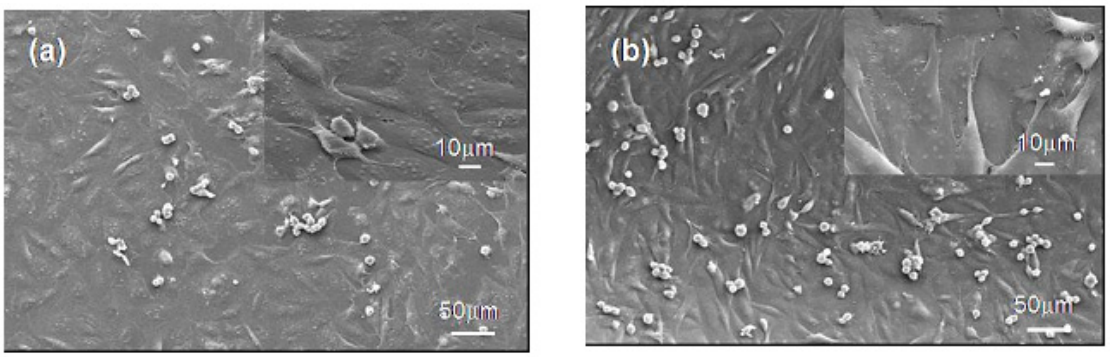

Figure 3.4 SEM micrographs showing SaOs-2 cultured for 3 days on the surface of plasma treated (a) and VSA grafted (b) membranes.

3.4.6 MTS assay

The MTS tests were carried out in order to further evaluate cell viability on treated and untreated membranes (Figure 3.5). Metabolically active cells are capable of reducing a tetrazolium compound (MTS) in an aqueous soluble formazan product. Non-viable cells rapidly lost their ability to reduce the MTS. Therefore, the production of the colored formazan products is proportional to the number of viable cells.

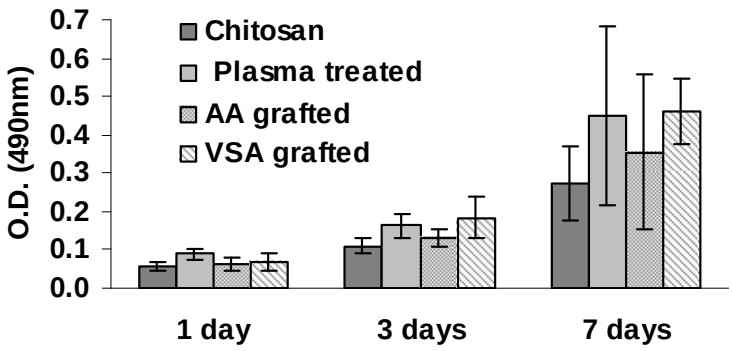

Figure 3.5 Viability of SaOs-2 adhered to untreated and modified surfaces after 1, 3 and 7days of culture at 5% CO_2 at 37ºC.

Considering the results reported above on the cell morphology, plasma treated and VSA grafted materials were expected to present better cell viability and proliferation than the untreated and AA grafted samples. The MTS results confirm those differences; the optical density measurements indicate that plasma and VSA treatments lead to a higher number of viable cells adhered to the surface of the materials after 1 day of culture compared to untreated or AA grafted chitosan membranes. The observed effect increases with the time of culture. Once again, these results supported the hypothesis that plasma and VSA treatment induce a positive effect on osteoblast-like cells.

3.5 Conclusions

A successful surface modification by plasma induced radical polymerization of acrylic and sulfonic polar monomers onto solvent cast chitosan membranes was performed. XPS results confirmed the polymer grafting on the membranes surface. FTIR-ATR spectra indicated that this modification took place only on a very thin layer of the surface and the materials bulk properties were not affected. Contact angle measurements showed that the total surface energy does not change significantly after the applied treatments. However, an increased polar component was found for all treated materials. Moreover, the AB method showed that this increase is generally due to Lewis base's contribution. Cell direct contact test with SaOs-2 showed that oxygen plasma treatments and VSA grafting substantially improved cell adhesion and proliferation compared with untreated chitosan. These results were correlated with both polar and basic components of the Surface Energy, showing that materials with intermediate polar and basic components positively affect cell adhesion and proliferation.

3.6 Acknowledgments

The authors acknowledge EU Marie Curie Actions, Alea Jacta EST for providing the PhD Grant to Paula M. López-Pérez, Portuguese Foundation for Science and Technology (FCT) for provide the postdoctoral grant to I. Pashkuleva (BPD/8491/2002). This work was carried out under the scope of the European NoE EXPERTISSUES (NMP3-CT-2004-500283).

3.7 References

1. Gallardo, A.; Aguilar, M.R.; Elvira, C.; Peniche, C.; San Roman, J. *Chitosan-Based Microcomposites- From Biodegradable Microparticles to Self-Curing Hydrogels*. Biodegradables Systems in Tissue Engieering and Regenerative Medicine, ed. R.L. Reis and J. San Roman. 2005, Boca Raton, U.S.A.: CRC Press. 145-161.

2. Kumar, M.N.V.R. A review of chitin and chitosan applications*. Reactive & Functional Polymers*, 2000, **46,** (1), 1-27.

3. Khor, E.; Lim, L.Y. Implantable applications of chitin and chitosan*. Biomaterials*, 2003, **24,** (13), 2339-2349.

4. Silva, R.M.; Silva, G.A.; Coutinho, O.P.; Mano, J.F.; Reis, R.L. Preparation and characterisation in simulated body conditions of glutaraldehyde crosslinked chitosan membranes*. Journal of Materials Science-Materials In Medicine*, 2004, **15,** (10), 1105-1112.

5. Zhu, X.; Chian, K.S.; Chan-Park, M.B.E.; Lee, S.T. Effect of argon-plasma treatment on proliferation of human-skin-derived fibroblast on chitosan membrane in vitro*. Journal of Biomedical Materials Research Part A*, 2005, **73A,** (3), 264-274.

6. Mori, T.; Okumura, M.; Matsuura, M.; Ueno, K.; Tokura, S.; Okamoto, Y.; Minami, S.; Fujinaga, T. Effects of chitin and its derivatives on the proliferation and cytokine production of fibroblasts in vitro*. Biomaterials*, 1997, **18,** (13), 947-951.

7. Boyan, B.D.; Hummert, T.W.; Dean, D.D.; Schwartz, Z. Role of material surfaces in regulating bone and cartilage cell response*. Biomaterials*, 1996, **17,** (2), 137-146.

8. Elvira, C.; Yi, F.; Azevedo, M.C.; Rebouta, L.; Cunha, A.M.; San Ramon, J.; Reis, R.L. Plasma- and chemical-induced graft polymerization on the surface of starch-based biomaterials aimed at improving cell adhesion and proliferation*. Journal of Materials Science-Materials in Medicine*, 2003, **14,** (2), 187-194.

9. Pashkuleva, I.; Marques, A.P.; Vaz, F.; Reis, R.L. Surface modification of starch based blends using potassium permanganate-nitric acid system and its effect on the adhesion and proliferation of osteoblast-like cells*. Journal of Materials Science-Materials in Medicine*, 2005, **16,** (1), 81-92.

10. Sun, H.X.; Zhang, L.; Chai, H.; Chen, H.L. Surface modification of poly(tetrafluoroethylene) films via plasma treatment and graft copolymerization of acrylic acid*. Desalination*, 2006, **192,** (1-3), 271-279.

11. Klee, D.; Ademovic, Z.; Bosserhoff, A.; Hoecker, H.; Maziolis, G.; Erli, H.J. Surface modification of poly(vinylidenefluoride) to improve the osteoblast adhesion*. Biomaterials*, 2003, **24,** (21), 3663-3670.

12. Pashkuleva, I.; Reis, R.L. *Surface activation and modification- a Way for Improving the Biocompatibility of Degradable Biomaterials*. Biodegradables Systems in Tissue Engieering and Regenerative Medicine, ed. R.L. Reis and J. San Roman. 2005, Boca Raton, U.S.A.: CRC Press. 429-454.

13. Chu, P.K.; Chen, J.Y.; Wang, L.P.; Huang, N. Plasma-surface modification of biomaterials. *Materials Science & Engineering R-Reports*, 2002, **36,** (5-6), 143-206.

14. Hirai, A.; Odani, H.; Nakajima, A. Determination Of Degree Of Deacetylation Of Chitosan By H-1-Nmr Spectroscopy. *Polymer Bulletin*, 1991, **26,** (1), 87-94.

15. Terbojevich, M.; Cosani, A.; Muzzarelli, R.A.A. Molecular parameters of chitosans depolymerized with the aid of papain. *Carbohydrate Polymers*, 1996, **29,** (1), 63-68.

16. Owens, D.K.; Wendt, R.C. Estimation of Surface Free Energy of Polymers. *Journal of Applied Polymer Science*, 1969, **13,** (8), 1741.

17. Reis, R.L.; Mendes, S.C.; Cunha, A.M.; Bevis, M.J. Processing and in vitro degradation of starch/EVOH thermoplastic blends. *Polymer International*, 1997, **43,** (4), 347-352.

18. Briggs, D. *Surface analysis of polymers by XPS and static SIMS*. 1998, Cambridge: Cambridge University Press. 47-87.

19. Li, Y.P.; Liu, L.; Fang, Y.E. Plasma-induced grafting of hydroxyethyl methacrylate (HEMA) onto chitosan membranes by a swelling method. *Polymer International*, 2003, **52,** (2), 285-290.

20. Ratner, B.D. *Surface properties of materials*. Biomaterials Science, ed. B.D. Ratner, et al. 1996, San Diego, U.S.A: Academic Press. 21-35.

21. Vanoss, C.J.; Chaudhury, M.K.; Good, R.J. Monopolar Surfaces. *Advances in Colloid and Interface Science*, 1987, **28,** (1), 35-64.

22. Liu, L.Y.; Chen, S.F.; Giachelli, C.M.; Ratner, B.D.; Jiang, S.Y. Controlling osteopontin orientation on surfaces to modulate endothelial cell adhesion. *Journal of Biomedical Materials Research Part A*, 2005, **74A,** (1), 23-31.

23. Kaelble, D.H.; Moacanin, J. Surface-Energy Analysis of Bioadhesion. *Polymer*, 1977, **18,** (5), 475-482.

24. Ostuni, E.; Chapman, R.G.; Holmlin, R.E.; Takayama, S.; Whitesides, G.M. A survey of structure-property relationships of surfaces that resist the adsorption of protein. *Langmuir*, 2001, **17,** (18), 5605-5620.

Chapter 4

Surface phosphorylation of chitosan significantly improves Osteoblast cells viability, attachment and proliferation

4.1 Abstract

Chitosan biocompatibility is often associated with the structural similarities with glycosaminoglycans (GAGs). Although all of the GAGs are build from repeating disaccharide units and some of them contain N-glucosamine (the main hexosamine in the chitosan backbone), all of them do also contain negatively charged functional groups. These charged units are believed to have a crucial role for the formation of proteoglycans and hence for key biochemical processes/signaling related with cell functionality and survival. Lack of these groups in chitosan structure could be the reason for the previously observed poor cell adhesion to this material. Herein, we are reporting that plasma induced grafting of negatively charged phosphonic groups can induce remarkably distinguishable cell response and to significantly improve the adhesion, proliferation and viability of osteoblast cells. The proposed plasma induced polymerization is very simple and versatile method and can be easily adapted to other materials and different negatively charged units.

This chapter is based on the following publication:
Paula M. López-Pérez; Ricardo M.P. da Silva; Carmen Serra; Iva Pashkuleva; Rui L. Reis. **Journal of Materials Chemistry**, 2010, 20 (3): 483-491.

4.2 Introduction

The presence of complex polysaccharides in different tissues has been recognized for more than 100 years. In connective tissues, for example cartilage, they comprise about 30 wt%[1]. Some polysaccharides represent the main constituent part of extracellular matrix (ECM). Hence, they are involved in a plethora of biological processes and thus they are crucial in the control of their normal metabolic course. Structural investigation revealed similarities in between these polysaccharides [1]: they are composed from disaccharide repeating units; all contain hexosamine (glucosamine or galactosamine) and finally they do contain negative functionalities (mostly carboxyl and sulfate) as well. Their common name, glycosaminoglycans (GAGs), comprises these similarities.

Chitosan, a linear polysaccharide composed of *N*-glucosamine and *N*-acetylglucosamine units, has been accepted in the biomaterials field as a structural analogue of GAGs. Its structure together with its relatively low price has imposed an intensive investigation on this polysaccharide as a material for a wide range of biomedical applications such as wound healing, gene/drug delivery, bone tissue repair and remodeling [2, 3]. Furthermore, its biodegradation leads to the release of aminosugars that can easily be excreted or incorporated into glycoproteins and GAGs metabolic pathways [4].

Besides these similarities, chitosan pKa value is about 6.1-7 [5] and recently, it was reported [6] that chitosan membranes isoelectric point (zeta potential equal to zero) occur at physiological conditions (pH 7.4). Hence, the positive surface charge arising from protonated amino groups, often claimed to predict cell adhesion to chitosan, should be excluded. Because the negative charge of the GAGs is associated with their bioactivity (via interactions with the positively charged amino groups of proteins), the lack of these groups in chitosan could be the reason for the poor cell adhesion on chitosan membranes reported previously by us [7, 8] and other authors [9-11]. Several studies have been investigating the possibility to overcome this major drawback by incorporation of carboxyl or sulfate groups into the chitosan backbone mimicking GAGs structure [6, 7, 12, 13]. However, when regeneration of mineralized tissues such as bone is the target, additionally to the protein-polysaccharide interactions, osseointegration and osteoconduction is also a must. These processes are triggered by the presence of other negatively charged groups, the phosphate groups. The importance of these groups has been recognized by the biomaterials scientific community for a long time and nowadays, phosphate coated (e.g. calcium phosphate) materials are commonly used for the purposes of bone regenerative medicine. Alternatively, polymers with grafted phosphate groups have been also designed to mimic the interactions occurring *in vivo*. In contrast to physically coated polymers,

grafting process results in formation of covalent bonds between the graft chains/groups and the polymer surface and therefore avoids their delamination assuring long term stability of the introduced chains. The fundamental step in grafting is the formation of reactive groups on the substrate surface. So far, only chemical activation/functionalization has been reported for obtaining phosphorylated derivatives of chitosan [14-20]. These reactions usually involve the use of organic solvents and high temperatures and therefore can easily affect the bulk properties (e.g. mechanical properties, degradation behavior) of the material. Hence, we are proposing an alternative approach for surface phosphorylation of chitosan membranes by plasma induced polymerization. Previously, we have demonstrated [7] that this method is an effective way for grafting of vinyl monomers. Its main advantage is that the surface properties can be enhanced selectively, while the bulk attributes of the materials remain unchanged. In this particular study, we are reporting the use of vinyl phosphonic acid (VPA) as a monomer. Polymers of VPA are known to be non-cytotoxic and had been successfully included onto polymers structures for cell behavior enhancement [21, 22]. It must be also noticed that the herein proposed method for surface phosphorylation does not remove the amino groups from the chitosan surface. The preservation of these distinct functionalities in chitosan is very important because they are associated with the specific biological properties of chitosan [6].

4.3 Materials and methods

4.3.1 Materials

Chitosan (CTS) from crabs' shells was purchased from Sigma Aldrich and purified prior use. Briefly, a 1% (w/v) chitosan solution in 1% aqueous acetic acid (AcOH) solution was prepared and filtered in order to remove the insoluble impurities. Subsequently, chitosan was coagulated adding NaOH (0.1 M) solution (final pH > 8) and the formed gel was washed with distilled water until a stable pH was reached. The obtained product was dehydrated by immersion in absolute ethanol, freeze-dried, ground to powder and dried overnight at 60ºC.

The degree of *N*-deacetylation (DD) of chitosan (93%) was determined by first derivative UV spectrophotometry, using both glucosamine (GluN) and *N*-acetylglucosamine (GluNAc) as standards for calibration [23]. A molecular weight of 790kDa was determined by viscometry using a 0.5 M AcOH/0.2 M AcONa aqueous solution. The measurements were performed at 25ºC and the Mark-Houwink parameters ($k = 3.5 \times 10^{-4}$; $a = 0.76$) [24] were

used for the calculations. Vinyl phosphonic acid (VPA) was purchased from Sigma-Aldrich and was used without further purification.

4.3.2 Preparation and modification of chitosan membranes

Chitosan 1% (w/v) was dissolved in 1% aqueous AcOH at slow stirring speed to avoid air bubble entrapment. The chitosan solution was poured into plastic Petri dishes at a ratio of 0.5 mg/cm^2. After drying at air, the membranes were neutralized by immersion in 0.1 M NaOH for 10 minutes and washed thoroughly with distilled water. The obtained membranes presented a smooth surface and thickness of around 50 μm.
Poly-(phosphonic acid) PVPA was grafted on the membranes surface by plasma induced polymerization. Chitosan membranes were placed into a radio frequency (13.56 MHz) plasma reactor (Plasma Prep5 equipment from Gala Instrument, Germany) and exposed to Oxygen plasma at 30 W of power for 15 minutes. During the treatment the pressure inside the reactor was maintained below 20 Pa by adjusting the gas flow. The so-activated membranes with free radicals formed on the surface were immersed in 100mM degassed solution of VPA in isopropanol and shaken at 37ºC for 2 hours. Subsequently, the membranes were thoroughly washed with isopropanol to remove the unreacted monomer and dried at room temperature.

4.3.3 Surface characterization

Surface chemical composition

Surface elemental analyses of non treated and modified samples was performed by X-Ray Photoelectron Spectroscopy (XPS) using an ESCALAB 200A instrument (VG Scientific, UK) with an aluminium anode (Al-Kα monochromatic radiation hν=1486.6 eV) operating at 15 kV (300 W). The measurements were performed at take off angle of 90º relative to the samples surface and a constant Analyser Energy mode (CAE). PISCES software was used for data acquisition and analysis. Survey spectra were acquired using pass energy of 50 eV over a binding energy range of 0 to 1100 eV and were used to calculate the elemental composition of the surfaces. High-resolution spectra for different elements (C1s, O1s and P2p) were obtained using a pass energy of 20 eV. Deconvoltion into subpeaks was performed by least-squares peak analysis software, XPSPEAK version 4.1, using the Gaussian/Lorenzian sum function. Background counts were subtracted

using a linear baseline and the sample charging was corrected assigning a binding energy of 285.0 eV to the saturated hydrocarbons C1s peak.

Time-of-Flight Secondary Ion Mass Spectrometry (ToF-SIMS) studies were performed using a ToF-SIMS IV instrument from ION-TOF GmbH, Germany. ToF-SIMS produces positive and negative mass spectra from the outer 10–20 Å of materials, and thus is capable of providing detailed information about the molecular structure of surfaces. The sputtering process is central to the SIMS technique and it can be described as a collision cascade of particles in the sample being analyzed. In this study, the samples were bombarded with a pulsed bismuth ion beam (25 keV) at 45° incidence over an area with size 500 μm^2. The energy of these primary ions is enough for bond breaking near to the collision site and therefore, the process results in extensive fragmentation and emission of secondary particles (neutral atoms and molecules, electrons, and ions). Particles produced in the top 2–3 monolayers of the sample have sufficient energy to overcome the surface binding energy and leave the sample. Only a small fraction of them are charged (10^{-6}–10^{-1}), and their positive or negative state depends on their electron configuration. The generated secondary ions were extracted with a voltage of 10 kV and their mass was determined by measuring their time of flight from the sample to the detector. Electron flood gun for charge compensation was necessary during the measurements. The experimental conditions (ion type, beam voltage and primary ion dose) were maintained constant for comparative studies. The mass spectra in both positive and negative mode and some specific informative secondary ion images for treated and modified samples are reported in the following section. Additionally, high mass resolution spectra were obtained by bunching the raw pulse. These spectra can be attained without concurrent loss of counts, however, this is at cost of spatial resolution (in this mode no better than 2-5 μm).

Surface topography

The topography of the samples was characterized by two different techniques: Optical profiler analysis was performed by an Interferometric profiler Wyko-NT 1100 (Veeco) using Vertical Scanning Interferometry (VSI) mode. The images were processed and analyzed with the analytical software package WycoVision®32. The Atomic Force Microscopy (AFM) characterization was performed in air atmosphere using a Multimode Nanoscope V (Veeco). Tapping mode was employed with non coated Phosphorous (n) dopped Silicon probe with cantilever length of 115 to 135 μm and resonant frequency from 257 to 342 kHz. Images were processed and analyzed by multimode software version V7.20 and analytical software package WycoVision®32.

Surface energy and water wettability

Static contact angle values were obtained by sessile drop method. Measurements were performed using a contact angle meter OCA 15+ (DataPhysics Instruments, Germany) with high performance image processing system. A 1 µl drop of the tested liquid was added at room temperature on the sample surface by a motor driving syringe. We used the three-solvent system: water (γ_s=72.8 mN/m) and glycerol (γ_s=64.0 mN/m) as polar liquids and methylene iodide (γ_s=50.8 mN/m) as non-polar one. At least six contact angle replicates per liquid-solid couple were measured and averaged. We calculated the surface tension from the contact angle data by two different methods: the Owens, Wendt, Rabel and Kaelble (OWRK) method [25] that discerns polar and dispersive components of the surface energy; and the acid-base method (AB method), which allows calculation of the Lewis acid and basic contributions using the van Oss-Chaudury-Good theory (vOCG) [26].
The chosen three solvent system can be used to compute the surface energy using the vOCG method, since it produces a set of well-conditioned equation system (low conditioning number) [27]. The surface energy components were calculated using the values of the liquid surface tension components obtained by Della Volpe and Siboni, which consider a reference scale for water that takes into consideration the different "strength" of water as acid or base [28].
Pure water adhesion tension was also calculated because it can be considered as a key measure of the water self-association structure. As a matter of fact, a straightforward correspondence has been claimed to occur between the physicochemical interfacial properties of water (scaled as water adhesion tension) and the biological response to biomaterials [29].

4.3.4 Cell culture

Since the materials studied in this work are to be used for mineralized tissue regeneration, the effect of the surface modifications was assessed by cells with the osteoblastic phenotype, the principal cell type facing these devices *in vivo*. A human osteosarcoma cell line (SaOs-2), an immortalized cell line with an osteoblastic phenotype, was purchased from European Collection of Cell Cultures (ECACC, UK) and cells were maintained at 37 ºC and 5% CO_2 in a humidified atmosphere. Dulbecoo's modified Eagle's medium (DMEM; Sigma-Aldrich, Inc, USA) supplemented with 10000 U/ml penicillin-G sodium, 10000 µg/ml streptomycin sulfate and 25 µg/ml amphotericin B in a 0.85% saline (Gibco,

Invitrogen Corporation, UK) and 10% of heat-inactivated fetal bovine serum (FBS; Biochrom AG, Germany) was used as cell culture medium.

Membranes were cut in a circular shape (ϕ=14 mm) and were sterilized by 70% ethanol aqueous solution. Subsequently, the substrates were washed with sterile phosphate buffered saline solution (PBS, Sigma Chemical Co., USA) to remove the remaining ethanol. The sterile samples were placed into 24 well culture plates and seeded with SaOs-2 ($3.3x10^4$cells/ml). Cells were cultured onto the materials for 1, 3, 7 and 14 days at 37 ºC, 5% CO_2 in a humidified atmosphere in order to follow their behavior in contact with the studied surfaces.

The morphology of SaOs-2 cells growing on untreated and modified chitosan membranes was observed by Scanning Electron Microscopy (S360, Leica Cambridge, UK). After each predetermined incubation time, cells were fixed using a 2.5% glutaraldehyde (Sigma, USA) solution in PBS. Prior the analysis, the samples were dehydrated by graded ethanol solutions (25%, 50%, 70%, 90% and 100%).

MTS assay and calcein-AM (MolecularProbes) staining were used to analyze cell viability. The cultured materials were incubated (3 hours, 37ºC, humidified atmosphere of 5% CO_2) with 500 µl of MTS solution in DMEM culture medium without phenol red (Sigma-Aldrich, Inc, USA). Optical Density (OD) was read in a microplate reader (Bio-Tek, USA) at 490 nm. For Calcein AM staining, the samples were treated with 0.002% calcein-AM solution in DMEM culture medium and incubated in dark for 15 minutes at 37ºC in a humidified atmosphere of 5% CO_2. Cells fluorescence was examined by an Axioplan Imager Z1 from Zeiss, Germany.

Cell proliferation was evaluated by DNA quantification. Cells were lysed by osmotic and thermal shock and the obtained supernatant was used for DNA analyse. DNA content along the time of culture using the PicoGreen dsDNA kit (MolecularProbes) and the fluorescence was read (485 nm/528 nm of excitation/emission) in a microplate reader and the DNA amounts calculated from a standard curve.

The MTS and DNA quantification data were subjected to statistical analysis and are reported as mean $\pm$ standard deviation. ANOVA test for independent samples were performed and the differences were considered statistically significant if $p < 0.05$.

4.4 Results and discussion

4.4.1 Surface Chemistry

The XPS spectrum of untreated chitosan membranes confirms the presence of C (63.2%), O (27.3%) and N (5.1%). Although at lower percentage, Si (4.3%) was also detected in the atomic composition of chitosan surface. Silicon is a component of crustacean shells, from which chitin is extracted and then converted into chitosan and it seems to be not completely removed during that process. After the applied surface treatment, the survey spectrum of PVPA grafted membranes showed two additional peaks (see support information Figure 4.SI1), allocated at 128.3 and 185.2 eV. These peaks were assigned to P2p and P2s respectively and confirmed the successful grafting with PVPA, incorporating 2 atomic% (at%) of phosphorous (see support information Table 4.SI1). Additional details about the surface chemical composition were obtained by high resolution spectra of C1s, O1s and P2p of unmodified and PVPA grafted chitosan membranes (Figure 4.1). The corresponding relative peaks are listed in Table 4.1.

Table 4.1 Relative peaks composition (%) of C1s, O1s high resolution spectra

C1s core level			O1s core level		
Peak BE/eV	**CTS**	**CTS-VPA**	**Peak BE/eV**	**CTS**	**CTS-VPA**
285.0	40.5	36.6	531.8	0.0	20.2
286.6	44.6	44.4	533.1	58.2	45.1
288.2	14.9	19.0	533.7	41.8	34.6

The C1s high resolution spectrum of chitosan is composed by three components. The peak at 285.0 eV was assigned to C-H/C-C chemical bonds of the chitosan backbone. Because amines presence induces a small chemical shift (around 0.6 eV) [30], the C-NH_2 signal does not appear as individual peak but it is overlapped by the C-H/C-C. The second peak is centered at 286.7 eV and was assigned to C-OH, C-O and C-N- bonds. Finally, the C=O and O-C-O/N-C=O groups from the acetylated rings appeared at 288.2 eV. The C1s high-resolution spectrum of PVPA grafted samples was very similar to the spectrum of untreated chitosan. The characteristic C-PO_3 signal (around 287.5 eV) [31] is overlapped by the peak centered at 288.1 eV and the increased relative area measured for this peak compared with untreated chitosan (Table 4.1) is consistent with this overlapping.

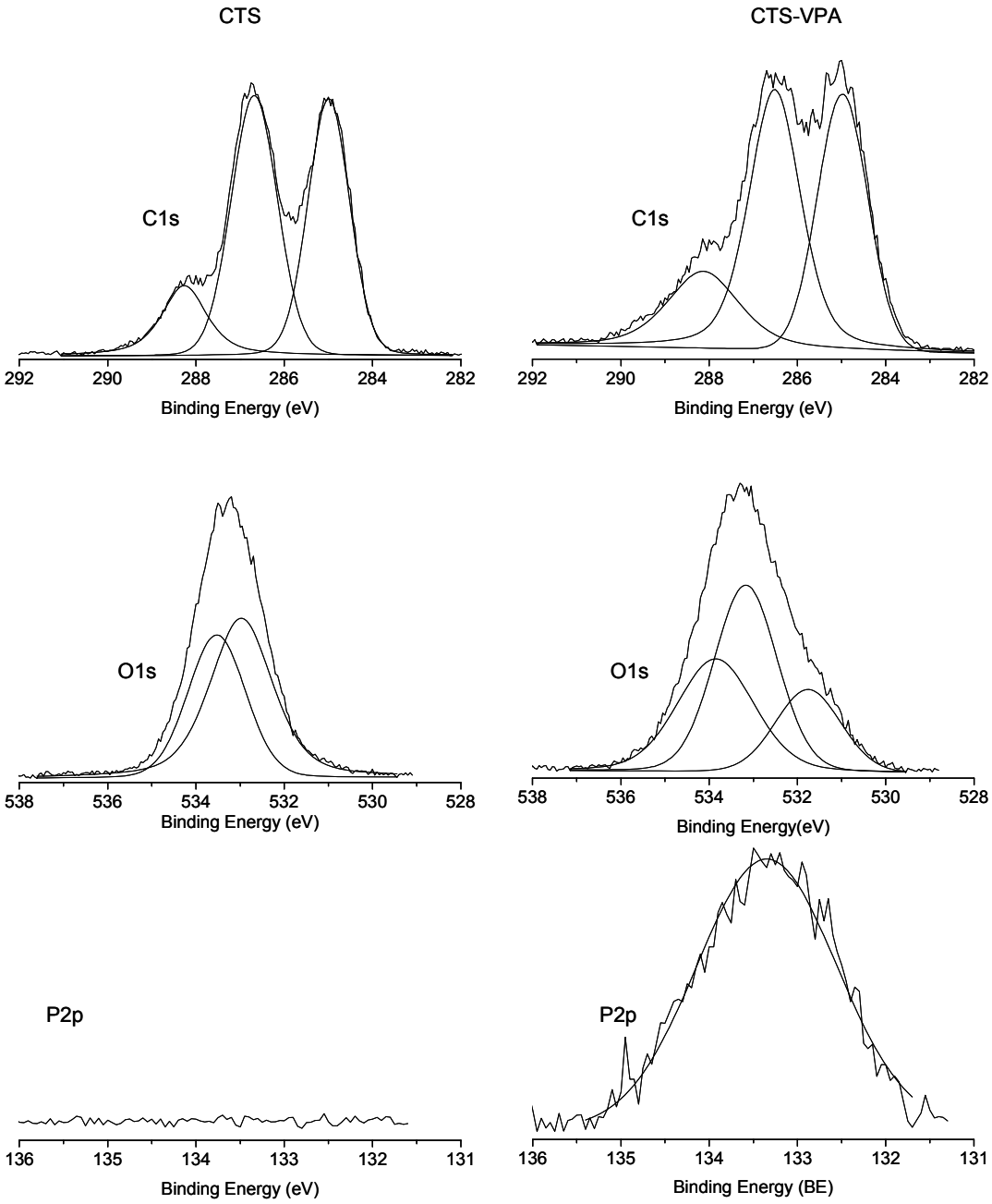

Figure 4.1 C1s, O1s, P2p core level spectra of native and PVPA grafted chitosan membranes.

O1s high resolution spectrum of chitosan showed two peaks centered at 533.0 and 533.5 eV, which correspond to C-OH and O-C-O bonds respectively [16]. After PVPA grafting a new signal at 531.8 eV was observed in the O1s spectrum, assigned to O atoms involved in -PO_3 bonds [32]. Considering the presence of elemental P on the surface (2at %) and the fact that three O atoms are bound to each P atom (–PO_3), the expected phosphorous-bind oxygen should be 6% of the total elemental composition on the surface. The deconvolution of the O1s high resolution spectrum gave a relative oxygen abundance in

the $–PO_3$ of 20.2% (Table 4.1). Because the total surface content of oxygen was found to be 32.1 at% (support information Table 4. SI1), the final experimental value for elemental phosphorous-bind oxygen is calculated to be 6.4% of the total elemental composition on the surface, which is in good agreement with the theoretical value. Finally, the P2p high resolution spectrum for PVPA grafted samples showed a single peak centered at 133.3 eV and assigned to phosphonic species [33-35]. The observed full width at half-maximum (FWHM) for this signal is wide (1.86 eV), as can be expected for P2p, since this signal correspond to $P2p_{1/2}$ and $P2p_{3/2}$ core-line doublets.

Additionally to XPS, ToF-SIMS analysis is used to identify the chemical and molecular composition of a surface. Small variations in the samples can be detected by differences in the fragmentation pattern in the mass spectra. Figure 4.2 displays both positive and negative ion survey spectra of the chitosan surface prior and after the applied modification.

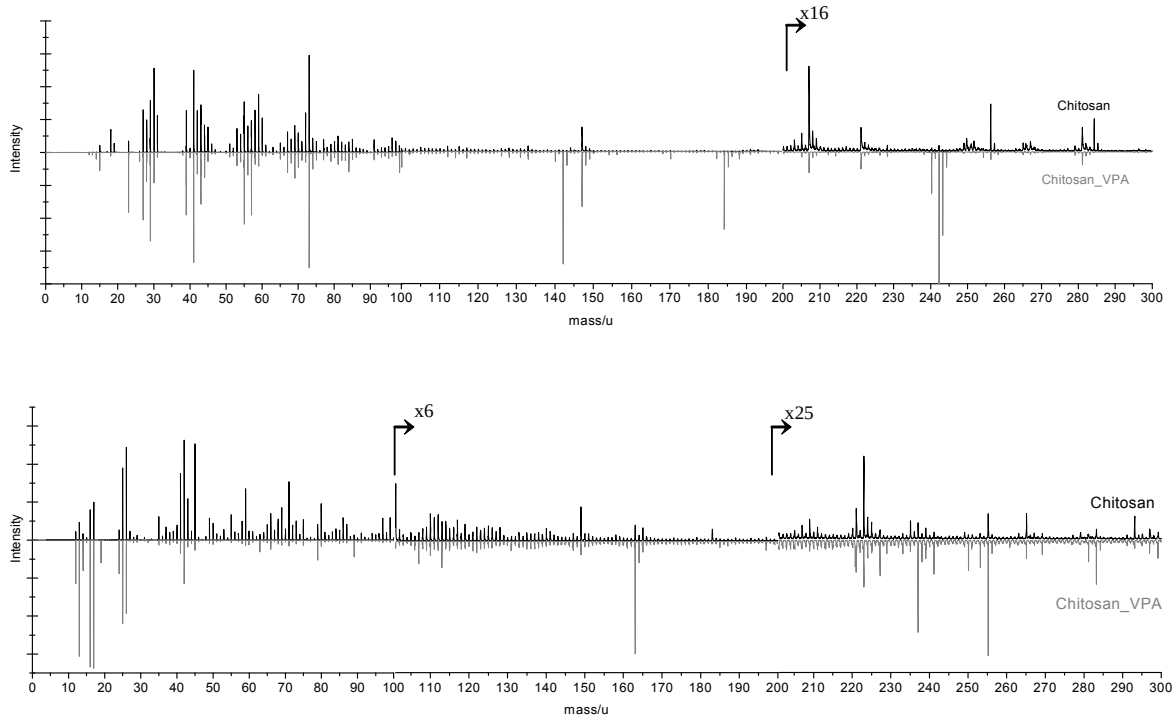

Figure 4.2 Positive (up) and negative (down) ToF-SIMS spectra of chitosan before and after (displayed in reverse) modification with poly (vinyl phosphonic acid).

Chitosan is composed of randomly distributed D-glucosamine (molecular mass 179) and N-acetyl-D-glucosamine (molecular mass 221) units. Hence, fragmentation patterns observed in the mass spectra of these glucosamines were also expected in the chitosan spectrum. Indeed, the ions M18 (NH_4), M30 (CH_4N), M59 (C_2H_5NO), M73 (C_3H_7NO), and the characteristic M207 ($C_7H_{13}NO_6$) and M221 ($C_8H_{15}NO_6$) [36] were detected in the positive ToF-SIMS spectra of chitosan (modified and non-modified). After PVPA grafting, we were

not able to detect the expected M31 (P) and M15 (NH) in positive polarity. However, it must be stated that P signal at this polarity present a very low intensity and therefore it is rather difficult to detect. On the other hand, the negative spectrum of PVPA-grafted chitosan showed clearly the presence of the specific fragments at M63 (PO_2) and M79 (PO_3). Additionally, the high resolution ToF-SIMS (Figure 4.3) also confirmed the presence of phosphorus with the characteristic peak at 30.975 present only in the spectrum of the modified material. Moreover, much higher concentration of M15 (NH) was detected after plasma modification demonstrating the simultaneous occurring of both processes grafting on one hand and etching/cleaning of the surface during the plasma activation on the other hand.

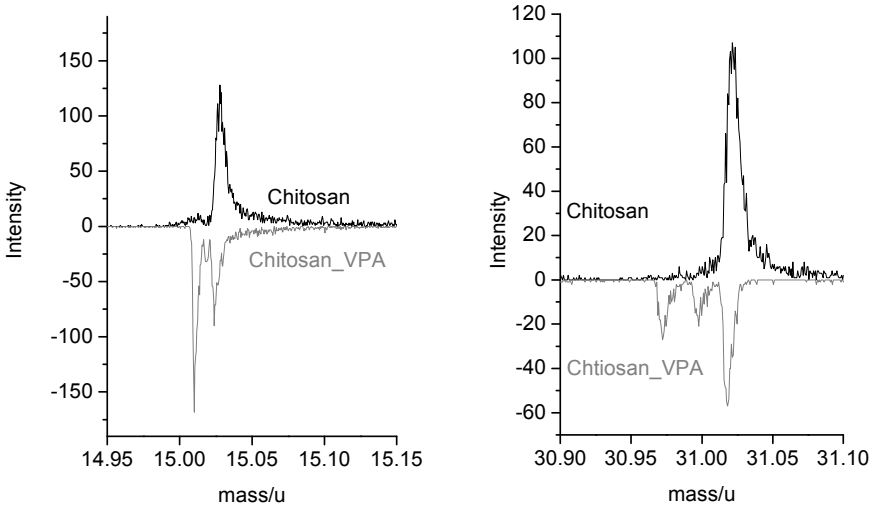

Figure 4.3 High resolution ToF-SIMS, showing both higher concentration of NH (left) and presence of P(right) as a result of the applied treatment (the spectra displayed in the reverse).

Further investigation of the spatial distribution of the new functionalities introduced by the applied modification was performed by ToF-SIMS mapping (Figure 4.4). The mapping confirmed that the grafting was successful and phosphorous containing groups at high concentration (brightest regions) were clearly observed on the overall surface. Although, it must be noticed that the modified surface was not chemically homogeneous and some regions with lower concentration of PO_2 and PO_3 fragments were observed.

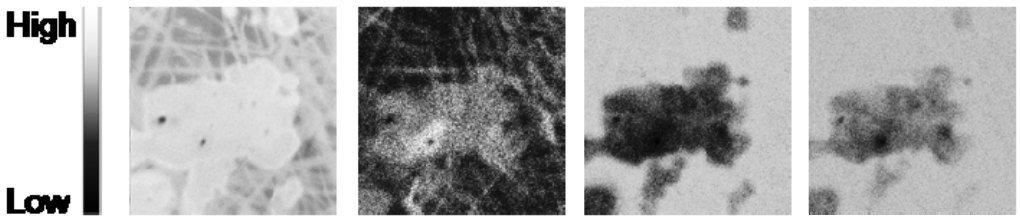

Figure 4.4 Images of a 500 μm^2 area of VPA-grafted chitosan surface as reconstructed from the negative ion mass spectrum measured by static ToF-SIMS. From left to right: all ions; M59 (C2H3O2); M63 (PO2); M79 (PO3).

4.4.2 Surface Topography

In theory, surface modifications can be envisaged to vary independently the surface topography and chemistry. However, in practice this is very difficult to achieve and in fact is impossible to prove that both properties are independent [37]. Hence, surfaces subjected to chemical modifications should be also evaluated for topographical changes. This is especially relevant for biomaterials surfaces where topography is known to have a striking effect on biological response [38, 39].

Optical profiler analyses were performed in order to analyze the presence of microfeatures on the surfaces. We have detected ring-like structures on the unmodified chitosan membranes air-face side. These features, with characteristic radius between 2 and 15 μm, disappeared after the treatment probably because of the etching process occurring during the plasma activation (Figure 4.5).

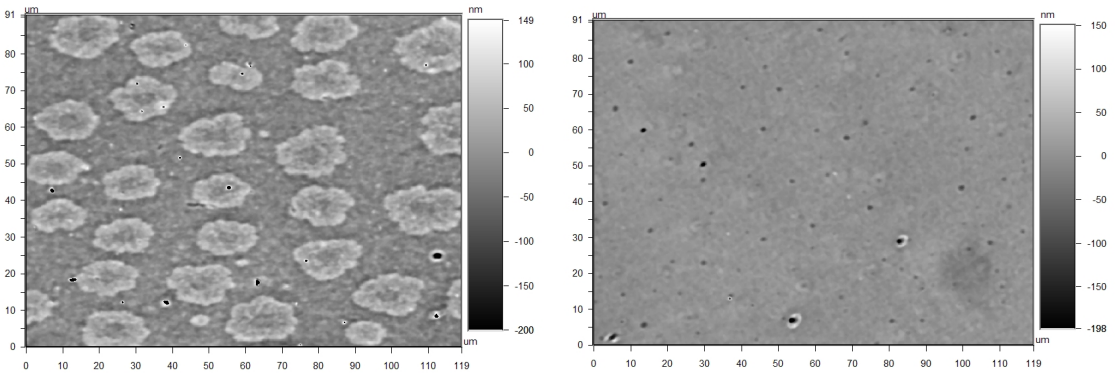

Figure 4.5 90x120μm^2 Optical Profiler images of chitosan (left) and PVPA grafted (right) membranes. Both images were taken in the membranes face dried in contact with the air.

Although optical profilometry offers quick analysis of surface topography without surface contact, it is limited in lateral resolution. Scanning probe microscopy is also non-damaging

method for surface observation because of the very light forces used and extends the lateral resolution to atomic dimensions. Therefore, high resolution (1x1 μm^2) AFM images were used to evaluate Ra (average absolute distance from average flat surface) and Rq (root mean square from average flat surface) values before and after the modification. Both surfaces showed nanopit-like textures of similar diameter and with random distribution. It could be also observed that modification process results in a small increase of the surface roughness with changes in Ra from 1.52 to 9.13 nm and in Rq from 1.91 to 11.57 nm for chitosan and CTS-PVPA, respectively (see Figure 4. SI2 in the support information).These differences at the nanoscale are in agreement with previously reported [8, 40] results for chitosan membranes modified by plasma and are also related with the etching process occurring during the activation step. Although the found differences in the roughness after PVPA grafting are small, these differences might be enough to affect cell behavior.

In their natural environment cells are in permanent contact with Nan topographic surfaces. For instance, basement membranes of various tissues are composed by pits, pores, protrusions and fibers in the range of 5-200 nm. Recent studies have shown that cells display differential performance depending on the topography at the nanoscale [41-43]. Lim *et al.* have showed that human fetal osteoblastic cells (hFOB) attachment and spreading as well as specific integrin expression were enhanced for cells cultured on 14-29 nm deep pits relative to flat surfaces or 45nm deep pits [42].

4.4.3 Surface energy and water wettability

Surface energy and water wettability of biomaterials significantly affect the biological process at the sub-cellular (protein adsorption) and cellular level (cell attachment, spreading, proliferation, etc) [37, 44-47]. The surface wettability can be directly determined by contact angle measurements, whereas it does not exist technique for direct determination of the surface energy of solids. Instead, measurements of contact angle, and several indirect empirical and semiempirical methods can provide the information required to compute the surface energy. The calculation methods are mostly based on the assumption that the free energy of a solid surface can be split into different components representing different independent interactions. There is still an intense debate [27, 28] on the applicability and correctness of using each method, as well as on the true physical meaning of some surface energy components. In this work we have calculated the surface energy both using the classical “paradigm” of Owens, Wendt, Rabel and Kaelble (OWRK) [25] and the perhaps more controversial van Oss-Chaudury-Good (vOCG) theory

[26-28], which provides additional information (Lewis acid-basic contributions), if taken and evaluated within the method assumptions and constrains.

Table 4.2 shows the water contact angle and the water adhesion tension for modified and untreated chitosan membranes. Water adhesion tension (τ) often used to predict or explain biomaterial-cell interactions as an alternative to surface energy, is defined as:

$$\tau = \gamma_w \cdot \cos\theta \tag{4.1}$$

where γ_w is the water surface tension (72.8 mN/m) and θ is the water contact angle.

Table 4.2 Equilibrium water contact angle and adhesion tension for PVPA grafted and non-treated chitosan membranes

Sample	Water contact angle (º)	Adhesion tension(τ) (mN/m)
CTS	98.5 ± 2.5	-10.8 ± 3.1
CTS-VPA	69.0 ± 10.2	25.7 ± 12.2

Relatively high water contact angle (98.5º) was measured for the untreated chitosan membranes. After PVPA grafting, the contact angle value decreases significantly (69.0º). Consequently, water tension adhesion values increased from -10.8mN/m to 25.7mN/m. According to the literature, values of water tension adhesion of 30mN/m (contact angle 65º) distinguish the hydrophobic and hydrophilic regimes [29, 48]. This value limits the region where long-range attractive (hydrophobic) forces become repulsive (hydration) forces. Being so, the water adhesion tension (Table 4.2) of untreated chitosan membranes discloses a hydrophobic surface. As expected, PVPA grafting increased the water adhesion tension as a consequence of the introduction of phosphonic groups. Nevertheless, the water adhesion tension value for PVPA grafted membranes is still in the hydrophobic regime, although within the limit where hydrophobic attraction is substituted by hydration driven repulsive forces [29].

Surface energy computed using the OWRK method split the surface energy γ_s into a dispersive γ_s^d and a polar component γ_s^p, according to the equation:

$$\gamma_s = \gamma_s^d + \gamma_s^p \tag{4.2}$$

High dispersive component is usually observed for polymers while the polar contribution is associated with the presence of polar groups on the surface. As shown in Table 4.3, the total surface energy (35.6 mN/m) determined by the OWRK method was higher for modified membranes than for untreated material (29.0 mN/m). The value of the polar component for unmodified chitosan was particularly low (0.22 mN/m), thus confirming

reported results for chitosan [7, 49]. As it was expected, the introduction of the polar phosphonic groups resulted in drastic increase in γ_s^p (8.3 mN/m).

Table 4.3 Surface Energy and its components calculated by OWRK and AB methods

Sample	OWRK method			AB method			
	γ_s (mN/m)	γ_s^d (mN/m)	γ_s^p (mN/m)	γ_s (mN/m)	γ_s^{LW} (mN/m)	γ_s^+ (mN/m)	γ_s^- (mN/m)
CTS	29.0±0.0	28.8±0.0	0.22±0.0	28.0±0.0	28.8±0.0	0.0±0.0	0.91±0.3
CTS-VPA	35.6±0.1	27.3±0.0	8.3±0.1	33.5±0.1	33.5±0.0	0.0±0.0	32.7±2.0

In turn, according to vOCG theory, the surface energy can be calculated as a combination of dispersive and Lewis acid-base contributions:

$$\gamma_S = \gamma_S^{LW} + \gamma_S^{AB} \tag{4.3}$$

where γ_S^{LW} is the surface energy corresponding to Lifshitz-van der Waals forces and γ_S^{AB} describes the contribution of the acid-base interaction to the surface energy:

$$\gamma_S^{AB} = 2 \cdot \left(\gamma_S^- \cdot \gamma_S^+\right)^{1/2} \tag{4.4}$$

where γ_S^- and γ_S^+ represent respectively the electron donor (Lewis base) and the electron acceptor (Lewis acid) contributions or, more specifically, the particular sub-set of Lewis acid-base interactions known as hydrogen bonding.

The results obtained from the vOCG method are in accordance with the results obtained in our previous study where chitosan was functionalized with sulfonic and carboxyl groups [7]. Both, untreated and modified samples presented a monopolar character with acid component being zero (Table 4.3). The basic component was strongly affected by the incorporation of phosphonic groups at the surfaces, increasing from 0.91 mN/m for chitosan to 32.7 mN/m for PVPA grafted sample. We used the scale proposed by Della Volpe and Sibone (DVB) [28], who assumed a ratio for the reference water acid-base components that better describes the different “strength” of water as Lewis acid and base. By using this scale, Della Volpe and Sibone calculated the acid-base coefficients for a wide set of materials, obtaining coefficients that described correctly the chemical properties commonly expected for all tested materials. Thus, the DVB scale corrects the artifact introduced by the former vOCG scale that uses equal acid-base components for water and generates values in which all surfaces seemed to be strongly basic. This tendency has been observed even for polymer surfaces that should present pronounced

Lewis acid character according to the general chemical sense [28]. For this reason, we were surprised to found that, according to the calculated acid-base components, unmodified chitosan membranes presented only hydrogen bond acceptor character. This is an odd result, since hydroxyl groups can act as both hydrogen bond donor (electron acceptor) and acceptor (electron donor).

4.4.4 Cell behavior

The influence of the surface modification on the biocompatibility of the studied materials was evaluated *in vitro* by osteoblast cell line (SaOs-2). We have observed by SEM a significant change of SaOs-2 morphology after the performed PVPA grafting (Figure 4.6).

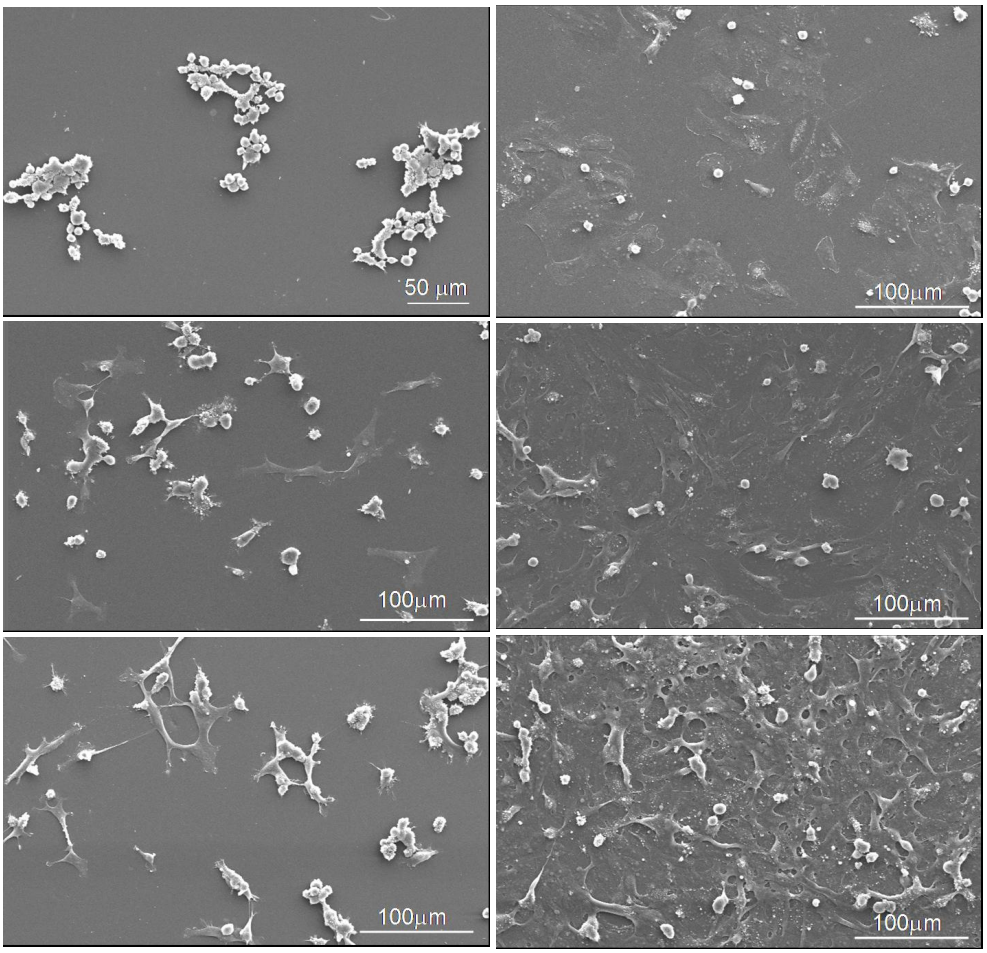

Figure 4.6 SEM micrographs of SaOs-2 cultured on chitosan (left) and PVPA (right) membranes during 1, 7 and 14 days (from up to down).

While SaOs-2 cultured on untreated membranes presented a rather round shape and low adhesion during all studied period, cells seeded on grafted membranes showed spread

morphology and higher number of cells attached to the surface. After one day of culture, a considerable number of adhered spread cells were observed on modified materials. In the following days the cells formed a homogeneous layer covering the entire surface. In agreement with our results, for instance Lim et al. [47] reported that cytoskeletal features between osteoblastic cells cultured on hydrophilic and hydrophobic materials are notable different. Cells on hydrophilic materials presented distinct, large plaques of integrins (α_v and β_3 subunits) co-localized with actin stress fibers whereas there was much less development of such adhesion structures on hydrophobic surfaces.

SaOs-2 cultured on chitosan membranes (τ=-10.8 mN/m) formed clump-like structures which grown in size and number with the culture time. Similar behavior has been recently reported for human foetal osteoblastic cells and three different osteoblast-like cell lines on hydrophobic substrates [46]. Although the number of viable cells as indicated by Calcein AM stained increased with the culture time for both materials, the few viable cells (Figure 4.7) adhered on chitosan membranes did not present the typical osteoblast-like morphology, being round sparsely distributed and forming clump-like structures. On the contrary, the modified samples were covered by a homogeneous layer of viable cells.

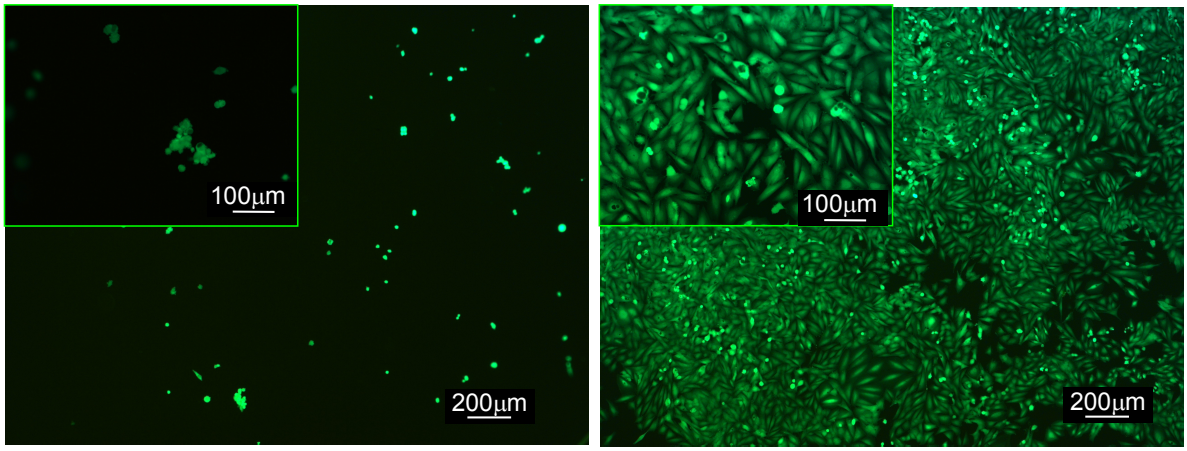

Figure 4.7 Calcein AM staining of SaOs-2 cultured for 7 days on chitosan (up) and PVPA (down) substrates.

MTS assay (Figure 4.8) showed a higher number of viable cells on PVPA grafted substrates. This difference became more evident with the increase of the culture time, indicating that the modification process have a positive effect on the long-term material response.

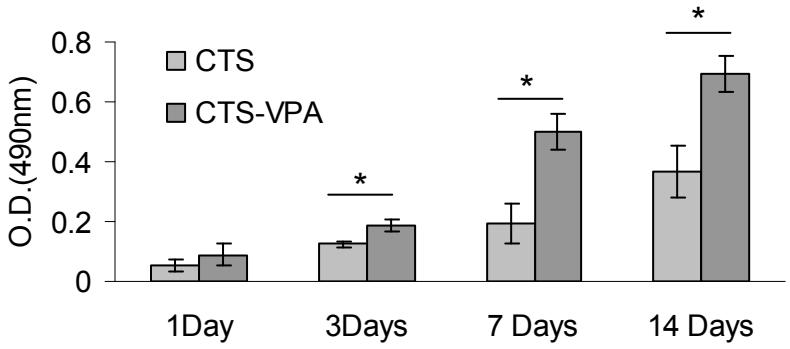

Figure 4.8 Cell viability (by MTS assay) of SaOs-2 cultured on unmodified and PVPA grafted membranes.* Significantly different (ANOVA test, $p<0.05$).

The same tendency was observed for cell proliferation (Figure 4.9). In fact, after 1 day of culture, the number of cells for PVPA grafted substrates was significantly higher than in chitosan membranes and this tendency was kept along all studied time periods. Therefore, it can be concluded that grafting process of PVPA on chitosan membranes' surface improved the osteoblast-like cells attachment, spreading, viability and proliferation.

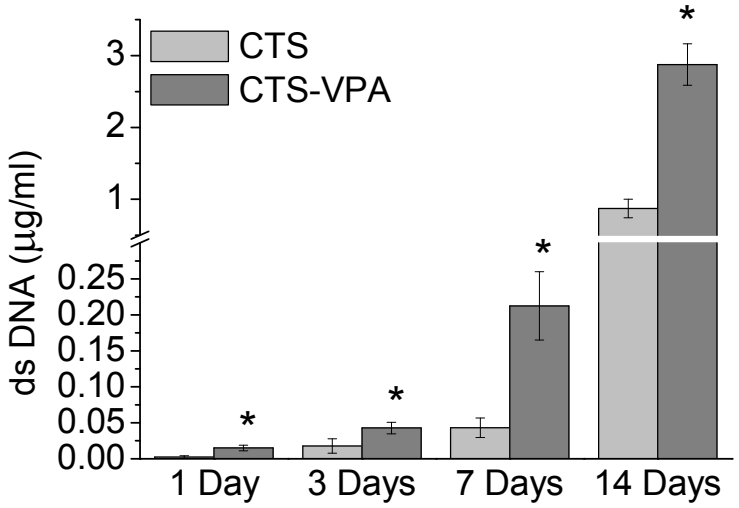

Figure 4.9 DNA concentration corresponding to SaOs-2 cultures in direct contact with CTS and PVPA substrates. * Significantly different (ANOVA test, $p<0.05$).

Whitesides and co-workers examined a group of around 60 mixed self-assembled monolayers (SAMs) suggesting that functional groups that made the surfaces inert had four common features: they were (i) hydrophilic, (ii) hydrogen bond acceptors, (iii) not hydrogen bond donors, and (iv) overall electrically neutral [50]. However, a few exceptions were found to this general rule; oligo(ethylene glycol) (OEG), mannitol (sugar alcohol) and maltose (disaccharide) surfaces have many hydrogen bond donors and also resisted

protein adsorption and cell adhesion [50-52]. Interestingly, mannitol-presenting surface was able to resist much longer than OEG to cell adhesion on patterned surfaces [51]. Although cell adhesion and proliferation is very limited on chitosan membranes, they are not fully inert because they do not inhibit those processes completely. Nevertheless, the lack of cell adhesion on monosaccharide-based model SAM surfaces can give us some cues for the limited ability of neutral polysaccharides such as chitosan to sustain mammalian cells growth. Moreover, the isoelectric point of chitosan membranes is around the physiological and culture pH (7.4) (overall electrically neutral). Therefore, these membranes should present physicochemical properties similar to other inert surfaces. Chitosan has many hydroxyl groups that should be able to perform both as hydrogen bond donor and acceptor, which would include chitosan within the few exceptions to the general rule stated before [50]. Nevertheless, the unexpected null value for the surface energy acid component (hydrogen bond donor) of unmodified chitosan membranes should mean that chitosan membranes' surface mainly performs as a hydrogen bond acceptor. Perhaps, this is more than a coincidence, but extending the discussion beyond would be premature and too speculative at the moment. Finally, the cell adhesion on the treated membranes can be explained by the negatively charged nature of the grafted polymer [50] which is expected to be ionized at the physiological pH.

4.5 Conclusions

Surface chemistry characterization by XPS and ToF-SIMS indicated that chitosan membranes could be successfully grafted with poly-(phosphonic acid) by plasma induce polymerization. The modification induces changes in the surface topography at the nanoscale associated to the etching process during the plasma activation step. We found that grafting of negatively charged groups such as phosphonic groups induced remarkably different osteoblast-like cells (SaOs-2) response in terms of attachment, spreading, viability and proliferation. Unmodified chitosan membranes presented very limited cell adhesion and the formation of sparsely located clump-like structures occurred for longer culture time periods. The physicochemical features of chitosan that grant its partial resistance to cell adhesion might be related with the inertness reported for other neutral saccharide-based surfaces. The plasma induced polymerization is very simple and versatile method and it was shown to be an effective grafting methodology to render a relatively inert polysaccharide the suitable surface properties for cell adhesion of proliferation.

4.6 Acknowledgements

The authors acknowledge funding from EU Marie Curie Actions, Alea Jacta Est (MEST-CT-2004-008104) and Portuguese Foundation for Science and Technology (FCT) (SFRH/BPD/34545/2007). This work was carried out under the scope of the European NoE EXPERTISSUES (NMP3-CT-2004-500283).

4.7 References

1. Marler, E.; Davidson, E.A. Structure of Polysaccharide Protein Complex. *Proceedings of the National Academy of Sciences of the United States of America*, 1965, **54,** (2), 648-656.

2. Kumar, M.; Muzzarelli, R.A.A.; Muzzarelli, C.; Sashiwa, H.; Domb, A.J. Chitosan chemistry and pharmaceutical perspectives. *Chemical Reviews*, 2004, **104,** (12), 6017-6084.

3. Muzzarelli, R.A.A.; Muzzarelli, C., *Chitosan chemistry: Relevance to the biomedical sciences*, in *Advances in Polymer Science*, T.T. Heinze, Editor. 2005, Springer-Verlag Berlin: Berlin. 151-209.

4. Pangburn, S.H.; Trescony, P.V.; Heller, J. Lysozyme Degradation Of Partially Deacetylated Chitin, Its Films And Hydrogels. *Biomaterials*, 1982, **3,** (2), 105-108.

5. Sorlier, P.; Denuziere, A.; Viton, C.; Domard, A. Relation between the degree of acetylation and the electrostatic properties of chitin and chitosan. *Biomacromolecules*, 2001, **2,** (3), 765-772.

6. Yeh, H.Y.; Lin, J.C. Surface characterization and in vitro platelet compatibility study of surface sulfonated chitosan membrane with amino group protection-deprotection strategy. *Journal of Biomaterials Science-Polymer Edition*, 2008, **19,** (3), 291-310.

7. Lopez-Perez, P.M.; Marques, A.P.; da Silva, R.M.P.; Pashkuleva, I.; Reis, R.L. Effect of chitosan membrane surface modification via plasma induced polymerization on the adhesion of osteoblast-like cells. *Journal Of Materials Chemistry*, 2007, **17,** (38), 4064-4071.

8. Silva, S.S.; Luna, S.M.; Gomes, M.E.; Benesch, J.; Pashkuleva, I.; Mano, J.F.; Reis, R.L. Plasma surface modification of chitosan membranes: Characterization and preliminary cell response studies. *Macromolecular Bioscience*, 2008, **8,** (6), 568-576.

9. Chung, T.W.; Lu, Y.F.; Wang, S.S.; Lin, Y.S.; Chu, S.H. Growth of human endothelial cells on photochemically grafted Gly-Arg-Gly-Asp (GRGD) chitosans. *Biomaterials*, 2002, **23,** (24), 4803-4809.

10. Cuy, J.L.; Beckstead, B.L.; Brown, C.D.; Hoffman, A.S.; Giachelli, C.M. Adhesive protein interactions with chitosan: Consequences for valve endothelial cell growth on tissue-engineering materials. *Journal Of Biomedical Materials Research Part A*, 2003, **67A,** (2), 538-547.

11. Li, J.; Yun, H.; Gong, Y.D.; Zhao, N.M.; Zhang, X.F. Investigation of MC3T3-E1 cell behavior on the surface of GRGDS-coupled chitosan. *Biomacromolecules*, 2006, **7,** (4), 1112-1123.

12. Jayakumar, R.; Nwe, N.; Tokura, S.; Tamura, H. Sulfated chitin and chitosan as novel biomaterials. *International Journal of Biological Macromolecules*, 2007, **40,** (3), 175-181.

13. Lin, C.-W.; Lin, J.-C. Surface characterization and platelet compatibility evaluation of surface-sulfonated chitosan membrane. *J. Biomater. Sci. Polymer Edn.*, 2001, **12,** (5), 543-557.

14. Jayakumar, R.; Nagahama, H.; Furuike, T.; Tamura, H. Synthesis of phosphorylated chitosan by novel method and its characterization. *International Journal of Biological Macromolecules*, 2008, **42,** (4), 335-339.

15. Amaral, I.F.; Granja, P.L.; Melo, L.V.; Saramago, B.; Barbosa, M.A. Functionalization of chitosan membranes through phosphorylation: Atomic force microscopy, wettability, and cytotoxicity studies. *J Appl Pol Sci*, 2006, **102,** (1), 276-284.

16. Amaral, I.F.; Granja, P.L.; Barbosa, M.A. Chemical modification of chitosan by phosphorylation: an XPS, FT-IR and SEM study. *Journal of Biomaterials Science-Polymer Edition*, 2005, **16,** (12), 1575-1593.

17. Jayakumar, R.; Selvamurugan, N.; Nair, S.V.; Tokura, S.; Tamura, H. Preparative methods of phosphorylated chitin and chitosan - An overview. *International Journal of Biological Macromolecules*, 2008, **43,** (3), 221-225.

18. Wan, Y.; Creber, K.A.M.; Peppley, B.; Bui, V.T. Synthesis, characterization and ionic conductive properties of phosphorylated chitosan membranes. *Macromolecular Chemistry and Physics*, 2003, **204,** (5-6), 850-858.

19. Li, Q.L.; Chen, Z.Q.; Darvell, B.W.; Liu, L.K.; Jiang, H.B.; Zen, Q.; Peng, Q.; Ou, G.M. Chitosan-phosphorylated chitosan polyelectrolyte complex hydrogel as an osteoblast carrier. *Journal of Biomedical Materials Research Part B-Applied Biomaterials*, 2007, **82B,** (2), 481-486.

20. Yokogawa, Y.; Nishizawa, K.; Nagata, F.; Kameyama, T. Bioactive properties of chitin/chitosan-calcium phosphate composite materials. *Journal of Sol-Gel Science and Technology*, 2001, **21,** (1-2), 105-113.

21. Gemeinhart, R.A.; Bare, C.M.; Haasch, R.T.; Gemeinhart, E.J. Osteoblast-like cell attachment to and calcification of novel phosphonate-containing polymeric substrates. *Journal Of Biomedical Materials Research Part A*, 2006, **78A,** (3), 433-440.

22. Tan, J.; Gemeinhart, R.A.; Ma, M.; Saltzman, W.M. Improved cell adhesion and proliferation on synthetic phosphonic acid-containing hydrogels. *Biomaterials*, 2005, **26,** (17), 3663-3671.

23. da Silva, R.M.P.; Mano, J.F.; Reis, R.L. Straightforward determination of the degree of N-acetylation of chitosan by means of first-derivative UV spectrophotometry. *Macromolecular Chemistry and Physics*, 2008, **209,** (14), 1463-1472.

24. Terbojevich, M.; Cosani, A.; Muzzarelli, R.A.A. Molecular parameters of chitosans depolymerized with the aid of papain. *Carbohydrate Polymers*, 1996, **29,** (1), 63-68.

25. Owens, D.K.; Wendt, R.C. Estimation of Surface Free Energy of Polymers. *Journal of Applied Polymer Science*, 1969, **13,** (8), 1741-1747.

26. van Oss, C.J.; Chaudhury, M.K.; Good, R.J. Interfacial Lifshitz-Vanderwaals and Polar Interactions in Macroscopic Systems. *Chemical Reviews*, 1988, **88,** (6), 927-941.

27. Della Volpe, C.; Maniglio, D.; Siboni, S.; Morra, M. Recent theoretical and experimental advancements in the application of van Oss-Chaudury-Good acid-base theory to the analysis of polymer surfaces - I. General aspects. *Journal of Adhesion Science and Technology*, 2003, **17,** (11), 1477-1505.

28. Della Volpe, C.; Siboni, S. Acid-base surface free energies of solids and the definition of scales in the Good-van Oss-Chaudhury theory. *Journal of Adhesion Science and Technology*, 2000, **14,** (2), 235-272.

29. Vogler, E.A. Structure and reactivity of water at biomaterial surfaces. *Advances in Colloid and Interface Science*, 1998, **74**, 69-117.

30. Briggs, D., in *Surface analysis of polymers by XPS and static SIMS*. 1998, Cambridge University Press: Cambridge 47-87.

31. Siow, K.S.; Britcher, L.; Kumar, S.; Griesser, H.J. *Characterization of sulfate and phosphate containing plasma polymer surfaces*. in *Nanoscience and Nanotechnology, 2006. ICONN '06. International Conference on*. 2006. Brisbane, Australia.

32. Adden, N.; Gamble, L.J.; Castner, D.G.; Hoffmann, A.; Gross, G.; Menzel, H. Phosphonic acid monolayers for binding of bioactive molecules to titanium surfaces. *Langmuir*, 2006, **22,** (19), 8197-8204.

33. Wagner, C.D.; Naumkin, A.V.; Kraut-Vass, A.; Allison, J.W.; Powell, C.J.; Rumble, J.R.J., *NIST Standard Reference Database 20 Version 3.5* 2003, National Institute of Standards and Technology.

34. Textor, M.; Ruiz, L.; Hofer, R.; Rossi, A.; Feldman, K.; Hahner, G.; Spencer, N.D. Structural chemistry of self-assembled monolayers of octadecylphosphoric acid on tantalum oxide surfaces. *Langmuir*, 2000, **16,** (7), 3257-3271.

35. Tosatti, S.; Michel, R.; Textor, M.; Spencer, N.D. Self-assembled monolayers of dodecyl and hydroxy-dodecyl phosphates on both smooth and rough titanium and titanium oxide surfaces. *Langmuir*, 2002, **18,** (9), 3537-3548.

36. Grenha, A.; Seijo, B.; Serra, C.; Remunan-Lopez, C. Surface characterization of lipid/chitosan nanoparticles assemblies, using X-ray photoelectron spectroscopy and time-of-flight secondary ion mass spectrometry. *Journal Of Nanoscience And Nanotechnology*, 2008, **8,** (1), 358-365.

37. Liu, X.M.; Lim, J.Y.; Donahue, H.J.; Dhurjati, R.; Mastro, A.M.; Vogler, E.A. Influence of substratum surface chemistry/energy and topography on the human fetal osteoblastic cell line hFOB 1.19: Phenotypic and genotypic responses observed in vitro. *Biomaterials*, 2007, **28,** (31), 4535-4550.

38. Anselme, K.; Bigerelle, M.; Noel, B.; Dufresne, E.; Judas, D.; Iost, A.; Hardouin, P. Qualitative and quantitative study of human osteoblast adhesion on materials with various surface roughnesses. *Journal of Biomedical Materials Research*, 2000, **49,** (2), 155-166.

39. Deligianni, D.D.; Katsala, N.; Ladas, S.; Sotiropoulou, D.; Amedee, J.; Missirlis, Y.F. Effect of surface roughness of the titanium alloy Ti-6Al-4V on human bone marrow cell response and on protein adsorption. *Biomaterials*, 2001, **22,** (11), 1241-1251.

40. Ogino, A.; Kral, M.; Yamashita, M.; Nagatsu, M. Effects of low-temperature surface-wave plasma treatment with various gases on surface modification of chitosan. *Applied Surface Science*, 2008, **255,** (5 PART 1), 2347-2352.

41. Kunzler, T.P.; Huwiler, C.; Drobek, T.; Voros, J.; Spencer, N.D. Systematic study of osteoblast response to nanotopography by means of nanoparticle-density gradients. *Biomaterials*, 2007, **28,** (33), 5000-5006.

42. Lim, J.Y.; Dreiss, A.D.; Zhou, Z.Y.; Hansen, J.C.; Siedlecki, C.A.; Hengstebeck, R.W.; Cheng, J.; Winograd, N.; Donahue, H.J. The regulation of integrin-mediated osteoblast focal adhesion and focal adhesion kinase expression by nanoscale topography. *Biomaterials*, 2007, **28,** (10), 1787-1797.

43. Lim, J.Y.; Hansen, J.C.; Siedlecki, C.A.; Runt, J.; Donahue, H.J. Human foetal osteoblastic cell response to polymer-demixed nanotopographic interfaces. *Journal of the Royal Society Interface*, 2005, **2,** (2), 97-108.

44. Lee, J.H.; Lee, H.B. A Wettability Gradient As A Tool To Study Protein Adsorption And Cell-Adhesion On Polymer Surfaces. *Journal Of Biomaterials Science-Polymer Edition*, 1993, **4,** (5), 467-481.

45. Kim, M.S.; Khang, G.; Lee, H.B. Gradient polymer surfaces for biomedical applications. *Progress in Polymer Science*, 2008, **33,** (1), 138-164.

46. Lim, J.Y.; Shaughnessy, M.C.; Zhou, Z.Y.; Noh, H.; Vogler, E.A.; Donahue, H.J. Surface energy effects on osteoblast spatial growth and mineralization. *Biomaterials*, 2008, **29,** (12), 1776-1784.

47. Lim, J.Y.; Taylor, A.F.; Li, Z.Y.; Vogler, E.A.; Donahue, H.J. Integrin expression and osteopontin regulation in human fetal osteoblastic cells mediated by substratum surface characteristics. *Tissue Engineering*, 2005, **11,** (1-2), 19-29.

48. Vogler, E.A. Water and the acute biological response to surfaces. *Journal Of Biomaterials Science-Polymer Edition*, 1999, **10,** (10), 1015-1045.

49. Cunha, A.G.; Fernandes, S.C.M.; Freire, C.S.R.; Silvestre, A.J.D.; Pascoal, C.; Gandini, A. What is the real value of chitosan's surface energy? *Biomacromolecules*, 2008, **9,** (2), 610-614.

50. Ostuni, E.; Grzybowski, B.A.; Mrksich, M.; Roberts, C.S.; Whitesides, G.M. Adsorption of proteins to hydrophobic sites on mixed self-assembled monolayers. *Langmuir*, 2003, **19,** (5), 1861-1872.

51. Luk, Y.Y.; Kato, M.; Mrksich, M. Self-assembled monolayers of alkanethiolates presenting mannitol groups are inert to protein adsorption and cell attachment. *Langmuir*, 2000, **16,** (24), 9604-9608.

52. Prime, K.L.; Whitesides, G.M. Self-Assembled Organic Monolayers - Model Systems for Studying Adsorption of Proteins at Surfaces. *Science*, 1991, **252,** (5009), 1164-1167.

4.8 Support information

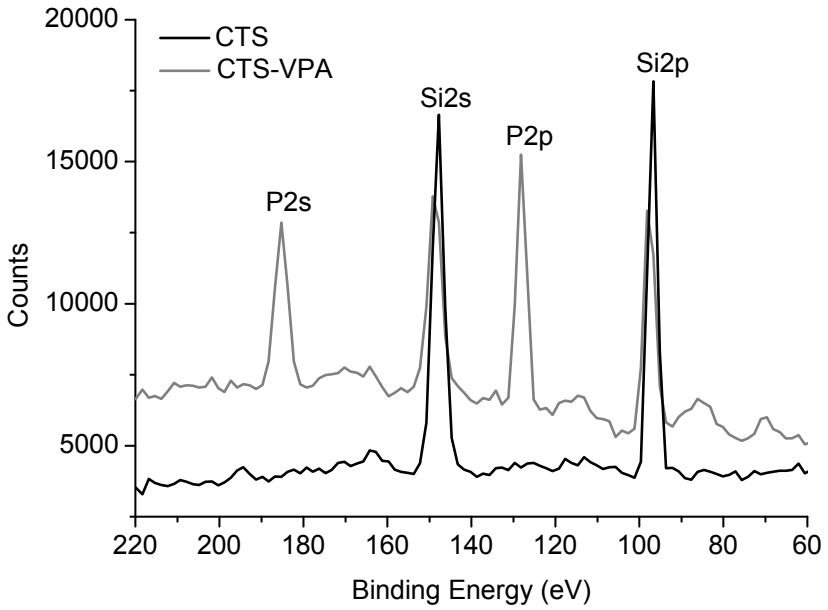

Figure 4.SI1 XPS Survey spectra of non-treated and PVPA grafted materials.

Table 4.SI1 Chemical composition in atomic percentage of native and PVPA grafted chitosan membranes determined by XPS

Material	C_{1s} (at%)	O_{1s} (at%)	N_{1s} (at%)	Si_{1s} (at%)	P_{2p} (at%)
CTS	63.2	27.3	5.1	4.3	0.0
CTS-VPA	56.5	32.1	6.8	2.6	2.0

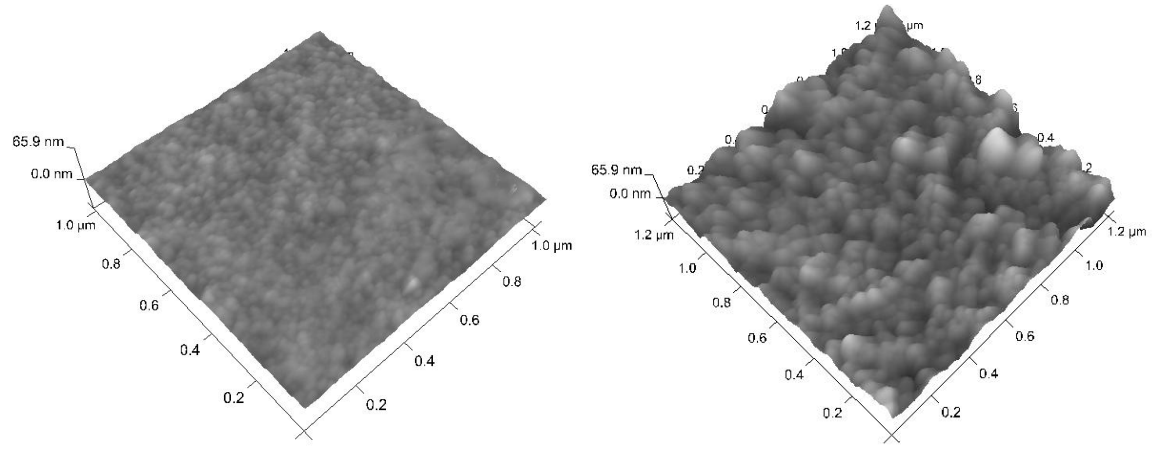

Figure 4.SI2 AFM images of chitosan (left) and PVPA grafted (right) membranes.

Chapter 5

Plasma-induced polymerization as a tool for surface functionalization of polymer scaffolds for bone tissue engineering: an *in vitro* study

5.1 Abstract

A commonly applied strategy in tissue engineering (TE) field is the use of temporary three dimensional scaffolds for supporting and guiding tissue formation in various *in vitro* strategies and *in vivo* regeneration approaches. The interactions of these scaffolds with the highly sensitive bioentities such as living cells and tissues primary occur through the material surface. Hence, surface chemistry and topological features have the principal role in coordinating biological events at molecular, cellular and tissue levels on time scales ranging from seconds to weeks. However, tailoring the surface properties of scaffolds with complex shape and architecture remains a challenge in the materials science. Commonly applied wet chemical treatments often involve the use of toxic solvents whose oddments in the construct could be fatal in the subsequent application. Aiming to shorten the culture time *in vitro* (i.e. prior the implantation of the construct), in this work we propose a modification of previously described bone TE scaffolds made from a blend of starch with polycaprolactone (SPCL). The modification method involves surface grafting of sulfonic or phosphonic groups via plasma-induced polymerization of vinyl sulfonic and vinyl phosphonic acid, respectively. We demonstrate herein that the presence of these anionic functional groups can modulate cell adhesion mediated through the adsorbed proteins (from the culture medium). At the studied conditions, both vitronectin adsorption and osteoblasts proliferation and viability increase in the following order SPCL<< sulfonic grafted SPCL< phosphonic grafted SPCL. The results revealed that plasma induced polymerization is an excellent alternative route, when compared to the commonly used wet chemical treatments, for the surface functionalization of biodevices with complex shape and porosity.

This chapter is based on the following publication:
Paula M. López-Pérez; Ricardo M.P. da Silva; Rui A. Sousa; Iva Pashkuleva; Rui L. Reis. *Submitted*

5.2 Introduction

Tissue engineering (TE) emerged as an interdisciplinary field confronting the transplantation crisis caused by the shortage of donor tissues and organs. Since its inception, scaffolds composed of synthetic and natural polymers have been key elements of different TE approaches [1]. The use of an appropriate template to provide physical support and a local environment for cells and hence to enable and facilitate tissue development is an essential issue for a successful regeneration strategy. Nowadays, it is well accepted [2-4] that the ideal scaffold for bone TE must possess adequate porosity, resulting in interconnected and permeable structure which allows the ingress of nutrients and cells. It is also believed that proper mechanical and physical properties, controlled biodegradability, biocompatibility, and ability to promote cellular interactions and tissue development are other main requirements for TE scaffolds [2, 5-8]. Last but not least, cells and surrounding tissues interact with any external devise primarily through the surface and therefore, properties as surface chemistry and topography are also key determinants for the material-bioentities crosstalk.

Starch based polymers have been studied as valuable materials for several biomedical applications [4, 9]. Their biocompatibility and non-cytotoxicity has been confirmed by both *in vitro* [4, 10-12] and *in vivo* [13] assays. In this work, we have chosen fiber mesh scaffolds made from a blend of starch and ε-polycaprolactone (SPCL) which have been already proposed for bone tissue engineering [4, 8, 10, 11]. Previous works have been targeting their optimisation in terms of degradability [7-9], porosity [4] and mechanical properties [9, 14] but so far there are just few studies focused on their surface properties [15] and the possibility to improve them [12, 16]. Herein, we propose plasma-induced polymerization as a way to render an appropriate surface for enhancing cell adhesion and speed up cell proliferation which will shorten the culture time *in vitro*, i.e. prior the implantation. Previously, we have demonstrated [17, 18] that this method is a very effective way for grafting of vinyl polymers on 2D, regular structures without modifying the bulk properties of the material. In this study, we are further reporting the effectiveness of this method for functionalization of 3D structures with complex shape with the negatively charged sulfonic and phosphonic groups and the influence of these groups on osteoblast cells behavior *in vitro*.

Anionic scaffolds have been investigated because of their capability to facilitate morphogenetic processes for tissue engineering substitutes [19, 20]. For example, the negative charge of glucosaminoglycans (GAGs) is associated with their bioactivity. GAGs interact with the positively charged amino groups of extracellular proteins and these interactions determine cell-matrix adhesion. Recent studies with sulfated derived materials

indicate enhanced adhesion and proliferation of osteoblast-like cells as a result of sulfate groups presence [18, 21]. On the other hand, the introduction of phosphate groups have been also proposed as an attractive modification strategy when bone tissue engineering applications are being targeted [17, 22-24]. The rationale for the use of this functionality stems from mimicry of bone promoting-proteins and mineral bone matrix. Phosphate rich proteins are known to initiate nucleation of bone and tooth mineralized matrix. It is also reported that many bone promoting proteins naturally interact with acidic polymers [25].

5.3 Materials and methods

5.3.1 Materials

In this work, we used a commercially available blend (Mater-Bi ZI01U, Novamont, Italy) composed of thermoplastic starch and poly(ε-polycaprolactone) (SPCL, 30/70 wt%) [26, 27]. The material was supplied in a granular form and processed by melt spun into fibers. Vinyl phosphonic acid (VPA) and vinyl sulfonic acid (VSA) were purchased from Sigma-Aldrich and used without further purification.

5.3.2 SPCL meshes production and modification

Fibers of SPCL were produced by melt spinning using a modular co-rotating twin screw extruder (Leistritz AG-LSM 36/25D, Germany), at a screw speed of 3 rpm and a temperature profile in the barrel (from feed to die zones) between 60 and 130 °C. The average output rate was 0.3 kg/h. Upon extrusion through the die, the filament was spun in two consecutive steps to a final draw ratio of approximately 1:100. The cooling of the filament was performed in air (average temperature of 17 °C). Melt spun fibers presented a diameter in the 105-345 μm range and a mean fiber diameter of 213 ± 50 μm. The fibers were cut into 0.5 mm length segments and used in the production of fiber mesh scaffolds by a custom-designed mould. Fiber bundles were randomly displaced into the mould cavities and subjected to thermal treatment at 60 °C for 30 minutes before predefined compression levels along the Z-axis were applied for assuring the bonding between neighboring fibers using a final compression ratio of 22 %. Upon demoulding, scaffolds with dimensions 2.2 ± 0.2 mm thickness and 6mm diameter were obtained. Their porosity

was measured by micro computed tomography (μCT) and the obtained averaged value was 64.4 ± 4.4 % (Figure 5.1).

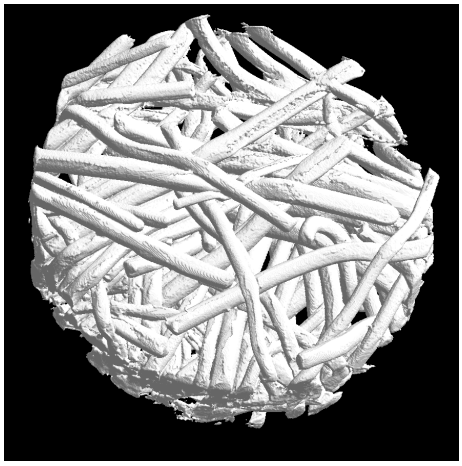

Figure 5.1 Micro computed tomography image from SPCL fiber mesh scaffold.

SPCL meshes were further modified by plasma-induced polymerization. Scaffolds were placed in a radio frequency (13.56 MHz) plasma reactor (Plasma Prep5, Gala Instrument, Germany) and exposed to O_2 plasma at 30 W of power for 15 minutes. During the treatment the pressure inside the reactor was maintained below 20 Pa by adjusting the gas flow. The activated meshes with free radicals formed on the surface were subsequently immersed in a degassed solution of vinyl phosphonic (VPA, 100 mM in 2-propanol) or vinyl sulfonic acid (VSA, 10 v/v% aqueous solution) at ratio 2 ml/scaffold. The reaction was carried out at room temperature for 2 hours under stirring. The scaffolds were thoroughly washed with the solvent used for the reaction in order to remove the unreacted monomer and at the end, the modified samples were dried at room temperature.

5.3.3 Surface chemical composition

Surface elemental analysis of untreated and modified samples was performed by X-Ray Photoelectronspectroscopy (XPS). The spectra were obtained using an ESCALAB 200A instrument from VG Scientific (UK) with PISCES software for data acquisition and analysis. The spectrophotometer was calibrated with reference to Ag 3d5/2 (368.27 eV). Monochromatic Al-Kα radiation (hv = 1486.60 eV) operating at 15 kV (300 W) was used and the measurements were performed at take off angle of 90 ° relative to the samples surface and a constant Analyser Energy mode (CAE). Survey spectra were acquire using

a pass energy of 50 eV over a binding energy range of 0 to 1100 eV, and were used to calculate the elemental composition of the surfaces. High resolution spectra for different regions were obtained using a pass energy of 20 eV. The peaks were fitted using a least-squares peak analysis software, XPSPEAK version 4.1 and the Gaussian/Lorenzian sum function. Background counts were subtracted using a linear baseline and the sample charging was corrected assigning a binding energy of 285.0 eV to the saturated hydrocarbons C1s peak.

5.3.4 Surface topography

The topography of the samples was characterized by Optical profiler analysis using an Interferometric profiler Wyko-NT 1100 (Veeco) operating in Vertical Scanning Interferometry (VSI) mode. The images were processed and analyzed with the analytical software package WycoVision®32.

5.3.5 Protein adsorption

The effect of the surface treatments on protein adsorption was analyzed by fluorescent immunolabeling. Two adhesion proteins were studied: fibronectin (Fn) because it is commonly used in a standard procedures applied to improve adhesion of cells and Vitronectin (Vn) because of its influence on cell spreading and migration. Unmodified and grafted SPCL scaffolds were incubated for 1 hour at the same conditions used for *in vitro* cell culture, i.e. complex protein solution composed of 10 v/v% heat-inactivated fetal bovine serum (FBS; Biochrom AG, Germany) in Dulbecoo's modified Eagle's medium (DMEM; Sigma-Aldrich, Inc, USA). Samples immersed in Phosphate Buffered Saline solution (PBS; Sigma-Aldrich, Inc, USA), were used as blanks. After the incubation time was over, the samples were washed with PBS and incubated at room temperature for 1 hour with primary antibody mouse anti-cow Vn (Santa Cruz, USA) or mouse anti-cow Fn (Santa Cruz, USA). Both primary antibodies were diluted at ratio 1:50 (v/v) in 1% (w/v) Bovine Serum Albumin (BSA, Sigma-Aldich, USA) solution in PBS. All samples were again washed and incubated for 1 hour at room temperature with goat anti-mouse Alexa Fluor 488 IgG (H+L) secondary antibody (Invitrogen, USA). Labeled samples were analyzed by an Olimpus IX81 Confocal Laser Scanning Microscope (CLSM).

5.3.6 Cell culture conditions and seeding

A human osteosarcoma cell line (SaOs-2), an immortalized cell line with an osteoblastic phenotype, was obtained from European Collection of Cell Cultures (ECACC, UK) and was used in the cell culture studies. The cells were cultured in DMEM supplemented with 10000 U/ml penicillin-G sodium, 10000 µg/ml streptomycin sulfate and 25 µg/ml amphotericin B in a 0.85 % saline (Gibco, Invitrogen Corporation, UK) and 10 % of FBS in a humidified atmosphere with 5 % of CO_2. A suspension of 2×10^5 cells was added to each scaffold. The scaffolds were incubated for 3, 7 and 14 days under standard culture conditions (37 °C, 5 % CO_2, humidified atmosphere).

The morphology of SaOs-2 cells was observed by Scanning Electron Microscopy (S360, Leica Cambridge, UK). Cells were fixed using 2.5 % (v/v) glutaraldehyde (Sigma, USA) solution in PBS. Prior the analysis, the samples were dehydrated by graded ethanol solutions.

Cell viability was analyzed by MTS assay. The cultured materials were incubated (3hrs, 37ºC, humidified atmosphere of 5 % CO_2) with 500 µl of MTS solution in DMEM culture medium without phenol red (Sigma-Aldrich, Inc, USA). Optical Density (OD) was read in a microplate reader (Bio-Tek, USA) at 490 nm.

DNA quantification was used to evaluate cell proliferation. Cells were lysed by osmotic and thermal shock and the obtained supernatant was used for DNA analysis. DNA content along the time of culture was determined using the PicoGreen dsDNA kit (MolecularProbes) and the fluorescence was read (485 nm/528 nm of excitation/emission) in a microplate reader. The DNA amounts were calculated from a standard curve.

Triplicates were analyzed at each time point for both assays (MTS and DNA). Statistical analysis was performed and the data are reported as mean ± standard deviation. ANOVA test for independent samples were performed and the differences were considered statistically significant if $p < 0.05$.

5.4 Results and discussion

Surface design of biomedical devices applied in direct contact with the body is crucial for their acceptance or rejection from the surrounding tissues. The modification of the surface chemistry and/or topography is a way to improve the biological performance of a biomaterial without changing its bulk properties. One of the most versatile and effective tools to tailor surface chemistry and properties of solids is the polymer grafting. In contrast to physical coating, grafting has several advantages such as covalent attachment of graft

chains onto a polymer surface which avoids their delamination and assures long term stability of introduced functionalities. Several approaches have been proposed for surface grafting on 2D structures, but not all of those are viable for complex 3D architectures. The hypothesis checked out in this study is the application of plasma induced polymerization for grafting of phosphonic and sulfonic groups on SPCL fiber mesh scaffolds.

5.4.1 Surface chemistry

The success of the applied treatment was primary checked out by surface elemental analysis. XPS survey spectra were used to assess the surface elemental composition (at %) of untreated and modified SPCL scaffolds. Two main elements, C and O, were present on the surface of untreated samples. The found ratio between them was similar to the theoretically calculated one for PCL (Table 5.1). This result indicates that the synthetic component is predominant on the surface of the sample and it is in agreement with previously reported results for SPCL materials [12, 15].

Table 5.1 Elemental composition of untreated and modified SPCL fiber meshes determined by XPS

Material	$C1_s$ (at%)	$O1_s$ (at%)	$P2_p$ (at%)	$S2_p$ (at%)	C:O ratio
Starch (theoretical)	50.0	50.0	-	-	1.0
PCL (theoretical)	75.0	25.0	-	-	3.0
SPCL (theoretical)	67.4	32.6	-	-	2.1
SPCL meshes	75.1	24.9	-	-	3.0
VSA grafted SPCL	67.8	32.0	-	0.2	2.1
VPA grafted SPCL	51.1	44.3	4.6	-	1.1

Plasma-induced polymerization resulted in higher oxygen content. Additionally, new peaks appear in the spectrum of the vinyl phosphonic acid (VPA) grafted sample corresponding to P2p (128.5 eV) and P2s (185.5 eV), confirming the introduction of phosphonic groups. We have calculated the presence of phosphorous on the surface from P2p transition and a concentration of 4.6 %at was found (Table 5.1). The presence of sulfur peak (0.2 %at) in XPS spectrum of the sample treated with vinyl sulfonic acid (VSA), confirms the success

of the grafting process with this monomer although with a lower efficiency than the VPA grafting. Some impurities (Si, N, Na, Sn and Cu) appear in the surface spectra of some samples, usually at very low concentration, and were excluded from the calculations of the elemental analysis (at %) showed in Table 5.1.

C1s, O1s, P2p and S2p core level spectra of untreated and grafted materials were analyzed in order to obtain additional details about the surface chemical composition. Figure 5.2a shows the binding energy region corresponding to C1s peak (279.8-291.9 eV) for SPCL sample. The peak-fitting was performed taking into consideration both PCL and starch chemical structures (Figure 5.3).

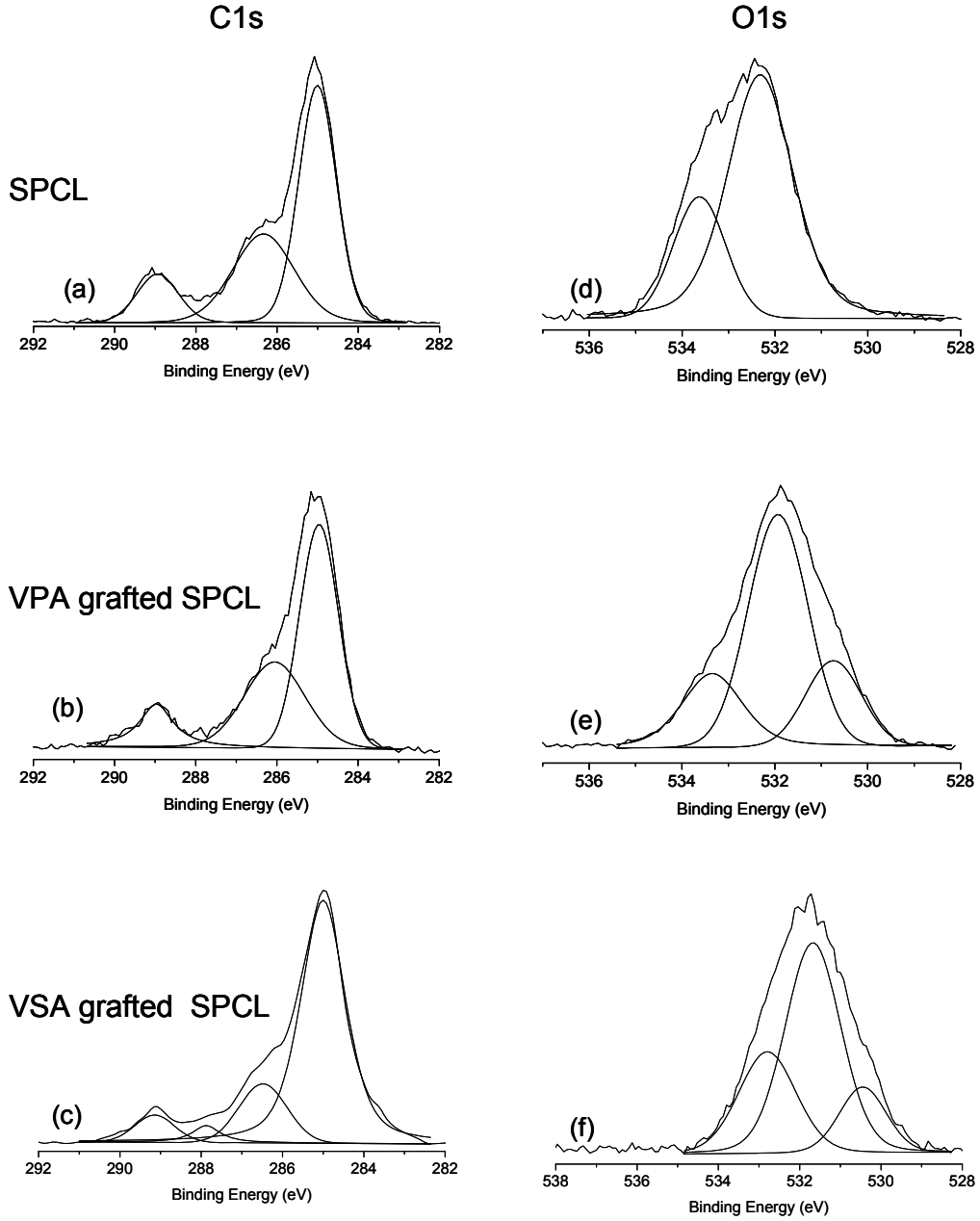

Figure 5.2 XPS core level spectra of untreated and grafted samples in the regions of C1s (left) and O1s (right).

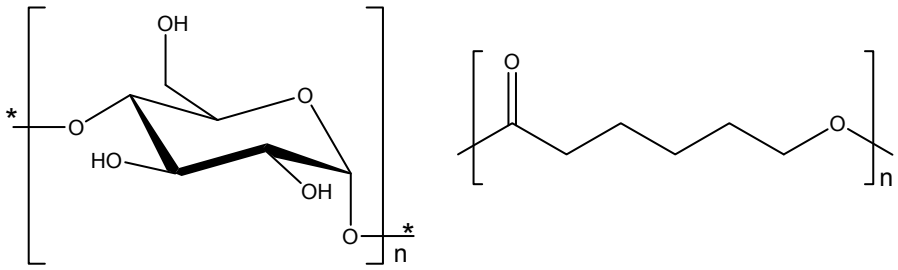

Starch poly (ε–caprolactone)

Figure 5.3 Chemical structures of the components of the blend.

The peak at 285.0 eV was assigned to C-H/C-C chemical bonds of the starch backbone and C-C chain from PCL. The signal centered at 286.3 eV corresponds to hydroxyl bonded carbons (C-OH) from starch and the ester bonded carbons (C-O) from PCL. The peak observed at 288.9 eV was assigned to O-C-O bonds from starch and the C=O bond from the synthetic component [28]. C1s spectrum of VPA grafted samples (Figure 5.2b) did not reveal significant changes when compared with untreated SPCL scaffolds. The expected binding energy of C-P is around 286-286.4 eV [29, 30] and therefore the C1s peak correspondent to C-PO_3 is probably overlapped by the C-OH/C-O peak. For VSA grafted samples, a new peak was detected at 287.9 eV and it assigned to C-S bonds from sulfonic acid (Figure 5.2c). To our knowledge there are only few work focused on the chemical shift of C-S and there is not agreement in the reported values [31-33]. Two peaks were identified in the high resolution O1s spectrum of SPCL scaffolds (Figure 5.2d). The peak at 532.3 eV was assigned to C=O bonds from PCL [29, 33] and the peak at 533.6 eV to C-OH/O-C-O from starch and C-O-C from both synthetic and natural components of the blend [33]. After VPA grafting (Figure 5.2e), additional peak at 531.0 eV appears in the O1s spectrum which was attributed to the P=O group. The second peak at 532.0 eV was assigned to the C=O and the last peak at 533.4 eV corresponds to C-O-/C-OH/C-O-C and the P-OH groups for which binding energies between 533.0 eV and 533.6 eV have been reported [29, 30, 34]. The O1s core level spectra of VSA grafted samples (Figure 5.2f), showed a new additional peak compared to the untreated SPCL scaffolds. This peak is allocated at 531.1 eV and it was assigned to O=S bonds [31, 32]. The P2p signal which appears in the spectrum of VPA grafted fiber meshes is a non-resolved doublet with 2p1/2 and 2p3/2 core levels. The peak is allocated at 133.6 eV and present a full width at half-maximum (FWHM) of 2.1eV [29, 34] (graph not shown).

5.4.2 Surface topography

When a polymer surface is treated by plasma, together with surface functionalization, surface degradation or etching may also occur [35]. Hence, chemical surface modification is usually associated with changes of surface topography/morphology. Consequently, the protein and cell interactions with the material may be also modified. An optical profiler analyze was performed to evaluate the eventual topographical changes on the surface of the fibers as a result of the applied treatment. As it can be seen in Figure 5.4, no significant changes were detected on the fiber surfaces after the performed modification.

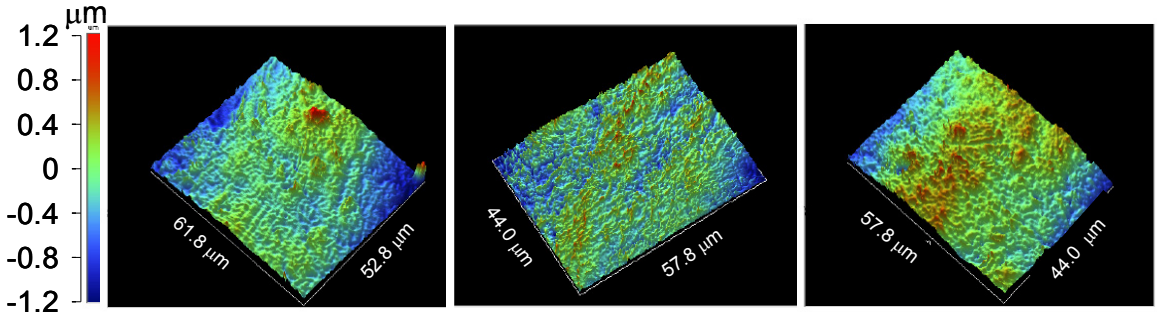

Figure 5.4 Optical profile images: From left to right untreated SPCL, VSA grafted and VPA grafted scaffolds.

Although the roughness calculated from 107X magnification images seems to increase in absolute value after the plasma treatment (Table 5.2), it must be noticed that this tendency is not enough evident because of the difference in the roughness between the fibers in the same scaffold.

Table 5.2 Values for the roughness, calculated from the optical profiler images (107X magnification)

	SPCL	VSA grafted SPCL	VPA grafted SPCL
Ra /nm	219.0 ± 22.7	245.1 ± 16.0	255.1 ± 14.0
Rq /nm	283.7 ± 34.6	308.3 ± 11.7	335.6 ± 20.5

5.4.3 *In vitro* biological evaluation

When a biomaterial is brought in a contact with a physiological milieu, it is very unlikely that cells will make a direct contact with its surface. The very first event either *in vivo* or *in vitro* is the protein adsorption from blood or serum to the material surface. The surface

properties set the characteristics of the adsorbed protein layer and the nature of the established protein-surface interactions will modulate cell adhesion and consequently cell biochemical mechanisms via interactions with cell-surface molecules, such as integrins. Figure 5.5 demonstrates that Vn adsorbed on all (untreated and modified) SPCL scaffolds, whereas Fn was not detected on any of the studied materials. This result is no surprising and it is in an agreement with previously reported data for SPCL materials showing predominant adsorption of Vn versus Fn from complex protein solutions [12, 36]. In fact, Vn is present at higher concentration than Fn in FBS. FBS for cell culture is prepared by clotting at 4 °C which can lead to a considerable depletion of Fn but not of Vn [37]. Another process which is associated with the lower protein adsorption of Fn *vs.* Vn is the so-called Vroman effect [38] which involves inhibition of Fn adsorption from serum by the ability of other proteins to displace it from the surface. This effect has been observed for Fn when serum with concentration above 3 % is used [39]. Because we have been working with 10 % FBS, the lack of Fn adsorption is an expectable result. On the other hand at this conditions, Vn can be adsorbed from the medium (Figure 5.5) and therefore to participate in the mediation of the following events such as cell adhesion, spreading and growth [40]. Vn adsorption profile on untreated and modified materials showed that the fluorescence intensity for SPCL scaffolds increase after the modification with VSA and even more after VPA grafting.

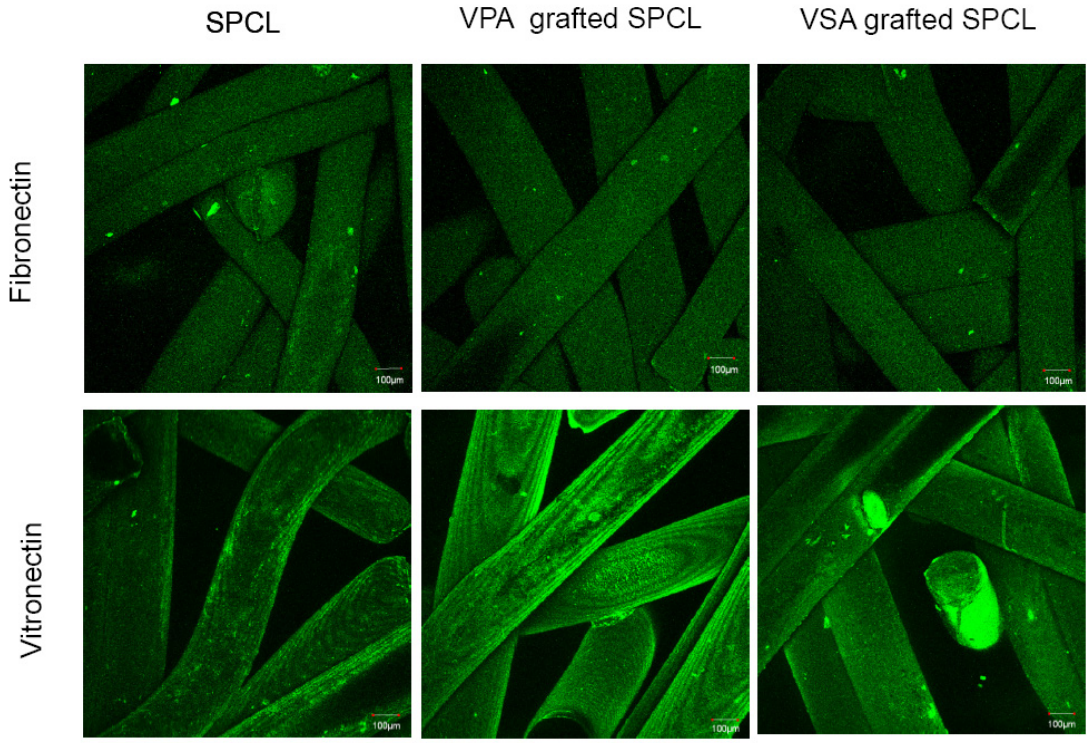

Figure 5.5 Confocal Laser Scanning Microscopy photographs of non-modified and grafted scaffolds stained for Fn and Vn.

These results indicate that the surface chemical composition significantly influences both the content of the adsorbed protein layer and the interactions between the material surface and the adsorbed proteins [41]. Vn plays an essential role on bone-derive cells attachment and spatial distribution [42, 43]. Hence, it is expected that the observed difference in Vn adsorption on untreated and modified scaffolds will change the behavior of those cells. Therefore, we tested osteoblast-like cells cultured in direct contact with the studied materials. Osteoblast cells *in vitro* have been shown to depend primarily on the adsorbed Vn or Fn for initial adhesion and spreading on materials [44]. Therefore, the ability of materials to support cell adhesion and spreading is mainly determined by their capability to adsorb these proteins from serum in an active state.

Figure 5.6 shows the SEM micrographs of SaOs-2 seeded on the surfaces of modified and untreated samples after 3, 7 and 14 days of culture. After 3 days of culture cells were able to attach and spread on all the surfaces, showing the typical morphology of osteoblast cells with polygonal shape. However, some differences were observed between the untreated SPCL and the grafted samples. While on modified scaffolds the cells were able to extend and to bridge between fibers, on untreated samples these bridges were not observed. Prolongation of the cultured periods to 1 and 2 weeks resulted in higher cell density, indicating the ability of SaOs-2 to proliferate in all the materials. At 14 days of culture, SaOs-2 formed a complete monolayer covering all the fibers, as well as some of the contact junction between fibers.

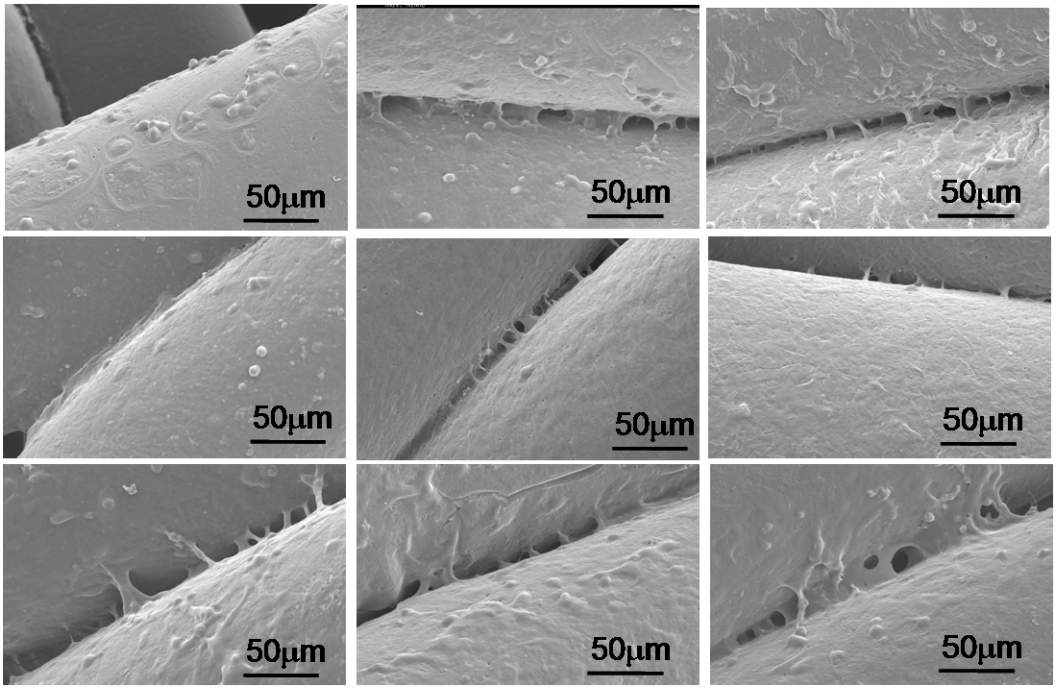

Figure 5.6 SEM microphotographs of SaOs-2 cultures on SPCL, VSA grafted and VPA grafted scaffolds (from left to right) after 3, 7 and 14 days of culture (from up to down).

Surface properties can induce not only morphological changes but they can also influence the metabolic activity of the cells. MTS was used to evaluate the effect of the grafted functional groups on the cell viability at different time points. MTS is an indirect test that determines cell mitochondrial activity which in turn can be related with the number of viable cells. For all studied materials, an increasing number of viable cells was detected with prolonged culture times. These results show the capability of both unmodified and treated scaffolds to support cell proliferation. However, Figure 5.7 demonstrates that the VPA grafting significantly increases the number of viable cells, when compared with untreated SPCL scaffolds, and this tendency was kept during the all studied period. The presence of phosphate functional groups also increases the cell viability compared with sulfonic groups grafted at the same conditions.

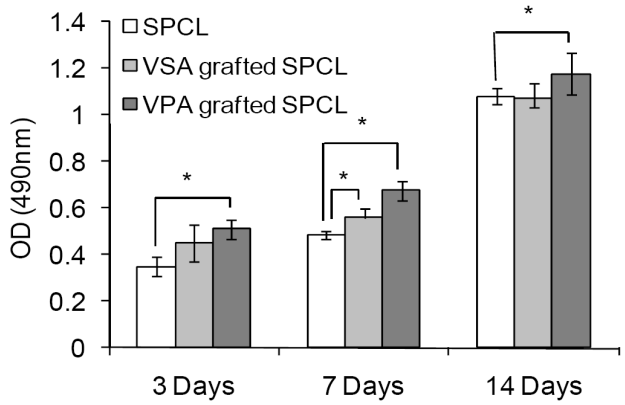

Figure 5.7 Viability of SaOs-2, evaluated by MTS assay, cultured on untreated and grafted SPCL fiber meshes. * Significantly different (ANOVA test, $p<0.05$).

DNA quantification was used to obtain more accurate quantitative results and to determine the cell proliferation profiles (Figure 5.8). DNA quantification confirmed the positive effect of the VSA and VPA grafting on the proliferation of SaOs-2. Once again the same order was kept: SPCL<VSA grafted SPCL< VPA grafted SPCL.

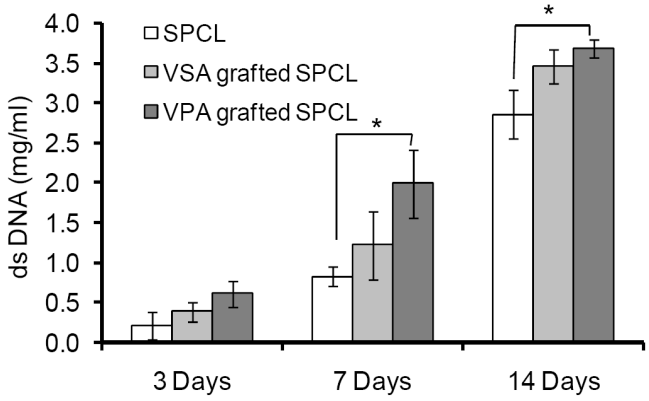

Figure 5.8 DNA concentration corresponding to SaOs-2 cultured on non-modified and functionalized scaffolds. * Significantly different (ANOVA test, $p<0.05$).

5.5 Conclusions

Plasma-induced polymerization is herein proposed as an effective method for 3D porous scaffolds functionalization. The results from the surface analyses confirmed that using this method we were successful in grafting sulfonic or phosphonic groups on the materials with complex shape without to change the surface morphology and topography. Although this method can be extended to different materials and monomers, it must be noticed that its efficiency is dependent on the used monomer: we have found that the reaction was more efficient for VPA with 4.6 %at of P measured on the surface, whereas only 0.2 %at of S was registered in the surface composition of VSA grafted surfaces. The introduced functional groups modulate the protein adsorption from serum as indicated by the confocal microscopy analysis. In this study, we have observed that Vn adsorption is favored on both modified samples compared with untreated SPCL scaffolds. Moreover, comparing treated samples between them, VPA grafted samples presented a higher quantities of adsorbed Vn compared with VSA grafted ones. Vn adsorption profiles were correlated with cell adhesion and proliferation studies; materials with higher Vn adsorption presented higher cell adhesion and proliferation. We further found that grafting of negatively charged units such as sulfonic and phosphonic groups induced remarkably different osteoblast-like cells (SaOs-2) response in terms of adhesion and proliferation: VPA grafted samples showed the highest cell adhesion and proliferation.
Overall, the results from this study further testify the potential of surface grafting of functional groups by plasma-induced polymerization in the context of bone tissue engineering.

5.6 Acknowledgements

The authors acknowledge funding from EU Marie Curie Actions, Alea Jacta Est (MEST-CT-2004-008104) and Portuguese Foundation for Science and Technology (FCT) (SFRH/BPD/34545/2007). This work was carried out under the scope of the European NoE EXPERTISSUES (NMP3-CT-2004-500283). The authors also acknowledge Dr M.I. Santos and C. Serra for their assistance on CLSM and XPS experiments.

5.7 References

1. Vacanti, J.P.; Langer, R. Tissue engineering: the design and fabrication of living replacement devices for surgical reconstruction and transplantation. *Lancet*, 1999, **354**, 32-34.

2. Liu, X.; Ma, P.X. Polymeric Scaffolds for Bone Tissue Engineering. *Annals of Biomedical Engineering*, 2004, **32,** (3), 477-486.

3. Luo, Y.; Engelmayr, G.; Auguste, D.T.; Ferreira, L.d.S.; Karp, J.M.; Saigal, R.; Langer, R., *25. Three-Dimensional Scaffolds*, in *Principles of Tissue Engineering*, R. Lanza, R. Langer, and J.P. Vacanti, Editors. 2007, Elsevier, Inc. 359-373.

4. Gomes, M.E.; Holtorf, H.L.; Reis, R.L.; Mikos, A.G. Influence of the porosity of starch-based fiber mesh scaffolds on the proliferation and osteogenic differentiation of bone marrow stromal cells cultured in a flow perfusion bioreactor. *Tissue Engineering*, 2006, **12,** (4), 801-809.

5. Stevens, B.; Yang, Y.; Mohandas, A.; Stucker, B.; Nguyen, K.T. A review of materials, fabrication methods, and strategies used to enhance bone regeneration in engineered bone tissues. *Journal of Biomedical Materials Research - Part B Applied Biomaterials*, 2008, **85,** (2), 573-582.

6. Tuzlakoglu, K.; Reis, R.L. Biodegradable Polymeric Fiber Structures in Tissue Engineering. *Tissue Engineering Part B-Reviews*, 2009, **15,** (1), 17-27.

7. Azevedo, H.S.; Gama, F.M.; Reis, R.L. In vitro assessment of the enzymatic degradation of several starch based biomaterials. *Biomacromolecules*, 2003, **4,** (6), 1703-1712.

8. Martins, A.M.; Pham, Q.P.; Malafaya, P.B.; Sousa, R.A.; Gomes, M.E.; Raphael, R.M.; Kasper, F.K.; Reis, R.L.; Mikos, A.G. The Role of Lipase and alpha-Amylase in the Degradation of Starch/Poly(epsilon-Caprolactone) Fiber Meshes and the Osteogenic Differentiation of Cultured Marrow Stromal Cells. *Tissue Engineering Part A*, 2009, **15,** (2), 295-305.

9. Gomes, M.E.; Azevedo, H.S.; Moreira, A.R.; Ella, V.; Kellomaki, M.; Reis, R.L. Starch-poly(epsilon-caprolactone) and starch-poly(lactic acid) fibre-mesh scaffolds for bone tissue engineering applications: structure, mechanical properties and degradation behaviour. *Journal of Tissue Engineering and Regenerative Medicine*, 2008, **2,** (5), 243-252.

10. Gomes, M.E.; Sikavitsas, V.I.; Behravesh, E.; Reis, R.L.; Mikos, A.G. Effect of flow perfusion on the osteogenic differentiation of bone marrow stromal cells cultured on

starch-based three-dimensional scaffolds*. Journal of Biomedical Materials Research Part A*, 2003, **67,** (1), 87-95.

11. Santos, M.I.; Fuchs, S.; Gomes, M.E.; Unger, R.E.; Reis, R.L.; Kirkpatrick, C.J. Response of micro- and macrovascular endothelial cells to starch-based fiber meshes for bone tissue engineering*. Biomaterials*, 2007, **28,** (2), 240-248.

12. Santos, M.I.; Pashkuleva, I.; Alves, C.M.; Gomes, M.E.; Fuchs, S.; Unger, R.E.; Reis, R.L.; Kirkpatrick, C.J. Surface-modified 3D starch-based scaffold for improved endothelialization for bone tissue engineering*. Journal of Materials Chemistry*, 2009, **19,** (24), 4091–4101.

13. Marques, A.P.; Reis, R.L.; Hunt, J.A. An in vivo study of the host response to starch-based polymers and composites subcutaneously implanted in rats*. Macromolecular Bioscience*, 2005, **5,** (8), 775-785.

14. Pavlov, M.P.; Mano, J.F.; Neves, N.M.; Reis, R.L. Fibers and 3D mesh scaffolds from biodegradable starch-based blends: Production and characterization*. Macromolecular Bioscience*, 2004, **4,** (8), 776-784.

15. Pashkuleva, I.; Azevedo, H.S.; Reis, R.L. Surface structural investigation of starch-based biomaterials*. Macromolecular Bioscience*, 2008, **8,** (2), 210-219.

16. Pashkuleva, I.; Marques, A.P.; Vaz, F.; Reis, R.L. Surface modification of starch based blends using potassium permanganate-nitric acid system and its effect on the adhesion and proliferation of osteoblast-like cells*. J. Mat.Sci.: Mat. Med.*, 2005, **16**, 81-92.

17. Lopez-Perez, P.M.; da Silva, R.M.P.; Serra, C.; Pashkuleva, I.; Reis, R.L. Surface phosphorylation of chitosan significantly improves Osteoblast cells viability, attachment and proliferation*. Submitted*, 2009.

18. Lopez-Perez, P.M.; Marques, A.P.; da Silva, R.M.P.; Pashkuleva, I.; Reis, R.L. Effect of chitosan membrane surface modification via plasma induced polymerization on the adhesion of osteoblast-like cells*. Journal of Materials Chemistry*, 2007, **17,** (38), 4064-4071.

19. Moreira, P.L.; An, Y.H.; Santos, A.R.; Genari, S.C. In vitro analysis of anionic collagen scaffolds for bone repair*. Journal of Biomedical Materials Research Part B-Applied Biomaterials*, 2004, **71,** (2), 229-237.

20. Chen, Y.M.; Shiraishi, N.; Satokawa, H.; Kakugo, A.; Narita, T.; Gong, J.P.; Osada, Y.; Yamamoto, K.; Ando, J. Cultivation of endothelial cells on adhesive protein-free synthetic polymer gels*. Biomaterials*, 2005, **26,** (22), 4588-4596.

21. Chaterji, S.; Gemeinhart, R.A. Enhanced osteoblast-like cell adhesion and proliferation using sulfonate-bearing polymeric scaffolds*. Journal of Biomedical Materials Research Part A*, 2007, **83,** (4), 990-998.

22. Gemeinhart, R.A.; Bare, C.M.; Haasch, R.T.; Gemeinhart, E.J. Osteoblast-like cell attachment to and calcification of novel phosphonate-containing polymeric substrates. *Journal Of Biomedical Materials Research Part A*, 2006, **78A,** (3), 433-440.

23. Tan, J.; Gemeinhart, R.A.; Ma, M.; Saltzman, W.M. Improved cell adhesion and proliferation on synthetic phosphonic acid-containing hydrogels. *Biomaterials*, 2005, **26,** (17), 3663-3671.

24. Viornery, C.; Guenther, H.L.; Aronsson, B.O.; Pechy, P.; Descouts, P.; Gratzel, M. Osteoblast culture on polished titanium disks modified with phosphonic acids. *Journal of Biomedical Materials Research*, 2002, **62,** (1), 149-155.

25. He, G.; Dahl, T.; Veis, A.; George, A. Nucleation of apatite crystals in vitro by self-assembled dentin matrix protein, 1. *Nature Materials*, 2003, **2,** (8), 552-558.

26. Bastioli, C.; Belliotti, V.; Cella, G.; Del Guidice, L.; Montino, S.; Perego, G., *Bodegradable polymeric compositions comprising starch and a thermoplastic polymer*, PCT, Editor. 1998, Novamont S. p. A., Novara, italy.

27. Bastioli, C.; Bellotti, V.; Del Tredici, G.; Lombi, R., *Biodegradable polymeric compositions based on starch and thermoplastic polymers*, E.P. Office, Editor. 1997, Novamont S.p.A.: Italy.

28. Clark, D.T.; Cromarty, B.J.; Dilks, A. A theoretical investigation of molecular core binding and relaxation energies in a series of oxygen-containing organic-molecules of interest in the study of surface oxidation of polymers. *Journal of Polymer Science Part a-Polymer Chemistry*, 1978, **16,** (12), 3173-3184.

29. Adden, N.; Gamble, L.J.; Castner, D.G.; Hoffmann, A.; Gross, G.; Menzel, H. Phosphonic acid monolayers for binding of bioactive molecules to titanium surfaces. *Langmuir*, 2006, **22,** (19), 8197-8204.

30. Viornery, C.; Chevolot, Y.; Leonard, D.; Aronsson, B.O.; Pechy, P.; Mathieu, H.J.; Descouts, P.; Gratzel, M. Surface modification of titanium with phosphonic acid to improve bone bonding: Characterization by XPS and ToF-SIMS. *Langmuir*, 2002, **18,** (7), 2582-2589.

31. Nasef, M.M.; Saidi, H. Surface studies of radiation grafted sulfonic acid membranes: XPS and SEM analysis. *Applied Surface Science*, 2006, **252,** (8), 3073-3084.

32. Ruangchuay, L.; Schwank, J.; Sirivat, A. Surface degradation of alpha-naphthalene sulfonate-doped polypyrrole during XPS characterization. *Applied Surface Science*, 2002, **199,** (1-4), 128-137.

33. Wagner, C.D.; Naumkin, A.V.; Kraut-Vass, A.; Allison, J.W.; Powell, C.J.; Rumble, J.R.; Jr, *NIST Standard Reference Database 20 Version 3.5* 2003, National Institute of Standards and Technology.

34. Textor, M.; Ruiz, L.; Hofer, R.; Rossi, A.; Feldman, K.; Hahner, G.; Spencer, N.D. Structural chemistry of self-assembled monolayers of octadecylphosphoric acid on tantalum oxide surfaces. *Langmuir*, 2000, **16,** (7), 3257-3271.

35. Chu, P.K.; Chen, J.Y.; Wang, L.P.; Huang, N. Plasma-surface modification of biomaterials. *Materials Science & Engineering R-Reports*, 2002, **36,** (5-6), 143-206.

36. Alves, C.M.; Reis, R.L.; Hunt, J.A. Preliminary study on human protein adsorption and leukocyte adhesion to starch-based biomaterials. *Journal of Materials Science-Materials in Medicine*, 2003, **14,** (2), 157-165.

37. Hayman, E.G.; Pierschbacher, M.D.; Suzuki, S.; Ruoslahti, E. Vitronectin - a Major Cell Attachment-Promoting Protein in Fetal Bovine Serum. *Experimental Cell Research*, 1985, **160,** (2), 245-258.

38. Vroman, L. Effect of Adsorbed Proteins on the Wettability of Hydrophilic and Hydrophobic Solids. *Nature*, 1962, **196,** (4853), 476–477.

39. Knox, P. Kinetics of Cell Spreading in the Presence of Different Concentrations of Serum or Fibronectin-Depleted Serum. *Journal of Cell Science*, 1984, **71**, 51-59.

40. Underwood, P.A.; Bennett, F.A. A Comparison of the Biological-Activities of the Cell-Adhesive Proteins Vitronectin and Fibronectin. *Journal of Cell Science*, 1989, **93**, 641-649.

41. Bale, M.D.; Wohlfahrt, L.A.; Mosher, D.F.; Tomasini, B.; Sutton, R.C. Identification of Vitronectin as a Major Plasma-Protein Adsorbed on Polymer Surfaces of Different Copolymer Composition. *Blood*, 1989, **74,** (8), 2698-2706.

42. McFarland, C.D.; Mayer, S.; Scotchford, C.; Dalton, B.A.; Steele, J.G.; Downes, S. Attachment of cultured human bone cells to novel polymers. *Journal of Biomedical Materials Research*, 1999, **44,** (1), 1-11.

43. Thomas, C.H.; McFarland, C.D.; Jenkins, M.L.; Rezania, A.; Steele, J.G.; Healy, K.E. The role of vitronectin in the attachment and spatial distribution of bone-derived cells on materials with patterned surface chemistry. *Journal of Biomedical Materials Research*, 1997, **37,** (1), 81-93.

44. Steele, J.G.; McFarland, C.; Dalton, B.A.; Johnson, G.; Evans, M.D.M.; Howlett, C.R.; Underwood, P.A. Attachment of Human Bone-Cells to Tissue-Culture Polystyrene and to Unmodified Polystyrene - the Effect of Surface-Chemistry Upon Initial Cell Attachment. *Journal of Biomaterials Science-Polymer Edition*, 1993, **5,** (3), 245-257.

Chapter 6

Hydrophobic-electrostatic balance driving the LCST offset aggregation-redissolution behavior of *N*-alkylacrylamide based ionic terpolymers

6.1 Abstract

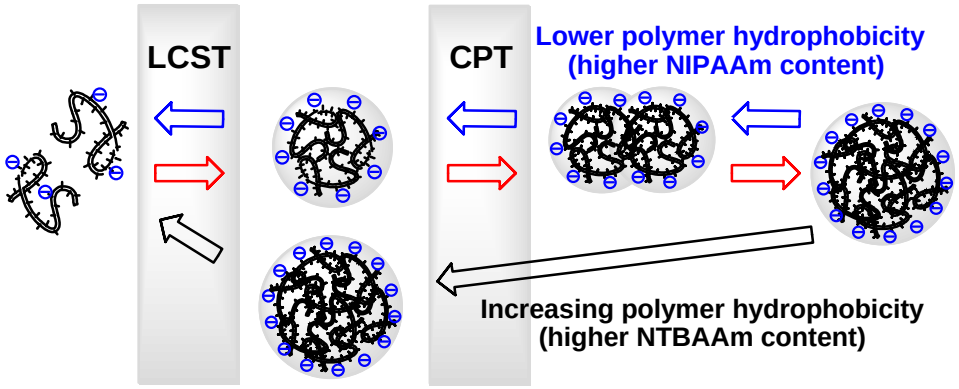

A series of random terpolymers composed of *N*-isopropylacrylamide (NIPAAm), 2-acrylamido-2-methyl-1-propanesulfonic acid (AMPS) and *N-tert*-butylacrylamide (NTBAAm) monomers were synthesized by free radical polymerization. The molar fraction of the negatively charged monomer (AMPS) was maintained constant (0.05) for all studied terpolymer compositions. Turbidity measurements were used to evaluate the influence of the relative amount of NIPAAm and NTBAAm, polymer concentration, and solution ionic strength on the cloud point and redissolution temperatures (macroscopic phase separation). Dynamic light scattering (DLS) was employed to elucidate some aspects regarding the molecular scale mechanism of the temperature-induced phase separation and to determine the low critical solution temperature (LCST). The aqueous solutions of terpolymers remained clear at all studied temperatures; turbidity was only observed in the presence of NaCl. The cloud point temperature (CPT) determined by turbidimetry was found to be systematically much higher than the LCST determined by DLS; nanosized aggregates were observed at temperatures between the LCST and the CPT. Both CPT and LCST decreased when increasing the molar ratio of NTBAAm (increased hydrophobicity). It was found that above a critical molar fraction of NTBAAm (0.25-0.30) the aggregation rate suddenly decreased. Polymers with NTBAAm content lower than 0.25 showed a fast macroscopic phase separation, but the formed large aggregates are disaggregating during the cooling ramp at temperatures still higher than the LCST. On the contrary, polymers with NTBAAm contents above 0.30 showed a slow macroscopic phase

separation and the formed large aggregates only redissolved when LCST was reached. These differences were explained on the basis of a delicate balance between the electrostatic repulsion and the hydrophobic attractive forces, which contribute cooperatively to the formation of metastable nanosized aggregates.

This chapter is based on the following publication:
Paula M. López-Pérez; Ricardo M.P. da Silva;Iva Pashkuleva; Francisco Parra; Rui L. Reis; Julio San Roman. **Langmuir**, 2010, DOI 10.1021/la903904t, *in press*

6.2 Introduction

Several polymers that are soluble in a certain solvent at low temperature undergo phase separation above a critical temperature value known as lower critical solution temperature (LCST). At the macroscopic level the phenomenon is similar for all polymer solutions that present LCST; a clear solution becomes "milky" upon heating (cloud point). Polymers showing this behavior in aqueous solution, such as poly(*N*-isopropylacrylamide) (pNIPAAm) and other *N*-substituted acrylamide polymers, had been extensively studied [1-7] because of their theoretical significance and technological potential. It has been shown that isolated pNIPAAm polymer chains undergo an abrupt conformational transition from expanded and flexible coil to an insoluble compact globule, as the temperature is raised above the Flory Θ-temperature [2-7], which is the theoretical limit between good and poor solvent regions. The coil-to-globule transition of these synthetic macromolecules provides a simple phenomenological model for many biological systems, such as protein folding, native DNA packing, and network collapse [8]. For example, (i) the molten globule state of proteins has been also observed for single pNIPAAm chains [3]; (ii) when copolymerized with small amounts of acrylic acid, collapsed polymer chains form thermodynamically stable interchain aggregates stabilized by surface charge [9], resembling protein quaternary structure; (iii) the ability of salts to influence pNIPAAm LCST follows the same trend recurrently found for the precipitation of proteins (salting out), known as the Hofmeister series [10]. From the technological point of view, these polymers have been proposed for applications such as pulsatile drug delivery systems [11], polymer supports in catalysis and synthesis [12], biomolecule affinity separation [13], nondestructive harvesting in mammalian cell culture [14, 15], just to enumerate a few.

In terms of polymer-solvent interactions, the coil-to-globule transition involves combined hydrophobic hydration and hydrogen bonding effects. During phase separation, hydrogen bonds between water molecules and polymer amide groups are disrupted and replaced by intramolecular hydrogen bonds among the dehydrated amide groups [16, 17]. If the polymer concentration is not exceptionally low, intrachain condensation is readily followed by aggregation and coalescence of the collapsing globules, prompted by hydrophobic interactions and interchain hydrogen bonding [4-7, 16]. The intrachain coil-to-globule transition and the interchain aggregation are two independent, but competing, processes [4-7, 9]. Except on extremely diluted solutions, where interactions between different polymer chains are kept at insignificant levels [3-7], both processes occur concomitantly in most practical situations.

N-Alkyl-substituted polyacrylamides are a class of homopolymers that combine simultaneously in the same monomer hydrophilic amide groups able to form hydrogen bonds with the hydration water and hydrophobic *N*-alkyl groups, forcing hydration water to assume a more organized structure [18]. Thus, it is not surprising that the behavior of a *N*-substituted acrylamide homopolymer in solution depends markedly on the *N*-substituent nature. Whereas the *N*-isopropyl-substituted acrylamide phase separation appears at around 32 ºC [4-7], more hydrophobic substituents lower the LCST and more hydrophilic ones increase the LCST [1]. Moreover, its copolymerization with more hydrophobic or hydrophilic monomers has the same effect on the LCST, providing a suitable route to fine-tune the LCST, by just making polymers with subtle differences in the composition [1, 19-21]. Interestingly, a LCST behavior was observed for nonionic copolymers of "very hydrophobic" or "very hydrophilic" *N*-substituted polyacrylamides that produce either completely insoluble or completely soluble homopolymers, respectively [1]. The LCST of these nonionic copolymers could be adjusted between the freezing and boiling points of the aqueous solutions by varying the composition [1]. On the other hand, ionic copolymer gels of *N*-*tert*-butylacrylamide (NTBAAm) and 2-acrylamido-2-methyl-1-propanesulfonic acid (AMPS) presented a discontinuous phase separation only in a limited compositional range. When the amount of the negatively charged AMPS was increased over a certain limit, the repulsive electrostatic interactions avoided the sudden collapse of the polymer network, and consequently a continuous-type swelling was observed with the temperature increase [21].

In this study, a series of ionic terpolymers of three different *N*-substituted acrylamide monomers (NIPAAm, NTBAAm, and AMPS) was synthesized, and the effect of NaCl and polymer concentrations in the solution behavior was evaluated. Our interest in ionic thermoresponsive polymers relies on their technological relevance because of their ability to form surfactant-free nanoparticles stabilized by surface charge above the LCST [9] or to interact with oppositely charged macromolecules, allowing for the construction of thermoresponsive polyelectrolyte complexes [22]. AMPS was chosen to afford a negative charge to the terpolymers because it is a strong acid [23] (pK_a=1.9) that dissociates completely in the pH range of most envisaged applications. An AMPS molar ratio of 0.05 was chosen to ensure a sharp phase separation, since it is reasonably below the limit wherein p(AMPS-co-NTBAAm) gels lose their discontinuous phase separation behavior [21]. Furthermore, the functional sulfonic group position in AMPS gives the terpolymers a continuous structural similarity along the polymer backbone, composed of isopropyl and *tert*-butyl side groups *N*-linked to inner amide groups. The sulfonic groups bound to some of the *tert*-butyl side groups are located on the periphery of the macromolecule (see Figure 6.1). This avoids the disruption of the continuity of the *N*-alkyl groups, which has

been referred in the literature to decrease hydrophobic aggregation force necessary for the cooperative chain collapse, thus decreasing phase separation sharpness [15, 24]. All terpolymers were synthesized containing the same relative amount of AMPS, i.e., containing the same charge. In order to adjust the LCST, terpolymer hydrophobic content was varied by changing NTBAAm to NIPAAm monomer ratio.

6.3 Materials and Methods

N-Isopropylacrylamide (NIPAAm, Acros Organics) and 2,2'-azobis-isobutyronitrile (AIBN) (Fluka) were recrystallized from a *n*-hexane/diethyl ether (5:1) mixture and methanol, respectively. 2-Acrylamido-2-methyl-1-propanesulfonic acid (AMPS) and *N-tert*-butylacrylamide (NTBAAm) were both purchased from Sigma-Aldrich and used as received as all other materials.

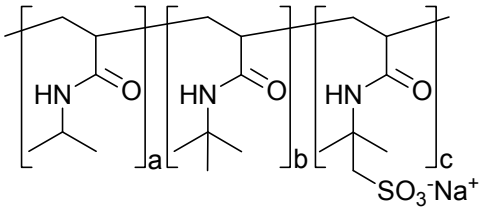

Figure 6.1 poly(NIPAAm-*co*-NTBAAm-*co*-AMPS) chemical structure

6.3.1 Copolymers synthesis and characterization

Linear terpolymers p(NIPAAm-*co*-NTBAAm-*co*-AMPS) were synthesized by free-radical copolymerization using AIBN as initiator. The copolymers are designed as *XX*/*YY*/*ZZ* being *XX*, *YY* and *ZZ* the molar percentages of NIPAAm, NTBAAm, and AMPS in the reaction mixture, respectively. Monomers with a total concentration of 0.5 M were dissolved in an 50:50 isopropanol:water mixture and AIBN (1 mol % with respect to the total monomer) was added to the solution. After degasification of the reactants solution with nitrogen for about 15 min, the reaction vessel was sealed and placed in an oven at 60 ºC for 16 h. The solution containing the obtained polymers was neutralized with NaOH, dialyzed against distilled water using dialysis tubes with a cutoff molecular weight of 3500 Da, and freeze-dried.

Terpolymers composition was analyzed by Elemental analyses (Leco CHNS-932) and ^{1}H NMR using $CDCl_3$ as solvent (Varian Inova 300). Molecular weight and polydispersity were determined by gel permeation chromatography (GPC) using 0.1% (w/v) LiBr solution

in DMF as eluent at a flow rate of 0.3 mL min^{-1} at 70 ºC and narrow disperse poly(ethylene glycol) (PEG) as calibration standards.

6.3.2 Turbidity measurements

The cloud point temperature (CPT) of the polymer solutions was measured in a Varian-Cary 3 UV/vis spectrophotometer, equipped with a Peltier cell holder for temperature control. The turbidity of the solutions was monitored as a function of temperature at 400 nm and under magnetic stirring. Solutions were prepared using distilled water with varying NaCl concentrations. These solutions were expected to be roughly neutral because AMPS is a fairly strong acid and the terpolymers had been previously converted in the salt form. Solutions were frozen at -20 ºC to ensure complete dissolution. Immediately after melting, solutions were placed in a cuvette, and heating scans were performed between 15 and 80 ºC at a scanning rate of 1 ºC/min. The first measured point at 15 ºC was used as blank which corresponds to the clear polymer solution. The transmittance of the polymer solution at different concentration and ionic strength (adjusted with NaCl) was monitored as a function of temperature. Cooling scans were performed between 80 and 5 ºC immediately after heating at the same rate. The aggregation kinetic isotherms were evaluated for an aqueous solution of 60/35/5 (1 g/L) in NaCl (0.154 M). Solutions were frozen before each temperature measurement, and blank was record at 15 ºC, as for the temperature scanning experiments. Afterwards, the solutions were rapidly heated to set temperature values near and above the CPT, and transmittance was recorded as a function of time.

6.3.3 Dynamic Light Scattering (DLS)

Dynamic light scattering was performed using a Zetasizer NanoZS Instrument (ZEN3600, Malvern Instruments, Worcestershire, UK) equipped with a 4 mW He-Ne laser (λ_0=633 nm) and with noninvasive backscattering (NIBS) detection at a scattering angle of 173º. Owing to this configuration, the equipment can decrease the scattered light path length through the sample by adjusting automatically the measuring position, hence reducing multiple scattering for larger particle size, i.e., opaque samples. This is especially useful in colloidal aggregation experiments, where scattered light intensity can rapidly increase several orders of magnitude, because it reduces the need of sample dilution. Both measuring position and attenuator were adjusted automatically before each

measurement. The autocorrelation function was converted in a volume-weighted particle size distribution with Dispersion Technology Software 5.06 from Malvern Instruments. The apparent hydrodynamic diameters (D_h) were taken as the mean position of the peak in volume-D_h distributions. The measurements were performed in the temperature range 5-85 ºC with a temperature interval of 2 ºC and an equilibration time of 2 min. Regarding the stability measurements, samples were initially frozen, melted, and equilibrated at 5 ºC inside the measurement cell to ensure complete dissolution. Thereafter, samples were submitted to a temperature jump and measured at constant temperature for 12 h. Terpolymer solutions with varying salt concentration were prepared in ultrapure water and filtered using a 0.20 µm disposable PES membrane filter (TPP, Trasadingen, Switzerland).

6.4 Results and Discussion

Several NIPAAm-*co*-NTBAAm-*co*-AMPS copolymers containing different NIPAAm/NTBAAm ratios and a constant 5 mol % of AMPS in the feed were prepared. Their composition and molecular weight are summarized in Table 6.1. The composition of the copolymers is quite close to the reaction feed composition, according to the expected from the chemical structure of the monomers and reactivity ratios reported in the literature [25, 26].

Table 6.1 Copolymers composition and molecular weight

Sample	Molar fraction in polymer			$M_w/10^3$ (g/mol)	$M_n/10^3$ (g/mol)	M_w/M_n
	NIPAAm[a]	NTBAAm[a]	AMPS[b]			
45/50/5	0.47	0.48	0.04	17.2	6.3	2.7
50/45/5	0.49	0.46	0.04	17.2	6.0	2.6
55/40/5	0.53	0.42	0.06	15.3	5.8	2.6
60/35/5	0.58	0.37	0.04	18.2	6.3	2.9
70/25/5	0.67	0.28	0.04	19.7	6.9	2.8
75/20/5	0.69	0.27	0.05	18.9	7.0	2.7
80/15/5	0.76	0.19	0.05	18.5	7.1	2.6
90/5/5	0.83	0.12	0.05	18.8	7.1	2.7
95/0/5	0.95	0.0	0.05	16.4	6.3	2.6

[a] Calculated by ^{1}H NMR considering AMPS 5.0%; [b] Calculated by elemental analysis

The AMPS molar fraction was experimentally determined to be around 0.05 for all copolymers, and the small differences observed fall under the technique uncertainty.

Besides, the small error fluctuations in the AMPS molar fraction do not correlate with the other monomer ratio. Therefore, we can exclude biased effects caused by polymer charge trends when analyzing properties related with the other two monomer frequencies. Moreover the weight average molecular weight (M_w) and polydispersity (M_w/M_n), determined by GPC, are also similar for all polymer samples, showing that these parameters are not affected by the monomers feed ratio.

Turbidimetry is a common technique used to estimate the LCST of thermoresponsive polymers in aqueous solutions, motivated by the tendency of polymer molecules to aggregate at the poor solvent region above the $\Theta-$ temperature, which causes a marked change in the solution optical properties [6, 7]. However, complications might arise from variations in the size of precipitated aggregate and the settling of precipitates, which is especially critical in aged solutions. The cloud point, measured at the onset of the turbidity increases with the temperature, should be an overestimation of the LCST. However, cloud point can still provide an acceptable estimation of the LCST for a stipulated temperature scanning rate if aggregation kinetics is faster enough. This fact, allied with the experimental simplicity, makes turbidimetry a primary choice in the literature for a fast estimation of the LCST. The concentration of the polymer solution (diluted regimes), the presence of surfactants, or the polymer ionic charge are some of the several factors that might influence aggregation kinetics. Nonetheless, turbidimetry provides a fast way of obtaining valuable information about the macroscopic phase separation behavior, even if the CPT does not match exactly the coil-to-globule transition. We have characterized our terpolymers solution behavior by means of turbidimetry, and the results were analyzed taking into consideration the referred shortcomings. Some of the terpolymer solutions were not stable at temperatures immediately above to the cloud point, but aggregation occurred at an extremely low rate. Therefore, it was not feasible to perform the experiments at a scanning rate lower enough to not influence the turbidimetry curves because it would require very long measurement times. The curves slope can still be used to compare the aggregation rate, providing that the measurements were done at the same scanning rate. In this sense, we did all temperature scanning measurements at a constant rate of 1 ºC/min.

In general, water solutions of the terpolymers remained clear at any temperature. The thermoresponsive behavior was only manifested in the presence of salts. Figure 6.2 shows the typical temperature dependence of transmittance for solutions of copolymers with a rational composition variation, on both heating (Figure 6.2a) and cooling (Figure 6.2b). Figure 6.3a shows the cloud point temperature extracted from Figure 6.2a and defined as the temperature at 98% light transmittance on heating. The phase separation sharpness was evaluated considering the temperature interval at which light transmittance

changes from 98% down to 2% (ΔCPT) during the heating scan, and it is represented in Figure 6.3a as a function of the NTBAAm content.

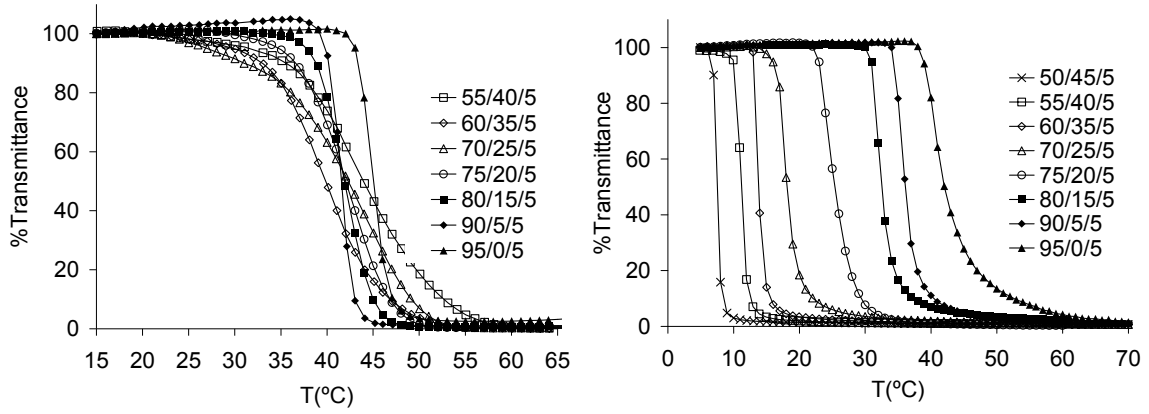

(a) (b)

Figure 6.2 Turbidity curves showing the effect of copolymer composition on the macroscopic phase separation for heating (a) and cooling (b) scans (1 g/L, 0.154M NaCl, 1 ºC/min).

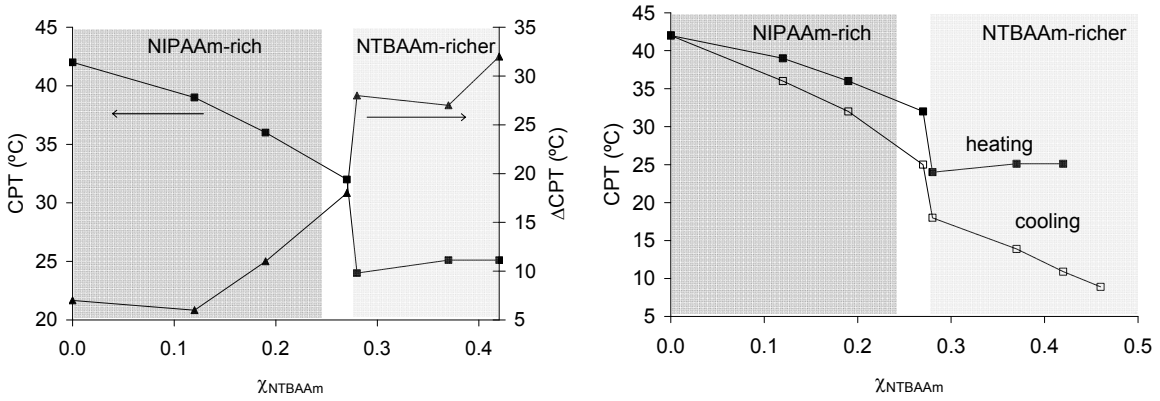

(a) (b)

Figure 6.3 Cloud point temperature (CPT) (filled squares) and macroscopic phase separation sharpness (ΔCPT) (filled triangles) in function of NTBAAm molar fraction (x_{NTBAAm}) (a). Comparision between CPT (filled squares) and redissolution temperature (empty squares) as a function of NTBAAm molar ratio (b).

It has been reported that linear NIPAAm homopolymer present a LCST around 31-33 ºC in water [3-7] and that LCST is slightly depressed when NaCl is added at the concentration range used in this work [10]. When NIPAAm was copolymerized with a small amount of AMPS (95/0/5), i.e., a more hydrophilic (ionic) monomer, the CPT (~42 ºC) was raised as expected. The macroscopic phase separation is sharp and occurs in a narrow

temperature range (Figures 6.2a and 6.3a). On the other hand, the CPT was reduced as expected by increasing the NTBAAm content, which results from an increased overall hydrophobic character of the copolymers (Figures 6.2a and 6.3a). Furthermore, it could be observed that as greater is the NTBAAm content on the copolymers, as slower is the aggregation process, leading to a decreased slope in the turbidity curves (Figure 6.2a) and consequently an increased ΔCPT (Figure 6.3a). It is interesting to notice that there is a composition interval (around 0.25-0.30 molar fraction of NTBAAm) at which the macroscopic phase separation changes from sharp to wide. Such alteration in the aggregation behavior is accompanied by an equally steep variation in the CPT. We have denominated these two composition ranges with very distinct aggregation behaviors as NTBAAm-richer and NIPAAm-rich polymers (shadowed areas of Figure 6.3). Considering that all copolymers possess identical charge (similar content of AMPS), the repulsive electrostatic forces are expected to be equivalent at the same ionic strength. Therefore, it is reasonable to conclude that the lower aggregation rate is only correlated with a higher NTBAAm (lower NIPAAm) content. This result is apparently contradictory with the colloidal aggregation principles. At the first glance, one could expect that the resultant of repulsive electrostatic and attractive hydrophobic forces would favor a faster aggregation process for the more hydrophobic NTBAAm-richer polymers.

Aggregation isotherms were determined for 60/35/5 (sample with broad aggregation profile), keeping the same polymer and NaCl concentrations (Figure 6.4). The temperature of the sample was rapidly increased to certain temperatures near and above the CPT, and transmittance values were measured with time. These measurements allowed us to elucidate that the studied system was not thermodynamically stable (or metastable) above the CPT, and that broadening of turbidity variation was caused by temperature-dependent aggregation kinetics. Figure 6.4 shows that the turbidity increases continually with the time at all studied temperatures, but the process is much faster at higher temperatures, whereas aggregation is “virtually prevented” for temperatures close to the CPT. According to these results, we could hypothesize that the observed decrease of the slope with increasing NTBAAm content does not mean that the volume transition became continuous. In fact, as we will discuss afterward, there is an observable discontinuous phase separation process at the microscopic level.

Immediately after the heating scan, the copolymer solutions were subjected to a cooling step in order to study the redissolution temperature. The onset of the turbidity decrease in the redissolution curves might not be well-defined because settling of aggregates also contributes to decrease the turbidity. Hence, redissolution temperature was considered to be at 50% light transmittance to avoid the effect of settling. Besides, this option is further

justified by the fast redissolution process observed for all the samples presented in Figure 6.2b.

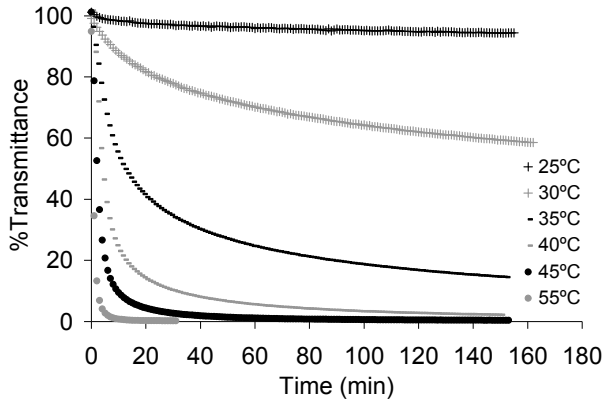

Figure 6.4 Isothermal aggregation kinetics of 60/35/5 (1g/L) dissolved in 0.154M NaCl aqueous solution at temperatures above the cloud point temperature.

As expected, the redissolution temperature decreases with increasing NTBAAm content in the terpolymer composition (Figure 6.2b), and it is always lower that the CPT (Figure 6.3b). The measured hysteresis is enhanced for NTBAAm-richer polymers. Moreover, as can be seen in Figure 6.2b, the curves of transmittance vs temperature in the cooling cycle are sharp for any ratio of NTBAAm, indicating that the redissolution occurs immediately below a certain temperature. The difference in the macroscopic phase separation sharpness between heating and cooling scans can be understood in terms of electrostatic repulsion and hydrophobic attraction. During polymer aggregation the molecules charge density counteracts the hydrophobic forces, eventually delaying or hindering aggregation. When the system is cooled below the LCST, the copolymer rehydration cancels the attractive hydrophobic forces responsible for aggregates cohesion, and the electrostatic repulsion provides the driving force for the fast redissolution.

When plotting the redissolution temperature against the molar ratio of NTBAAm (Figure 6.3b), it was possible to observe an abrupt variation at the same composition range (0.25-0.30) in which a similar steep variation is observed for CPT and aggregation rate (Figure 6.3a). These observations motivated us to study the effect of the ionic strength and polymer concentration on the macroscopic phase separation for two different copolymers: one representative of the NTBAAm-richer polymer behavior (60/35/5) and the other typifying the NIPAAm-rich polymers (80/15/5).

Salt concentration might act both on the LCST and on the aggregation profile. Since both copolymers are polyelectrolytes, it was not surprising to observe that the ionic strength

influences both polymers CPT in the same manner; when the NaCl concentration is increased, the CPT decreases (Figure 6.5). It was reported that, at the concentration range used in this study, the influence of NaCl in the pNIPAAm LCST is rather small (<1 ºC) [10, 20] if compared with the reduction extent that we observed in the CPT for both terpolymers (>30 ºC). This divergence might indicate that the CPT is detected above the θ–temperature. If this is correct, the unexpectedly stronger dependence of the CPT on the NaCl concentration is related to the effect of salt concentration over the colloidal aggregation kinetics, rather than the θ–temperature. The addition of salt to the solution shields the repulsive Coulombic interactions between charged sulfonic groups (screening effect), facilitating colloidal aggregation if the system is above the θ–temperature. Although the CPT is similarly affected for both NTBAAm-richer and NIPAAm-rich copolymers, the transition rate is not equally affected. The turbidity rising rate strongly depends on the ionic strength for the more hydrophobic copolymer (60/35/5), being slower at lower salt content and more abrupt at higher concentrations. On the contrary, the ΔCPT is not affected by changes in the salt concentration for 80/15/5; in all cases a fast aggregation was observed. The strong dependence of the aggregation rate on the salt concentration for NTBAAm-richer polymers reveals that the colloidal stabilization effect is electrostatic in nature. Thus, why is this effect not observed for NIPAAm-rich polymers? A possible explanation is that, for NTBAAm-richer polymers, the stronger hydrophobic forces in action above the LCST are able to override the electrostatic potential energy increment caused by a higher charge density of the colloidal particles. In this situation, the increased charge density would provide an additional energy barrier for further colloidal aggregation, especially if charged segments were oriented toward the surface.

The effect of the ionic strength on the redissolution temperature was also evaluated (Figure 6.5). The NTBAAm-richer copolymer showed a fast redissolution profile for all tested salt concentrations. Moreover, the transmittance vs temperature curves are almost superimposed showing coincident redissolution temperature around 15 ºC regardless of the ionic strength. On the other hand, a sharp redissolution profile was also observed for NIPAAm-rich polymers, but in this case the temperature at which the aggregates are redissolved depends on the salt concentration. Although a certain hysteresis was observed between heating and cooling, both aggregation and redissolution processes of the NIPAAm-rich polymer are influenced in a very similar extent by the solution ionic strength.

The dependence of the CPT on the polymer concentration is shown in Figure 6.6. In this case, the aggregation and redissolution behavior is very similar for NTBAAm-richer and NIPAAm-rich polymers. The aggregation rate increased and CPT decreased at higher polymer concentration, whereas the redissolution profile was fast and not dependent on

the polymer concentration. The results are in agreement with the general principles of colloidal aggregation, where the aggregation is dependent on the particle concentration. In turn, disaggregation should be mainly ruled by particle intrinsic structural features.

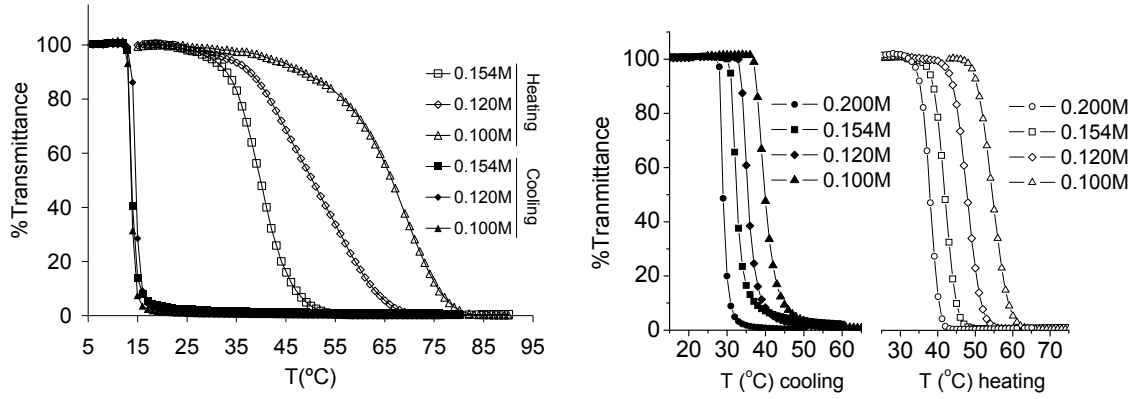

(a) (b)

Figure 6.5 Effect of the NaCl concentration on the turbidity vs temperature curves on heating and cooling scans for 60/35/5 (a) and 80/15/5 (b). In both curves the polymers concentrations and scan rates were 1g/L and 1 ºC/min respectively.

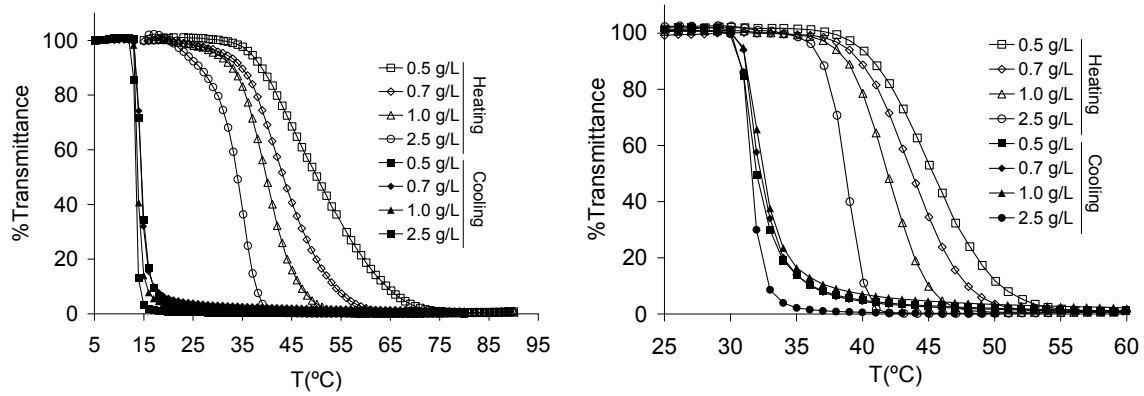

(a) (b)

Figure 6.6 Effect of the polymer concentration on the transmittance vs temperature curves on heating and cooling scans for 60/35/5 (a) and 80/15/5 (b). In both curves the salt concentrations and scan rates were 0.154M and 1 ºC/min respectively

Since some of the studied polymer solutions do not present sharply defined cloud points, we used dynamic light scattering (DLS) in order to elucidate the apparently contradictory behavior observed with the copolymer composition (more hydrophobic polymers showed lower aggregation rates). DLS permits the analysis of size variations at the molecular scale, and therefore, it is possible to analyze early stages of aggregation. Figure 6.7 shows the temperature dependence of apparent hydrodynamic diameter (D_h) on the NaCl

concentration for 60/35/5, at a fixed polymer concentration of 1 g/L. It could be observed that in the absence of salt a sharp increase of D_h is observed at 23 ºC indicating the aggregation of individual ionomer chains in solution. Above this temperature value, the D_h increases slightly with the temperature. The formed colloidal particles remained stable at 27 ºC for at least 11h (result not shown). Qiu et al. reported a similar behavior for low molecular mass poly(*N*-isopropylacrylamide-*co*-acrylate) in water at a comparable concentration [27]. They suggested that when short chains are analyzed by DLS, the intrachain collapse is not observed since its effect on the overall chain dimension is negligible and is faster than the interchain aggregation. Because of this reason, the decrease on D_h due to the coil-to-globule transition typically observed for larger polymers in very diluted solution [4, 6, 7] was not observed for the studied terpolymers with shorter chains. Even though the coil-to-globule transition is not observed, this first aggregation step should be very close to the θ-temperature [9], providing our best estimation of the LCST. Being so, we will use the term LCST to denominate this early aggregation observed by DLS and the CPT to denote only the value obtained by turbidimetry, for the sake of clarity.

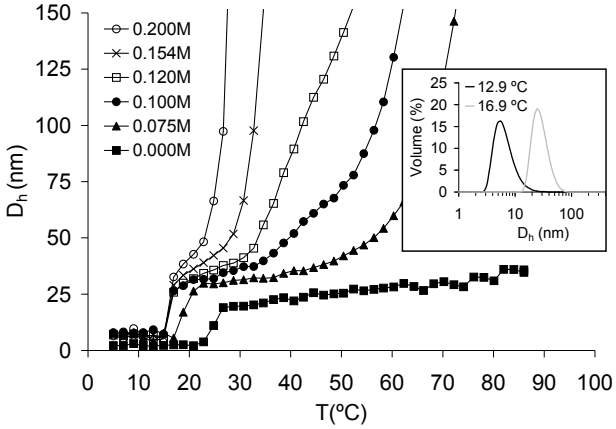

Figure 6.7 Temperature dependence of the apparent hydrodynamic diameter (D_h) at several NaCl concentrations for 60/35/5 (polymer concentration 1g/L). The inset figure shows the hydrodynamic diameter distribution at temperatures before and after the aggregation (0.120M NaCl).

When NaCl was added to the solution, a similar early aggregation behavior was observed, but the aggregates were not stable in the entire temperature range, ultimately leading to a further increase of the D_h above a certain temperature. Comparing the CPT (Figure 6.5a) with the LCST (Figure 6.7) of 60/35/5 at several NaCl concentrations, it is possible to see that there is no correspondence between both values. This observation raises great

concerns on the use of turbidimetry to evaluate the LCST of charged polymers. In fact, CPT is related with the massive aggregation observed in Figure 6.7 at higher temperatures, being the first formed metastable aggregates (LCST) undetected by turbidimetry. If in our results the CPT does not match precisely the temperature at which a more pronounced D_h increment is observed, it is because scanning rate is lower in the DLS measurements due to the relatively longer times required for data acquisition and temperature stabilization. The gap between the metastable nanosized aggregates (LCST) and the faster aggregation (CPT) is more pronounced at lower salt concentrations. When salt concentration increases, the stability range of the colloidal particles decreases. Thus, it is reasonable to conclude that the effect of NaCl concentration on the CPT is solely related with the screening effect over the charge, reducing colloidal stability and accelerating aggregation. Hypothetically, the LCST dependence on the NaCl concentration can only determine the temperature at which the first metastable aggregates are formed.

The inset in Figure 6.7 shows the hydrodynamic diameter distribution at temperatures immediately before and after the aggregation when 0.120M NaCl was added to the solution. At 12.9 ºC, slightly below the LCST, only one peak centered at ~8 nm was observed. This peak corresponds to individual copolymer chains, as it was confirmed by measuring the size distribution of the polymer in a good solvent (tetrahydrofuran). The obtained volume-D_h distribution was equivalent to that obtained in water below the LCST (graph not shown). The size distribution above the LCST at 16.9 ºC is narrower and corresponds to an average D_h of ~25 nm, reflecting the interchain aggregation.

The stability of the aggregates before the massive aggregation was tested isothermally by measuring the D_h and the scattered light intensity with the time at set temperatures close to the LCST (Figure 6.8). The light intensity is very sensitive to small changes in the scatters size and should be constant, at fixed scattering angle and temperature, if there is no aggregation. 60/35/5 in 0.120M NaCl showed the first aggregation at ~15 ºC (Figure 6.7) and it could be observed that at 19 ºC both D_h and light intensity are stable for at least 11 h (Figure 6.8. However, when the solution was left at 25 ºC, the light intensity and D_h increased with the time, indicating that aggregation occurs at this temperature. It seems that the aggregation rate increases continuously with the temperature, so that a limit between two aggregation regimes is not well-defined. In this sense, the separation of the aggregation behavior in two stages, early metastable aggregation and later massive coagulation, is merely descriptive.

It is interesting to notice that the temperature observed for the first aggregation in DLS (LCST) corresponds to the redissolution temperature observed by turbidimetry. Hence, for this specific case, we can state that the redissolution temperature is more representative

of the LCST than the CPT. On the other hand, after the massive coagulation the produced aggregates are stable in the cooling scan; i.e., there is no redissolution as long as the temperature is kept above the LCST.

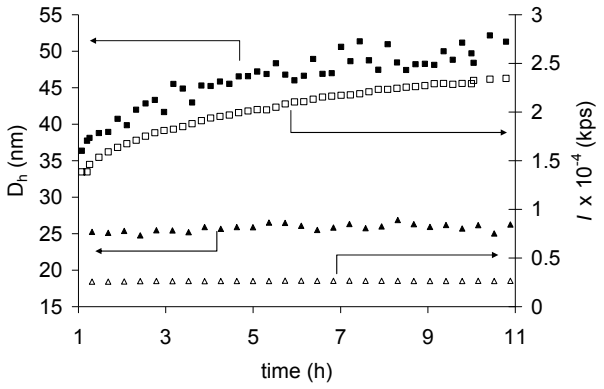

Figure 6.8 Isothermal aggregation kinetics of 60/35/5 determined by DLS (1g/L polymer concentration and 0.120M NaCl) at 19 ºC (triangles) and 25 ºC (square). Filled symbols represent the hydrodynamic diameter and empty symbols represent scattered light intensity (173º).

The LCST of the NIPAAm-rich polymer (80/15/5) (Figure 6.9) was higher than the LCST of 60/35/5 for all tested NaCl concentration, as expected. A quite different behavior was observed for 80/15/5 water solution (inset graph). Substantially bigger scatters are detected at the first aggregation, which increases continuously with the temperature, but never reaching a massive coagulation stage.

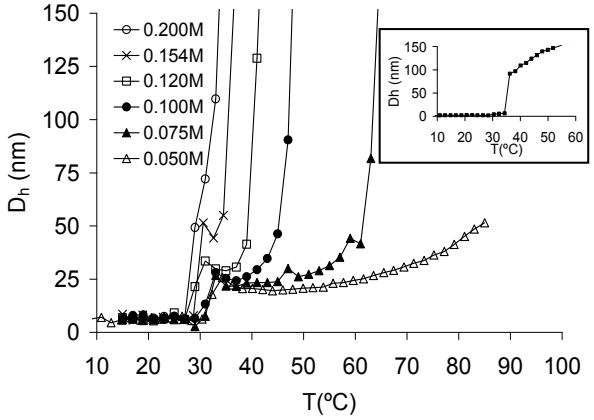

Figure 6.9 Temperature dependence of the apparent hydrodynamic diameter (D_h) at several NaCl concentrations for 80/15/5 (polymer concentration 1g/L). Inset shows the temperature dependence of D_h in water.

The lower percentage of NTBAAm monomer in this copolymer composition should imply that weaker hydrophobic aggregation forces are active above the LCST. Therefore, hydrophobic interactions may not be able to bring the charges close enough to provide an effective surface charge density, hindering electrostatic stabilization of the aggregates. Interestingly, when small quantities of salt are added to the solutions, it could be observed that the formed aggregates were smaller and showed an early metastable aggregation stage, recalling the aggregation behavior observed for NTBAAm-richer polymer. This supports the explanation given before, since the screening effect produced by the added salt are expected to reduce electrostatic repulsion inside the aggregates. In this sense, there should be a salt concentration in which the cohesive hydrophobic forces are sufficient to overcome the reduced internal repulsion and provide an effective surface charge density for colloidal stabilization.

Comparing Figure 6.7 and Figure 6.9 we can conclude that both polymers showed similar behavior with the formation of small aggregates that remain stable at lower temperature, after which a massive coagulation occurs. However, the coagulation rate showed a sharper acceleration for NIPAAm-rich than for NTBAAm-richer samples. Another common feature of both samples is that the CPT determined by turbidimetry is not representative of the LCST for any tested condition; nanosized aggregates are always observed by DLS at lower temperatures than the CPT determined by turbidimetry. In some cases, as for low salt concentrations, the observed differences could be as great as 30 ºC. Nevertheless, the comparison of DLS and turbidity results for NIPAAm-rich polymer showed that the redissolution of the bigger aggregates occurs at temperatures higher than the LCST. On the other hand, when the same comparison is performed for NTBAAm-richer polymer, we could observe that the aggregates formed at higher temperatures only disaggregate in the cooling ramp when the LCST is reached. This observation confirms that the internal cohesion of 60/35/5 formed aggregates is enough to compensate the electrostatic repulsion at any temperature above the LCST. In NIPAAm-rich polymer the hydrophobic interactions are weaker and the aggregates are redissolved at temperatures higher than the LCST. Moreover, it is interesting to notice that for this polymer (80/15/5) the redissolution temperature changed with the salt concentration. Increasing salt concentration results in the enhancement of charge screening, and subsequently the electrostatic repulsion is progressively reduced. Therefore, the hydrophobic interactions are enough to support the aggregates stability at lower temperatures.

6.5 Conclusions

p(NIPAAm-*co*-NTBAAm-*co*-AMPS) aqueous solution did not show turbidity changes (macroscopic phase separation) with the temperature. The CPT was only observed when NaCl was added to the solutions. However, the formation of metastables nanosized aggregates (LCST) was observed by DLS in both water and aqueous saline solutions. The macroscopic phase separation is always observed at higher temperatures than the formation of the nanoaggregates. Therefore, there is no correlation between CPT and LCST. These results raise serious concerns about the validity of using turbidimetry measurements to obtain a reliable estimation of the LCST for charged thermoresponsive polymers.

Both the CPT and the LCST decreased with the increase of hydrophobicity (increased NTBAAm content). However, the aggregation profile observed by turbidimetry dramatically change above a critical amount of NTBAAm (0.25-0.30). Terpolymers with NTBAAm content below the critical value showed a fast macroscopic phase separation for all studied conditions. Moreover, the formed large aggregates redissolve in the cooling ramp at different temperature depending on the salt concentration and always at temperatures higher than the LCST. On the other hand, NTBAAm-richer terpolymers showed a slower aggregation process whose rate was found to depend on salt concentration. In this case, the formed large aggregates during the heating scan disentangled always at the same temperature which is coincident with the LCST. The differences observed on copolymers solutions can be explained as the result of a fine balance between hydrophobic attractive forces and electrostatic repulsion, which leads to formation of intermediate metastable nanosized aggregates. The hydrophobic cohesion forces for polymers with higher NTBAAm content are stronger, thus able to withstand a higher surface charge density. Therefore, the aggregation is slower due to the electrostatic repulsion that acts as stabilizer of the aggregates. Furthermore, the redissolution only occurs at the LCST because the stronger internal cohesion is enough to compensate the electrostatic repulsion. On the other hand, the hydrophobic forces in polymers with lower content of NTBAAm are weaker and not able to bring charges close enough to provide an effective surface charge density, hindering electrostatic stabilization of the aggregates with a consequent fast coagulation. Moreover, the larger aggregates formed meanwhile are redissolved before reaching the LCST in the cooling ramp because the hydrophobic interactions are not strong enough to counteract the electrostatic repulsion.

6.6 Acknowledgements

The authors acknowledge funding from EU Marie Curie Actions, Alea Jacta Est (MEST-CT-2004-008104), and Portuguese Foundation for Science and Technology (FCT) (SFRH/BPD/34545/2007). This work was carried out under the scope of the European NoE EXPERTISSUES (NMP3-CT-2004-500283).

6.7 References

1. Liu, H.Y.; Zhu, X.X. Lower critical solution temperatures of N-substituted acrylamide copolymers in aqueous solutions. *Polymer*, 1999, **40,** (25), 6985-6990.
2. Graziano, G. On the temperature-induced coil to globule transition of poly-N-isopropylacrylamide in dilute aqueous solutions. *International Journal of Biological Macromolecules*, 2000, **27,** (1), 89-97.
3. Wu, C.; Zhou, S.Q. First observation of the molten globule state of a single homopolymer chain. *Physical Review Letters*, 1996, **77,** (14), 3053-3055.
4. Wu, C.; Zhou, S.Q. Laser-Light Scattering Study of the Phase-Transition of Poly(N-Isopropylacrylamide) in Water .1. Single-Chain. *Macromolecules*, 1995, **28,** (24), 8381-8387.
5. Wu, C.; Zhou, S.Q. Thermodynamically Stable Globule State of a Single Poly(N-Isopropylacrylamide) Chain in Water. *Macromolecules*, 1995, **28,** (15), 5388-5390.
6. Kubota, K.; Fujishige, S.; Ando, I. Single-Chain Transition of Poly(N-Isopropylacrylamide) in Water. *Journal of Physical Chemistry*, 1990, **94,** (12), 5154-5158.
7. Fujishige, S.; Kubota, K.; Ando, I. Phase-Transition of Aqueous-Solutions of Poly(N-Isopropylacrylamide) and Poly(N-Isopropylmethacrylamide). *Journal of Physical Chemistry*, 1989, **93,** (8), 3311-3313.
8. Baysal, B.M.; Karasz, F.E. Coil-globule collapse in flexible macromolecules. *Macromolecular Theory and Simulations*, 2003, **12,** (9), 627-646.
9. Qiu, X.P.; Li, M.; Kwan, C.M.S.; Wu, C. Light-scattering study of the coil-to-globule transition of linear poly(N-isopropylacrylamide) ionomers in water. *Journal of Polymer Science Part B-Polymer Physics*, 1998, **36,** (9), 1501-1506.
10. Zhang, Y.J.; Furyk, S.; Bergbreiter, D.E.; Cremer, P.S. Specific ion effects on the water solubility of macromolecules: PNIPAM and the Hofmeister series. *Journal of the American Chemical Society*, 2005, **127,** (41), 14505-14510.
11. Alarcon, C.D.H.; Pennadam, S.; Alexander, C. Stimuli responsive polymers for biomedical applications. *Chemical Society Reviews*, 2005, **34,** (3), 276-285.

12. Bergbreiter, D.E.; Case, B.L.; Liu, Y.S.; Caraway, J.W. Poly(N-isopropylacrylamide) soluble polymer supports in catalysis and synthesis. *Macromolecules*, 1998, **31,** (18), 6053-6062.

13. Nagase, K.; Kobayashi, J.; Okano, T. Temperature-responsive intelligent interfaces for biomolecular separation and cell sheet engineering. *Journal of the Royal Society Interface*, 2009, **6**, S293-S309.

14. da Silva, R.M.P.; Mano, J.F.; Reis, R.L. Smart thermoresponsive coatings and surfaces for tissue engineering: switching cell-material boundaries. *Trends in Biotechnology*, 2007, **25,** (12), 577-583.

15. Ebara, M.; Yamato, M.; Hirose, M.; Aoyagi, T.; Kikuchi, A.; Sakai, K.; Okano, T. Copolymerization of 2-carboxyisopropylacrylamide with N-isopropylacrylamide accelerates cell detachment from grafted surfaces by reducing temperature. *Biomacromolecules*, 2003, **4,** (2), 344-349.

16. Cheng, H.; Shen, L.; Wu, C. LLS and FTIR studies on the hysteresis in association and dissociation of poly(N-isopropylacrylamide) chains in water. *Macromolecules*, 2006, **39,** (6), 2325-2329.

17. Schild, H.G.; Tirrell, D.A. Microcalorimetric Detection of Lower Critical Solution Temperatures in Aqueous Polymer-Solutions. *Journal of Physical Chemistry*, 1990, **94,** (10), 4352-4356.

18. Tamai, Y.; Tanaka, H.; Nakanishi, K. Molecular dynamics study of polymer-water interaction in hydrogels .2. Hydrogen-bond dynamics. *Macromolecules*, 1996, **29,** (21), 6761-6769.

19. Feil, H.; Bae, Y.H.; Jan, F.J.; Kim, S.W. Effect of Comonomer Hydrophilicity and Ionization on the Lower Critical Solution Temperature of N-Isopropylacrylamide Copolymers. *Macromolecules*, 1993, **26,** (10), 2496-2500.

20. Mao, H.B.; Li, C.M.; Zhang, Y.J.; Furyk, S.; Cremer, P.S.; Bergbreiter, D.E. High-throughput studies of the effects of polymer structure and solution components on the phase separation of thermoresponsive polymers. *Macromolecules*, 2004, **37,** (3), 1031-1036.

21. Varghese, S.; Lele, A.K.; Mashelkar, R.A. Designing new thermoreversible gels by molecular tailoring of hydrophilic-hydrophobic interactions. *Journal of Chemical Physics*, 2000, **112,** (6), 3063-3070.

22. Wong, J.E.; Diez-Pascual, A.M.; Richtering, W. Layer-by-Layer Assembly of Polyelectrolyte Multilayers on Thermoresponsive P(NiPAM-co-MAA) Microgel: Effect of Ionic Strength and Molecular Weight. *Macromolecules*, 2009, **42,** (4), 1229-1238.

23. Travas-Sejdic, J.; Easteal, A. Swelling equilibria and volume phase transition of polyelectrolyte gel with strongly dissociated groups. *Polymer Gels and Networks*, 1997, **5,** (6), 481-502.

24. Aoyagi, T.; Ebara, M.; Sakai, K.; Sakurai, Y.; Okano, T. Novel bifunctional polymer with reactivity and temperature sensitivity. *Journal of Biomaterials Science-Polymer Edition*, 2000, **11,** (1), 101-110.

25. Gibbons, O.; Carroll, W.M.; Aldabbagh, F.; Yamada, B. Nitroxide-mediated controlled statistical copolymerizations of N-isopropylacrylamide with N-tert-butylacrylamide. *Journal of Polymer Science Part a-Polymer Chemistry*, 2006, **44,** (21), 6410-6418.

26. Zhang, C.; Easteal, A.J. Study of free-radical copolymerization, of N-isopropylac lamide with 2-acrylamido-2-methyl-1-propanesulphonic acid. *Journal of Applied Polymer Science*, 2003, **88,** (11), 2563-2569.

27. Qiu, X.P.; Kwan, C.M.S.; Wu, C. Laser light scattering study of the formation and structure of poly(N-isopropylacrylamide-co-acrylic acid) nanoparticles. *Macromolecules*, 1997, **30,** (20), 6090-6094.

Chapter 7

Temperature as a single on-off parameter controlling nanoparticles growing, stabilization and fast disentanglement

7.1 Abstract

Thermoresponsive nanoparticles are synthesized from ionic random terpolymer precursors. A distinct temperature dependent aggregation-redissolution behavior is observed within a subtle balance between polymer ionic charge and hydrophobic content, which is used for colloidal synthesis of nanoparticles in aqueous medium and without surfactants. The solution thermal history provides a robust mean to customize the size of nanoparticles that can be disentangled on command.

This chapter is based on the following publication:
Paula M. López-Pérez; Ricardo M.P. da Silva; Iva Pashkuleva; Julio San Roman; Rui L. Reis. *Submitted.*

7.2 Introduction

The small size of nanoparticles, together with increased surface area and reactivity, allows them to translocate cell membranes, target specific tissues or organs (by adsorption or surface binding of signaling molecules), and catalyze chemical reactions. [1, 2] Owing to its unique properties, organic nanoparticles (polymer or lipid) hold a great potential to be used in various biomedical applications, especially as intracellular drug and gene delivery systems. [3-5] Small size is a key attribute enabling nanoparticles to overcome various biological barriers such as the blood-brain barrier, the reticuloendothelial system (RES), tumor blood vessels with enhanced permeability, extracellular matrix components, cell membrane and other intracellular barriers. [1, 2] Herein we describe a method for the synthesis of thermoresponsive nanoparticles that provides a good control over particle size (between 35 - 200 nm). We have designed random thermoresponsive terpolymers that possess a fine balance between hydrophobic attractive forces and electrostatic repulsion above the lower critical solution temperature (LCST). In the literature, block copolymers have been a primary choice to trigger macromolecular assembly in aqueous environment, based on a lipid-like amphiphilic nature. [6-13] In this work, the choice of random copolymers instead was inspired by their resemblance with the intercalated nature of hydrophobic and charged residues found in the primary structure of proteins. The method reported herein allows nanoparticles to be processed in aqueous medium without surfactants, using temperature as a single on-off parameter controlling particle growing, stabilization and fast disentanglement.

The most widespread methods for nanoparticles production include the previous preparation of an emulsified system. [14] Thereafter, particles are formed in the discontinous phase either by polymer precipitation/gelation or by monomer polymerization. Two immiscible phases are required and the oil phase is not always easy to remove. Surfactants are often required to stabilize the emulsion and to avoid nanoparticle aggregation. Furthermore, emulsion-based methods often require use of crosslinkers. [14]

Alternative methods to prepare nanoparticles in aqueous medium are based on polymer precipitation or macromolecular self-assembly in conditions of spontaneous dispersion formation. These methods avoid the use of organic solvents, crosslinkers and/or surfactants. [14] Thermoresponsive polymers offer unique properties that have been elegantly adapted to trigger the spontaneous formation of nanoparticles, which can be used for burst drug release on demand. [3, 9-13]

Thermoresponsive polymers such as poly(*N*-isopropylacrylamide) (PNIPAAm) are hydrophilic at low temperature and became hydrophobic above the LCST. Graft or linear

block copolymers using PNIPAAm can form core-shell micellar assemblies, with the thermoresponsive building block working as either the solvated shell [6-8] or the hydrophobic core, [9-13] depending on the nature of the other block and on the temperature. If PNIPAAm is coupled to more hydrophobic blocks, stable polymeric micelles are formed below the LCST. [6-8] Hydrophobic drugs can be loaded into the inner corona, while the hydrophilic PNIPAAm shell permits the aqueous solubilization and temperature-responsiveness. This architecture does not differ from other non-thermoresponsive micelles assembled from block copolymer amphiphiles, except in that the hydrophilic shell can turn hydrophobic upon temperature increase, [6-8] eventually destabilizing the inner core of the micelle and triggering drug release. [6] The core-shell structure is formed when the polymer, previously dissolved in a water miscible organic solvent, is mixed with water. [6-8]

In the case of block copolymers of PNIPAAm with a hydrophilic block such as poly(ethylene glycol) (PEG) [9-12] or single-stranded DNA, [13] the macromolecule can be dissolved in water below the LCST. Stable core-shell nanoparticles are produced above the LCST, when the PNIPAAm block became hydrophobic. The hydrophilic block forms a hydrated shell that prevents further aggregation of collapsed PNIPAAm chains. [9-13] Inducing macromolecular assembly above the LCST in water circumvents the need of using organic solvents. Furthermore, these methods allow nanoparticles to be reversibly disassembled lowering the temperature, which might be useful to release drugs locally applying simple ice packs or clinical instruments such as deeply penetrating cryoprobes.[15]

Similarly, polymeric nanogels can also be obtained with thermoresponsive random copolymers, being macromolecular assembly in water induced above the LCST. In this case, the electrostatic repulsion between charged surfaces stabilizes the colloidal nanoparticles above the LCST. [16-18] In a recent work, [18] we have found that charged terpolymers composed of NIPAAm, *N-tert*-butylacrylamide (NTBAAm) and 2-Acrylamido-2-methyl-1-propanesulphonic acid (AMPS) form metastable colloidal nanoparticles upon heating above the LCST. The original method described herein is based on the distinct aggregation-redissolution behavior observed for some of these thermoresponsive terpolymers.

7.3 Results and discussion

Linear random terpolymers were synthesized by radical polymerization containing a constant ratio of 5% of AMPS in feed. The small ratio of charged monomer ensures enough electrostatic repulsion intended for nanoparticles stabilization, but is not enough to disrupt the discontinuous type coil-to-globule transition. [19] Terpolymer hydrophobicity was

varied by changing the ratio between NIPAAm and a more hydrophobic monomer (NTBAAm) in order to adjust the LCST. Terpolymers with NIPAAm/NTBAAm/AMPS ratios of 80/15/5 and 60/35/5 were studied, representing two different aggregation-redissolution behaviors, which changed above a critical amount of NTBAAm (0.25-0.30). [18]

Turbidimetry measurements were performed to picture the macroscopic observation of the phase separation (Figures 7.1a and 7.1b, right y-axis). The cloud point temperature (CPT) was extracted from heating scans at the transmittance decrease onset, whereas a redissolution temperature can be observed on cooling. Dynamic light scattering (DLS) provides an insight of the early macromolecular aggregation (Figures 7.1a and 7.1b, left y-axis). Above the LCST a sharp increase of the hydrodynamic diameter (D_h) is observed indicating the aggregation of individual ionomer chains in solution. Although the size of the polymers synthesized by us did not allow direct observation of the molecular contraction during coil-to-globule transition (single molecules are not observed above the LCST), this first aggregation step provides a good estimation of the LCST. [20] For the sake of clarity, we will use the term LCST to denominate this early aggregation observed by DLS and the CPT to denote the value obtained by turbidimetry.

The more hydrophobic polymer (60/35/5) presented lower LCST, CPT and redissolution temperature. The redissolution temperature was lower than the CPT for both copolymers (Figures 7.1a and 7.1b). The general aggregation profile observed by DLS was also similar for both copolymers (Figures 7.1a and 7.1b). An early aggregation (LCST) occurs with formation of small aggregates that remain stable at temperatures near and above the LCST. Further increasing the temperature, a “massive” coagulation happens with the formation of bigger aggregates. This “massive” coagulation corresponds to the CPT observed by turbidimetry.

The copolymer containing lower NTBAAm ratio (80/15/5) (Figure 7.1a) showed a sharp macroscopic phase separation on heating and a fast increase of the D_h in the second aggregation step. Moreover, it was observed that redissolution on cooling occurs at higher temperatures than the early aggregation observed by DLS. It seems that the colloidal particles formed on heating are disrupted on cooling before reaching the LCST.

On the other hand, the more hydrophobic copolymer (60/35/5) showed slower macroscopic phase separation (Figure 7.1b). This is in agreement with the slower second aggregation observed by DLS at higher temperature (Figure 7.1b). In this case, the large aggregates formed during the heating scan seem to dissolve only after cooling below the LCST (Figure 7.1b), at temperature lower than the early small metastable nanoaggregates formed on heating.

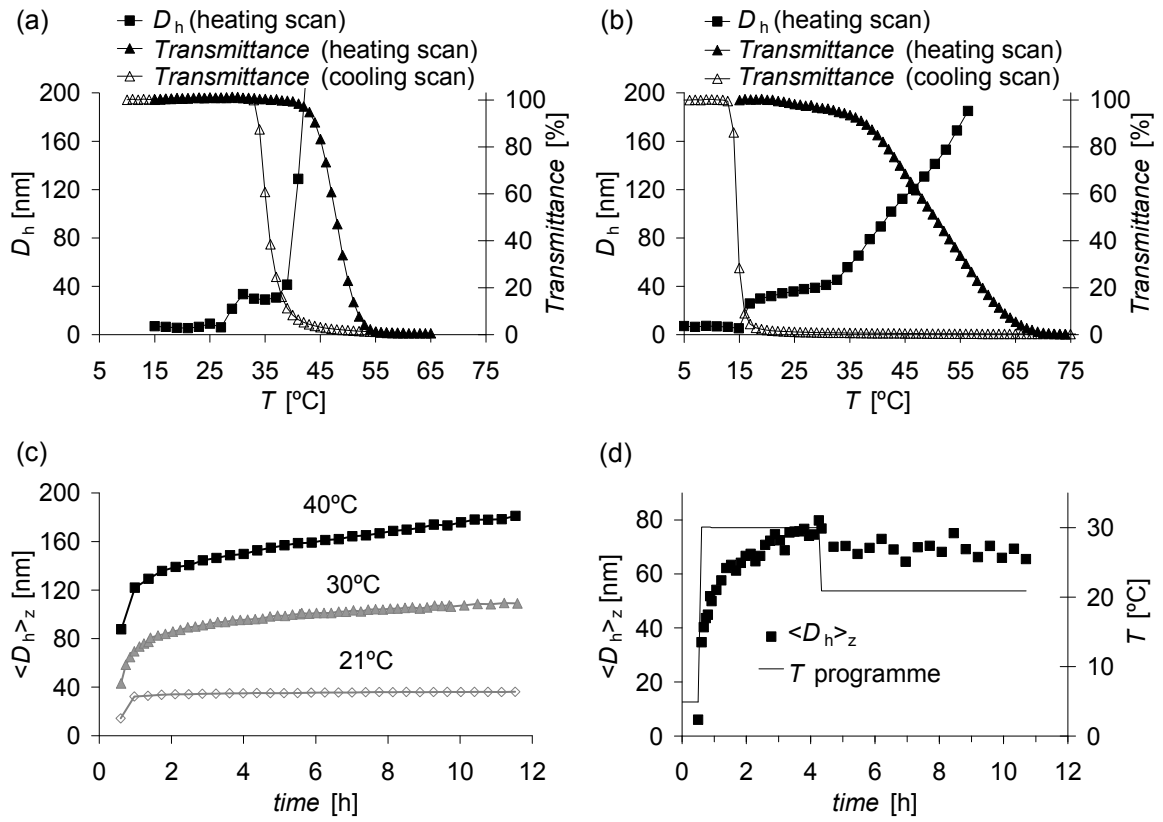

Figure 7.1 Hydrodynamic diameter (D_h) and solution turbidity (*Transmittance*) changes observed as a function of temperature for (a) 80/15/5 and (b) 60/35/5. (c) Aggregation isotherms for 60/35/5 above the LCST. (d) Nanoparticles size control using a temperature programme. All measurements were done at polymer concentration of 1 g/l in NaCl aqueous solution (0.120M).

Aggregation isotherms were determined for 60/35/5 (Figure 7.1c). Samples were initially equilibrated at 5 ºC in order to assure complete dissolution. Thereafter, solutions were submitted to a temperature jump and z-average D_h ($<D_h>_z$) was recorded at constant temperature. It was observed that metastable colloidal particles of around 35 nm were formed at 21 ºC; size remained stable for at least 12 h. When the solution was kept at 30 ºC the $<D_h>_z$ increased with the time indicating that aggregation occurs slowly at this temperature. The aggregation rate increases with the temperature as could be verified by measuring the aggregation isotherm at 40 ºC (Figure 7.1c). Taking into consideration the smooth growth of colloidal particles observed at 30 and 40 ºC (Figure 7.1c), together with the fact that larger colloidal aggregates only completely redissolve when cooled below the LCST (Figure 7.1b), we hypothesized that the aggregates, meanwhile formed at higher temperatures, would not disentangle and could be stabilized at temperatures near and above the LCST (21 ºC). In fact, it can be observed in Figure 7.1d particles that have been grown at 30 ºC for some time. When temperature is decreased to 21 ºC the $<D_h>_z$

remains constant. In a separate experiment, we observed that nanoparticle size was constant for at least one week (not shown). This behavior can be used to deliver customized particle size, just maintaining the polymer solution at high temperature for some time and decreasing the temperature to 21 ºC when particles achieve the desired size. Figures 7.2a and 7.2b show nanoparticles obtained at 30 and 40 ºC, respectively. A schematic representation of the manipulation of nanoparticles size is depicted in Figure 7.2c. Nanoparticles with sizes between 40 and 100 nm can be obtained by growing them at 30 ºC for different time periods (Figure 7.2a). When colloidal nanoparticles were formed at 40 ºC, sizes in the range 100-200 nm were obtained (Figure 7.2b). Nanoparticles can also be reversibly disentangled at temperature below the LCST, with recovery of soluble terpolymer chains. This type of systems might be very useful for instance in intracellular drug delivery and actuators for burst release applications.

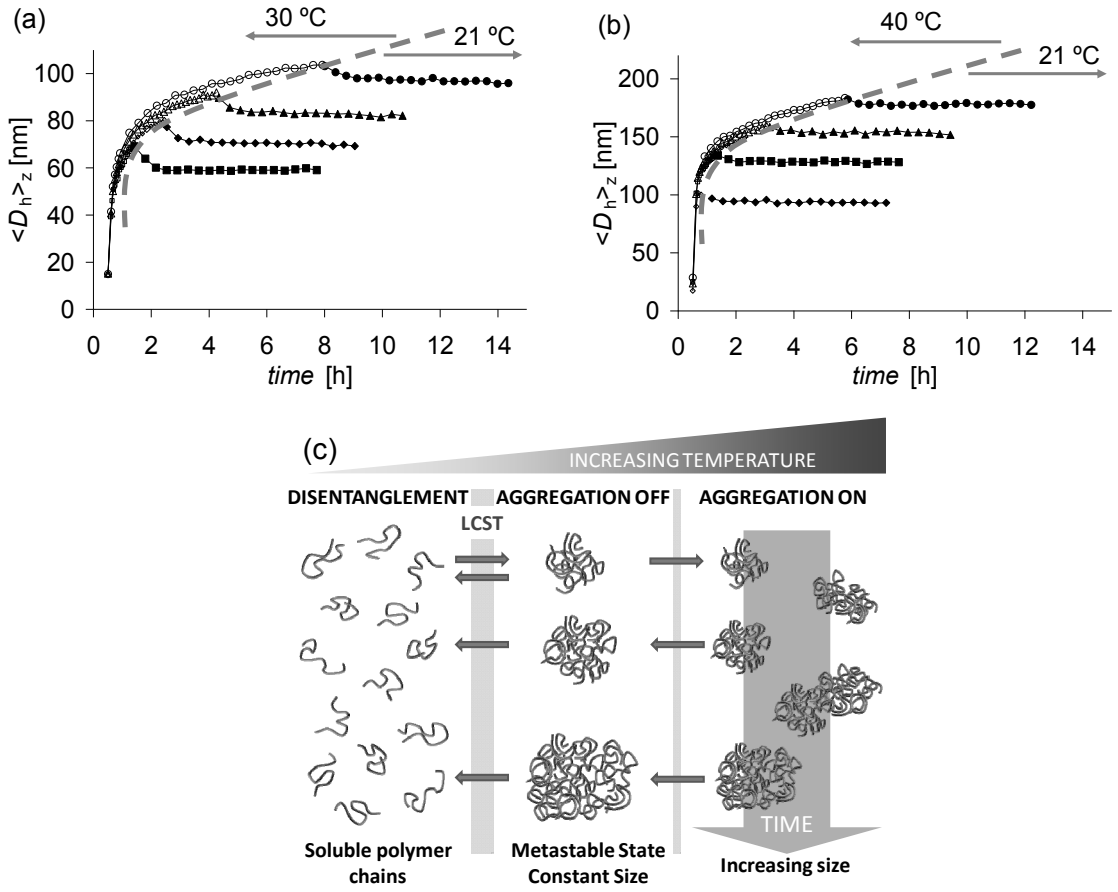

Figure 7.2 Nanoparticles z-average hydrodynamic diameter (<D_h>$_z$) observed as a function of temperature for 60/35/5. Aggregation is triggered at (a) 30 ºC or at (b) 40 ºC for well defined time periods and subsequently inhibited at 21 ºC. All measurements were done at polymer concentration of 1 g/l in NaCl aqueous solution (0.120M). (c) Schematic representation of the nanoparticles size manipulation using the thermoresponsive aggregation behavior.

Electrostatic stabilization through the anionic groups of AMPS was initially though to be the most important stability mechanism for this system. Therefore, electrophoretic mobility (μ_e) measurements were performed to evaluate particles surface charge. It was observed (Figure 7.3a) that below the LCST μ_e value remains sensibly constant. Above the LCST the absolute value of μ_e increases in a pseudo-linear manner with the temperature. In general, a higher $|\mu_e|$ would imply an improved stability because of the electrostatic repulsion. However we observed exactly the opposite. Interestingly, μ_e was independent on both temperature scanning rate and particle size. As seen in Figure 7.3b the electrophoretic mobility at a fixed temperature remained constant during at least 9 h, regardless occurrence or not of colloidal aggregation. It was also observed that decreasing the temperature to 21 ºC after this time period at 30 or 40 ºC the μ_e recovers the value initially obtained at 21 ºC. The straightforward correlation between μ_e and temperature seems to indicate that the on-off aggregation above the LCST is ruled by surface phenomenon.

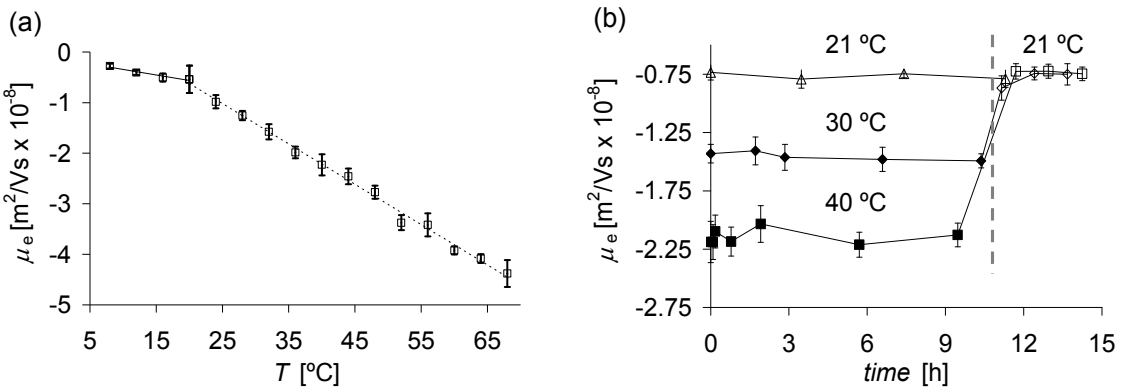

Figure 7.3 (a) Electrophoretic mobility (μ_e) observed as a function of temperature for 60/35/5. Linear regression trendlines are shown independently for the datasets above and below 21 ºC. (b) μ_e measured isothermally for the studied aggregation kinetic states, followed by isothermal determination at 21 ºC. All measurements were done at polymer concentration of 1 g/l in NaCl aqueous solution (0.120M).

It is well known that the driving force of the aggregation in thermoresponsive polymers is an increased hydrophobicity above the LCST. [21] Similarly, the driving force for increasing $|\mu_e|$ with temperature should also be an increasing hydrophobicity. Thus, if aggregation happens at higher surface charge, it is also because hydrophobic forces have been enhanced, being at a certain point able to counteract the electrostatic repulsion. In order to explain why aggregation is much faster for μ_e values where typically colloidal stability is attained, we might speculate that the non-crosslinked nature of the polymer aggregates

permits molecular rearrangements that minimize surface charge electrostatic repulsion when different colloidal particles approach each other. On the other hand, the low μ_e values also did not completely justify the colloidal stability found for temperatures closer to the LCST (21 ºC). Consequently, a different mechanism should be actuating, providing an additional (or main) energy barrier. A possible explanation can be an increased steric repulsion provided by an increased mobility of polymeric chains (lower polymer surface density) at lower temperature. In fact, the lower μ_e values are consistent with the hypothesis of lower polymer surface density.

7.4 Conclusions

In summary, we propose herein an original method to produce thermoresponsive nanoparticles by means of a temperature cycle. This method has several advantages; the nanoassemblies are formed in aqueous medium and surfactants are not needed for particles stabilization. The slow aggregation observed above the LCST was used to obtain a fine control over the particle size. Nanoparticles, grown at a higher temperature (30 and 40 ºC), are stabilized at the desired size by decreasing the temperature to 21 ºC. Finally, complete disentanglement of the nanoparticles can be triggered by further decreasing of the temperature (below 16 ºC). The thermoresponsive system reported here may be potentially useful for a range of applications, including drug and gene delivery, biosensing, or separation and purification of biological molecules and cells. Moreover, we believe that it would be possible to extend the method to other thermoresponsive polymers, both cationic and anionic, by fine tuning the balance between electrostatic repulsion and polymer hydrophobicity.

7.5 Experimental

N-isopropylacrylamide (NIPAAm, Acros Organics) and 2,2'-Azobis-isobutyronitrile (AIBN) (Fluka) were recrystallized from n-hexane/diethyl ether (5:1) and methanol, respectively. 2-Acrylamido-2-methyl-1-propanesulphonic acid (AMPS) and *N-tert*-butylacrylamide (NTBAAm) (Sigma-Aldrich) were used as received.

Linear random terpolymers P(NIPAAm-*co*-NTBAAm-*co*-AMPS) were synthesized as previously described. [18] Briefly, monomers (total concentration 0.5 M) were dissolved in isopropanol/water (50:50) and AIBN (1 mol % of total monomers) was added. Two different copolymers were synthesized using feed molar percentages of

NIPAAm/NTBAAm/AMPS in the reaction mixture of 60/35/5 and 80/15/5, respectively. After deoxygenation with N_2 (15 min), the reaction vessel was sealed and kept at 60 ºC for 16 h. Then, polymer solutions were neutralized with NaOH, dialyzed against distilled water (cut-off 3500 Da) and freeze-dried. Terpolymers composition was very similar to the reaction feed composition, as determined by Elemental analysis (Leco CHNS-932) and ^{1}H NMR using $CDCl_3$ as solvent (Varian Inova 300). [18] Molecular weight (~ 18 KDa) and polydispersity (~ 2.7) [18] were determined by gel permeation chromatography (GPC) using LiBr (0.1 %w/v) in DMF as eluent at a flow rate of 0.3 mL.min^{-1} at 70 ºC and narrow disperse poly(ethylene glycol) (PEG) as calibration standards.

The cloud point temperature (CPT) of the polymer solutions was measured in a Varian-Cary 3 UV/Visible spectrophotometer, equipped with a Peltier temperature controller. The transmittance (400 nm) was monitored as a function of temperature under magnetic stirring. Solutions were frozen at -20 ºC to ensure complete dissolution. Immediately after melting, solutions were placed in a cuvette and heating scans were performed between 15-80 ºC at a scanning rate of 1 ºC/min. The initially clear polymer solution was used as blank. Cooling scans were performed between 80-5 ºC immediately after heating at the same rate.

The hydrodynamic diameter was determined by Dynamic Light Scattering (DLS) using a Zetasizer NanoZS Instrument (ZEN3600, Malvern Instruments, Worcestershire, UK) equipped with a 4 mW He-Ne laser (λ_0=633 nm) and with non-invasive backscattering (NIBS) detection at a scattering angle of 173º. Both measuring position and attenuator were adjusted automatically before each measurement. Measurements at variable temperature were performed after an equilibration time of at least 2 min.

The electrophoretic mobility was obtained by Laser Doppler Velocimetry (LDV) using a Zetasizer NanoZS Instrument (ZEN3600, Malvern Instruments, Worcestershire, UK) at a scattering angle of 17º and capillary folded cells (DTS1060, Malvern, Worcestershire, UK). The measurements were performed with an applied voltage of ± 20 V in the temperature range 8-64 ºC after an equilibration time of 4 min. For both DLS and electrophoretic mobility measurements, the terpolymer solutions were prepared in ultrapure water and filtered using a 0.20 µm disposable PES membrane filter (TPP, Trasadingen, Switzerland).

7.6 Acknowledgements

The authors acknowledge funding from EU Marie Curie Actions, Alea Jacta Est (MEST-CT-2004-008104) and Portuguese Foundation for Science and Technology (FCT)

(SFRH/BPD/34545/2007). This work was carried out under the scope of the European NoE EXPERTISSUES (NMP3-CT-2004-500283).

7.7 References

1. Hussain, S.M.; Braydich-Stolle, L.K.; Schrand, A.M.; Murdock, R.C.; Yu, K.O.; Mattie, D.M.; Schlager, J.J. Toxicity evaluation for safe use of nanomaterials: Recent achievements and technical challenges. *Advanced Materials*, 2009, **21,** (16), 1549-1559.

2. De, M.; Ghosh, P.S.; Rotello, V.M. Applications of nanoparticles in biology. *Advanced Materials*, 2008, **20,** (22), 4225-4241.

3. Ganta, S.; Devalapally, H.; Shahiwala, A.; Amiji, M. A review of stimuli-responsive nanocarriers for drug and gene delivery. *Journal of Controlled Release*, 2008, **126,** (3), 187-204.

4. Rijcken, C.J.F.; Soga, O.; Hennink, W.E.; Nostrum, C.F.v. Triggered destabilisation of polymeric micelles and vesicles by changing polymers polarity: An attractive tool for drug delivery. *Journal of Controlled Release*, 2007, **120,** (3), 131-148.

5. Oliveira, J.M.; Kotobuki, N.; Marques, A.P.; Pirraco, R.P.; Benesch, J.; Hirose, M.; Costa, S.A.; Mano, J.F.; Ohgushi, H.; Reis, R.L. Surface engineered carboxymethylchitosan/poly(amidoamine) dendrimer nanoparticles for intracellular targeting. *Advanced Functional Materials*, 2008, **18,** (12), 1840-1853.

6. Chung, J.E.; Yokoyama, M.; Okano, T. Inner core segment design for drug delivery control of thermo-responsive polymeric micelles. *Journal of Controlled Release*, 2000, **65,** (1-2), 93-103.

7. Kohori, F.; Sakai, K.; Aoyagi, T.; Yokoyama, M.; Yamato, M.; Sakurai, Y.; Okano, T. Control of adriamycin cytotoxic activity using thermally responsive polymeric micelles composed of poly(N-isopropylacrylamide-co-N,N-dimethylacrylamide)-b-poly(D,L-lactide). *Colloids and Surfaces B-Biointerfaces*, 1999, **16,** (1-4), 195-205.

8. Zhang, L.; Guo, R.; Yang, M.; Jiang, X.; Liu, B. Thermo and pH dual-responsive nanoparticles for anti-cancer drug delivery. *Advanced Materials*, 2007, **19,** (19), 2988-2992.

9. Neradovic, D.; Soga, O.; Van Nostrum, C.F.; Hennink, W.E. The effect of the processing and formulation parameters on the size of nanoparticles based on block copolymers of poly(ethylene glycol) and poly(N-isopropylacrylamide) with and without hydrolytically sensitive groups. *Biomaterials*, 2004, **25,** (12), 2409-2418.

10. Zhu, P.W.; Napper, D.H. Effect of heating rate on nanoparticle formation of poly(N-isopropylacrylamide)-poly(ethylene glycol) block copolymer microgels. *Langmuir*, 2000, **16,** (22), 8543-8545.

11. Topp, M.D.C.; Dijkstra, P.J.; Talsma, H.; Feijen, J. Thermosensitive micelle-forming block copolymers of poly(ethylene glycol) and poly(N-isopropylacrylamide). *Macromolecules*, 1997, **30,** (26), 8518-8520.

12. Qiu, X.P.; Wu, C. Study of the core-shell nanoparticle formed through the "coil-to-globule" transition of poly(N-isopropylacrylamide) grafted with poly(ethylene oxide). *Macromolecules*, 1997, **30,** (25), 7921-7926.

13. Mori, T.; Maeda, M. Temperature-responsive formation of colloidal nanoparticles from poly(N-isopropylacrylamide) grafted with single-stranded DNA. *Langmuir*, 2004, **20,** (2), 313-319.

14. Vauthier, C.; Bouchemal, K. Methods for the Preparation and Manufacture of Polymeric Nanoparticles. *Pharmaceutical Research*, 2009, **26,** (5), 1025-1058.

15. Qin, S.; Geng, Y.; Discher, D.E.; Yang, S. Temperature-controlled assembly and release from polymer vesicles of poly(ethylene oxide)-block-poly(N-isopropylacrylamide). *Advanced Materials*, 2006, **18,** (21), 2905-2909.

16. Qiu, X.; Li, M.; Kwan, C.M.S.; Wu, C. Light-scattering study of the coil-to-globule transition of linear poly(N-isopropylacrylamide) ionomers in water. *Journal of Polymer Science, Part B: Polymer Physics*, 1998, **36,** (9), 1501-1506.

17. Qiu, X.P.; Kwan, C.M.S.; Wu, C. Laser light scattering study of the formation and structure of poly(N-isopropylacrylamide-co-acrylic acid) nanoparticles. *Macromolecules*, 1997, **30,** (20), 6090-6094.

18. Lopez-Perez, P.M.; da Silva, R.M.P.; Pashkuleva, I.; Parra, F.; Reis, R.L.; San Roman, J. Hydrophobic-electrostatic balance driving the LCST offset aggregation-redissolution behavior of N-alkylacrylamide based ionic terpolymers. *Langmuir*, 2010, **in press**.

19. Varghese, S.; Lele, A.K.; Mashelkar, R.A. Designing new thermoreversible gels by molecular tailoring of hydrophilic-hydrophobic interactions. *Journal of Chemical Physics*, 2000, **112,** (6), 3063-3070.

20. Qiu, X.P.; Li, M.; Kwan, C.M.S.; Wu, C. Light-scattering study of the coil-to-globule transition of linear poly(N-isopropylacrylamide) ionomers in water. *Journal of Polymer Science Part B-Polymer Physics*, 1998, **36,** (9), 1501-1506.

21. Takei, Y.G.; Aoki, T.; Sanui, K.; Ogata, N.; Sakurai, Y.; Okano, T. Dynamic Contact-Angle Measurement of Temperature-Responsive Surface-Properties for Poly(N-Isopropylacrylamide) Grafted Surfaces. *Macromolecules*, 1994, **27,** (21), 6163-6166.

Chapter 8

General conclusions and final remarks

In this thesis surface phenomena addressing two very different applications within the biomaterials field were studied. If fact, physical protein adsorption, a critical step in cell adhesion and subsequent fate, is mainly explained by the same surface phenomenon that rules colloidal aggregation processes.

In the first part of the present thesis (Chapters 3, 4 and 5), the surface of 2D and 3D biomaterial structures was functionalized with acidic anionic groups by plasma induced polymerization and the influence of the modification process on the surface properties and the material *in vitro* performance was evaluated. In the second part, (chapters 6 and 7) thermoresponsive ionic polymers were synthesized and characterized. The peculiar aggregation-redissolution behavior of some of the synthesized polymers was used for the production of nanoparticles with a well controlled size.

Surface functionalization by plasma induced polymerization

This part of the thesis dealt with the influence of anionic, acidic groups on the surface of biomedical devices and with the crosstalk of these devises with different bioentities present in the *in vitro* environment such as cells and proteins. Our attention to those groups was a consequence of the presence of negatively charged functional groups in all natural glycosaminoglycans and because of the proven crucial role of these charged units in the formation proteoglycans, and therefore in key biochemical process related to cell survival and functionality. In Chapters 3 to 5, we have tested the three most common for natural biomacromolecules negative moieties: -COOH, -SO_3H and –PO_3H. While the first two groups are common for the GAGs, the third one is closely related to biomineralization process triggering bone formation. In these studies (Chapters 3, 4 and 5) we have found that small changes in surface morphology and chemistry can induce remarkably distinguishable cell response. A negative effect of –COOH grafted chitosan on osteoblasts like cells (SaOs-2) attachment and proliferation was observed whereas tremendous improvement in cell behaviour on surfaces with –SO_3H and –PO_3H grafted groups was registered. The response of SaOs-2 cells to the modified surfaces was related to protein adsorption. We have investigated adsorption from complex protein solution such as serum where a competition between different proteins occurs. The detected improvement in cell

behaviour on both -SO_3H and –PO_3H containing surfaces was attributed to the adhesive vitronectin (Vn), the protein which adsorbed mostly at the studied conditions (the same as for the in vitro cell tests). Further comparison between the negative functionalities demonstrated increased adsorption of Vn on –PO_3H grafted samples. The same tendency was observed for the adhesion and proliferation of SaOs-2; higher DNA quantities were registered for SaOs-2 cultured on –PO_3H modified samples.

Chapter 5 of the thesis proved that the methodology for surface modification proposed in Chapters 3 and 4 is applicable to devices made from different polymers and with complex shapes. The translation of 2D to 3D surface modification is very important since the supports required in different tissue engineering strategies and biomedical applications are usually 3D, complex shaped scaffolds. The nowadays available strategies for functionalization of 3D structures usually involve wet chemical treatments which in many cases affect the bulk properties of the material.

Overall, the results from this part of the thesis further testify the potential of surface grafting of functional groups by plasma-induced polymerization in the context of bone tissue engineering.

Thermoresponsive alkylacrylamide based ionic terpolymers.

Ionic thermo-responsive polymers has the ability to form surfactant-free nanoparticles stabilized by surface charge above the LCST or to interact with oppositely charged macromolecules, allowing for the construction of thermo-responsive polyelectrolyte complexes. In the second part of this thesis (Chapter 6 and 7), a series of ionic terpolymers composed of *N*-isopropylacrylamide (NIPAAm), 2-Acrylamido-2-methyl-1-propanesulphonic acid (AMPS) and *N-tert*-butylacrylamide (NTBAAm) monomers were synthesized by free radical polymerization. In Chapter 6 the effect of polymer composition, salt and polymer concentration in the aggregation-redissolution behavior in solution was evaluated. Turbidity was used to assess the macroscopic phase separation and dynamic light scattering (DLS) was employed to elucidate some aspects regarding the molecular scale mechanism of the temperature-induced phase separation. In Chapter 7 the ionic polymers aggregation-redissolution profile observed for more hydrophobic polymers was used to propose a methodology for the production of nanoparticles with a well controlled size.

In the polymer design, AMPS was chosen to afford a negative charge to the terpolymers because it is a strong acid (pK_a=1.9) that dissociates completely in the pH range of most envisaged applications. An AMPS molar ratio of 0.05 was chosen to assure a sharp

phase-separation. Furthermore, the functional sulfonic group position in AMPS gives the terpolymers a continuous structural similarity along the polymer backbone. This avoids the disruption of the continuity of the *N*-alkyl groups, which has been referred in the literature to decrease hydrophobic aggregation force necessary for the cooperative chain collapse, thus decreasing phase-separation sharpness. All terpolymers were synthesized containing the same relative amount of AMPS, i.e., containing the same charge. In order to adjust the LCST, terpolymer hydrophobic content was varied by changing NTBAAm to NIPAAm monomer ratio. Poly(NIPAAm-*co*-NTBAAm-*co*-AMPS) aqueous solution did not show turbidity changes (macroscopic phase separation) with the temperature.

The CPT was only observed when NaCl was added to the solutions. However, the formation of metastables nanosized aggregates (LCST) was observed by DLS in both water and aqueous saline solutions. The macroscopic phase separation was always observed at higher temperatures than the formation of the nano-aggregates. Therefore, there was no correlation between CPT and LCST. These results raised serious concerns about the validity of using turbidimetry measurements to obtain a reliable estimation of the LCST for charged thermoresponsive polymers. Both the CPT and the LCST decreased with the increase of hydrophobicity (increased NTBAAm content). However, the aggregation profile observed by turbidimetry dramatically changed above a critical amount of NTBAAm (0.25-0.30). Terpolymers with NTBAAm content below the critical value showed a fast macroscopic phase separation for all studied conditions. Moreover, the formed large aggregates redissolve in the cooling ramp at different temperature depending on the salt concentration and always at temperatures higher than the LCST. On the other hand, NTBAAm-richer terpolymers showed a slower aggregation process whose rate was found to depend on salt concentration. In this case, the large aggregates formed during the heating scan disentangled always at the same temperature which is coincident with the LCST. The differences observed on copolymers solutions were explained as the result of a fine balance between hydrophobic attractive forces and electrostatic repulsion, which leads to formation of intermediate metastable nanosized aggregates. The hydrophobic cohesion forces for polymers with higher NTBAAm content are stronger, thus able to withstand a higher surface charge density. Therefore, the aggregation is slower due to the electrostatic repulsion that acts as stabilizer of the aggregates. Furthermore, the redissolution only occurs at the LCST because the stronger internal cohesion is enough to compensate the electrostatic repulsion. On the other hand, the hydrophobic forces in polymers with lower content of NTBAAm are weaker and not able to bring charges close enough to provide an effective surface charge density, hindering electrostatic stabilization of the aggregates with a consequent fast coagulation.

Moreover, the larger aggregates formed meanwhile were redissolved before reaching the LCST in the cooling ramp because the hydrophobic interactions are not strong enough to counteract the electrostatic repulsion.

Using the aggregation-redissolution profile of more hydrophobic copolymers we have proposed in this thesis a method to produce thermoresponsive nanoparticles by means of a temperature cycle (Chapter 7). The nanoassemblies were formed in aqueous medium and surfactants were not needed for particles stabilization. The slow aggregation observed above the LCST was used to obtain a fine control over the particle size. Nanoparticles, grown at a higher temperature (30/ 40ºC), were stabilized at the desired size by decreasing the temperature to 21ºC. Finally, complete disentanglement of the nanoparticles could be triggered by further decreasing the temperature (below 16ºC).

We believe that it would be possible to extend the method to other thermoresponsive polymers, both cationic and anionic, by fine tuning the balance between electrostatic repulsion and polymer hydrophobicity. This nanoparticle synthesis methodology may be potentially useful to obtain nanoparticles of customized size for a range of applications, including drug and gene delivery, biosensing, separation and purification of biological molecules and cells. The method avoids using surfactants or crosslinkers, avoiding their inherent drawbacks. The reversible disentanglement of the nanoparticles at temperature below the LCST, with recovery of soluble terpolymer chains, might be very useful for instance in intracellular drug delivery and burst release of drugs locally applying simple ice packs or clinical instruments such as deeply penetrating cryoprobes.

What does not kill me, makes me stronger

Friedrich Nietzsche *(Twilight of the Idols*, 1888*)*